Site-Specific Labelling of Nucleic Acids

by Catalyst-Free 1,3-Dipolar Cycloadditions

A thesis submitted to the National University of Ireland in fulfilment of the requirements for the degree of

Doctor of Philosophy

by

Colin Henry Freeman, B.Sc.

NUI MAYNOOTH

Ollscoil na hÉireann Má Nuad

Department of Chemistry,
National University of Ireland, Maynooth,
Maynooth,
Co. Kildare,
Ireland.

February 2012

Research Supervisor: Dr. Frances Heaney

Head of Department: Professor John Lowry

Table of Contents

To Harry and Caroline (the folks) and Ali and Sophie (the siblings)

Acknowledgements

First and foremost I'd like to thank my supervisor, Dr. Frances Heaney, for her advice, stewardship and of course, patience over the past four years. Simply put, I could not have asked for a better supervisor. A special mention also to Dr. Jeffrey Glennon – I wouldn't be at the tail end of a PhD thesis right now if it wasn't for him. Indeed, many thanks to all the academic staff in the chemistry department in NUI Maynooth, who have all at one stage or another offered me some sort of advice/help/kindness. I am most grateful to the technical staff, whose expertise and all-round helpfulness have been of great importance to me in countless ways over the course of my studies. Thanks also to the group of Dr. Joe Vyle in Queens University Belfast for their help with collecting the photochemical data for our azobenzene compounds. An enormous thank you as well to IRCSET for providing funding for my research.

A special mention must also go to the members of my own research group, both past and present. To former post-doc Ishwar, who was of enormous assistance throughout the first few years. To Linda, whose bench I inherited, and was always patient and helpful in my first year when my lab skills were a little less 'refined'. To our most recent addition Haowen, who to this day remains the only person I've seen produce a mushroom-cloud in the lab environment. And finally to my 'lab-buddie' Vickie, who finds herself finishing up at the same time as myself. Vickie is French and she's mad as a brush.

Keeping with the academic theme, I feel my secondary school chemistry teacher, Brendan Grehan, deserves a shout-out. A pretty mad guy – god knows where you are or what you're doing now Sir, but in my case you definitely made a difference.

Now onto my fellow chemistry postgrads. I didn't realise it when I signed up, but studying for a PhD in chemistry in NUI Maynooth is actually *serious* craic. Contrary to the popular opinion that all 4th level chemistry students are stuffy, annoying nerds, that's really only the case for about half of them. If it wasn't for my peers in the department, my time as a postgrad would have been infinitely more boring. Whether drinking cans and playing xbox with John, Joey and Conor, being pestered into displaying my phenomenal dance skills in Mantra by Roisin, Lor-d-na (that's Lorna with

a ‘d’), Lynn, Foxy and co., trying to figure out what Claire or Vickie were actually saying, or discussing which GAA players I hated the most with Declan Gavin, any time spent with the other postgrads was invariably great craic. I’ll certainly miss the banter in the lunch room. I may never again have access to such a tolerant forum for my rants, ramblings and rowdiness.

To the GAA community in NUI Maynooth, and of course, my home club St. Brigids: you make life a pleasure. Football is a huge part of my life, and whenever sporting and academic commitments have collided, there’s only been one winner. As I heard said by, of all people, a priest just last week, ‘Never let exams get in the way of your general education.’ Although, it has been a bit of a close call in recent weeks as this deadline approaches...

And finally, to my parents, Harry and Caroline – what can I say? You’ve been completely supportive of everything I’ve ever done, and probably everything I ever will do. All I can say is thank you for your financial and emotional support, for always taking an interest, for the roof over my head and of course, for your genes. I can’t forget my sisters either: Ali, who’s a secondary school teacher in Marino keeping all them youngsters from the ‘Sheriffer’ on their toes, and Sophie, who is now herself a 1st year science undergrad right here in NUI Maynooth. I pass the torch to you now Sophie...

Not really.

Declaration

I hereby certify that this thesis has not been submitted before, in whole or in part, to this or any other university for any degree and is, except where otherwise stated, the original work of the author.

Signed: _____ Date: _____

Abstract

The focus of the novel research reported in this thesis is the labelling of nucleic acids by catalyst-free 1,3-dipolar cycloaddition reactions. Both nitrile oxide-alkyne cycloadditions (NOAC) and strain-promoted azide-alkyne cycloadditions (SPAAC) were explored.

The possiblitity for 'pre-synthetic' functionalisation was demonstrated using non-nucleosidic phorphoramidite building blocks generated by NOAC. Three isoxazole phosphoramidites were prepared. Following *in situ* generation of the nitrile oxides from 1,2-, 1,3- or 1,4-disubstituted hydroxyethoxybenzaldehyde oximes and highly regioselective cycloadditions to a simple alkyne, the isomeric isoxazoles were obtained in excellent yields. Functional group interchange of the pendant hydroxy group to a phosphoramidite functionality facilitated coupling to DNA both by manual and instrument controlled solid phase DNA synthesis.

Photoresponsive DNA, incorporating isomeric isoxazole-linked azobenzene moieties, was prepared by 'post-synthetic' modification of alkyne-functionalised oligonucleotides by NOAC. The compatibility of the azobenzene functionality with NOAC protocols was first confirmed with small molecule examples; the resulting cycloadducts were characterised by NMR spectroscopy and mass spectrometry (MS). Oligonucleotides incorporating azobenzene moieties at either the 5'- or the 3'- termini, or at an internal position, were subsequently synthesised and the photochemical and kinetic properties of selected examples were determined. A relationship was found between the thermodynamic and photochemical properties of the modified oligonucleotides and the substitution pattern on the aryl rings of the azobenzene moiety.

DNA and 2'-OMe RNA sequences conjugated to a variety of chemically and biologically significant ligands were prepared by solid-phase SPAAC. A strained-cyclooctyne phosphoramidite was first conjugated to the 5'-terminus of oligonucleotides. Several azide labels were prepared, including benzyl, cinnamyl, biotinyl, cholesteryl and fluoresceinyl. Conjugation was clean and efficient in all cases. Oligonucleotides were characterised by HPLC and MALDI-TOF MS.

Abbreviations

A	Pre-exponential factor
Ac	Acetyl
Ar	Aryl
BMT	5-Benzylmercapto-1*H*-tetrazole
br s	Broad singlet
Bz	Benzoyl
Calcd.	Calculated
$CDCl_3$	Deuterated chloroform
Ch-T	Chloramine T
cm	Centimetre
CNE	2-Cyanoethyl
CPG	Controlled pore glass
CuAAC	Copper catalysed azide-alkyne cycloaddition
^{o}C	Degrees Celsius
d	Doublet
δ	Chemical shift
DA	Diode array detector
DCM	Dichloromethane
dd	Doublet of doublets
Δ	Reflux temperature
$\Delta H^{\ddagger}$	Enthalpy of activation
$\Delta S^{\ddagger}$	Entropy of activation
Dmf	Dimethylformamidyl
DMF	Dimethylformamide
DMP	Dess-Martin periodinane
DMSO	Dimethyl sulphoxide
d_6-DMSO	Deuterated dimethyl sulphoxide
DMT	Dimethoxytrityl
dsDNA	Double-stranded DNA
dsRNA	Double-stranded RNA
ε	Molar absorptivity
E_A	Activation energy
ESI	Electronspray ionisation
EtOH	Ethanol
FMO	Frontier molecular orbital
HCl	Hydrochloric acid
HPLC	High performance liquid chromatography

hr	Hour
HRP	Horseradish peroxidise
Hz	Hertz
*i*Bu	Isobutyrl
*i*Pr-Pac	Isopropyl phenoxyacetyl
Irr	Irradiated
k	Rate constant
J	Coupling constant
k_B	Boltzmann's constant
KOH	Potassium hydroxide
λ	Wavelength (nm)
LAH	Lithium aluminium hydride
LC/TOF-MS	Liquid chromatography time-of-flight mass spectrometer
LCAA	Long-chain amino alkyl
m	multiplet
M	Molar
MALDI-TOF	Matrix-assisted laser desorption/ionization-time of flight
MscL	Mechanosensitive channel of large conductance
Me	Methyl
MeOH	Methanol
MHz	Megahertz
min	Minute
mL	Millilitre
mmol	Millimole
m.p.	Melting point
µL	Microlitre
MS	Mass spectrometry
N_2	Dinitrogen
NaCl	Sodium chloride
NaOH	Sodium hydroxide
NBS	*N*-Bromosuccinimide
NCS	*N*-Chlorosuccinimide
nm	Nanometre
NMR	Nuclear magnetic resonance
NOAC	Nitrile oxide-alkyne cycloaddition
NTP	Nucleotide triphosphate
OEt	Ethoxide anion
Pac	Phenoxyacetyl
PCR	Polymerase chain reaction
pH	Logarithmic scale of concentration of hydronium ions ($-\log[H_3O^+]$)
ppm	Parts per million

R	Universal gas constant
RISC	RNA-induced silencing complex
RNAi	RNA interference
RNAP	RNA polymerase
q	Quartet
rt	Room temperature
s	Singlet
sl br s	Slightly broad singlet
siRNA	Small interfering RNA
$t_{1/2}$	Half-life
t	Triplet
T	Temperature
TCA	Trichloroacetic acid
TEA	Triethylamine
THF	Tetrahydrofuran
T_m	Melting temperature of a DNA/RNA duplex
UV/Vis	Ultraviolet/visible
χ	Mole fraction

Chapter 1

Introduction

1.1 Introduction

Ever since the elucidation of the structure of DNA by Watson and Crick,[1] the iconic double helix is an image that resonates with people from all walks of life. In the decades since, the role of nucleic acids in the storage and transmission of genetic information has become a hugely popular research topic. In light of recent breakthroughs in the fields of genetics and molecular biology including the mapping of the human genome and the discovery of the potential therapeutic value of RNA interference (RNAi) pathways, there is a demand for research at the interface of chemistry and biology to help in bringing molecular advances to their full clinical potential.

1.1.1 Structure of DNA and RNA

DNA is made up of four structurally related monomers called nucleosides: adenosine, cytidine, guanosine and thymidine (figure 1.1). Each consists of a sugar portion (deoxyribose) and a heterocyclic base portion. Adenosine and guanosine possess a purine-type base (adenine and guanine), whereas in cytidine and thymidine the base (cytosine and thymine) is of the pyrimidine type.

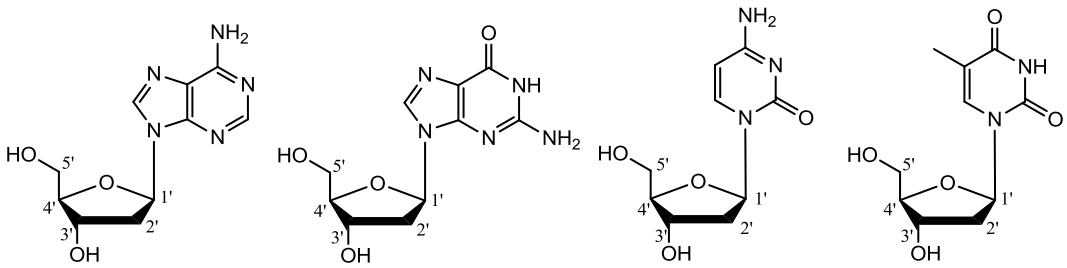

Figure 1.1. The four canonical DNA nucleosides

These monomer building blocks are linked together, in various combinations, *via* a phosphodiester linkage involving the oxygen atoms at the 3’ and 5’ carbons of adjacent sugar units to form individual strands of DNA. Consequently, each strand of DNA possesses a free hydroxy group at either end, one borne on a 5’-carbon and the other on a 3’-carbon. As such, sequences of DNA are read in a 5’ to 3’ (more common) or a

3’ to 5’ direction, *e.g.* the shorthand for the sequence shown in figure 1.2 is 5’-TCAGA-3’.

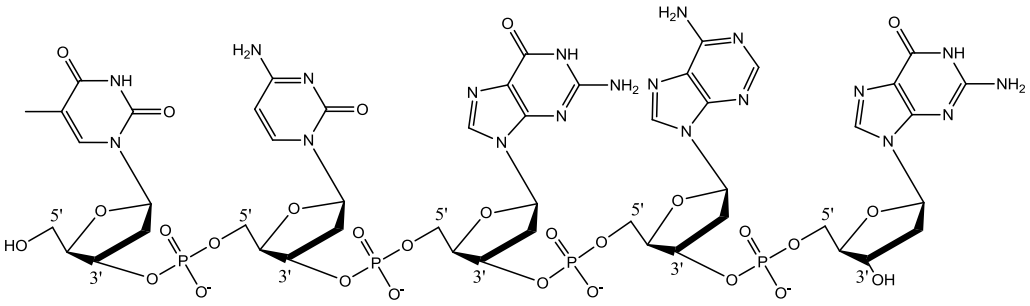

Figure 1.2. A 5-*mer* sequence of DNA, highlighting the phosphodiester linkages and the terminal 5’- and 3’- hydroxy groups

In the cellular environment it is rare to encounter DNA in its single-stranded form. DNA strands form stable duplexes *via* regular, predictable hydrogen bonding between the nucleoside bases on adjacent strands. Guanine pairs with cytosine *via* three hydrogen bonds, whereas adenine pairs with thymine *via* two hydrogen bonds; the two strands wind around each other to form a double helix (figure 1.3).

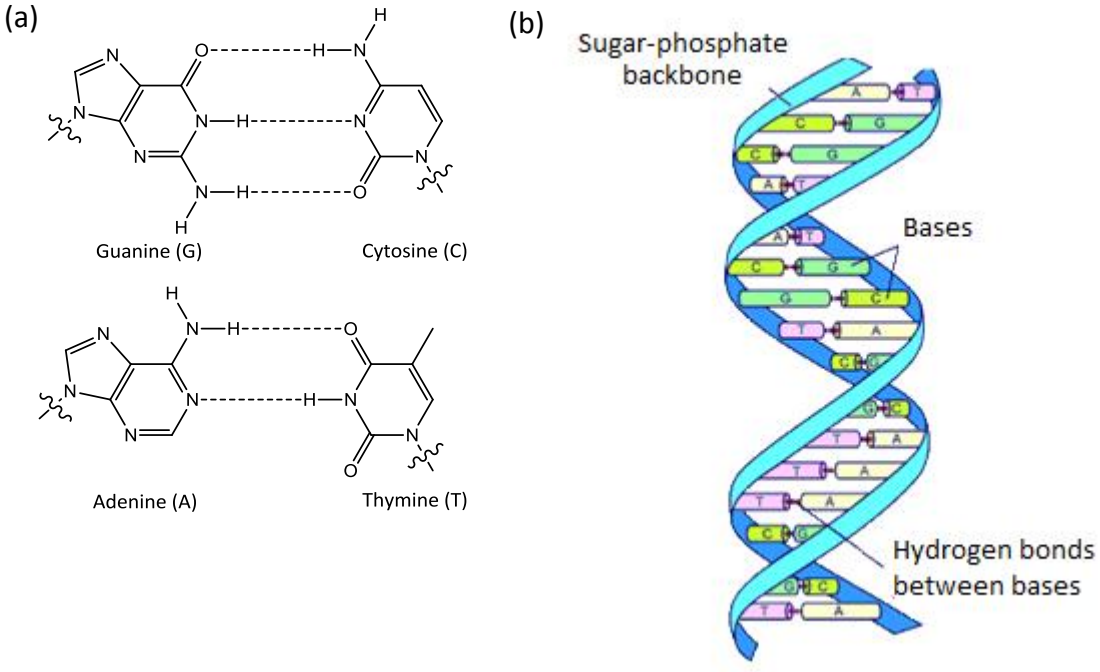

Figure 1.3. (a) Base-paring between purine and pyrimidine bases; (b) The double helical structure of DNA[2]

RNA closely resembles DNA in structure, yet there are a few key differences between the two. The sugar unit of RNA nucleosides (ribose) bears an extra hydroxyl group at the 2'-position (figure 1.4). The 3'-OH is not involved in the phosphodiester backbone; it remains 'free' and has the potential to act as a nucleophile. This additional reactivity renders RNA significantly less stable than DNA. In addition, in RNA the base thymine is replaced with uracil, which differs only in the absence of a methyl group. Finally, unlike DNA, RNA most commonly exists in cells in its single stranded form, although different sections of longer strands may base-pair with each other to form looped regions. Noteworthy examples of double-stranded RNA (dsRNA) include certain viruses, which possess dsRNA genomes, and short interfering RNAs (siRNA), which are key components of the RNA interference pathway.

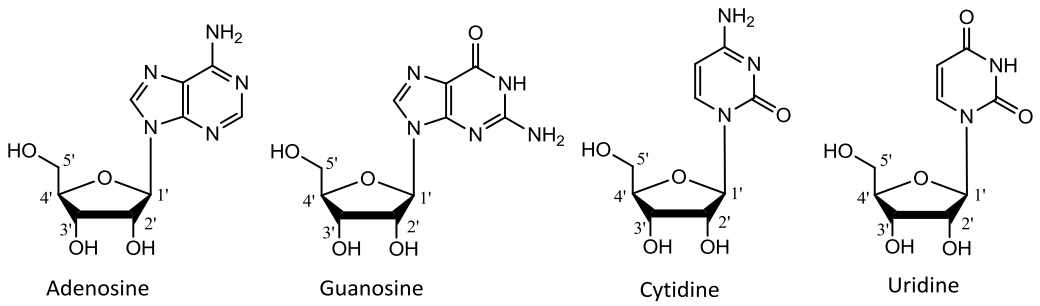

Figure 1.4. The four canonical RNA nucleosides

1.2 RNA interference

The discovery that gene expression in living cells can be controlled by base-pairing between small sequences of RNA and messenger RNA (mRNA) has ushered in a revolution in RNA biology. The role of RNAi in eukaryotic cells involves defence against parasitic genes (*e.g.* from viruses) in addition to regulation of the expression of endogenous genes. The diagnostic and therapeutic potential of RNAi first became apparent in the late 1990s when Craig C. Mello and Andrew Fire published their seminal report describing the selective control of gene expression following the introduction of exogenous RNA into *C. Elegans*.[3]

The mechanism of RNAi can be broken down into several steps, as shown in scheme 1.1.[4,5] Firstly, a long sequence of dsRNA, which may be exogenous or endogenous in origin, is cleaved into small RNA duplexes known as small siRNA by the RNase III enzyme Dicer. Secondly, these siRNA segments are unwound, and one of the strands is preferentially taken up into the RNA-induced silencing complex (RISC). The complex then searches the transcriptome for complementary sequences of messenger RNA (mRNA). Finally, the siRNA-derived, single-stranded RNA (ssRNA) of the RISC complex, known as the guide strand, directs the enzymatic component of the RISC complex, an Argonaute protein, to cleave the complementary sequence of mRNA.

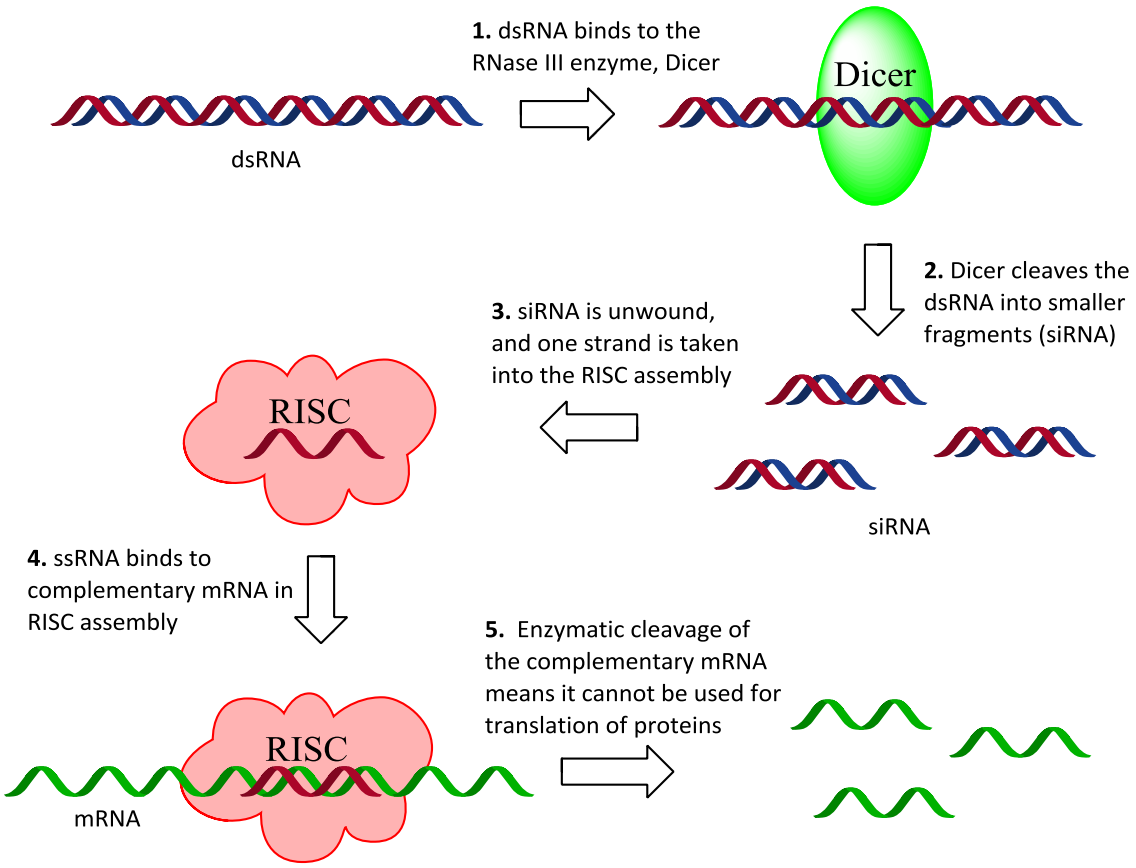

Scheme 1.1. The RNA interference pathway

RNAi has emerged as a powerful tool for research in molecular biology, which exploits its selective and robust ability to effect gene knockdown. The ability to selectively 'cancel out' genes thought to have a role in a particular cellular process can be invaluable in determining the physiological role of particular gene products. Studies

involving the model organisms *C. Elegans* and *Drosophila* have benefited greatly from this approach, and consequently the genes involved in many crucial biological pathways such as aging,[6] cell cycle regulation[7] and specific signalling pathways[8] have unambiguously been identified.

It is now commonplace for applications which exploit RNAi to employ chemically modified siRNAs.[9] Due to the relatively small size of siRNAs (~21-25 nucleotides in length), chemical synthesis of exogenous sequences is straightforward, and allows various chemical modifications to be introduced. Modifications are generally intended to increase stability, promote efficacy, or block binding to unintended targets. Since the 2'-OH group of the sugar is not required for active RNAi,[10] many modifications have been incorporated at this position. 2'-*O*-Methyl derivatives have been widely used; this modification significantly increases the stability of the sequence towards RNA digesting enzymes.[11] Increasing the half-life of small RNAs is of obvious importance for RNAi therapeutics, which must survive long enough *in vivo* to reach their site of action. Cellular uptake is another hurdle which must be overcome. Owing to their size and high density of negative charge, siRNAs cannot easily cross cell membranes. In this regard, modifications involving conjugation to lipophilic moieties such as cholesterol have proven useful.[12]

1.3 Nucleic acid modification

Applications which rely on the manipulation of oligonucleotides are not only limited to molecular research, genetic and therapeutic spheres; the reliable and predictable nature of base pairing between complementary strands of DNA has been exploited in the formation of two- and three- dimensional nanostructures.[13] In these cases the DNA scaffold is functionalised with groups which can impart new electrical[14,15] magnetic,[3,16] or light transporting[17] properties, which are useful for the construction of nanowires. DNA based asymmetric catalysis exploits the chiral nature of the double helix to facilitate enantioselective reactions between small molecules.[18] Diagnostic applications require the conjugation of small molecules such as fluorescent dyes, *e.g.*

fluorescein,[19] affinity tags, *e.g.* biotin,[20] or other biomolecules, *e.g.* carbohydrates[21] or peptides.[22]

1.3.1 Solid phase oligonucleotide synthesis

1.3.1.i Introduction

Chemically prepared oligonucleotides can be obtained from solid phase synthesis. The methodology most commonly employed involves phosphoramidite coupling chemistry to build sequences of up to ~250 nucleotides in length,[23] and can be fully automated. In a typical procedure, the starting material is a commercially available nucleoside which has its 5'-OH group protected with a dimethoxytrityl (DMT) moiety, and is covalently linked to a resin, *e.g.* controlled-pore glass (CPG), by way of a linker attached at its 3'-hydroxy group. One common linker consists of a succinyl moiety conjugated by means of an amide bond to a long-chain amino alkyl (LCAA) group, which is itself bound to the CPG support. The key building blocks are nucleoside phosphoramidites, which are DMT protected at the 5'-position and bear a reactive phosphoramidite group at the 3'-position [figure 1.5 (a)].

With the exception of thymine, the heterocyclic base portion of each nucleoside is nucleophilic, and protection is necessary prior to oligonucleotide synthesis. The commercially available nucleoside phosphoramidites are available with protecting groups pre-installed. Adenine and cytosine are typically protected with an acetyl (Ac) or benzoyl (Bz) group, while dimethylformamidyl (dmf) or isobutyryl (*i*Bu) protected guanine is commonly used [figure 1.5 (b)]. The phosphorus (III) atom of the phorphoramidite group is also protected with a 2-cyanoethyl (CNE) group.

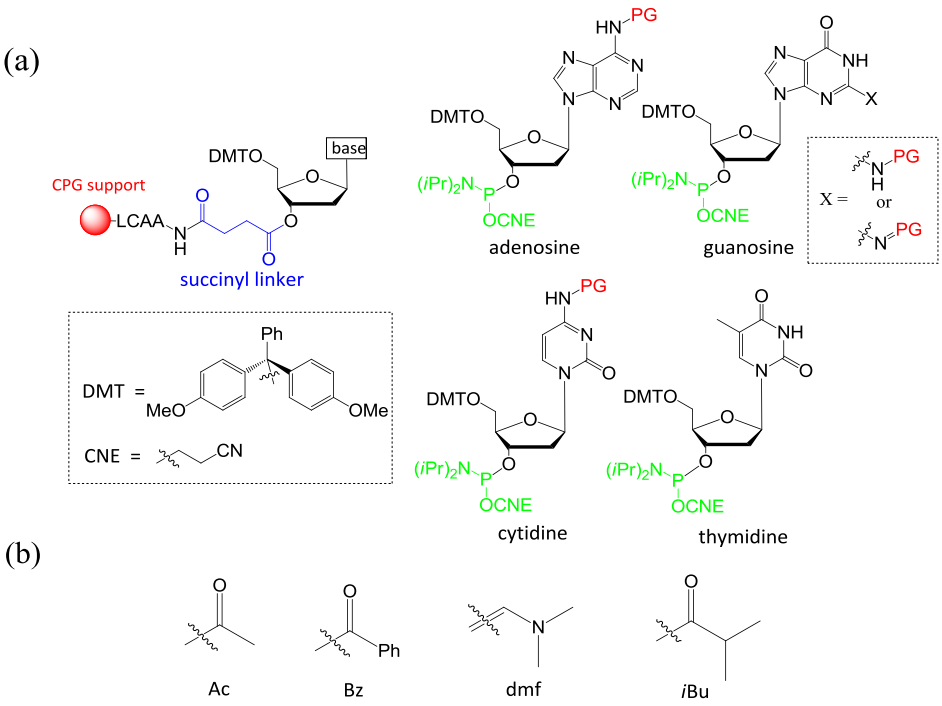

Figure 1.5. (a) General structure of a CPG-bound nucleoside and the structures of the four canonical deoxynucleoside phosphoramidites; (b) Common base protecting groups

Different resin pore sizes are available depending on the nature of the synthesis; 500 Å CPG is most suitable for the preparation of short (< 20 bases) sequences. Larger pore sizes of 1000 Å (20-80 bases) and 3000 Å (> 80 bases) can be used for larger scale syntheses. Many suppliers also offer different loadings of the nucleoside on the resin, these typically range from 15-100 µmol/g.

1.3.1.ii Synthetic cycle

Each cycle of oligonucleotide synthesis can be divided into four steps.

Step 1: Deblocking. The DMT protecting group is removed with a solution of acid (typically 2% trichloroacetic acid (TCA) in DCM). Immediately following exposure to the acid, an intense orange colour is observed as a result of the generation of the DMT cation. Many automated syntheses quantitatively detect the release of this chromophore at the beginning of each cycle to monitor the efficiency of coupling.

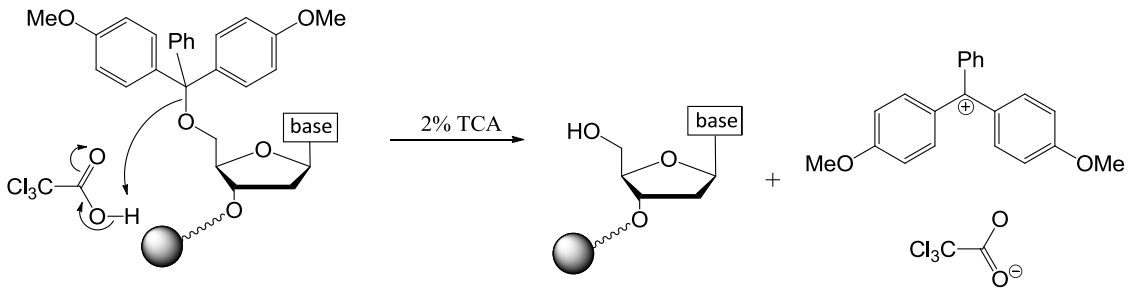

Scheme 1.2. First step of oligonucleotide synthesis – deblocking

Step 2: Coupling. The support-bound, 5'-deprotected nucleoside is exposed to a mixture of an acidic azole catalyst, *e.g.* 5-benzylmercapto-1*H*-tetrazole (BMT), and a solution of the second nucleoside bearing a phosphoramidite functionality at the 3'-position, which is in excess. The reaction solvent is anhydrous CH_3CN. Initial protonation of the isopropylamine group is followed by nucleophilic substitution with the BMT anion, thus activating the phosphoramidite moiety. Coupling then occurs between this activated phosphoramidite and the 5'-OH group of the CPG-nucleoside, forming a phosphite triester linker. Coupling is usually very rapid (~30 s), and once complete, all excess reagents are removed by washing.

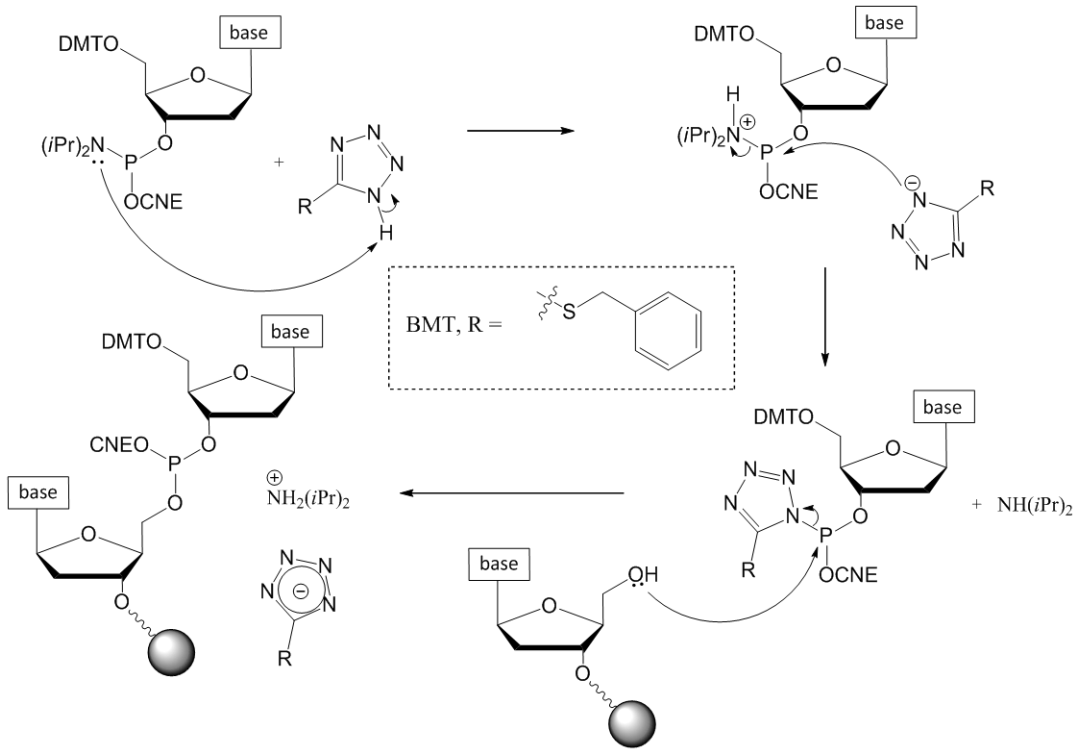

Scheme 1.3. Second step of oligonucleotide synthesis – coupling

Step 3: Capping. After each coupling step, a small amount (< 1%) of the resin-bound nucleoside/oligonucleotide may remain unreacted. The unreacted 5'-OH groups can potentially undergo further chain elongation in subsequent steps of the synthesis, leading to oligonucleotides with internal base deletions. Accumulation of these 'mutations' at each step can lead to a complex mixture of oligonucleotides. In order to avoid this, the free 5'-OH groups are capped after each coupling step. Capping involves exposure to a mixture of acetic anhydride and 1-methylimidazole. Acetylation of the OH group prevents further chain growth.

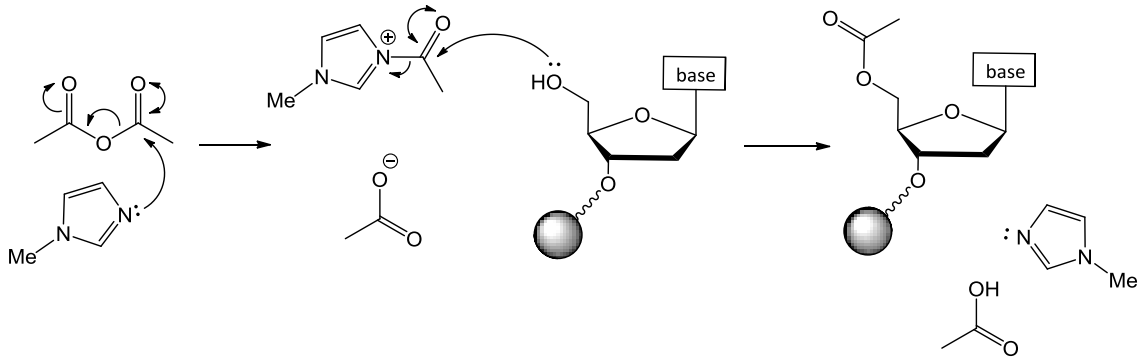

Scheme 1.4. Third step of oligonucleotide synthesis - capping

Step 4: Oxidation. The P(III) phosphite triester group formed during coupling is unstable under the acidic conditions necessary for the deblocking step which initiates the next synthetic cycle. To overcome this problem, iodine oxidation in the presence of H_2O and pyridine is conducted, leading to a P(V) species. The resulting phosphotriester retains the CNE protecting group to ensure no reactions occur at phosphorus during subsequent synthetic cycles.

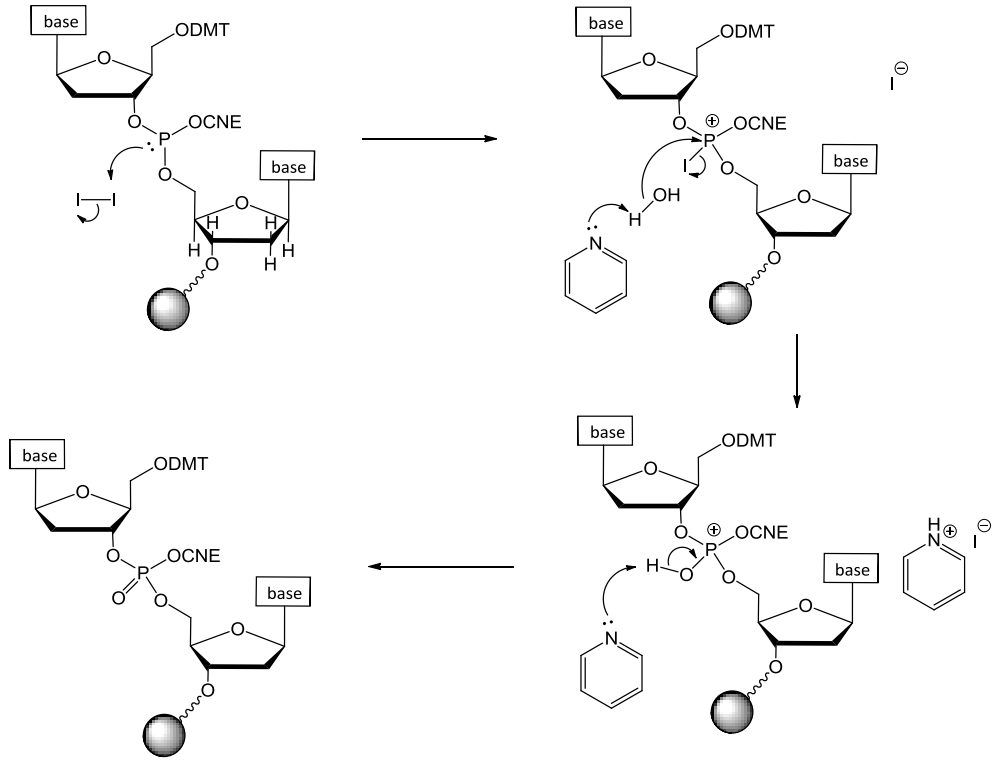

Scheme 1.5. Fourth step of oligonucleotide synthesis – oxidation

Upon completion of steps 1-4, the next cycle can begin by deblocking the 5'-O-DMT group of the previously coupled nucleoside.

1.3.1.iii Pre- and post-synthetic modifications

In addition to the canonical nucleosides functionalised with a phosphoramidite group, modified nucleosides bearing a label on either the sugar or the base portion can be incorporated into oligonucleotides in a similar manner.[24,25] Non-nucleosidic phosphoramidites can also be introduced in this way,[26] thus providing a means of incorporating quite different functionalities into the backbone of the sequence. The introduction of modified monomers into an oligonucleotide to yield a labelled sequence as the final product is known as pre-synthetic modification. A general representation of the pre-synthetic modification of an oligonucleotide sequence, involving preparation of a labelled nucleoside phosphoramidite by click chemistry (see section 1.4), is given in scheme 1.6. While the potential to fully automate site specific modification of oligonucleotides is appealing, there are many cases in which this

approach is compromised by poor coupling yield and/or extended coupling times for the introduction of the modified phosphoramidite(s). This can lead to problems downstream where oligonucleotide purification is required.

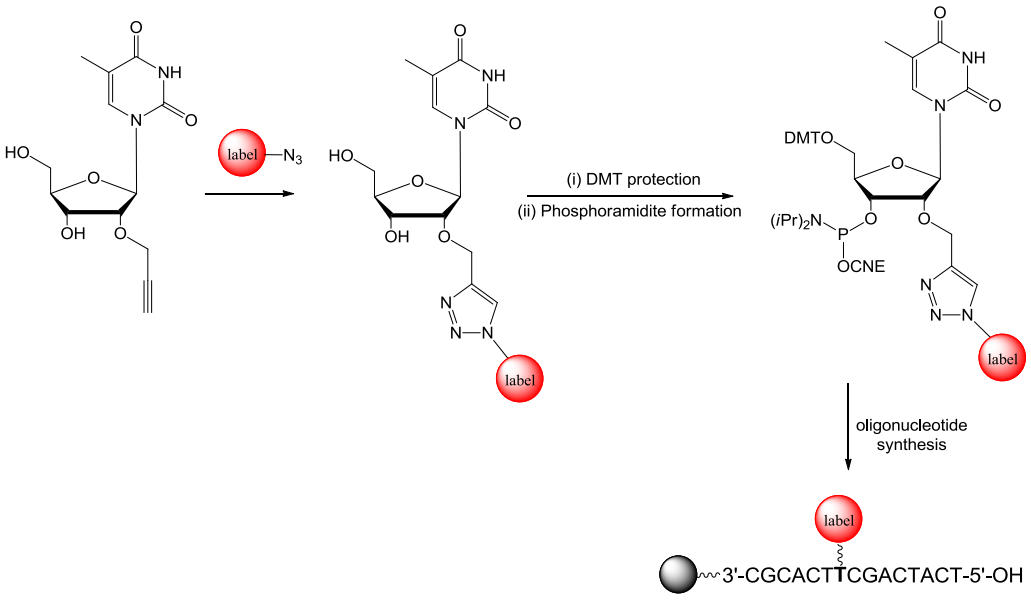

Scheme 1.6. Pre-synthetic modification of an oligonucleotide.

Post-synthetic modification of oligonucleotides adopts a similar approach to the pre-synthetic strategy; however, conjugation of the label of interest takes place after oligonucleotide synthesis is complete. Smaller, less disruptive modifications, *e.g.* alkynes,[27] are introduced into the sequence during automated synthesis; the small size of these groups means that coupling efficiency is not significantly reduced. The label of interest, bearing a complementary reactive group, *e.g.* an azide,[27] is conjugated to the functionalised oligonucleotide after the sequence has been assembled. A general representation of post-synthetic oligonucleotide modification is shown in scheme 1.7.

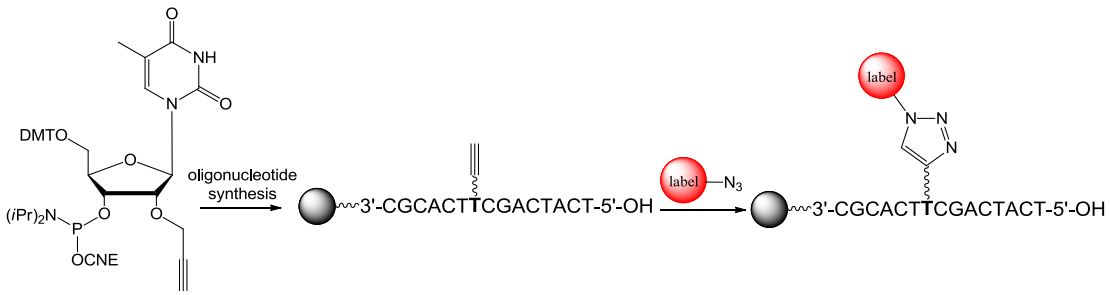

Scheme 1.7. Post-synthetic modification of an alkyne modified oligonucleotide

1.3.1.iv Cleavage and deprotection

Once the required oligonucleotide sequence has been prepared and the desired modifications have been introduced, cleavage from the solid support is necessary to obtain a solution of DNA/RNA for analysis or further application. Treatment with an aqueous solution of a base such as ammonium hydroxide or methylamine affords the cleaved oligonucleotide by hydrolysis of the ester linkage of the succinyl group (scheme 1.8).

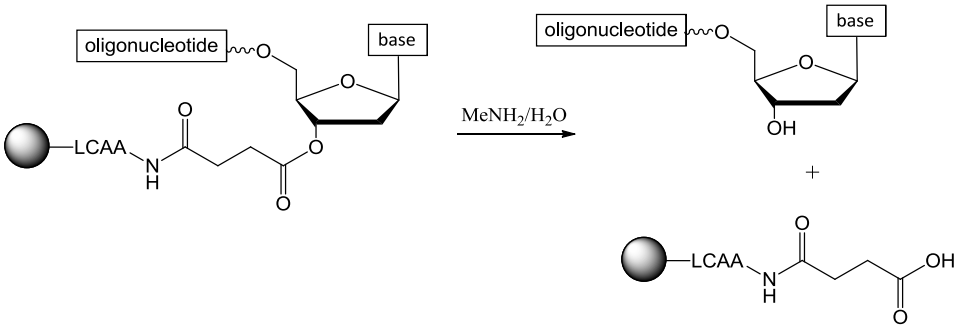

Scheme 1.8. Final step - oligonucleotide cleavage from the solid support

Base deprotection and removal of the CNE moiety used to protect the phosphate groups usually occurs in tandem with cleavage from the resin; the mechanism of removal of the CNE moiety is shown in scheme 1.9(a). A typical deprotection/cleavage procedure involves incubation in 40% aqueous $MeNH_2$ for 30 min at 65 ^{o}C. However, certain chemically modified oligonucleotides may be sensitive to these conditions. In such cases, use of more labile or 'ultramild' base protecting groups can facilitate milder deprotection following incubation in methanolic potassium carbonate at room temperature for 3 hr.[28] Popular examples of these ultramild protecting groups include phenoxyacetyl (Pac), isopropyl phenoxyacetyl (*i*Pr-Pac) and Ac groups for adenosine, guanosine and cytosine bases respectively [scheme 1.9 (b)].

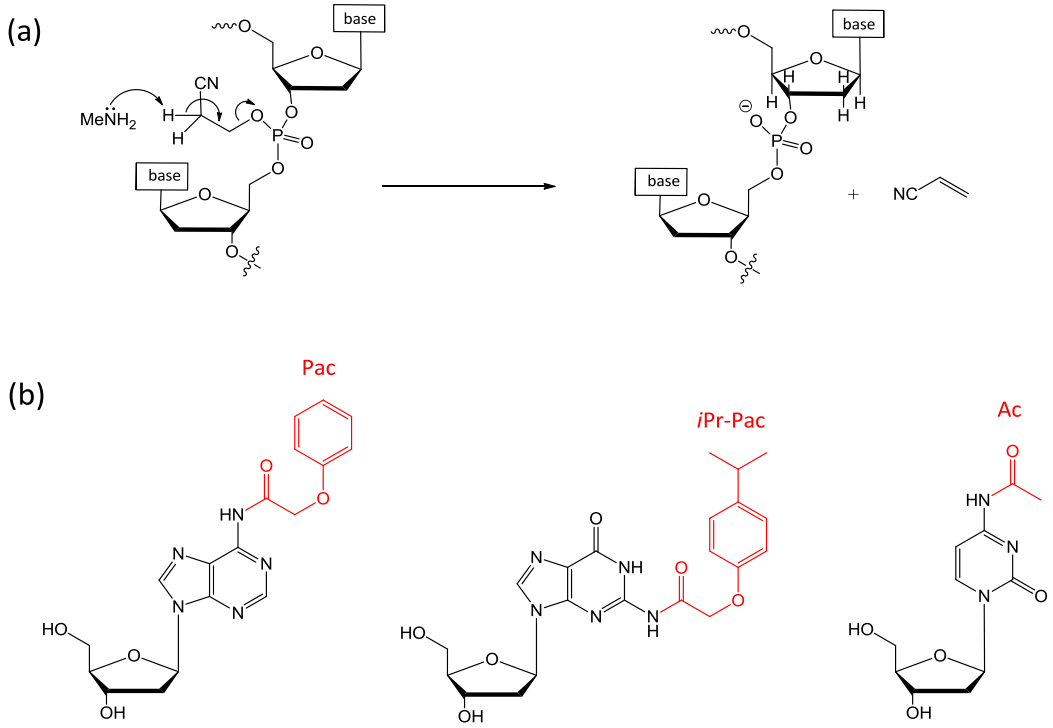

Scheme 1.9. (a) Deprotection of the phosphate group; (b) The 'ultramild' protecting groups Pac, *i*Pr-Pac and Ac

1.3.2 Enzymatic synthesis of modified nucleic acids

It is very difficult, or indeed impossible, to prepare densely functionalised sequences of DNA or RNA of > 50-60 nucleotides in length by the incorporation of modified phosphoramidites during chemical synthesis (see section 1.3.1.iii).[29] On the other hand, DNA and RNA polymerase enzymes have been shown to incorporate modifications into sequences up to 500 nucleotides in length.[30-33] A general approach to the preparation of long sequences of functionalised DNA is shown in scheme 1.10. In addition to a template sequence from which the strand to be synthesised is read, this technique requires a primer sequence from which to begin polymerisation. The length of the new, modified sequence is determined by the length of the template strand, which may be a gene segment,[30] or a synthetic sequence prepared by solid phase synthesis.[31] Nucleoside triphosphates (NTPs) are required as the monomeric building blocks; for modified NTPs, those which incorporate the modification at the 5-position of pyrimidines bases or at the 7-position of purine bases are found to be well

tolerated by DNA polymerases.[29] Although incorporation of modified NTPs bearing larger labels is frequently unpredictable, incorporation of smaller functional groups, *e.g.* azides, alkynes, is well tolerated.[34,35] Subsequent post-synthetic modification of these functionalised sequences can yield long sequences of densely labelled DNA.[27]

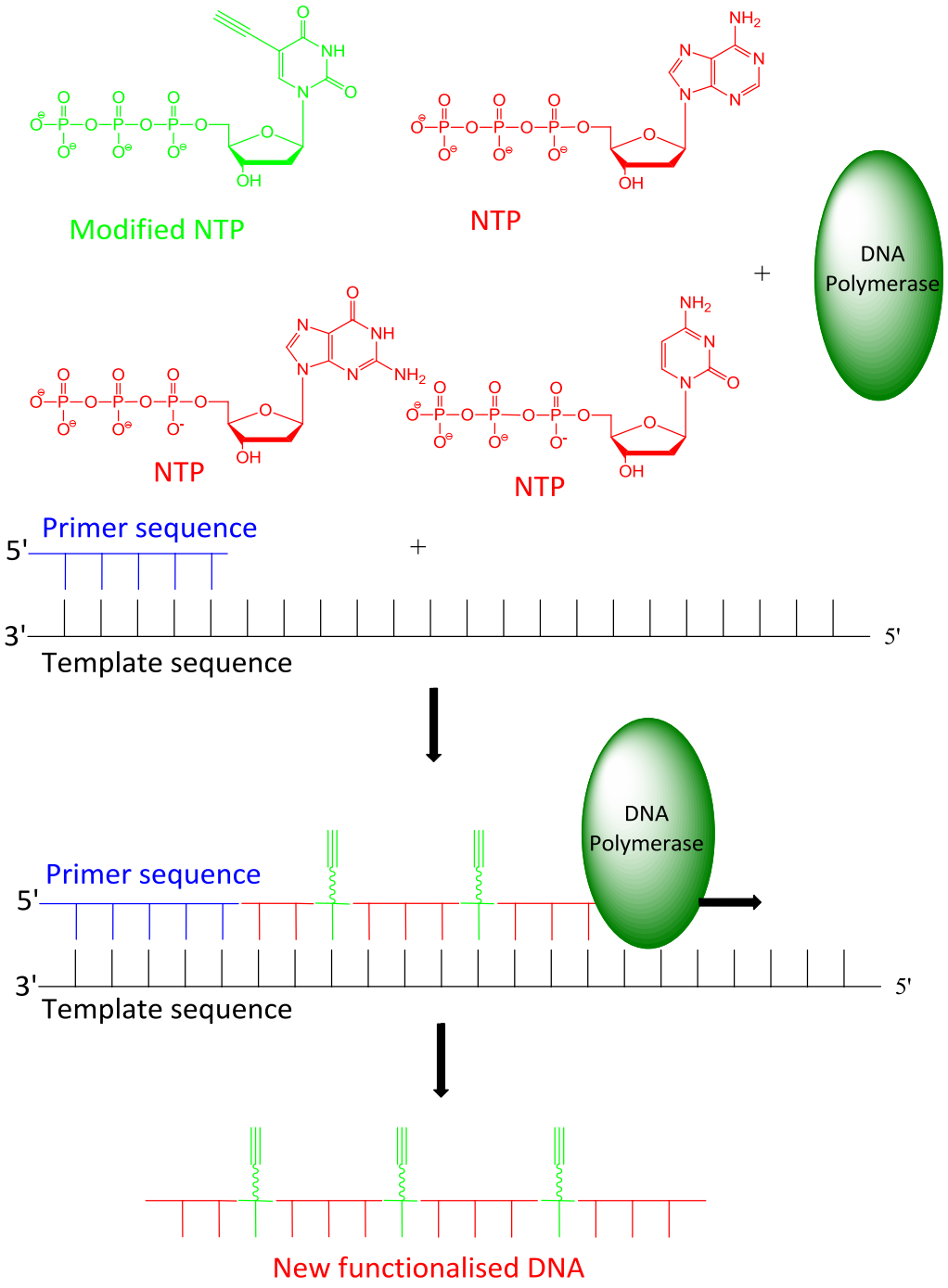

Scheme 1.10. Synthesis of modified DNA using a primer-template system and one modified NTP

1.3.3 Modified oligonucleotides by click chemistry

A range of chemical reactions have been exploited for the conjugation of different labels to nucleic acids. These include the Diels-Alder cycloaddition,[36] the Staudinger ligation[37] and and the Huisgen 1,3-dipolar cycloaddition.[38] These may be employed at the post-synthetic stage, or indeed for the preparation of modified nucleosides for use in pre-synthetic modification. Those reactions classified under the umbrella of 'click chemistry', a concept first outlined by Sharpless in 2001, have enormous potential for the modification of oligonucleotides, and will be discussed in more detail in the following sections.

1.4 Click chemistry

1.4.1 Introduction

The drive towards efficient, green syntheses has gathered significant momentum over the past decade. In addition to stricter environmental controls from regulatory bodies, pharmaceutical manufacturers also strive to lower the costs associated with the discovery, development and large scale production of drugs. Thus, any chemical philosophy which places an emphasis on efficient, environmentally friendly transformations has widespread appeal.

Since its inception by Sharpless in 2001,[39] the click chemistry ideology has attracted huge interest. Acknowledging that the ultimate goal of synthesis is not necessarily the production of compounds, but the production of properties, click chemistry focuses on the application of simple existing chemical strategies to the construction of complex structures by linking together small, modular building blocks. For a reaction to be considered a 'click' reaction, it must fulfil a set of criteria, many of which place an emphasis on green principles. These reactions must be wide in scope, modular, generate only inoffensive, easily removable by-products, and give reaction products in very high yields and with excellent control of stereoselectivity. Click reactions are further characterised by simple reaction conditions, benign solvent, or indeed no solvent at all, readily available starting materials and simple product isolation. Click

reactions should be thermodynamically favourable, and selective for the formation of a single product.

The most common click reactions result in the formation of carbon-heteroatom bonds. Reactions include substitution reactions, *e.g.* ring opening of strained heterocycles such as epoxides[40] and aziridines,[41] carbonyl chemistry of the non-aldol type such as formation of oximes ethers and hydrazones,[42] amides,[43] ureas[44] and thioureas,[45] and cycloadditions, in particular 1,3-dipolar cycloadditions.[46]

1.4.2 1,3-Dipolar cycloadditions

Also known as the Huisgen cycloaddition, the 1,3-dipolar cycloaddition is a classic reaction in organic chemisty, involving combination of a 1,3-dipole and a dipolarophile to form a variety of heterocycles (figure 1.6). The history of 1,3-dipoles dates back to the late 19th century, when Curtius discovered diazoacetic ester.[47] Shortly thereafter, the reaction of diazoacetic ester with *α,β*-unsaturated esters was described, demonstrating the first example of a 1,3-dipolar cycloaddition reaction.[48] The discovery of nitrones[49] and nitrile oxides[50] followed in the 1890s, and by the time the Diels-Alder reaction was discovered in 1928,[51] the synthetic value of cycloaddition chemistry was quite apparent. However, it was not perhaps until the 1960s, and Huisgen's systematic studies of the 1,3-dipolar cycloaddition,[52] that the true synthetic value of 1,3-dipoles became fully appreciated.

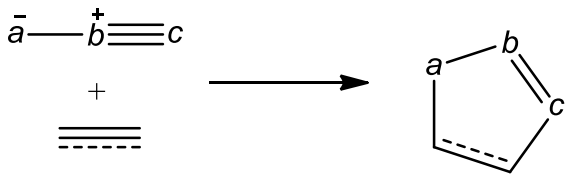

Figure 1.6. General representation of the 1,3-dipolar cycloaddition

1.4.2.i Types of dipoles and dipolarophiles

A large variety of dipoles and dipolarophiles exist, and consequently the scope for production of a range of heterocycles is huge. The most common dipolarophiles are alkenes and alkynes, but other molecules possessing multiple bonds beween carbon and heteroatom, or between two heteroatoms, such as nitriles and carbonyls, also fall into this category. A large number of 1,3-dipoles have been reported, but in practice only a small fraction of these have found widespread use. These can be divided into two different types: the allyl anion type and the propargyl/allenyl anion type. The non-linear allyl anion type have four π electrons spread between three parallel p_z orbitals, which are perpendicular to the plane at which the dipole is bent [figure 1.7 (a)]. Examples include nitrones, azomethine ylides, carbonyl ylides, carbonyl imines and nitro compounds. The linear propargyl/allenyl type have an extra π orbital orthogonal to the the allyl molecular orbital, which does not participate in cycloaddition [figure 1.7 (b)]. For the propargyl/allenyl family, the middle atom (*b*) is limited to nitrogen. Examples include nitrile oxides, azides and diazoalkanes.

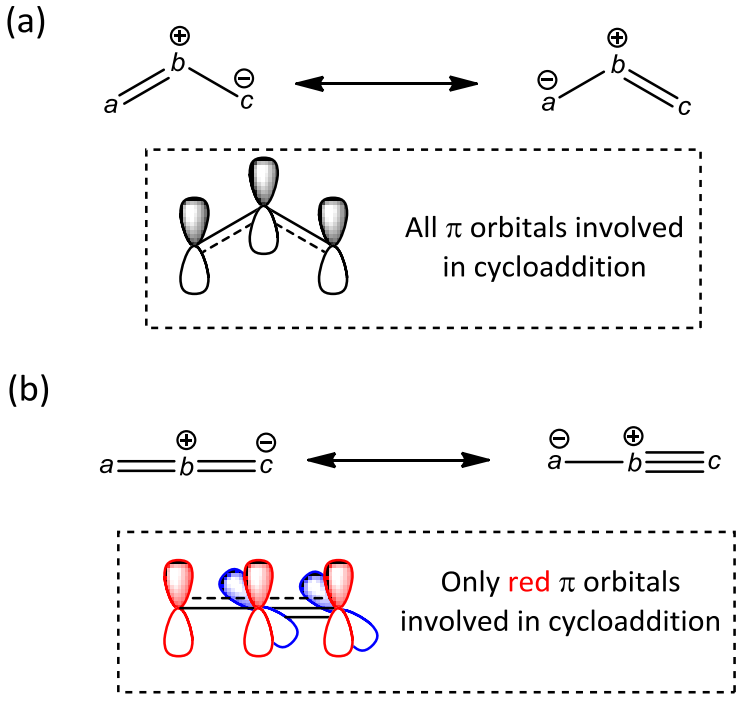

Figure 1.7. Resonance contributors and arrangement of π orbitals for (a) allyl anion type and (b) propargyl/allenyl anion type 1,3-dipoles

1.4.2.ii Frontier molecular orbital analysis of 1,3-dipolar cycloaddition

The regioselectivity and relative reactivity of 1,3-dipolar cycloadditions can be explained with reference to the relative energies of the frontier molecular orbitals (FMOs) of the reacting dipole and dipolarophile. The Sustman classification of 1,3-dipolar cycloadditions as type I, type II or type III depends on the dominant orbital interaction between dipole and dipolarophile FMOs.[53,54] In type I reactions, the dominant FMO interaction is that between the HOMO of the dipole ($HOMO_{dipole}$) and the LUMO of the dipolarophile ($LUMO_{dipolarophile}$); reactions involving electron-poor dipolarophiles usually fall into this category. In type II reactions, the similar energy gap between dipole and dipolarophile FMOs means that $HOMO_{dipole}$-$LUMO_{dipolarophile}$ and $HOMO_{dipolarophile}$-$LUMO_{dipole}$ interactions are both important. Type III reactions are dominated by the interaction of the $HOMO_{dipolarophile}$ with the $LUMO_{dipole}$; this is the most common interaction for reactions involving electron-rich dipolarophiles. These three types of interactions are represented in figure 1.8 below. For a given dipole, the rate of cycloaddition with a range of dipolarophiles is seen to increase as the energy gap between the reacting HOMO and LUMO decreases.[55]

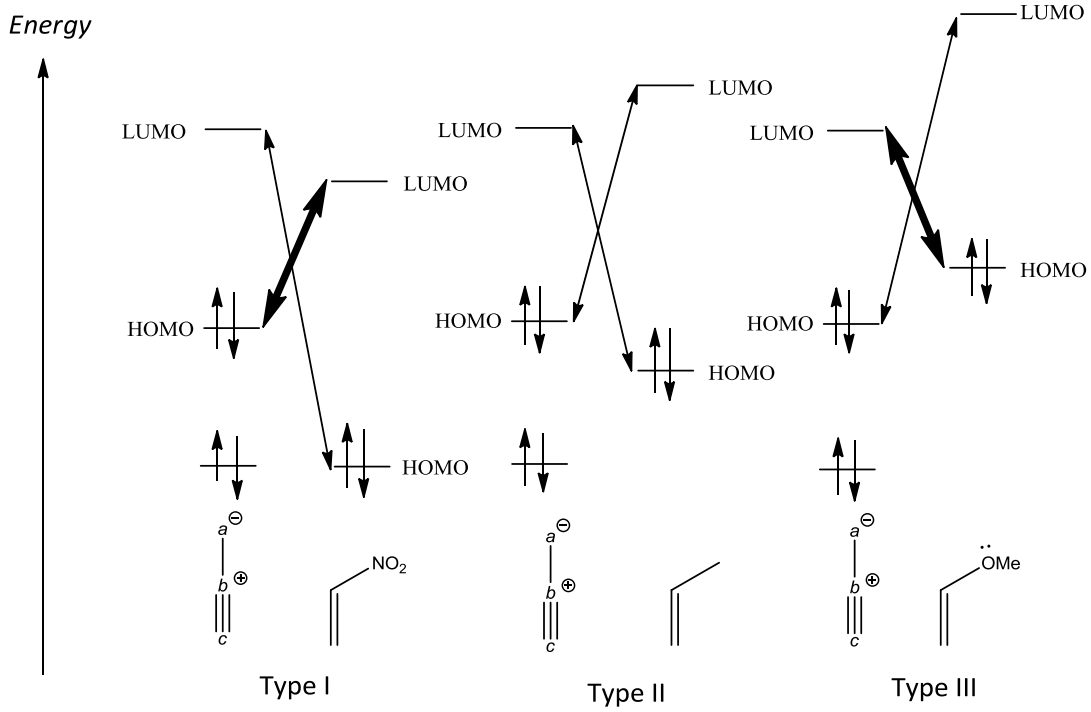

Figure 1.8. Frontier orbital interactions for 1,3-dipolar cycloaddition between a propargyl/allenyl type dipole and three differently substituted alkenes

In his book on the frontier orbital analysis of organic chemical reactions, Fleming presents an excellent discussion of the FMO considerations of 1,3-dipolar cycloadditions in relation to regioselectivity.[56] The experimentally observed regiochemical outcomes of a number of test case cycloadditions have been predicted by analysis of the interacting frontier orbitals. An interesting example is the reaction between azides and alkynes. Thermal cycloaddition affords nearly equal amounts of the 1,4- and 1,5-disubstituted triazole cycloadducts.[52] This is explained in terms of the relative energies and the coefficients of the frontier orbitals involved in figure 1.9. The coefficient of a particular atomic orbital is a measure of its contribution to the molecular orbital, or in other words the amount of electron density around the atom in question. In figure 1.9, the circles drawn around the atoms represent the relative sizes of the coefficients of each atomic orbital; the clear and darkened circles serve to identify the changes of sign in the wave-function. As can be seen from the relative energies of the dipole and dipolarophile FMOs, the transition states of azide-alkyne cycloadditions receive significant contributions from both $HOMO_{dipolarophile}$-$LUMO_{dipole}$ and $HOMO_{dipole}$-$LUMO_{dipolarophile}$ interactions. Each interaction will result in the molecular orbitals of the dipole and dipolarophile aligning in a distinct orientation in the transition state, with the coefficients matching (large with large, small with small). As each of these transitions states gives rise to a different regiosisomer, little regioselectivity is observed.

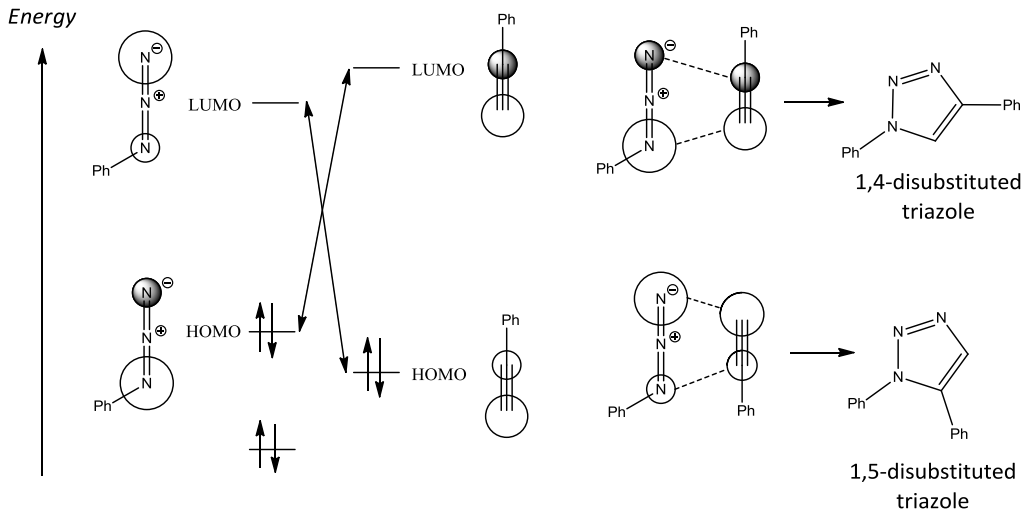

Figure 1.9. Frontier orbital model accounting for the lack of regioselectivity in the cycloaddition between phenyl azide and phenylacetylene

1.4.3 CuAAC

Often described as a 'near-perfect' chemical reaction, the copper-catalysed azide-alkyne cycloaddition (CuAAC) is synonymous with click chemistry. While the thermal version was first described over a century ago by Michael,[57] and later popularised by Huisgen,[52,58] the copper catalysed variant was first reported simultaneously and independently by the groups of Meldal and Sharpless in 2002.[59,60] Copper catalysts drastically change the mechanism and outcome of azide-alkyne cycloadditions, giving exclusively a 1,4-disubstituted triazole at room temperature in excellent yields. This is in stark contrast to the uncatalysed version, which requires prolonged heating and results in a mixture of 1,4- and 1,5-disubsituted triazolyl products with little or no regioselectivity. As discussed in section 1.4.2.ii, the poor regioselectivity is as a result of the similar energy gap between the HOMO-LUMO energy levels of the azide and the alkyne. CuAAC proceeds *via* a completely different mechanism to the 1,3-dipolar cycloaddition. The CuAAC reaction is also highly selective, which is important for conjugation between more complex molecules bearing diverse functionalities. Scheme 1.11 below shows a proposed catalytic cycle for the CuAAC reaction based on density functional theory (DFT) calculations.[61]

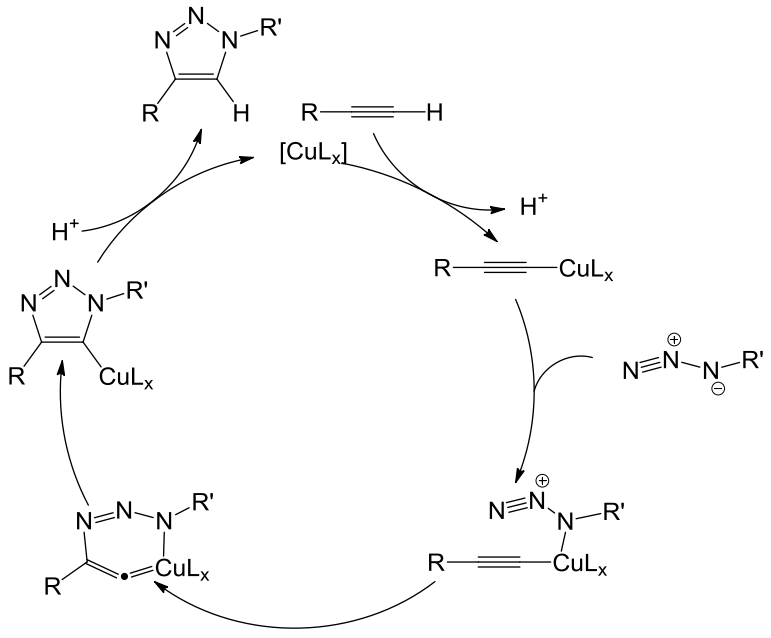

Scheme 1.11. Proposed mechanism of the CuAAC reaction based on DFT calculations.

The catalytic cycle is initiated by π coordination of the alkyne to Cu(I). This causes the alkyne proton to become more acidic, facilitating its removal by base. Subsequently, a σ-acetylide intermediate is formed. In the next step, the azide is activated by coordination to copper, which causes the azide's terminus to become more electrophilic. This is followed by the C-N bond forming event, resulting in a strained copper metallacycle. Subsequent formation of the copper triazolide intermediate is fast and energetically favourable. Finally, protonation of this species is followed by dissociation, giving the 1,4-disubstituted triazole and regenerating the catalyst ligand complex for more cycles.

Considering the numerous benefits described above, it is perhaps unsurprising that a diverse range of applications of this ligation strategy have been reported. The potential of CuAAC in the realm of drug discovery and biochemical studies has been the subject of a review by Kolb and Sharpless.[62] Other reviews have focused on polymer and materials science applications,[63,64] while the utility of CuAAC as a 'green' reaction has also received attention.[65] Exploitation of this reaction for bioconjugation represents a facile way to covalently link two large molecular entities, *e.g.* fusing two proteins together or attaching a peptide linker to a carbohydrate. In this regard, reviews covering the application of CuAAC to carbohydrate,[66] protein,[67] and DNA[68] conjugation have been reported.

1.5 Aims of thesis

The objective of this research was the conjugation of small molecules to DNA/RNA, which may impart upon these biopolymers desirable properties such as increased half-life, bioavailability, binding affinity, fluorescence *etc.* As mentioned in the preceding chapter, CuAAC has received much attention as a tool for chemical modification, yet application of other examples of the 1,3-dipolar cycloaddition to DNA conjugation have been somewhat neglected. In particular, the nitrile oxide-alkyne cycloaddition (NOAC) and strain-promoted azide-alkyne cycloaddtion (SPAAC) present viable, catalyst-free alternatives for the formation of functionalised nucleosides and oligonucleotides. The aim of this novel work was to explore both pre- and post-synthetic oligonucleotide

modification by exploitation of NOAC as well as SPAAC chemistry. Specific aims were as follows:

- Pre-synthetic modification of DNA employing modified phosphoramidite building blocks generated by NOAC (chapter 2).
- Post-synthetic functionalisation of DNA with an azobenzene photoswitch *via* NOAC and photochemical characterisation of the resulting conjugates (chapter 3).
- Post-synthetic labelling of a range of DNA and RNA sequences by solid-phase SPAAC, employing a simple monocyclic cyclooctyne as the dipolarophile.

Chapter 2

Nitrile oxide-alkyne cycloadditions 1: Pre-synthetic modification of DNA by NOAC

2.1 Introduction

2.1.1 Nitrile oxides

The chemistry of nitrile oxides is well documented in several important reviews and monographs.[69,70] The parent compound, fulminic acid, has been known for over two centuries, and many derivatives of this dipole have been prepared. The most common applications of nitrile oxides involve the formation of Δ^2-isoxazolines and isoxazoles, which result from their cycloaddition with alkenes and alkynes, respectively [scheme 2.1 (b)]. These reactions are thermodynamically favoured and do not generally require a catalyst. Most nitrile oxides are unstable, some are even explosive. Many small nitrile oxides dimerise to stable five-membered furoxans [scheme 2.1 (c)] upon storage either neat or in solution at such a high rate as to render them non-isolable. As a result, they are usually prepared *in situ* in the presence of a dipolarophile, which traps the nitrile oxide to form the heterocycle before the competing dimerisation can occur.

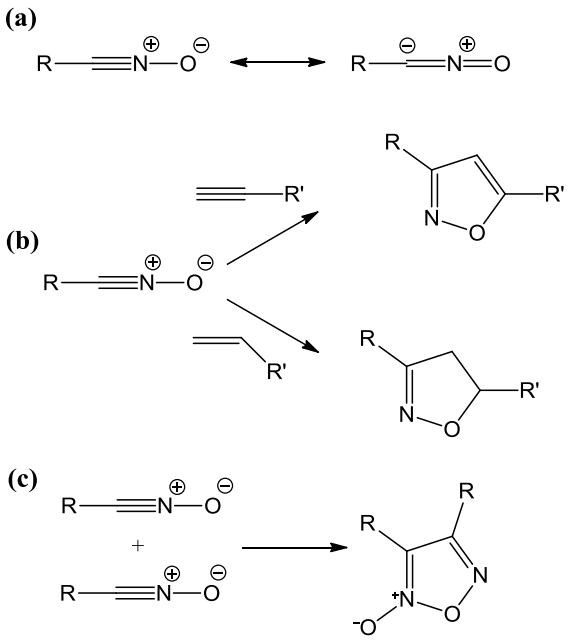

Scheme 2.1. (a) Main resonance contributors of the nitrile oxide dipole; (b) Reaction of nitrile oxides with monosubstituted alkynes and alkenes to form isoxazoles and isoxazolines, respectively; (c) Dimerisation of nitrile oxides to form furoxans

2.1.2 Generation of nitrile oxides

Generally speaking, nitrile oxides (**1**) are unstable, and as such are usually prepared *in situ* and used immediately. Suitable starting materials include oximes (**2**) which are prepared from the parent aldehyde (**3**).[71-73] From the oxime, a number of choices are available for generation of the dipole. Hydroximoyl halides (**4**) can be obtained by halogenation of the respective oximes,[74-76] and their subsequent base induced dehydrohalogenation is a common approach to *in situ* nitrile oxide formation.[77-79] The dehydration of nitroalkanes (**5**) with an aryl isocyanate, usually in the presence of triethylamine as a base, is another possible route; this is known as the Mukaiyama procedure.[80] The precursor nitroalkanes can be obtained *via* oxidation of the corresponding oxime[81] or *via* nucleophilic substitution of the parent haloalkane (**6**).[82] A less common approach involves the thermolysis of furoxans (**7**), which relies on extremely high temperatures.[83] Stable furoxans may however be convenient starting materials for the generation of short-lived nitrile oxides. These various strategies for the preparation of nitrile oxides are represented in scheme 2.2.

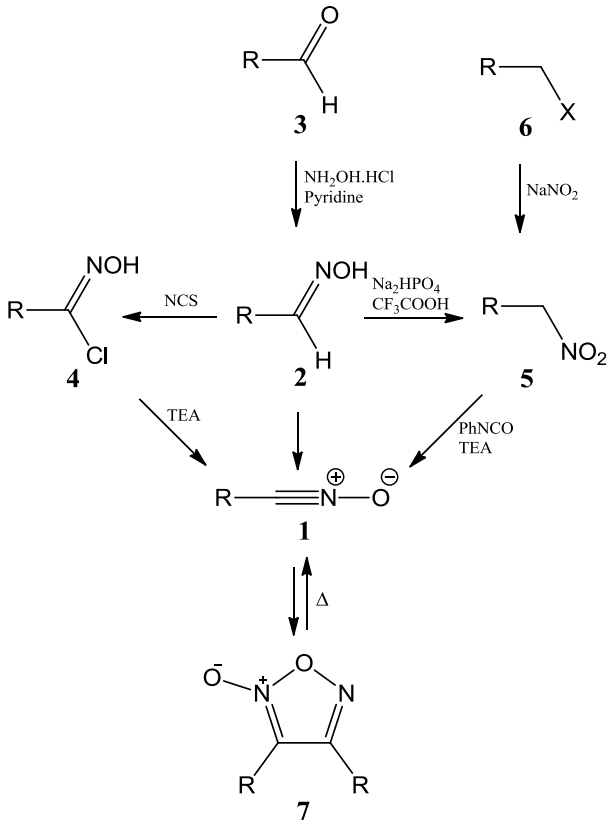

Scheme 2.2. The various routes available for the preparation of nitrile oxides

If a hydroximoyl halide is used as a nitrile oxide precursor, a one-pot synthesis starting from the parent oxime is the most common approach. A variety of halogenating agents such as *tert*-butyl hypochlorite, *N*-chlorosuccinimide (NCS) and *N*-bromosuccinimide (NBS) are available for generation of hydroximoyl halides, and *in situ* dehydrohalogenation in the presence of a base such as pyridine yields the nitrile oxide.

The halogenating agent selected by this author is chloramine-T (Ch-T) (**8**). The exact mechanism of dipole generation has been debated. Hassner and Rai proposed initial chlorination of the oxime followed by base-catalysed elimination of hydrogen chloride to give the nitrile oxide.[84] A more likely scenario, perhaps, is the mechanism proposed by Padmavathi *et al.* (scheme 2.3).[85] This involves initial deprotonation of the oxime OH proton, followed by nucleophilic substitution and finally elimination of a stoichiometric amount of tosyl amine to yield the nitrile oxide.

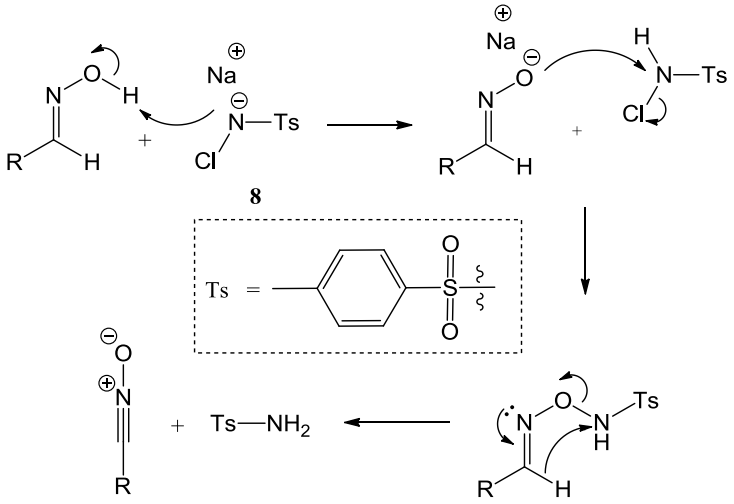

Scheme 2.3. Proposed mechanism of nitrile oxide formation by Ch-T[85]

2.1.3 1,3-Dipolar cycloaddition of nitrile oxides

Many aspects of the 1,3-dipolar cycloaddition have already been discussed in section 1.4.2. As highlighted therein, the application of FMO theory has had a formidable impact in helping to explain experimental results. FMO considerations of transition states resulting from the cycloaddition of nitrile oxides to alkenes and alkynes lead to

their classification as type II/borderline type III 1,3-dipolar cycloadditions,[46] *i.e.* the interaction of the $HOMO_{dipolarophile}$ with the $LUMO_{dipole}$ is slightly dominant, although the $LUMO_{dipolarophile}$/$HOMO_{dipole}$ interaction is also important. As such, both electron-withdrawing and electron-donating groups have been shown to increase the reactivity of the dipolarophile towards nitrile oxides. However, other factors such as the steric contributions of any substituents present also need to be considered to offer a more accurate explanation of observed reactivity.

Cycloaddition reactions of nitrile oxides with substituted alkenes/alkynes can theoretically lead to 3,5- and 3,4-disubstituted isoxazolines/isoxazoles [scheme 2.4 (a)]. In most cases the 3,5-disubstituted product is formed with high regioselectivity; this experimental observation is supported by *ab initio* and FMO calculations.[86,87] The nature of the substituents on the dipole has little or no influence on the regioselectivity when terminal alkenes/alkynes are used, although in some cases substitution of the dipolarophile can have an effect. In one example, β-cyclodextrin is tethered to the dipolarophile, and the host-guest interaction between aryl nitrile oxides and the cyclodextrin moiety is exploited to control the relative orientation of the dipole and dipolarophile, resulting in reversal of the usual regiochemistry [scheme 2.4 (b)].[88] It is more difficult to predict the regiochemical outcome using disubstituted dipolarophiles; in these cases the product ratio is seen to depend largely on the substitutents present on the alkene/alkyne.

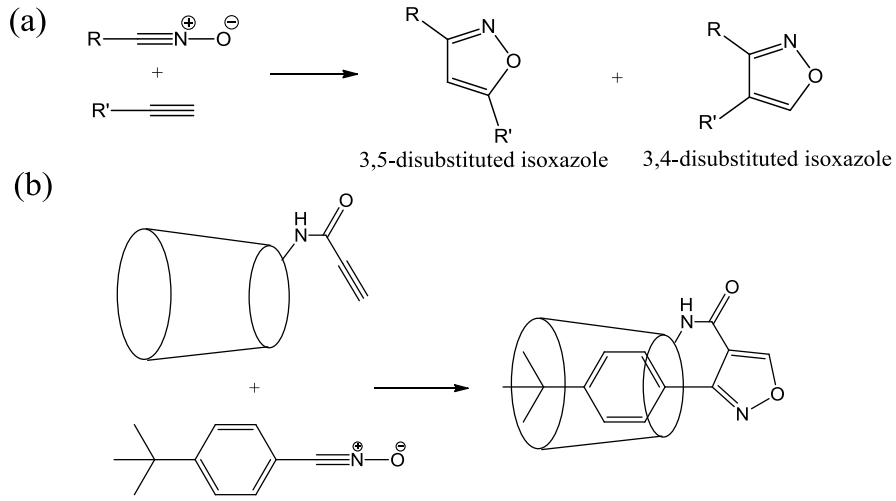

Scheme 2.4. (a) Nitrile oxide-alkyne cycloaddition resulting in formation of regioisomeric products; (b) Example of selective generation of a 3,4-disubstituted isoxazole[88]

The bulk of the literature describing the 1,3-dipolar cycloaddition of nitrile oxides concerns their reaction with alkenes to form isoxazolines. These reactions are highly regioselective, and huge scope exists for the synthesis of substituted heterocyclic products by synthetic manipulation of the dipole and dipolarophile. In addition, the isoxazoline heterocycle formed can serve as a synthon for other functional groups such as 3-hydroxycarbonyls and 3-amino alcohols.[89] The isoxazoline ring also has value in its own right. It exhibits significant pharmacological activity, and examples of isoxazoline containing compounds displaying anti-microbial,[90] anti-nociceptive[90,91] and anti-stress[92] activity have been reported.

In spite of the many benefits it shares with the alkene version, the nitrile oxide alkyne cycloaddition (NOAC) has received much less attention. Many isoxazole containing compounds display interesting biological activity, and their pharmacological properties include anti-inflammatory,[93] analgesic[94] and HIV inhibitory activity.[95] The relatively weak N-O bond of the heterocycle represents a potential site for cleavage, particularly under basic or reductive conditions. Ring cleavage can be used as a route to bifunctional compounds such as 1,3-dicarbonyls,[96] 3-hydroxycarbonyls[97] and enaminoketones.[98] One attractive feature of the NOAC is its high regioselectivity; it tends to yield 3,5-disubstituted isoxazoles almost exclusively.[38,99,100] In addition, NOAC forms planar heterocyclic products with no issues of diastereoselctivity to contend with.

2.1.4 Nucleic acid labelling by nitrile oxide cycloadditions

Huisgen 1,3-dipolar cycloaddition is known to be an effective approach for the modification of nucleic acids; in particular the CuAAC reaction has received much attention.[68] However, exposure to Cu(I) can lead to oxidative cleavage of DNA/RNA, and the cytotoxic effects of copper-contaminated oligonucleotide products remain an issue for biological applications. Copper-free methodologies can avoid these problems, and examples such as nitrone[101] and nitrile oxide[38] cycloadditions have been effectively employed in the preparation of modified nucleic acids. Our group has

demonstrated metal-free, regiospecific labelling of both DNA and RNA by NOAC, while others have reported similar findings employing alkenes as the dipolarophile. [27, 38]

In one example, Carell and co-workers synthesised a styrene modified nucleoside phosphoramidite, which was readily incorporated into a series of oligonucleotide sequences. These styrene-functionalised oligonucleotides then underwent efficient, regioselective reaction with a range of nitrile oxides, furnishing exclusively the 3,5-disubstituted isoxazoline products.[27] Our group employed an alternative strategy, in which the non-nucleosidic phosphoramidite **9** was prepared and used to introduce a terminal alkyne to the 5'- terminus of a resin-bound DNA sequence. 1,3-dipolar cycloaddition was then carried out between the alkyne-functionalised oligonucleotide and benzonitrile oxide on the solid phase, leading to regioselective formation of 3,5-disubstituted isoxazole-DNA conjugates (scheme 2.5).[38]

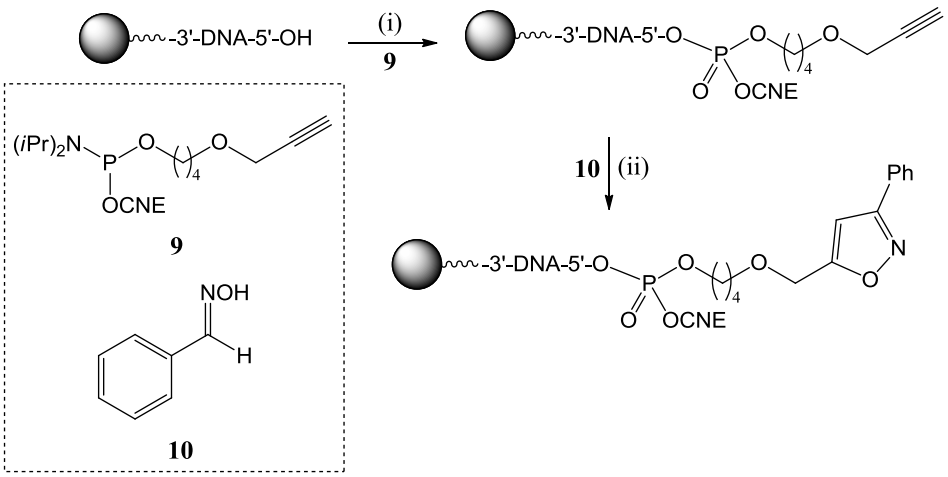

(i) BMT, CH_3CN, rt, 30 min, then I_2 (0.1 M) THF-pyridine-H_2O

(ii) Ch-T, aq. $NaHCO_3$ (4%), EtOH, rt, 30 min

Scheme 2.5. DNA conjugation by NOAC on the solid phase[38]

We were interested in developing an alternative to this post-synthetic approach to oligonucleotide modification. In this chapter, a pre-synthetic strategy is outlined, wherein modified phosphoramidite monomers generated by NOAC are employed to deliver modifications to DNA. This method, in which the NOAC reaction takes place off-resin, may represent a welcome alternative for large scale applications, or in cases where the oligonucleotide may carry additional functionalities sensitive to the conditions of the 'click' reaction.

2.2 Results and Discussion

2.2.1 Pre-synthetic oligonucletide modification involving NOAC

The desired strategy for oligonucleotide conjugation is contrasted with the standard post-synthetic cycloaddition approach in scheme 2.6. The 1,3-dipolar cycloaddition is potentially a powerful synthetic method, and careful selection of the dipole and dipolarophile components can afford heterocyclic products displaying a range of chemical properties. It is our hypothesis that if either the dipole or the dipolarophile bears a pendant hydroxy group that cycloaddition, followed by generation of the corresponding phosphoramidite, can yield a versatile building block which can facilitate convenient, catalyst-free oligonucleotide conjugation. This off-resin approach would certainly increase the versatility of click chemistry as it applies to oligonucleotide conjugation, and provide an alternative to more commonly used approaches such as solid phase oximation and CuAAC. There is large scope for the introduction of many different labels to DNA/RNA in this manner, potentially yielding nucleic acids tagged with a variety of reporting or targeting probes.

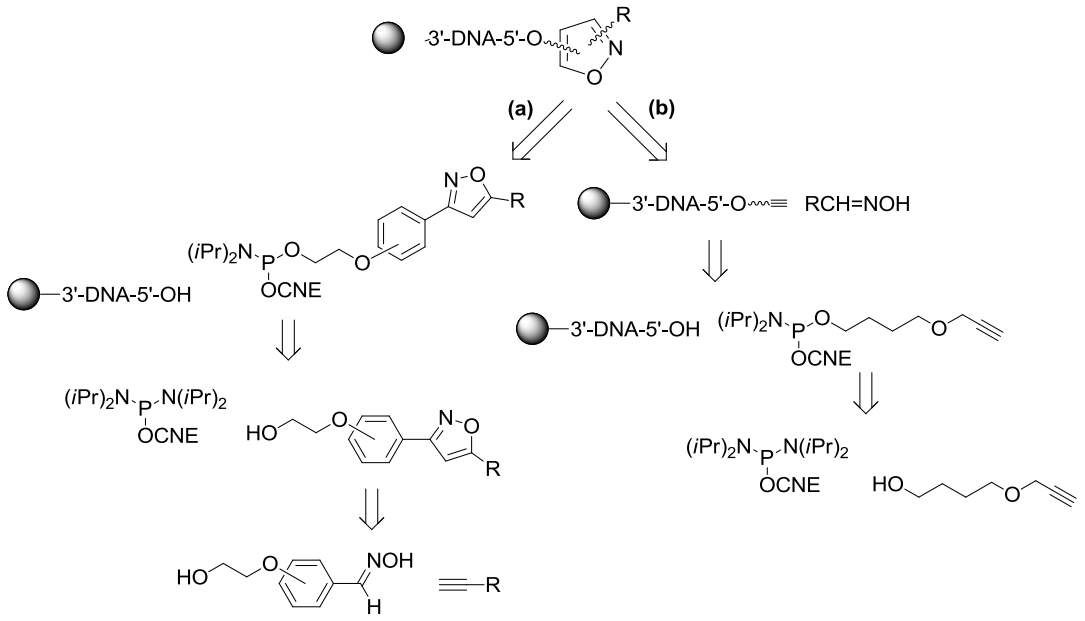

Scheme 2.6. Retrosynthetic (a) pre- and (b) post-synthetic approaches to chemically modified oligonucleotides

Applications which utilise products of the CuAAC reaction as key building blocks in the construction of modified nucleic acids have been reported. In one example, trivalent glycoclusters, themselves generated by CuAAC, have been conjugated to aminooxy terminated DNA by way of solid-supported oximation.[102] Other examples have employed phopshoramidite derivatives of click chemistry derived triazole monomers. The triazole moiety is most frequently borne at the C-5 position of pyrimidine bases including deoxyuridines,[103-105] cytidines,[24] and thymidines.[106] Location of the triazole component at the 5'-position of the sugar[25] and as a spacer between the base and sugar moieties[107] has also been demonstrated. Finally, non-canonical[108] and non-nucleosidic[26] triazole phosphoramidites have been described. It is perhaps surprising that, whilst isoxazoles are an interesting heterocyclic family with diverse applications, isoxazole bearing phosphoramidites are not well known. To the best of our knowledge, the D-threoninol derivative **11** (figure 2.1) prepared for inclusion in a library of cyclic oligonucleotides targeted to Hepatitis C virus NS5B, represents the only known example.[109]

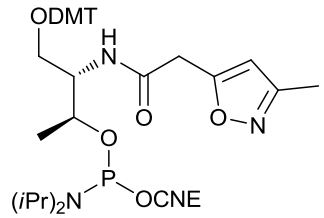

11

Figure 2.1. Isoxazole phosphoramidite **11**[17]

2.2.2 Synthesis of phosphoramidite monomers

Scheme 2.6 highlights the requirement of the pre-synthetic approach (route a) for isoxazole cycloadducts bearing a pendant hydroxy moiety which serves as the site of introduction for phosphoramidite groups. To this end, the isomeric hydroxyethoxybenzaldehyde oximes **13a-c** were selected as nitrile oxide precursors for the NOAC reaction. These were conveniently prepared from the commercially available aldehydes **12a-c**, and were obtained in excellent yield (86-96%) following

reaction with hydroxylamine hydrochloride in the presence of sodium acetate. In each case, complete conversion of the aldehyde to the desired oxime was confirmed by ^{1}H NMR spectral data. As a representative example, the ^{1}H NMR spectra of the *para*-disubstituted compounds **12c** and **13c** are shown (figure 2.2), highlighting loss of the resonance at 9.90 ppm representing the aldehyde proton and appearance of a new signal at 8.08 ppm characteristic of the imino proton of the oxime functional group. A small upfield shift of the doublet resonances representing the two pairs of equivalent aromatic protons is also observed.

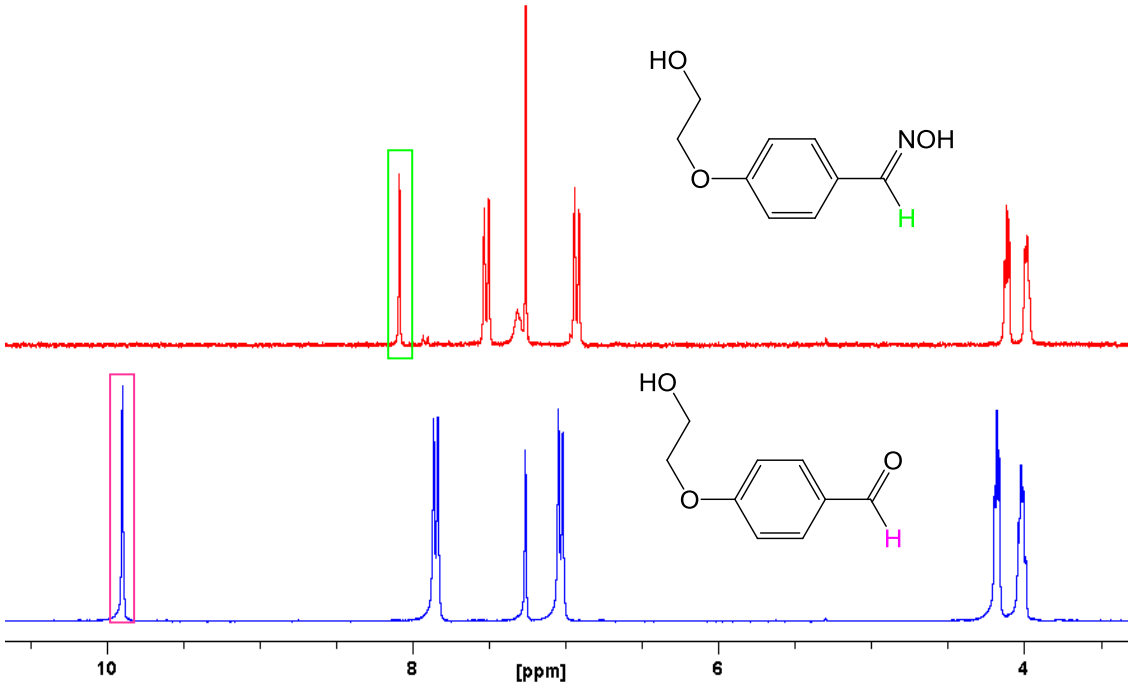

Figure 2.2. ^{1}H NMR spectra of *para*-disubstiuted hydroxyaldehyde **12c** (blue) and corresponding oxime **13c** (red)

The reaction of the oximes **13a-c** with Ch-T in aqueous ethanol afforded the corresponding nitrile oxides (**18a-c**), which were trapped *in situ* with propargyl phenyl ether (**14**) yielding the cycloaddition products **15a-c** (scheme 2.7). These isoxazole cycloadducts were obtained in 81-85% isolated yield following stirring of the reaction mixture for 18 hr at room temperature. Purification of the crude products was achieved by flash column chromatography.

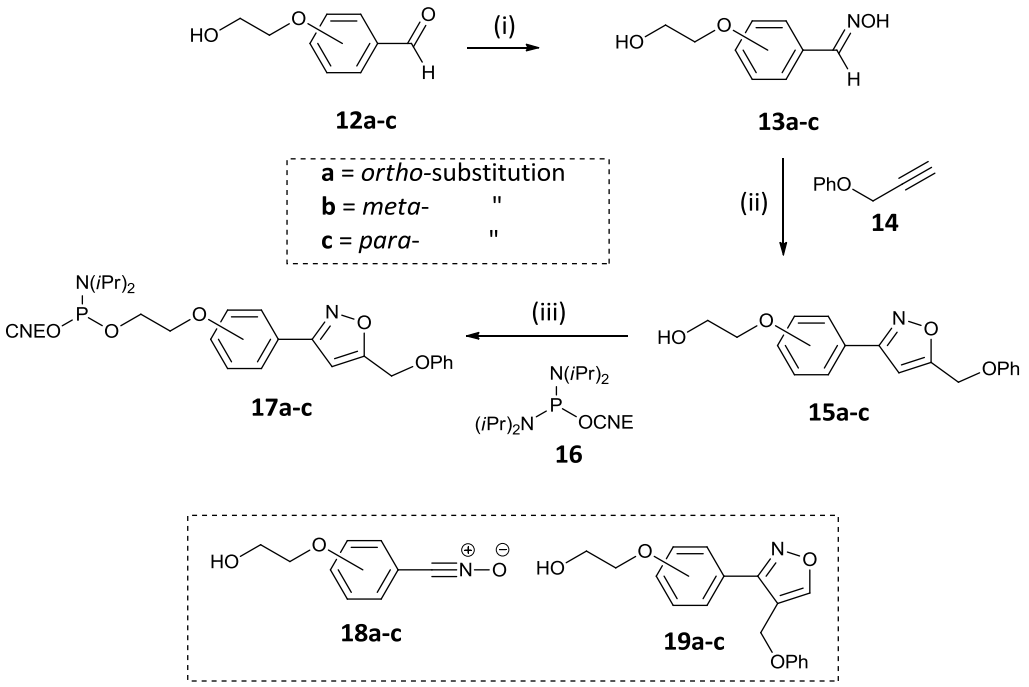

(i) $NH_2OH.HCl$, NaOAc, $EtOH/H_2O$, reflux, 1 hr

(ii) Ch-T, $EtOH/H_2O$, rt, 18 hr

(iii) BMT, CH_3CN, rt, 30 min

Scheme 2.7. Synthesis of the phosphoramidite monomers **17**

Each cycloaddition reaction displayed highly regioselective formation of the 3,5-disubstituted isoxazole cycloadduct. In each case, assignment of the regiochemistry of the product followed from analysis of the ^{1}H NMR spectral data. A singlet resonance in the range of 6.59-6.76 ppm was observed, which was deemed characteristic of a H-4 isoxazole ring proton; a H-5 proton resulting from 3,4-substitution would resonante in the region of 7.5-8.5 ppm.[110-112] Indeed, close examination of the ^{1}H NMR spectra of the crude cycloadducts revealed low intensity signals at ~8.5 ppm – evidence of the formation of small amounts of the 3,4-disubstituted isoxazole. In addition, a minor signal at ~4.9 ppm is observed in these spectra, which is deemed to represent the methylene protons adjacent to the 3,4-disubstituted isoxazole ring. In the case of the cycloadducts **15a** and **19a**, the two regioisomeric products could not be separated by chromatographic methods. The ^{1}H NMR spectrum of **15a** is shown (figure 2.3); in this case the relative integration of the signals corresponding to the regioisomeric adducts is ~1:21 in favour of the 3,5-disubstituted isoxazole.

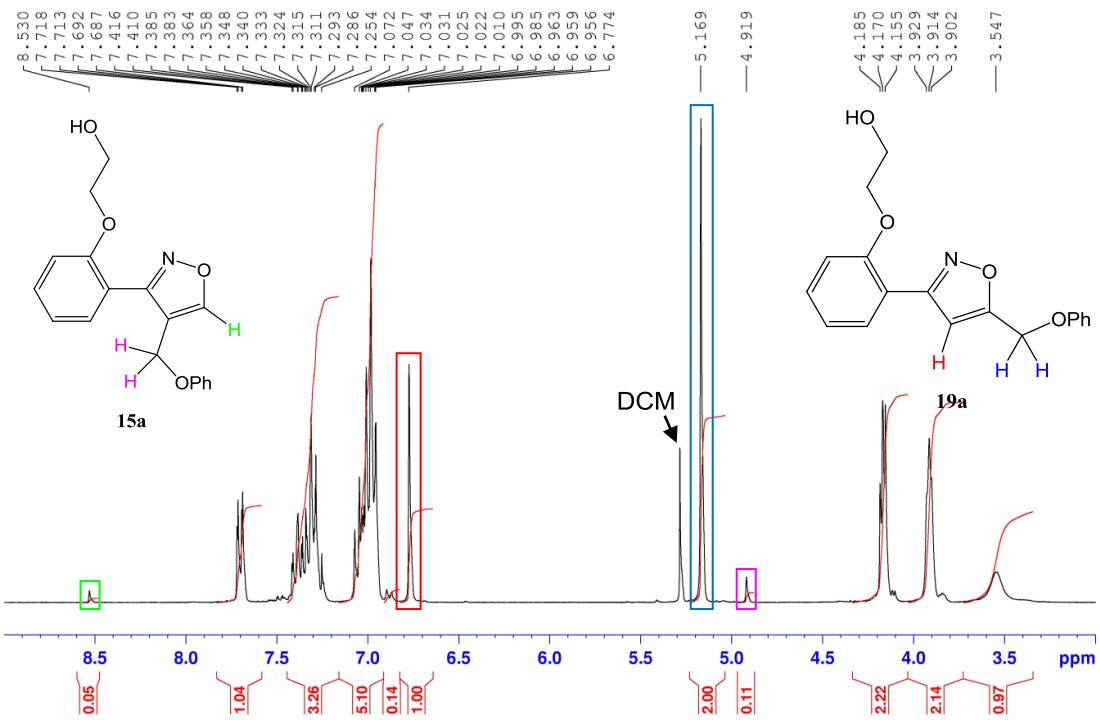

Figure 2.3. ^{1}H NMR spectrum of **15a**, highlighting minor amounts of **19a**

The phophoramidites **17a-c** were obtained in reasonable yield following coupling of the isoxazole cycloadducts **15a-c** with 2-cyanoethyl-*N,N,N'N'*-tetraisopropylphosphorodiamidite (**16**) in the presence of BMT as activator (scheme 2.8). After 30 min stirring of the reaction mixture at rt in anhydrous acetonitrile, complete consumption of the starting alcohol was confirmed by TLC analysis. An equimolar amount of BMT and the starting materials **15** and **16** were used to prevent formation of a *bis*-substituted P(III) byproduct. Generation of **17a-c** was supported by ^{31}P NMR spectroscopy; the spectra of the crude products each displayed a resonance in the region of ~148-149 ppm which is characteristic of phosphorus (III). Typically the ^{31}P NMR spectra of the crude samples displayed additional resonances in the region of ~10-20 ppm. Presumably these signals represent P(V) oxidation by-products, which are difficult to avoid given the air sensitive nature of the phosphoramidites.

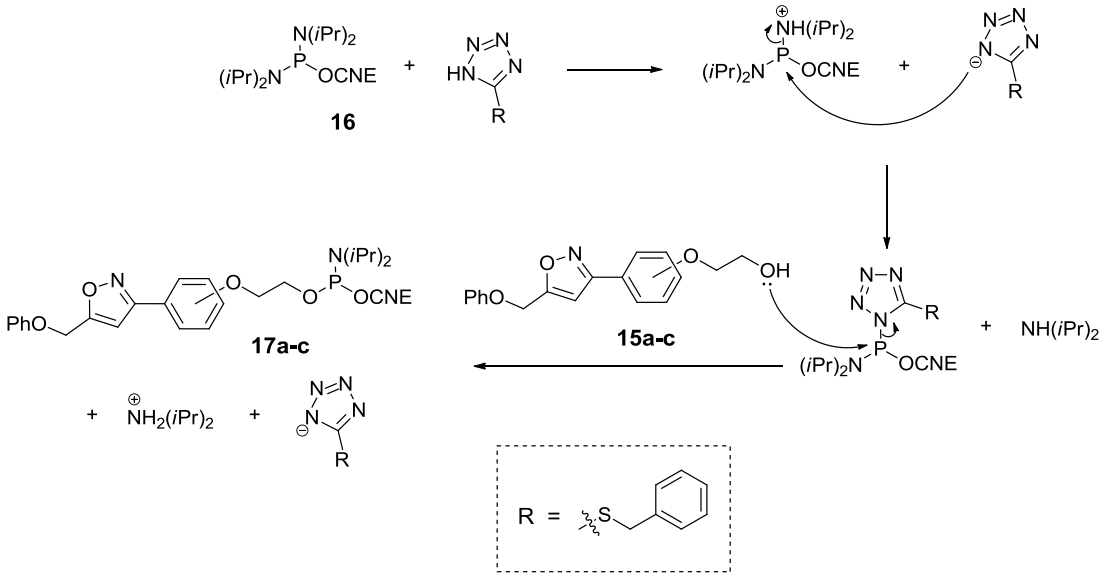

Scheme 2.8. Mechanism of formation of the isoxazole-phosphoramidites **17a-c**

Although **17a-c** were found to be suitable for solid phase coupling without purification, pure samples were required for characterisation purposes; therefore removal of the P(V) impurities was necessary. Purification of phosphoramidites *via* flash column chromatography can be tricky, as the weakly acidic nature of the silica stationary phase can be detrimental to these labile compounds. We found that neutralisation of the silica with 1% triethylamine (TEA) prior to column loading and elution under an atmosphere of nitrogen was sufficient for purification of the crude products without a significant sacrifice in yield. ^{31}P NMR spectral data for **17c** is shown before and after purification (figure 2.4).

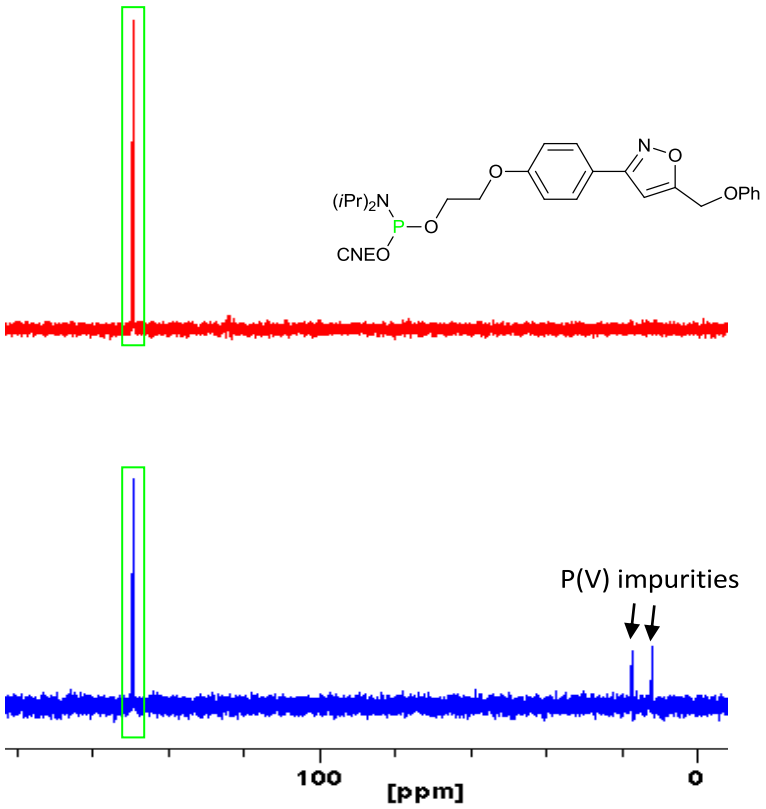

Figure 2.4. ^{31}P NMR spectra of crude (blue) and purified (red) **17c**

2.2.3 DNA labelling

Coupling between resin-bound DNA and the phosphoramidite monomers **17a-c** is represented in scheme 2.9. Conjugation of the phosphoramidite **17a** to CPG-thymidine (**20**) was explored as the test case reaction. Coupling was carried out manually on the solid phase on a 1 µmol scale. Firstly, the CPG-thymidine was placed in a DNA synthesis column, and a 1 mL syringe containing a solution of **17a** in anhydrous acetonitrile was attached to one end. At the other end, a second 1 mL syringe was attached containing a solution of BMT in the same solvent. The two solutions were then passed through the synthesis column for a period of 15 min. To ensure complete coupling, a second portion of each solution was then attached and the process was repeated for a further 15 min. Following oxidation of the resin-bound DNA conjugate with I_2, cleavage from the solid support was effected following incubation in aqueous $MeNH_2$ for 30 min at 65 ^{o}C. Reversed-phase (RP) HPLC analysis of the resulting aqueous solution confirmed >95% conversion to the desired product

(figure 2.6). A significant difference in rentention time between the starting material (thymidine, **21**) and the product **23a** was noted. This is unsurprising, since a relatively large non-polar molecule is introduced during the formation of the product. Evidently, the highly polar thymidine starting material (**21**) is weakly retained by the non-polar C_{18} column, and is thus eluted at a much earlier time than the less polar product **23a**. This empirical evidence for the formation of the isoxazole-conjugate **23a** is supported by mass spectral analysis.

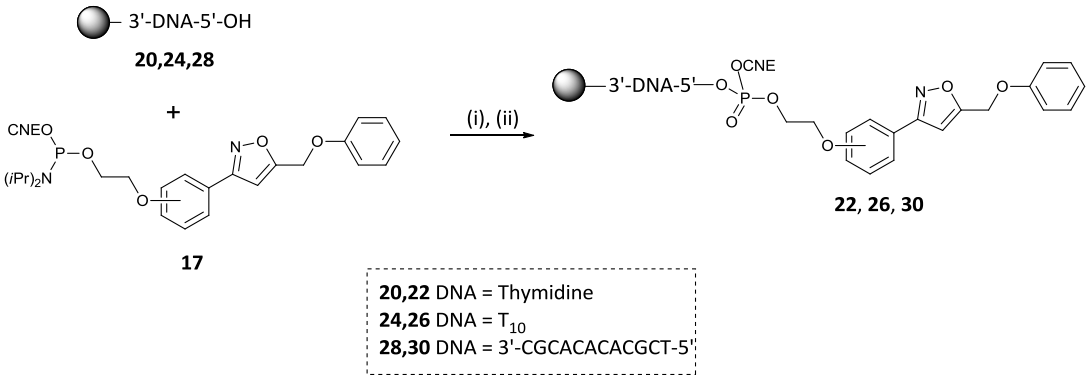

Scheme 2.9. (a) Solid phase synthesis of chemically modified nucleic acids using isoxazole-phosphoramidite monomers

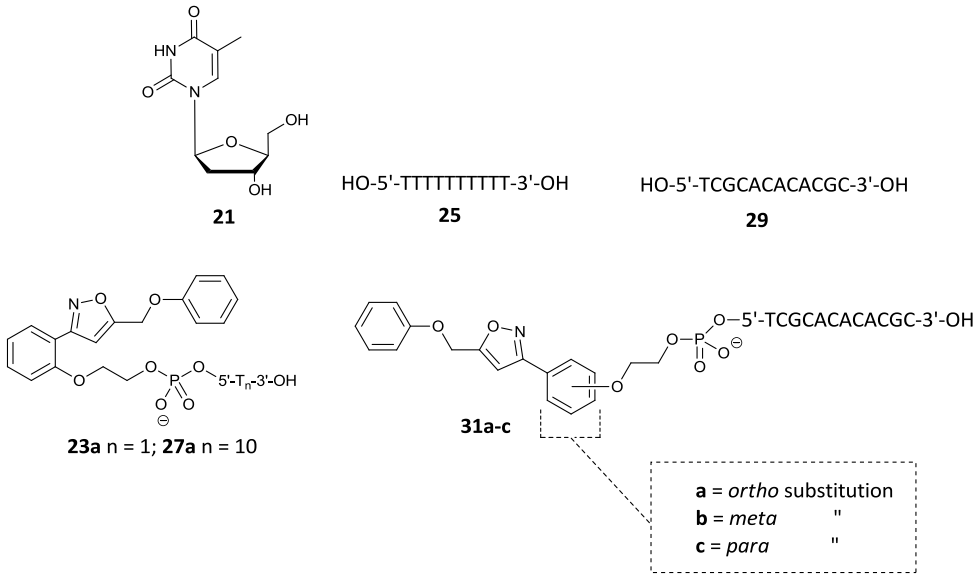

Figure 2.5. Structures of cleaved and deprotected DNA starting materials and products

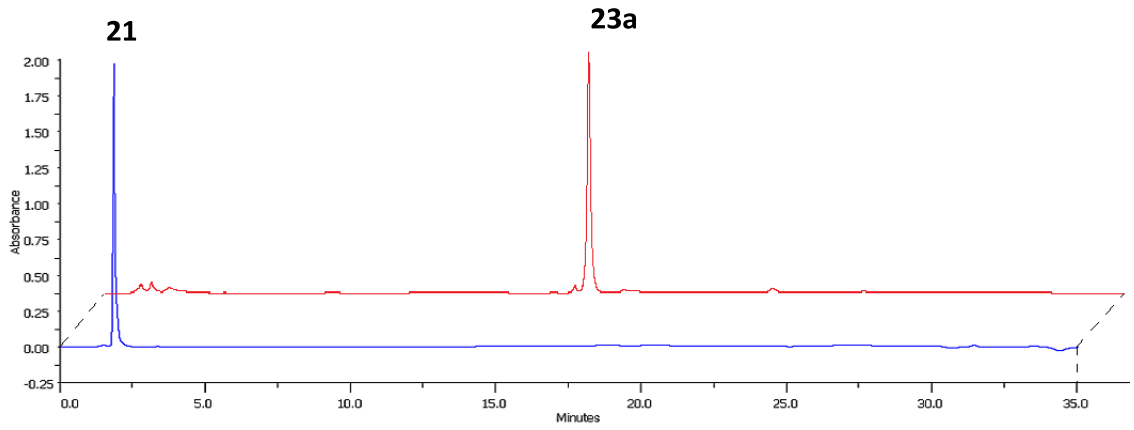

Figure 2.6. Overlaid chromatograms of thymidine starting material **21** (blue) and the labelled nucleoside **23a** (red)

Compatibility of the procedure with an oligonucleotide was confirmed when coupling of **17a** to CPG-decathymidine (**24**) was demonstrated under identical reaction conditions. RP-HPLC analysis of the crude product (figure 2.7) following cleavage from the resin indicated that the reaction proceeded smoothly in near quantitative yield, and formation of the product **27a** was supported by MALDI-TOF MS analysis. A significant increase in retention time of the oligonucleotide starting material and product was observed in comparison to the previous monomeric example. This is a trend generally observed for the analysis of oligonucleotides by RP-HPLC, *i.e.* retention time increases as chain length increases. Much like the previous example, the product **27a** was seen to elute at a later time than the oligonucleotide starting material **25**.

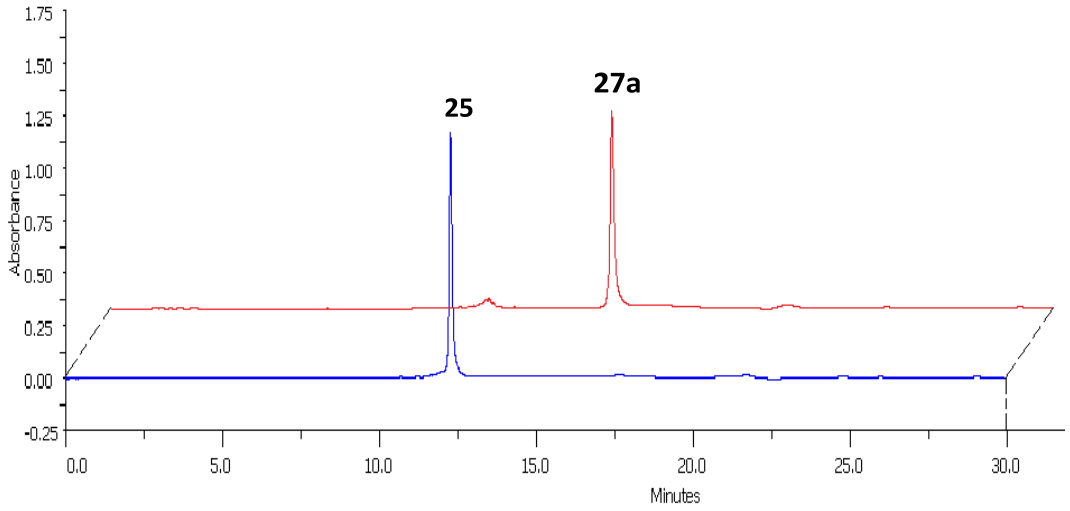

Figure 2.7. Overlaid chromatograms of decathymidine starting material **25** (blue) and the labelled oligonucleotide **27a** (red)

The scope of this reaction was further demonstrated in conjugation to the resin-supported 12-*mer* **28**, which contained all four bases with their standard protecting groups. Coupling of **28** with the phosphoramidite **17a** afforded the resin-bound conjugate **30a**. Cleavage and deprotection followed incubation in aqueous ammonium hydroxide for 24 hr at room temperature, and characterisation of the product by RP-HPLC and MALDI-TOF MS confirmed formation of **31a** in near quantitative yield. Similar results were observed when the regioisomeric phosphoramidite building blocks **17b** and **17c** were employed instead of **17a**. Thus, manual solid phase coupling of **17b** and **17c** to the resin-bound 12-*mer* **28** yielded the CPG-DNA-conjugates **30b** and **30c**. RP-HPLC analysis of the cleaved and deprotected products **31b,c** showed a similar profile to that of **31a** (figure 2.8). There was negligible difference in the retention time of all three isomeric conjugates, and all eluted more slowly than the parent 12-*mer* **29.** As expected, MALDI-TOF MS analysis supported formation of the desired products.

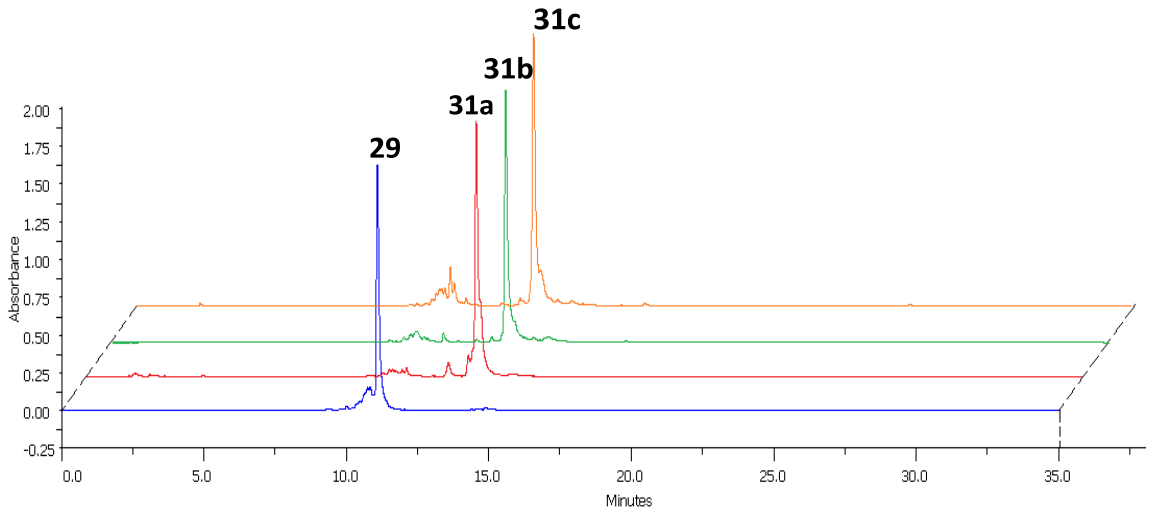

Figure 2.8. Overlaid chromatograms of mixed base 12-*mer* starting material **29** (blue), and the labelled oligonucleotides **31a** (red), **31b** (green), **31c** (orange), which were prepared by manual phosphoramidite coupling

These results were most encouraging, but we wished to take it further and explore the possibility to automate the introduction of 'click-prepared' phosphoramidite monomers to DNA in search of further convenience and flexibility. Thus, pure samples of **17a-c** were prepared with a view to automating coupling to the resin-supported 12-*mer* **28** on an Expedite DNA synthesiser. In the first example, a solution of the phosphoramidite **17c** in anhydrous acetonitrile and 0.2 µmol of **28** in a DNA synthesis

column were installed on the instrument. We employed the standard protocol used for the coupling of nucleosidic phosphoramidites, *i.e.* 37 equiv. of phosphoramidite and 1.5 min coupling time, in search of the support-bound conjugate **30c**. After standard work-up, coupling efficiency was adjudged by RP-HPLC analysis of the cleaved product **31c** to be >90%. However, conjugation of **17a** and **17b** to **28** under identical conditions displayed inferior coupling yields (figure 2.9); presumably the increased steric demand of these regioisomeric monomers offers an explanation for the poorer reactivity. Exposure of **28** to a larger amount of **17a** or **17b** (50 equiv.) for a longer time (15 min) was sufficient to increase the level of conversion to the products **30a** and **30b** to over 90%. In each case, HPLC data demonstrates a favourable comparison between manual and automated approaches.

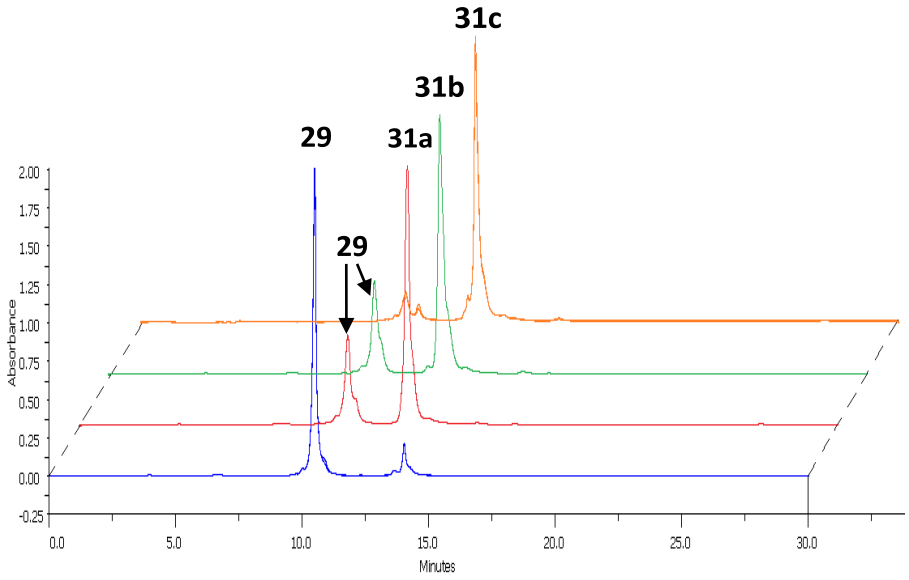

Figure 2.9. Overlaid chromatograms of the mixed base 12-*mer* starting material **29** (blue) and the labelled oligonucleotides **31a** (red), **31b** (green) and **31c** (orange) prepared on the DNA synthesiser using the standard coupling protocol.

2.2.4 Conclusions

Novel isoxazole building blocks have been prepared by copper-free NOAC. These heterocyclic products, bearing a pendant hydroxy functionality, were constructed from modular components of the NOAC reaction, and engineered to meet the chemical

specifications of automated DNA synthesis. Thus, the presence of the pendant hydroxy functionality facilitates introduction of a phosphoramidite group, which was exploited to conjugate these 'click-prepared' heterocycles to DNA on the solid phase. Coupling has been demonstrated on the level of a single nucleoside and also with oligonucleotides containing all four natural bases. While on-resin click chemistry with alkyne-functionalised oligonucleotides is well established, the off-resin or pre-synthetic approach described herein presents an alternative tool for nucleic acid modification. The ability to efficiently automate conjugation may be attractive for larger scale applications, and additionally oligonucleotides bearing functionalities incompatible with 1,3-dipolar cycloaddition conditions are spared this exposure. We believe that through preparation of various isoxazole cycloadducts bearing a pendant OH group(s), huge scope exists for the construction of diverse DNA, and indeed RNA conjugates.

Chapter 3

Nitrile oxide-alkyne cycloadditions 2: Preparation of photoresponsive DNA by NOAC

3.1 Introduction

3.1.1 Photoresponsive molecules

The ability to control the behaviour of biologically active molecules by external, easily controllable stimuli has many benefits. Whether one is investigating a particular cellular mechanism, or developing a drug, an important criterion to consider is how selectively the biological processes involved can be manipulated. For example, spatio-temporal control of drug activity may reduce side effects and increase efficacy. By designing molecules which respond to an external trigger, it becomes possible to effect their permanent or indeed reversible activation.

Light is an ideal trigger since it is highly orthogonal. In most biological examples, with the exception of a few highly specialised cell types such as those of the eye or those involved in photosynthesis in plants, cells do not react to light. In addition, cells are not harmed by light unless the wavelength used is very short. Light sensitive molecules may bear a photo-labile protecting group, in which case they are referred to as 'caged' and undergo an irreversible transition from an inactive to an active state upon irradiation with light of a certain wavelength. Alternatively, they may be photochromic compounds, *i.e.* they exist in equilibrium between two isomeric forms which absorb light of different wavelengths. These bistable photo-switches have an advantage over caged compounds in that they do not generate any by-products upon activation, which may lead to toxicity problems in biological settings.[113,114] This is offset, however, by the problem of finding the right location for attachment of the switching moiety, in addition to difficulties in achieving proper binary on/off behaviour.

The applications of light-activated caged compounds have been the subject of several review articles.[115-117] Photo-labile protecting groups have been recognised as a useful tool by synthetic chemists for many years. However, their greatest potential arguably lies at the interface of chemistry and biology. Placement of a caging group at the correct location can render an otherwise active molecule completely inactive. Factors

to consider when choosing a particular caging group include the quantum yield for the deprotection reaction and the toxicity of the inevitable by-product(s). Some of the most common photo-labile protecting groups include the *ortho*-nitrobenzyl group (**32**), nitrodibenzofurane (**33**), coumarin (**34**) and their derivatives (figure 3.1).

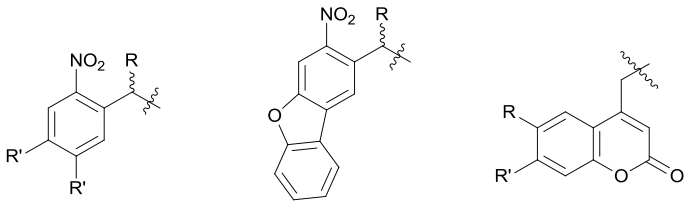

32 **33** **34**

Figure 3.1. Some common photo-labile protecting groups

The three most widely reported types of reversible photo-switches are diarylethenes, spiropyrans and azobenzenes. Diarylethenes typically consist of two thiophene rings bridged by a double bond. They isomerise reversibly *via* a 6-π electrocyclic reaction from an open-ring, unconjugated form to a conjugated, closed ring form upon absorption of light of the appropriate wavelength (figure 3.2). Significantly, this photo-switch is unaffected by thermal conditions. Diarylethenes also display excellent fatigue resistance, short response time and high quantum yield. However, they experience very little change in shape upon isomerisation, which limits their use to applications which exploit the reversible change in their electronic properties, such as polymer chemistry[118] and high density data storage.[119]

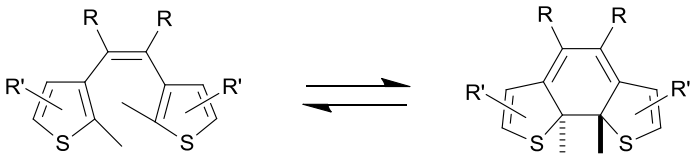

Figure 3.2. Isomerisation of a diarylethene

Spiropyrans, and the closely related spirooxazines, exist in equilibrium between two forms: a ring-closed spiro form and a conjugated, ring-opened merocyanine form (figure 3.3). In the spiro form, the conjugated system of the pyran/oxazine and another aromatic part of the molecule are seprated by an sp^3 hybridised 'spiro' carbon. Upon irradiation with UV light, the spiro carbon to oxygen bond breaks and the former

achieves sp^2 hybridisation, resulting in a planar, conjugated system. Consequently, the merocyanine form can absorb visible light and is therefore highly coloured, whereas the spiro form is colourless. Spiropyrans are widely reported in the literature, and their applications include metal complexation[120] (due to coordination of the metal to the phenolate anion in the merocyanine form), DNA intercalation[121]and modification,[122] and bio-imaging.[123]

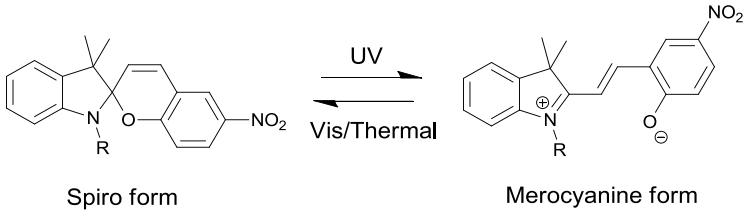

Figure 3.3. Reversible equilibrium of a spiropyran

A search of the literature reveals many examples of the functionalisation of nucleic acids with azobenzenes. There are of course many reasons why azobenzenes make ideal candidates for the construction of photoresponsive nucleic acids, which will be discussed in detail in the following section.

3.1.2 Azobenzenes

3.1.2.i Introduction

Azobenzene is the parent molecule of a class of compounds consisting of two phenyl rings separated by an azo bond. The defining feature of these compounds is their popularity as dyes and colourants. These compounds display a large electronic absorbance maximum, the position of which varies according to the location and nature of any substituents on the phenyl rings, allowing for chemical fine tuning of colour. Arguably their most interesting property, however, is their readily induced, reversible, *trans* to *cis* isomerisation upon the absorbance of light of a particular frequency. The geometric change which accompanies this photochemical transformation can have a significant effect on the chemical, mechanical, optical and

electronic properties of materials which incorporate azobenzenes into their overall structure.

3.1.2.ii Photchemistry and photophysics of azobenzenes

The *trans* isomer of azobenzene (**35**) is approximately 50 kJ·mol^{-1} more stable than the *cis* isomer,[124] and the barrier to isomerisation is ~200 kJ·mol^{-1}.[125] As a result, under dark conditions the *trans* form dominates. Absorbance of light anywhere within the broad *trans* absorbance band leads to isomerisation to the *cis* state in high quantum yield; this occurs on a timescale of picoseconds.[126,127] While the *trans* form is almost planar and has a dipole moment near zero, the *cis* isomer adopts a bent conformation with the phenyl rings twisted ~55^{o} out of the plane of the azo bond, and has a dipole moment of 3 Debye.[128] The structures and electronic absorption spectra of the individual geometric isomers are represented in figure 3.4.

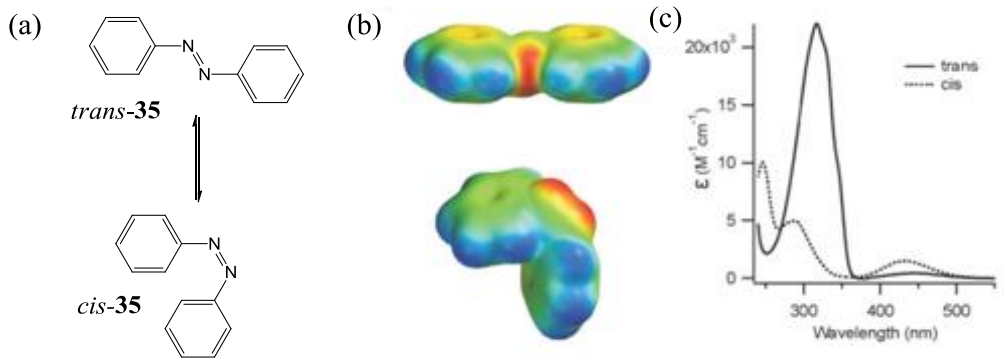

Figure 3.4. (a) Structures of *cis* and *trans* isomers of azobenzene (**35**); (b) Space-filling models, coloured by electrostatic potential (red-negative to blue-positive); (c) Electronic absorption spectra of the *trans* and *cis* isomers of azobenzene (ethanol).[129]

Once in its *cis* form, azobenzene may revert to the *trans* form, either through absorbance of light in the *cis* absorbance band, or *via* thermal relaxation. Due to overlapping of the absorption bands of the *cis* and *trans* isomers, it is impossible to obtain 100% of either isomer following irradiation. For example, in unsubstituted azobenzene, irradiation produces a photo-stationary state with a maximum of ≈80% *cis* and ≈95% *trans.*[129] The *cis* isomer will, however, thermally convert back to >99.99% of

the *trans* state. The quantum yield of each isomerisation process (φ_{cis} *and* φ_{trans}) and the thermal rate constants (*k*) are intimately related to the substitution pattern on the phenyl rings. These parameters will affect the amount of each isomer in the photo-stationary state; other influencing factors include irradiation intensity and wavelength, temperature, and the host matrix *viz* solution,[130] polymer matrix[131] or monolayer.[132]

3.1.2.iii Isomerisation mechanism

A single mechanism cannot satisfactorily explain all aspects of the isomerisation process, even for unsubstituted azobenzene. Four mechanisms have been proposed as pathways for azobenzene isomerisation – inversion, rotation, concerted inversion, and inversion-assisted rotation;[133-134] these are represented in figure 3.5.

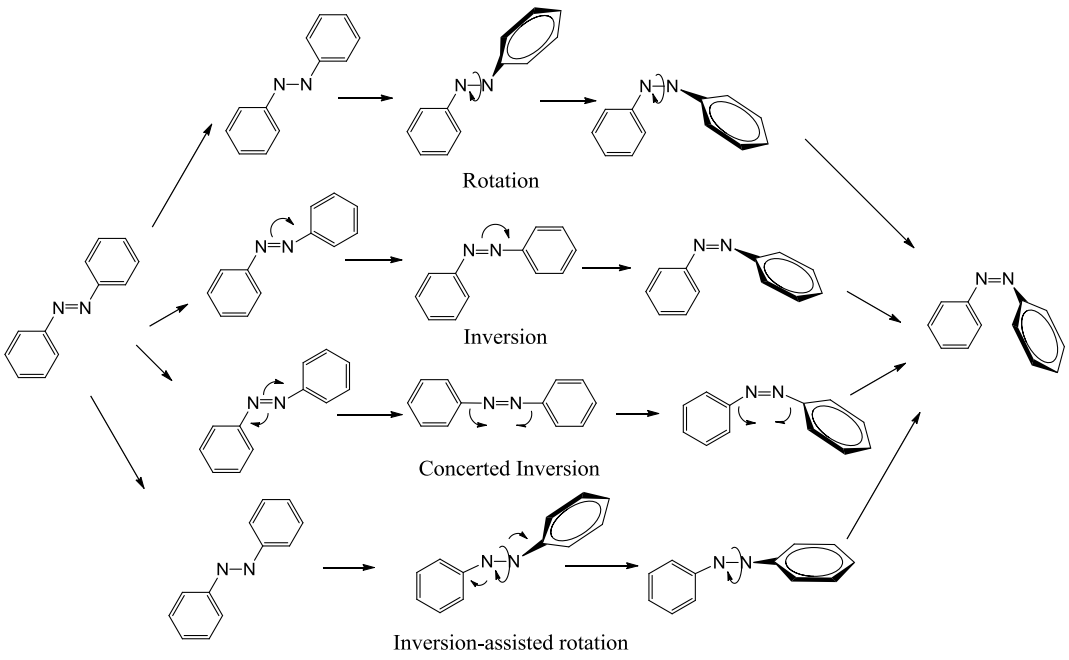

Figure 3.5. Proposed mechanisms for azobenzene isomerisation[135]

The inversion mechanism involves an increase in one N=N-C angle to 180°.[134] In the rotational mechanism, the N=N π bond breaks, allowing free rotation about the N-N bond. As a result, the C-N-N-C dihedral angle changes, while the N-N-C angle remains unchanged at ~120°.[136] The concerted inversion pathway involves both N=N-C angles increasing to 180°, resulting in a linear transition state. In inversion-assisted rotation,

a large change in the C-N-N-C dihedral angle and a small yet significant change in the N=N-C angle occur simultaneously. Significantly, the transition state that results from concerted inversion has no dipole moment, whereas the other three isomerisation pathways possess polar transition states. Since relaxation from all four of these transition states can yield either the *cis* or the *trans* isomer, each pathway predicts photo-stationary states comprising both isomers; the relative proportions of each will depend on the electronic and steric properties of the ring substituents.

3.1.2.iv Effects of substitution on the spectral and kinetic properties of azobenzenes

Azobenzene derivatives can be divided into three classes on the basis of their substitution pattern and the effect this has on their absorbance spectra; the azobenzene type, the aminoazobenzene type and the pseudo-stilbene type (figure 3.6).[137]

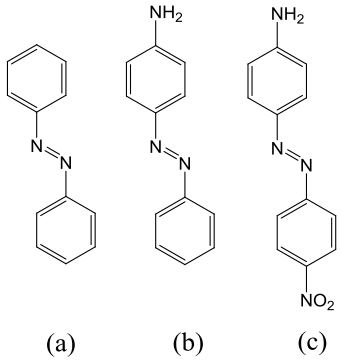

Figure 3.6. Examples of the three spectroscopic classes of azobenzenes : (a) azobenzenes, (b) aminoazobenzenes, and (c) pseudo-stilbenes

Substituted azobenzenes, like the parent azobenzene, are characterised by a high intensity π-π* band in the UV region and a low intensity n-π* band in the visible region. Compounds in the aminoazobenzene class generally possess electron donating groups (*e.g* NH_2) at the *ortho* and/or *para* positions. In these compounds, the π-π* and n-π* bands are very close and may be overlapping in the near visible UV region. Pseudo-stilbene type molecules are characterised by substitution at the 4- and 4'-position with an electron donor and an electron acceptor (a 'push-pull' substitution pattern), resulting in a strongly asymmetric electron distribution. In such molecules

the π-π* band is shifted toward the red (past that of the n-π*) to assume a reverse order with respect to the spectra of the parent azobenzene molecule. Due to the range of spectral properties resulting from substitution, different azobenzenes display characteristic rates and extents of isomerisation, and in general individual azobenzenes interact differently with light of a given wavelength.

Manipulation of the position of the λ_{max} of an azobenzene compound *via* substitution will alter the wavelength of light necessary to effect photo-isomerisation. Such manipulation may prove advantageous in biological applications, where irradiation with UV light can lead to tissue damage.[138]

It is also important to consider the correlation observed between the position of the *trans* π-π* absorption band (described here simply as λ_{max}) and the thermal relaxation of the *cis* isomer. In general, red-shifted azobenzenes, *i.e*. those with their λ_{max} in the visible region, are found to exhibit faster thermal relaxation processes.[139,140] The results of a study by Woolley *et al.* clearly show, for a series of *para* disubstituted azobenzenes, the relationship between the electron donating ability of the substituents, the value of λ_{max} and the thermal half-life of the *cis* isomer (figure 3.7).[141] In general, as λ_{max} shifted towards the visible region, a corresponding decrease was observed in the half-life ($t_{1/2}$) of the *cis* isomer.

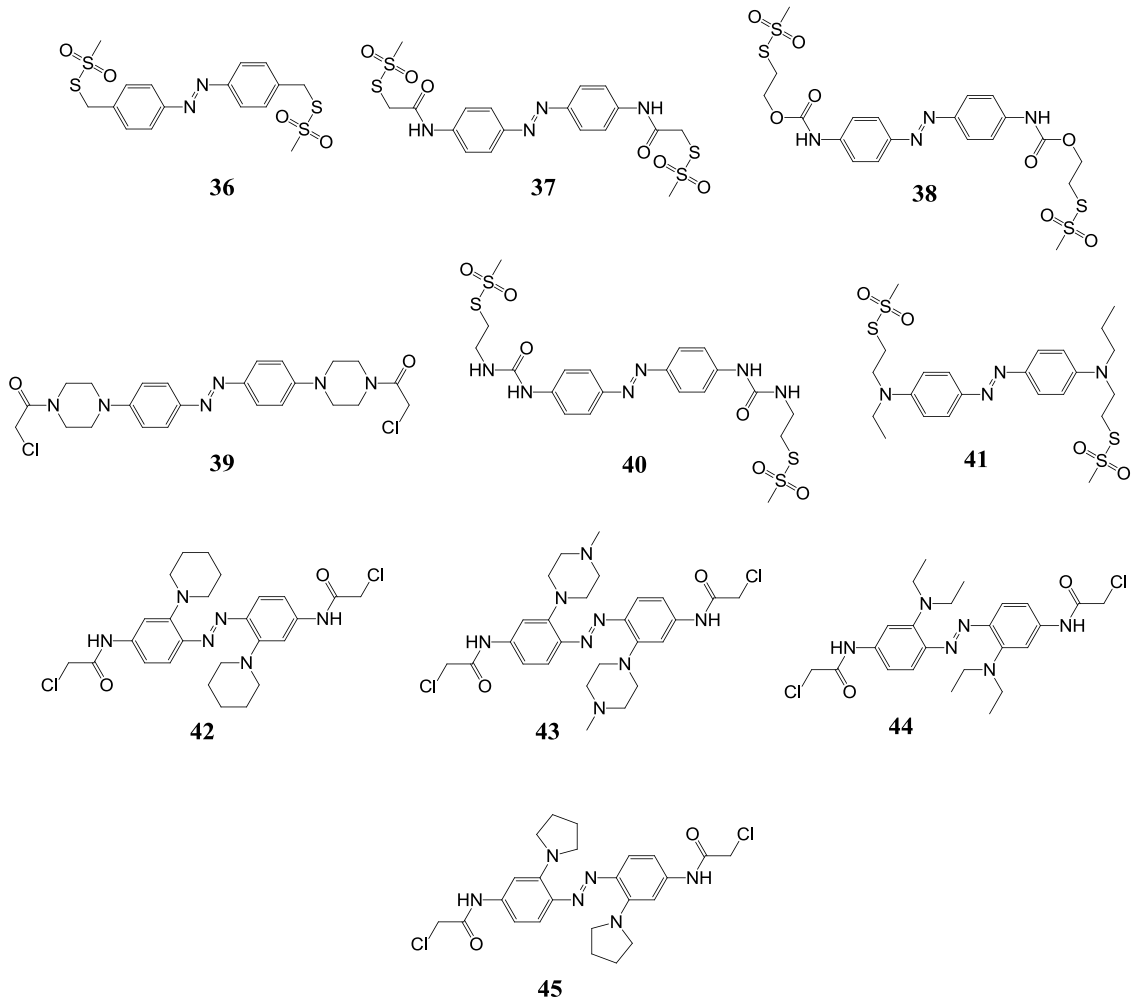

Compound	λ_{max} (*trans*)	$t_{1/2}$ (*cis-trans*)	Compound	λ_{max} (*trans*)	$t_{1/2}$ (*cis-trans*)
36	342 nm	43 hr	**41**	450 nm	2 ms
37	366 nm	12 min	**42**	445 nm	6 sec
38	372 nm	80 s	**43**	437 nm	5 min
39	382 nm	11 sec	**44**	488 nm	0.8 sec
40	480 nm	25 ms	**45**	530 nm	0.7 sec

Figure 3.7. The relationship between λ_{max} of the *trans* form and the $t_{1/2}$ of the *cis* form of a series of *para*-disubstituted azobenzenes.

The thermal stability of the *cis* form may be improved *via* introduction of substituents at the *ortho*[142] or *meta*[143] positions. When probing a biological process, increasing the stability of the *cis* isomer is often desirable, particularly if the process in question occurs on the timescale of minutes/hours. In such a case it would be preferable to maintain the on/off state of the photo-switch over this time period, rather than relying on constant irradiation. Conversely, if a pulsed conformational switch is desired as part of a biochemical switch, rapid return to the *trans* state would be preferable.

3.1.2.v General Applications

Azobenzenes have frequently been used to alter bulk material properties, and such applications have been the subject of several review articles.[144-146] Many if not all of these applications exploit the *cis* to *trans* photo-switch of the azobenzene chromophore, which is considered a remarkably clean photochemical reaction.[137] The main criteria for a useful photo-trigger include reversibility, large geometrical or electrical change, low sensitivity to the environment, fatigue resistance and high quantum yield;[144] azobenzenes meet all of these conditions, with the *proviso* that fatigue resistance and quantum yield are dependent on the substitution pattern of the phenyl rings.

In the fields of nanotechnology and materials science, azobenzenes have been incorporated into a variety of materials. In one example, an azobenzene substituted at its *meta* positions with two urethane moieties linked to two cholesteryl units (**46**) was used as an organogelator to gelatinise cyclohexane (figure 3.8).[147] Upon irradiation with light at 365 nm, photo-isomerisation from the *trans* to the *cis* form occurred; the subsequent change in geometry about the azo bond resulted in a loss of the hydrogen bonding between the N-H and C=O groups of the urethane units responsible for forming the gel, leading to a gel-sol transition. Sol-gel phase transition was effected upon irradiation at 436 nm, as a result of isomerisation from *cis* to *trans* geometry. Thus, photo-controlled gel-sol-gel phase transitioning through the breaking and reforming of hydrogen bonds was demonstrated.

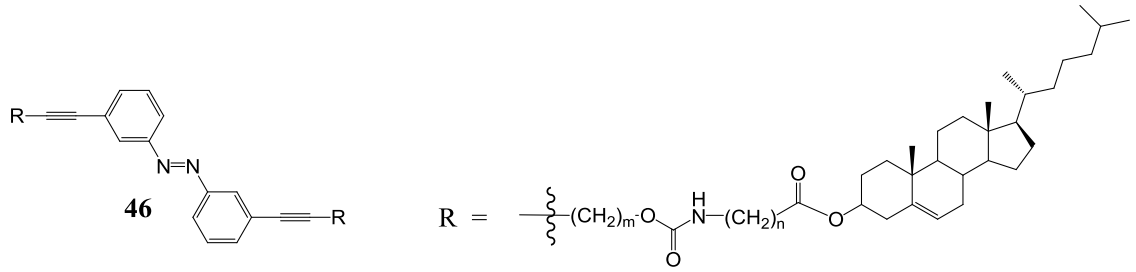

Figure 3.8. Substituted azobenzene **46** used in gel-sol-gel application

In an example of an azobenzene functioning as a photo-switchable organic monolayer, a silicon surface was functionalised with a pseudo-stilbene type azobenzene.[148] *Trans-cis* isomerisation resulted under alternate UV and visible light irradiation. The electrical conductivity of the material, measured under both conditions, showed a distinct difference between the *trans* and *cis* forms; such photo-regulation of electrical conductivity may have potential applications in microelectronics and molecular electronics.

Rotello and co-workers demonstrated that incorporation of azobenzene into the side-chains of polystyrene can be used to effect a reversible change in polymer structure.[149] Isomerisation of these side-chains into the more compact *cis* isomer can relax the polymer structure, allowing for enhancement of aromatic stacking and dipole-dipole interactions between the side chains.

The unique photophysical properties of azobenzenes have also been exploited in a range of biomolecular applications. In addition to nucleic acids (which will be covered in more detail in section 3.1.7), there are many examples of conformational control of azobenzene modified proteins and peptides.[150 -151] In one example, this conformational switch was exploited in a restriction enzyme to effectively photo-regulate DNA cleavage.[152] The photo-switchable moiety was incorporated into a single chain version of the restriction enzyme PvuII by cross-linking two suitably located cysteine residues with a bifunctional azobenzene derivative (figure 3.9). A range of modified variants of the enzyme were produced by altering the site of modification and by introducing multiple cross-links. Some of the modified variants, which carried the cross-links close to the catalytic centre, were modulated in their DNA cleavage activity by a factor of up to 16 following illumination with UV light (*trans-cis*) and blue

light (*cis-trans*). Significantly, this change in activity was achieved in seconds, and was fully reversible.

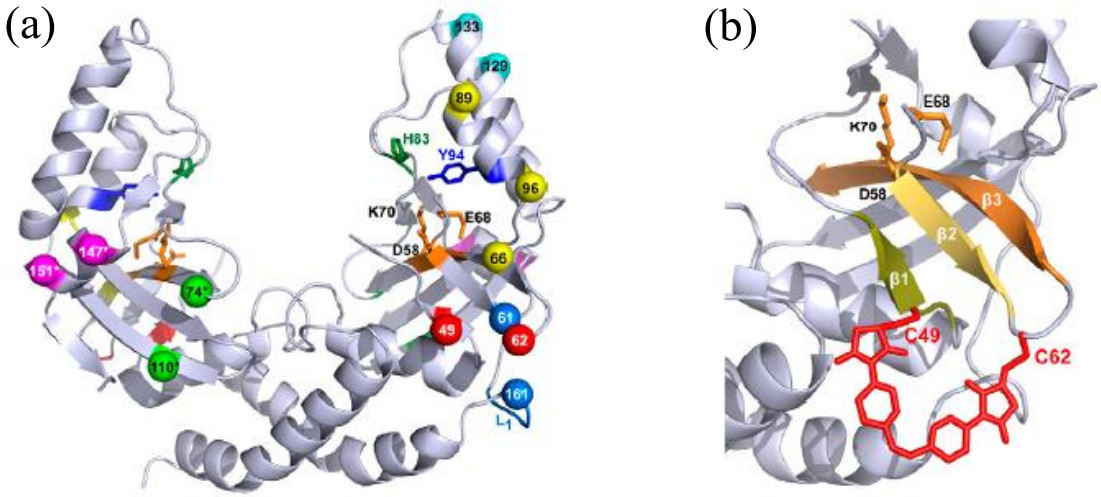

Figure 3.9. (a) The crystal structure of scPvuII with the residue pairs chosen for cross-linking in colour; (b) An expansion of the region comprising β strands β1, β2, and β3 and the catalytic centre, together with a model of the azobenzene photswitch cross-linking positions C49 and C62.[152]

Several studies have explored the potential of photochromic ligands to control the function of proteins through a reversible change in shape and/or polarity of an integral bistable photo-switch; examples include nicotinic acetylcholine receptor agonists,[153] enzyme inhibitors[154] and ionotropic glutamate receptor (iGluR) agonists.[155] In the latter example, an azobenzene substituted glutamate derivative was prepared and its *cis*/*trans* agonist profile was investigated. Reversible isomerisation of the photoresponsive agonist under irradiation at 380 nm and 500 nm was shown to effectively control iGluR activity, while maintaining good efficacy and affinity.

3.1.2.vi Nucleic acid applications

In the first reported example of an oligonucleotide modified with an azobenzene chromophore, Nakano and co-workers designed the azobenzene phosphoramidite building block **47**.[156] The key functionalities are borne, by way of amido linkages, at

the 4- and the 4'- positions; a DMT protected alcohol at one end, and a phosphoramidite group on the opposite side.

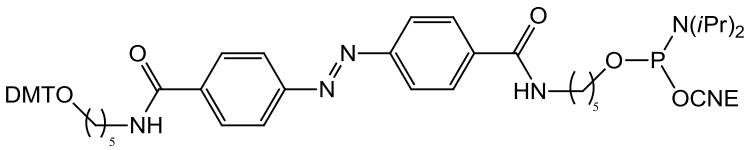

47

Figure 3.10. Azobenzene phosphoramidite **47** designed by Nakano[156]

The presence of these terminal groups, compatible with automated oligonucleotide synthesis, facilitated straight-forward incorporation of the azobenzene moiety into a growing oligonucleotide strand. Irradiation of the modified oligonucleotide with light at 313 nm resulted in a marked decrease in the characteristic absorbance of the *trans* isomer of azobenzene, showing isomerisation to the *cis* form. Significantly, the initial spectrum was regenerated completely upon exposure of the photosensitive oligonucletide to dark conditions, so displaying reversibly of the isomerisation. The authors also noted that the photo-isomerisation characteristics of the azobenzene unit were not affected by incorporation into the oligonucleotide.

While the potential to alter nucleic acid conformation *via* direct incorporation of azobenzene into the sugar-phosphate backbone was indeed interesting, the scope of these photosensitive modifications was subsequently broadened by incorporation of azobenzene residues into the side chains of oligonucleotides.[157] This was achieved by employing the non-natural phosphoramidite **48** (figure 3.11), which in contrast to linker **47**, bears a pendant azobenzene group which sits out of the sugar-phosphate backbone.

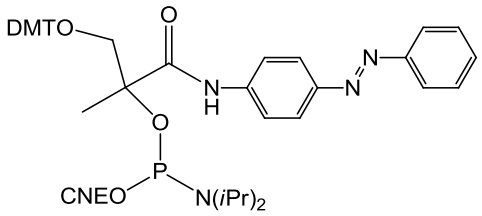

48

Figure 3.11. Azobenzene phosphoramidite **48** used by Komiyama and co-workers[157-159]

Komiyama and co-workers have demonstrated that photo-isomerisation of oligonucleotides modified with **48** destabilises duplex formation.[158,159] DNA melting studies indicated duplexes bearing a single modification on one strand were significantly destabilised when the azobenzene chromophore was isomerised from its *trans* to its *cis* form. This discovery lent considerable weight to the hypothesis that azobenzenes could be used to photo-regulate the structure, and in turn function, of DNA.

In an effort to elucidate the structural detail of photo-regulation, circular dichromism (CD) studies were undertaken; these help to determine the position of the azobenzene moiety in the secondary structure of the DNA duplex.[159] They indicated that the *trans* isomer, which has a planar structure,[160] intercalates between two base pairs of the double helix. This π stacking interaction stabilises the duplexes of modified oligonucleotides with respect to the native duplex. It is these interactions which are disrupted upon photo-isomerisation from the planar *trans* form to the non-planar *cis* form, evidenced by a significant decrease in the melting tempterature (T_m) of *cis*-azobenzene modified duplexes with respect to both the *trans*-azobenzene appended conjugates and the native duplex.

Exploitation of the optical control of duplex stability has helped to provide information on DNA recognition. Komiyama and co-workers have demonstrated photo-regulation of the DNA polymerase reaction,[161] DNA transcription[162,163] and RNA digestion.[164] In one elegant example, outlined in figure 3.12, optical control of DNA polymerisation was effected. A 54-mer DNA template was hybridised at two different positions to an 18-mer primer and a modulator sequence, which was modified with the azobenzene linker **48** near its 5' terminus. DNA elongation, mediated by T7 DNA polymerase, was blocked when the pendant azobenzene chromophore of the modifier sequence was present in its *trans* form, leading to the production of truncated 34-mer DNA. However, following irradiation with UV light ($300<\lambda<400$ nm), which effected the isomerisation to *cis* geometry, the full length 54-mer DNA was produced. It is the case that when the modifier sequence bears the azobenzene moiety in its *trans* form, a duplex forms with the template strand due to the relative ease of accommodation of the planar *trans*-azobenzene within the duplex. The T7 DNA polymerase requires

single-stranded DNA as a template, and thus as it moves along the DNA strand, it is blocked by the double-stranded region. Hence elongation ceases at the 5' terminus of the modulator strand. However, when the modulator strand carries the non-planar *cis* azobenzene moiety, dissociation of the duplex results due to steric repulsion. This allows the DNA polymerase to continue further along the template strand, yielding the full-length DNA.

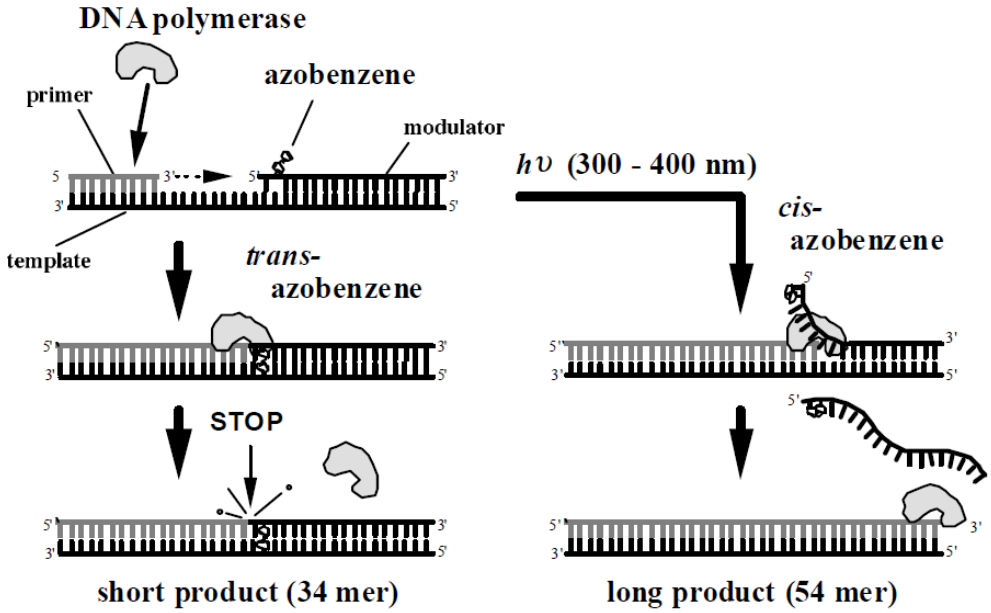

Figure 3.12. Mechanism of photo-regulation of DNA polymerisation[161]

Photo-regulation of gene expression has also been demonstrated. In this example, an azobenzene moiety was tethered to a T7 promoter sequence and transcription by T7 RNA polymerase (RNAP) was effected.[163] In terms of the position of the incorporation of the modified azobenzene subunit, two regions of the promoter were investigated – the loop binding region and the unwinding region. Kinetic studies demonstrated that the mechanism of transcription regulation differed depending on the site of incorporation of the azobenzene unit. When the azobenzene moiety was present in the loop-binding region of the promoter, the *trans* form strongly intercalated between base pairs, interfering with the binding of RNAP. Photo-isomerisation to the *cis* form following UV irradiation forced the the *cis*-azobenzene to flip out of the duplex, facilitating binding of the RNAP.

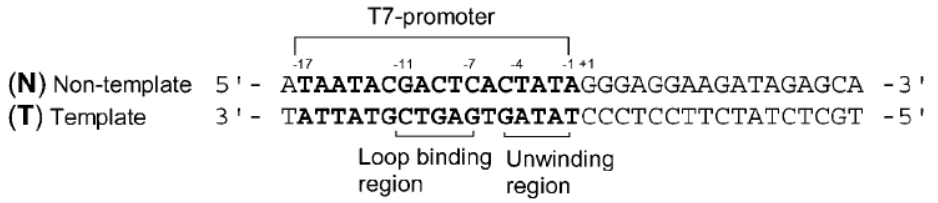

Figure 3.13. DNA sequence identifying promoter region, loop binding region and unwinding region[40]

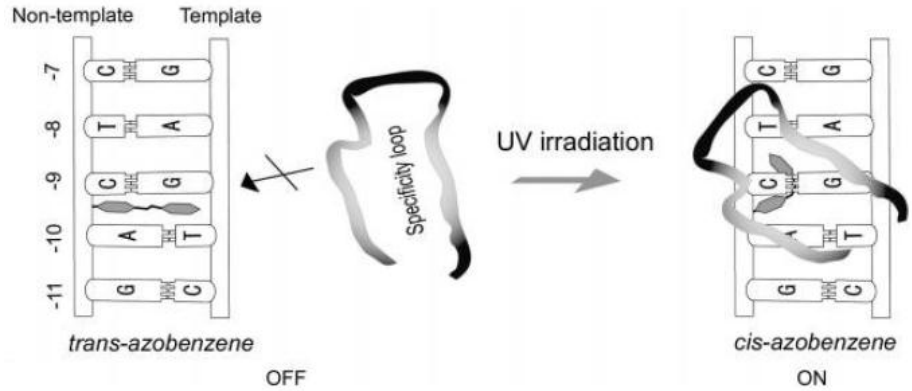

Figure 3.14. Mechanism of photo-regulation of gene expression with azobenzene modification in the loop-binding region

Incorporation of the modification into the unwinding region of the promoter sequence effected photo-regulation of transcription through a different mechanism. In the native duplex, the base pairs in the unwinding region of the duplex are melted by RNAP and the template strand is directed into the catalytic site of transcription. Intercalation of *trans*-AB, however, stabilises the duplex and prevents it from unwinding. On *trans-cis* isomerisation, melting of this region is facilitated due to the steric hindrance of nonplanar *cis*-AB.

In addition to DNA, construction of photoresponsive RNA strands has been successful.[165] A pendant azobenzene moiety was incorporated into a single RNA strand *via* a D-threoninol derivative using standard phosphoramidite coupling chemistry, and RNA/RNA duplex formation was investigated between the photoresponsive modified strand and unmodified, complementary RNA sequence

(a)

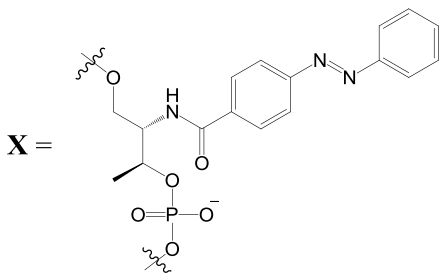

R_xG 5'-CUUAC**XG**CUGA-3'
RC 3'-GAAUG **C**GACU-5'
R_xA 5'-CUUAC**XA**CUGA-3'
RU 3'-GAAUG **U**GACU-5'
R_xU 5'-CUUAC**XU**CUGA-3'
RA 3'-GAAUG **A**GACU-5'
R_xC 5'-CUUAC**XC**CUGA-3'
RG 3'-GAAUG **C**GACU-5'

(b)

Duplex	T_m (°C)		
	trans	***cis***	**ΔT_m**
R_xG/RC	48.8	36.5	12.3
R_xA/RU	41.8	29.4	12.4
R_xU/RA	41.6	31.2	10.4
R_xC/RG	46.1	37.0	9.1

Figure 3.15. (a) Structure of azobenzene unit and sequences of RNA; (b) Thermal melting analysis data[165]

This study found significant changes in the T_m of the modified duplexes resulting from reversible *trans-cis* isomerisation of the azobenzene moiety and thus an efficient tool with which to photochemically regulate RNA duplex formation. Further duplex destabilisation was observed upon incorporation of 2',6'-dimethylazobenzene, most likely owing to the increased steric hindrance induced when trying to accommodate the non-planar *cis* form in the duplex. Comparison between azobenzene modified RNA duplexes and the unmodified, native RNA duplex showed a slight (~2 °C) destabilisation, indicating that even the *trans* form destabilised the duplex to some extent. This can be explained by the fact that the rigid A form structure of the RNA/RNA duplex does not easily accept intercalators between the base pairs.[166]

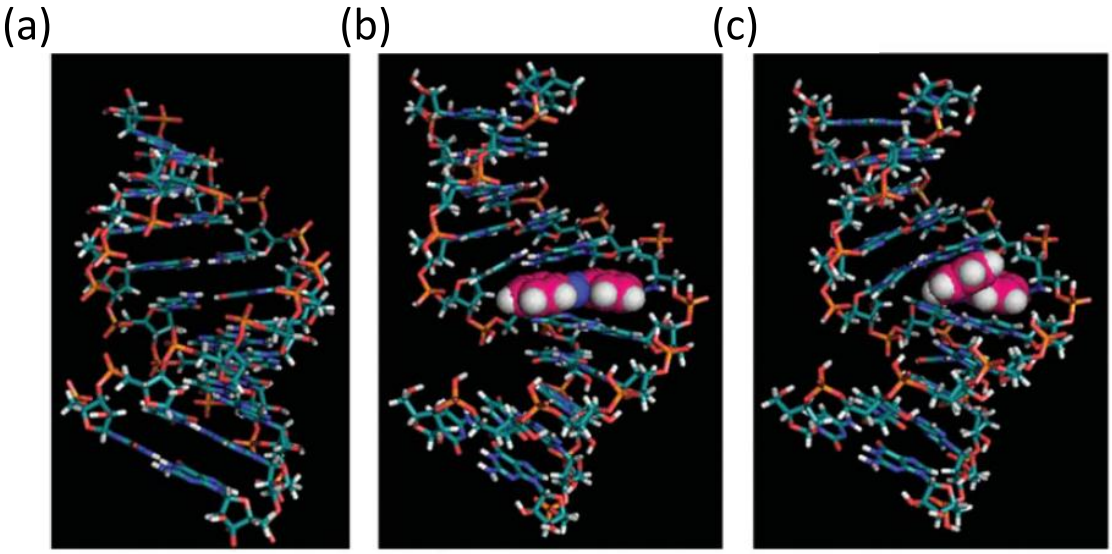

Figure 3.16. Energy-minimized structure of (a) the native RNA/RNA duplex (R_nG/RC), and the azobenzene modified RNA/RNA duplexes (b) *trans* R_XG/RC, and (c) *cis*-R_XG/RC[167]

The ability to efficiently photo-regulate RNA duplex formation may have applications in RNAi research, which requires RNA to be in the duplex form to be active. Single stranded RNA cannot be taken up by the RISC complex, and therefore cannot effect gene knockout/suspression. Construction of photoresponsive RNA duplexes may therefore provide a useful tool for the spatio-temporal control of siRNA activity (see section 1.2 for more information on RNAi).

3.1.2.vii Azobenzene-modified nucleic acids by click chemistry

The preparation of oligonucleotides covalently linked to an azobenzene moiety/moieties has most commonly been achieved by employing azobenzene-modified phosphoramidites as monomeric building blocks in solid phase synthesis. To the best of our knowledge, there are no reported examples of the assembly of azobenzene-modified oligonucleotides in which click chemistry has been used as the key conjugation step. Indeed, the application of click reactions such as 1,3-dipolar cycloadditions could be potentially valuable for the preparation of a range of photo-switchable oligonucleotides. Accordingly, this chapter will discuss the application of NOAC chemistry to the modification of oligonucleotides with azobenzenes.

3.2 Results and Discussion

3.2.1 Azobenzene-oligonucleotide conjugates by NOAC

The results presented in chapter 2 describe the synthesis of modified oligonucleotides prepared from NOAC-generated phosphoramidite building blocks. For the post-synthetic preparation of azobenzene-oligonucleotide conjugates by NOAC, one of the components of the cycloaddition (alkyne or nitrile oxide) must be incorporated into the oligonucleotide during solid phase synthesis. The alkyne moiety is better suited to this, as a variety of 2'-*O*-propargyl nucleosides are commercially available. Using the optimised conditions for NOAC outlined in chapter 2 as a starting point, we wished to examine the potential of this chemistry for the preparation of azobenzene-modified oligonucleotide sequences. The proposed retrosynthetic approach to the desired oligonucleotide conjugates **49** is shown in scheme 3.1.

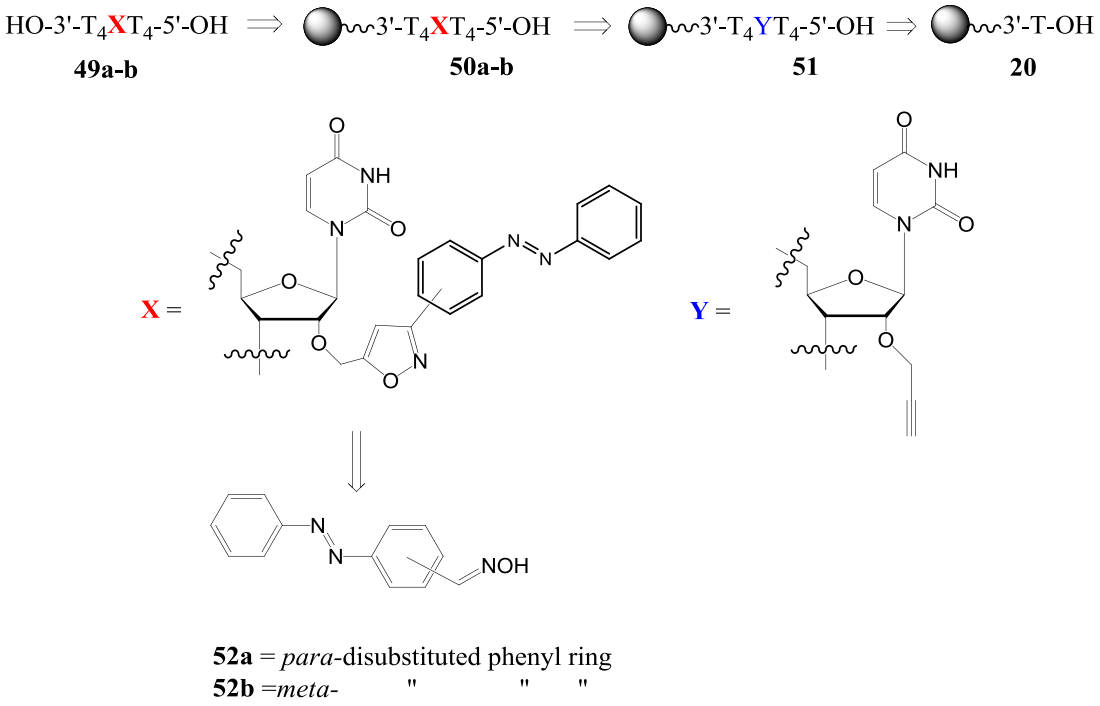

52a = *para*-disubstituted phenyl ring
52b =*meta*- " " "

Scheme 3.1. Retrosynthetic analysis of azobenzene-modified oligonucleotides

3.2.2 Preliminary cycloadditions, synthesis of 55a-d

The retrosynthetic approach outlined in scheme 3.1 requires the oximes **52a,b** as key intermediates. These oximes are not known compounds, and a trawl of the literature suggested their synthesis would require several steps. Thus, we elected to begin this study looking at small molecule examples of the NOAC involving some easily prepared azobenzene compounds (scheme 3.2).

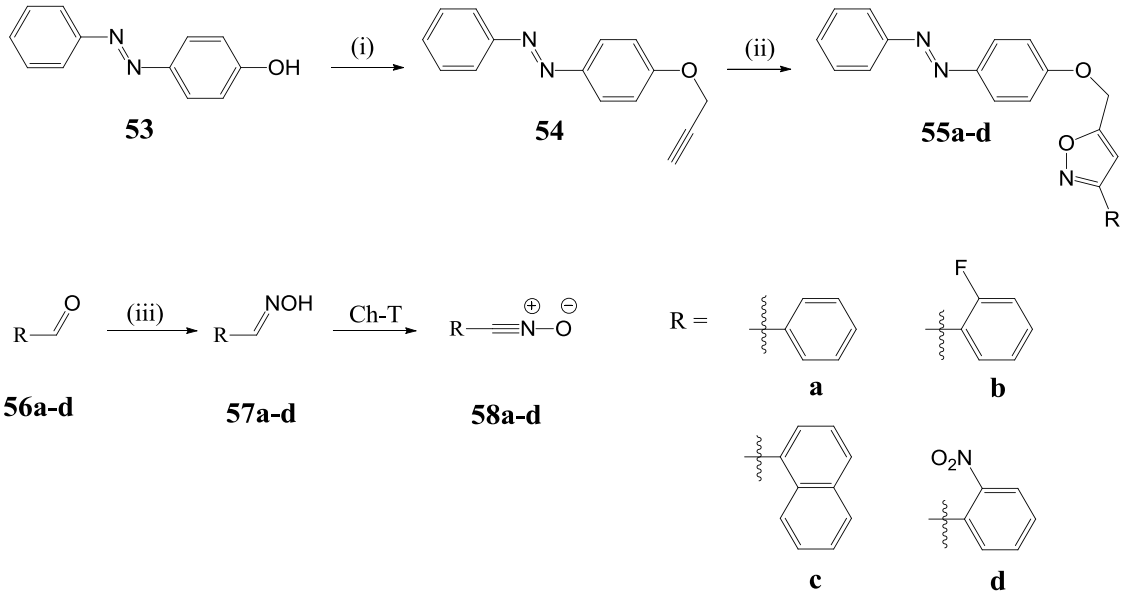

(i) K_2CO_3, $BrCH_2C(CH)$, acetone, 18 hr

(ii) Ch-T, RCHNOH (**57a-d**), $EtOH/H_2O$, 40°C, 1 hr

(iii) $NH_2OH.HCl$, C_5H_5N, EtOH, MW (120 °C, P_{max} = 300 W), 30 min

Scheme 3.2. Synthesis of cycloadducts **55a-d**

The first hypothesis tested was that the azo group would be compatible in the presence of Ch-T, which we used to prepare nitrile oxides *in situ* from oximes. To address this concern, the propargyl ether **54** was prepared. This compound, with its terminal triple bond, could potentially serve as the dipolarophile partner in a click cycloaddition reaction, and provide information on the inertness, or otherwise, of the azo group to the NOAC protocol. Nucleophillic substitution of propargyl bromide with the phenol **53** in the presence of K_2CO_3 gave **54** in quantitative yield. The ^1H NMR spectral data of **54** corresponded to that reported in the literature.[168] Click cycloaddition between **54** and benzonitrile oxide (**58a**), generated *in situ* from

commercially available benzaldehyde oxime (**57a**), furnished the cycloadduct **55a** as an orange solid in 91% yield; it can be inferred from this excellent yield that no adverse reaction occurred between the azo group and Ch-T. ^{1}H NMR spectral data, shown in figure 3.17, supports selective formation of a 3,5-disubstituted isoxazole cycloadduct. Loss of the triplet at 2.58 ppm confirms consumption of the starting alkyne **54**. Furthermore, the signal representing the methylene protons adjacent to the ether linkage, a doublet with a chemical shift of 4.78 ppm in **54**, shifts downfield to resonate at 5.28 ppm, presenting as a singlet. The singlet at 6.69 ppm is characteristic of the H-4 proton of the isoxazole; significantly there is no evidence of the regioisomeric 3,4-disubstituted product, which would have a characteristic signal in the range of 7.50-8.50 ppm.[110-112]

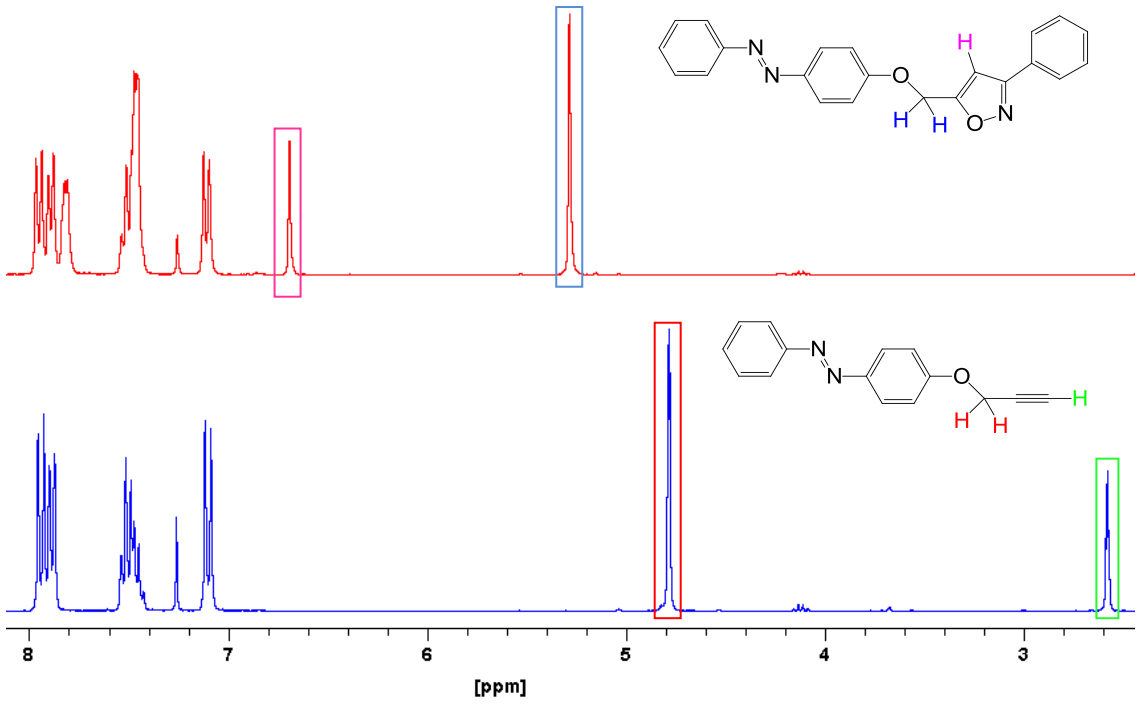

Figure 3.17. ^{1}H NMR spectra of alkyne click partner **54** (blue) and cycloadduct **55a** (red)

To investigate the influence of daylight on **55a**, a solution of the compound in $CDCl_3$ was left to stand on the laboratory bench. Evidence for light-induced *trans-cis* isomerisation was examined by recording ^{1}H NMR spectra over a time interval. After a period of three hours, the ^{1}H NMR spectrum (figure 3.18) indicated that a significant amount (~25%) of the thermally stable *trans* isomer was converted to the *cis* isomer. Several additional peaks appeared in the spectrum. Analysis of the spectrum shows an

extra signal in the region characteristic of the isoxazole proton; a singlet at 6.62 ppm is deemed to represent the *cis* isomer (the same proton in the *trans* isomer presents at 6.69 ppm). An additional resonance representing the methylene protons of the *cis* isomer is observed at 5.01 ppm. Significantly, upon standing overnight in the dark, isomerisation back to > 95% *trans*-**55a** was observed.*

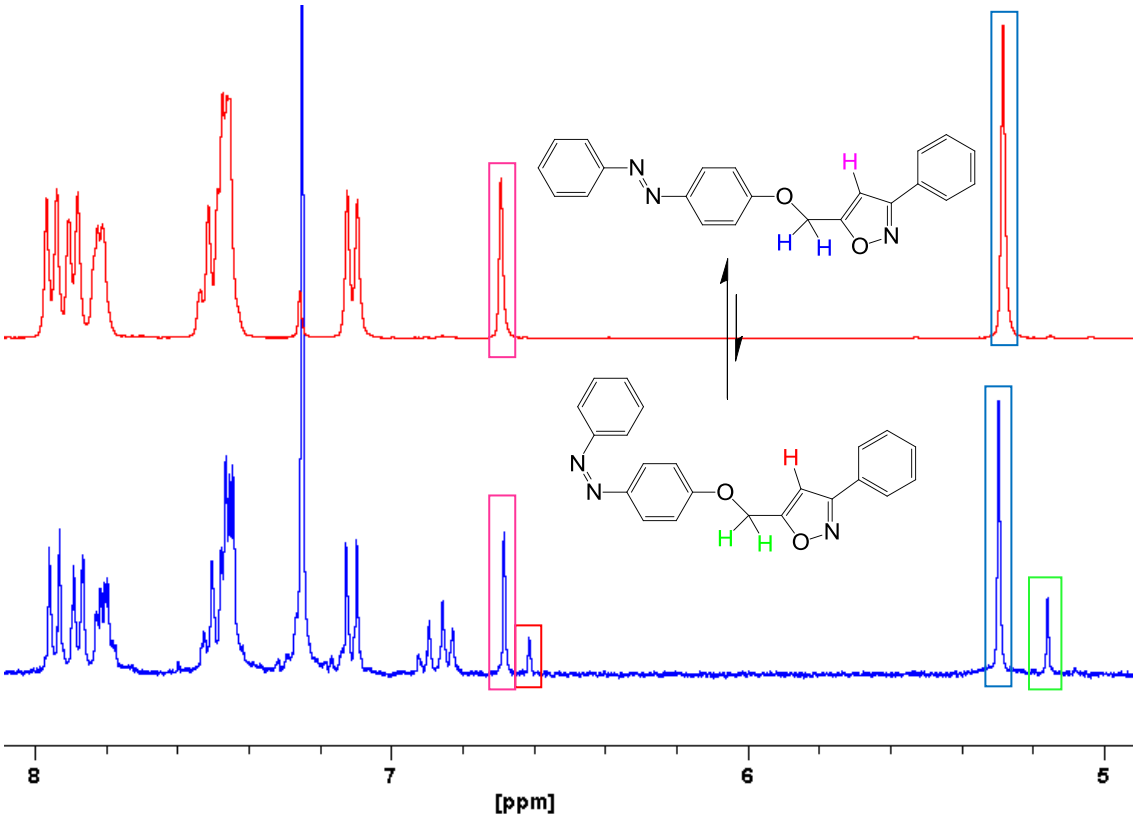

Figure 3.18. ^{1}H NMR spectra of pure *trans*-**55a** (red) and a mixture of *trans*-**55a** and *cis*-**55a** (blue) after 3 hr standing in daylight

To explore the generality of the cycloaddition with an azo-alkyne, further reactions were attempted between **54** and the aryl nitrile oxides **58b** and **58c**, themselves prepared *in situ* from their parent oximes, **57b** and **57c**. Oxime preparation followed

* For the sake of clarity, in all other schemes and NMR spectra in this chapter, only the thermodynamically more stable *trans*-azobenzene isomer will be illustrated.

from condensation of the aldehydes **56b** and **56c** with $NH_2OH.HCl$. Oximation was carried out in ethanol under microwave irradiation; sealed, pressurised vials, facilitating heating of the reaction mixture to a temperature above the boiling point of the solvent were employed. Consequently, formation of both **57b** and **57c** was complete in 30 mins, which is an improvement on the reaction time of 2 hr reported for the synthesis of similar oximes by conventional heating approaches.[72] Both **57b** and **57c** are known in the literature, and their ^{1}H NMR data corresponded to that previously reported. [71,73] The ensuing cycloadducts, **55b** and **55c**, were both obtained with isolated yields of 86%, and their structures were confirmed by ^{1}H NMR spectral data. The characteristic signals for the isoxazole ring proton in each case appeared at ~6.8 ppm. Significantly, in the case of the 2-fluorophenyl cycloadduct **55b**, this signal appeared as a doublet, with a coupling constant of 3.6 Hz (figure 3.19). Since fluorine[19] has a spin of ½ and a relative abundance of 100%, this multiplicity is a consequence of a five bond (^5J) coupling between the isoxazole proton and the fluorine atom present at the 2-position of the adjacent phenyl ring. This coupling interaction was confirmed when a ^{1}H NMR spectrum with ^{19}F decoupling showed the signal for the isoxazole proton collapsed to a singlet. Interpretation of the ^{13}C NMR spectrum of **55b** proved less trivial; it was complicated by the 2/3/4/5 bond coupling between the fluorine atom and the carbon atoms. In some cases CF coupling is very large, *e.g. J* = 250.3 Hz for the *ipso* carbon atom.

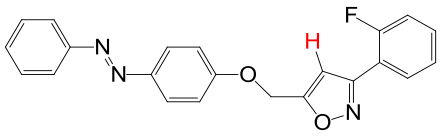

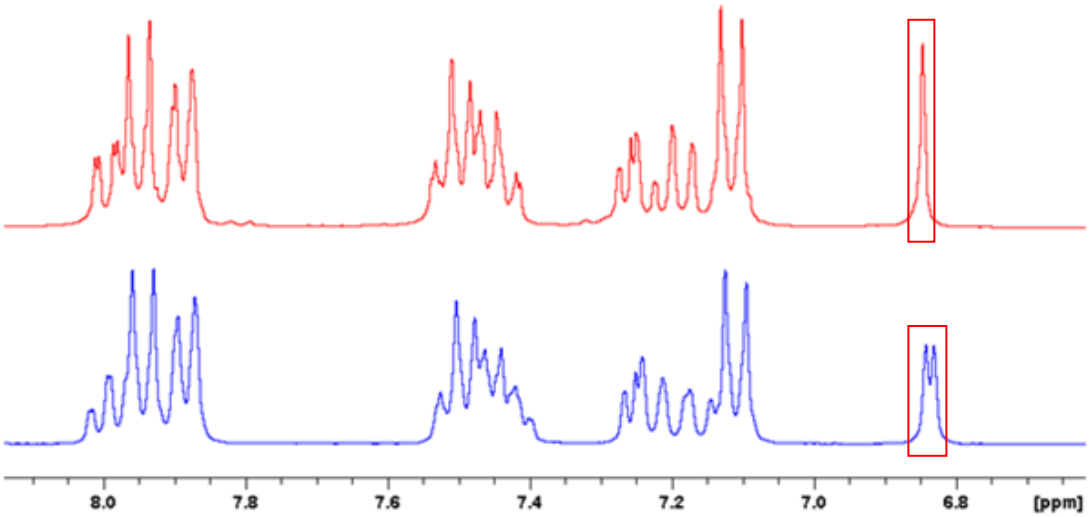

Figure 3.19. ^{1}H NMR spectrum of **55b** with (red) and without (blue) ^{19}F decoupling

Cycloaddition of **54** with 2-nitrophenyl nitrile oxide (**58d**) prepared *in situ* from commercially available 2-nitrobenzaldehyde oxime (**57d**) was less efficient than that observed with the analogous dipoles **58a-c.** A final isolated yield of 35% of **55d** was obtained**.** Presumably, the low yield was a result of the steric interference of the bulky nitro group at the *ortho* position impacting negatively on the alignment of the nitrile oxide to the dipolarophile in the transition state, leading to cycloaddition formation. A summary of the isolated yields obtained is provided in table 3.1.

Nitrile oxide	R	Product (% Yield)
58a	Ph	**55a** (91)
58b	2-Fluorophenyl	**55b** (86)
58c	1-Naphthyl	**55c** (86)
58d	2-Nitrophenyl	**55d** (35)

Table 3.1. Isolated yields of cycloadducts **55a-d** following cycloaddition of **54** with nitrile oxides **58a-d**

3.2.3 Amide cycloadditions, synthesis of 62-64

Following the success of the cycloaddition between a range of nitrile oxides and an azobenzene substrate with an ether linked alkyne moiety, we next sought to increase the structural complexity, and probed the potential of nitrile oxide cycloadditions with an azobenzene substrate carrying a propargyl moiety linked through an amide functional group (scheme 3.3).

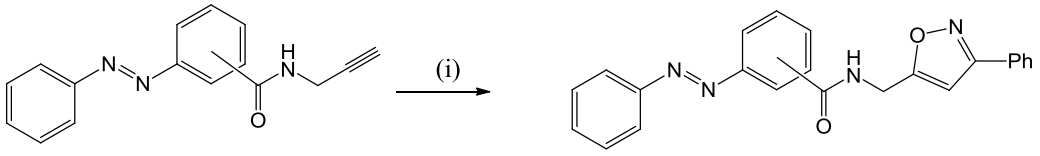

59-61 **62-64**

59,62 = *ortho*-disubstituted phenyl ring
60,63 = *meta*- " " "
61,64 = *para*- " " "

(i) Ch-T, PhCHNOH (**57a**), EtOH/H_2O, 40 ^oC, 1 hr

Scheme 3.3. Cycloadditions of the propargyl amides **59-61** with *in situ* generated phenyl nitrile oxide (**58a**)

The substrates **59-61** were gifted by our collaborators in Queens University, Belfast. These were obtained as orange solids following amide coupling between the parent carboxylic acids and propargyl amine.[169] Employing an identical experimental procedure used in the synthesis of **55a-d**, the cycloadducts **62-64** were obtained with isolated yields in the range of 70-81%. As a representative example, the ^1H NMR spectrum of the *para*-disubstituted cycloadduct **64** is shown (figure 3.20). As previously discussed, the characteristic isoxazole resonance at 6.62 ppm confirms regioselective formation of the 3,5-disubstituted isoxazole **64**. Suprisingly, the spectrum displays a large singlet resonance at 7.98 ppm, which integrates for 4 protons. This likely represents two out of the three pairs of equivalent protons H_a, H_b and H_c. One would expect these signals to appear distinct from each other, and appear as doublets (or in the case of H_a possibly a doublet of doublets). The amide proton has a chemical shift of 6.78 ppm, and appears a triplet as a result of coupling to

the adjacent methylene protons, which themselves present as a doublet resonance at 4.85 ppm.

These results confirm the compatibility of the amide functionality, as well as the azo group, with Ch-T. This may be of significance when employing NOAC in the conjugation of small molecules to proteins/polypeptides.

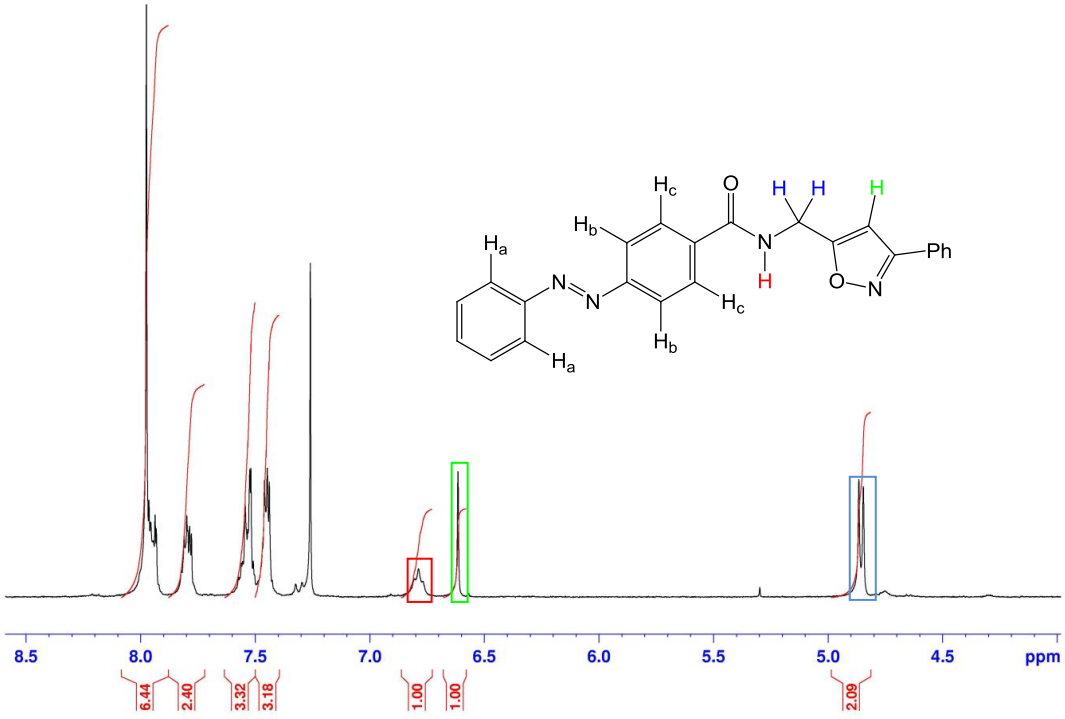

Figure 3.20. ^{1}H NMR spectrum of **64**

3.2.4 Synthesis of 3- and 4-(phenylazo)benzaldehyde oximes (52a,b)

3.2.4.i Synthesis of azo-aldehyde precursor 67a by a Grignard method

The initial attempts to synthesise the oxime **52a** focused on condensation of the phenyliminodimagnesium reagent **65** with 4-nitrobenzaldehyde (**66**) to form the aldehyde precursor **67a** (scheme 3.4) by modification of an experimental procedure described in the literature for the preparation of a series of mono- and bis-substituted azobenzenes.[170] The desired intermediate **65** was prepared following reaction of

aniline with two equivalents of ethyl magnesium bromide in anhydrous THF under an atmosphere of argon. 4-(Phenylazo)benzaldehyde (**67a**) was subsequently obtained following condensation of the freshly prepared solution of **65** with 4-nitrobenzaldehyde. In addition to the targeted azo-aldehyde **67a**, this reaction also produced a significant amount of the undesired azoxy derivative **68**. The ratio of the azo to the azoxy products varied from as low as 1:9 to a maximum of 1:1 as the concentration and number of equivalents of **65** were altered, and in our hands it was difficult to make the reaction reproducible.

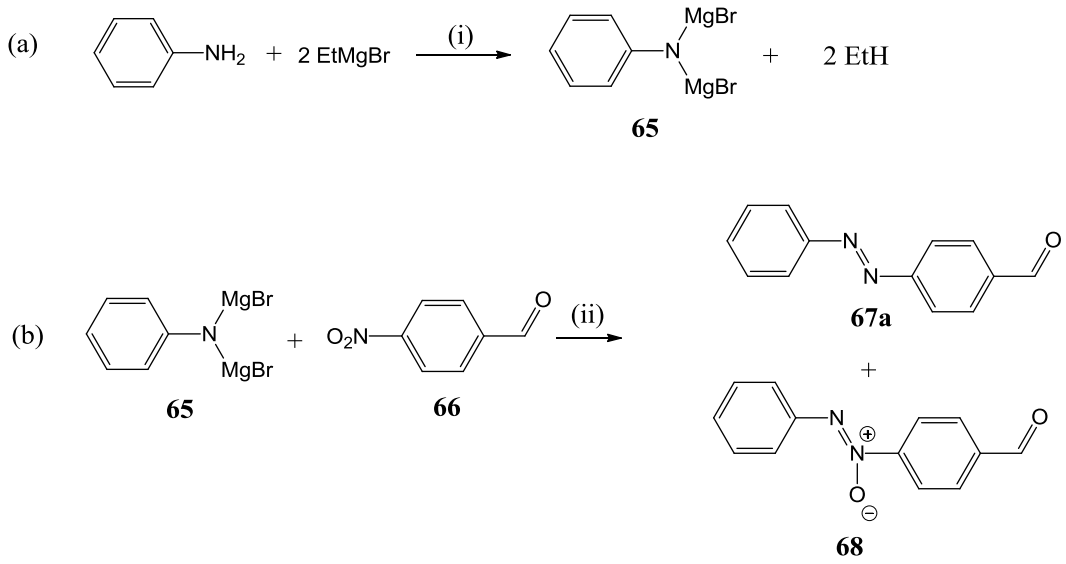

Scheme 3.4. Synthesis of the azo-aldehyde **67a** by the Grignard approach

It has been reported that azoxybenzene (**70**) is the intermediate species in the condensation of **65** with nitrobenzene (**69**), yielding azobenzene (**35**). It is further suggested that deoxygenation of **70** by a further portion of **65** yields the final product **35** (scheme 3.5).[170] With this in mind, we attempted to increase the ratio of **67a** to **68** in the crude product by increasing the number of equivalents of **65** from 5 to 8, relative to **66**. Under these modified conditions, the highest ratio of the azo to azoxy product was obtained; no further improvement was observed following an increase in the relative amount of **65** to 12 equivalents or increasing the reaction time from 3 to 18 hr.

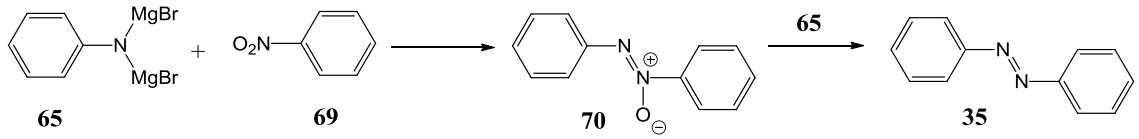

Scheme 3.5. Deoxygenation of azoxybenzene (**70**) with **65**, yielding azobenzene (**35**)

In spite of the poor chemoselectivity, a sample of the desired azo-aldehyde was obtained following separation of the azo and azoxy products by flash chromatography on silica gel. In terms of characterisation of the two species, ^{1}H and ^{13}C NMR spectroscopy were not particularly useful. Instead, a combination of mass analysis and UV-Vis spectroscopy were used. The overlaid UV spectra of the two products (EtOH) are shown in figure 3.21. The presence of a local maximum in the region of 413 nm is characteristic of a compound containing an azo bond; an azoxy group does not absorb light at this wavelength.[171] Thus, on the basis of UV data, samples were unambiguously identified as either azo-aldehyde **67a** or azoxy-aldehyde **68**. These findings were supported by mass analysis.

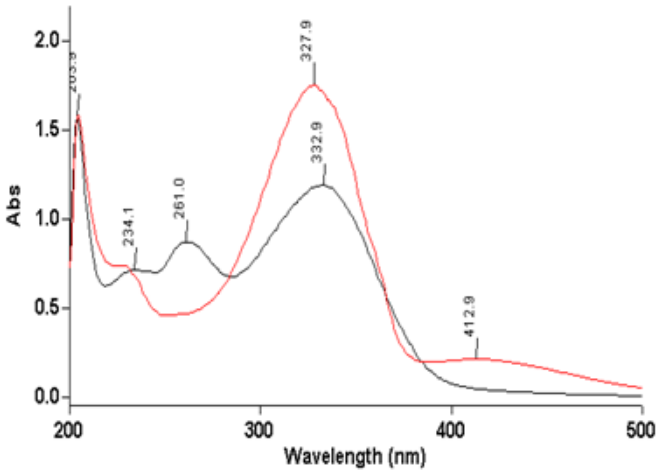

Figure 3.21. UV spectra of the azo-aldehyde **67a** (red) and the azoxy-aldehyde **68** (black), analysed in EtOH

Once **67a** and **68** had been differentiated on the basis of their UV and mass data, the small differences in their ^{1}H NMR spectra could be used as a tool to quantitatively determine the relative amounts of each compound in the crude product of future reactions. Thus, the chemical shift of the aldehyde proton of **68** resonated slightly

more downfield than the corresponding proton of **67a**. The ratio of the two products in the crude could then be determined by the relative integration of these two peaks.

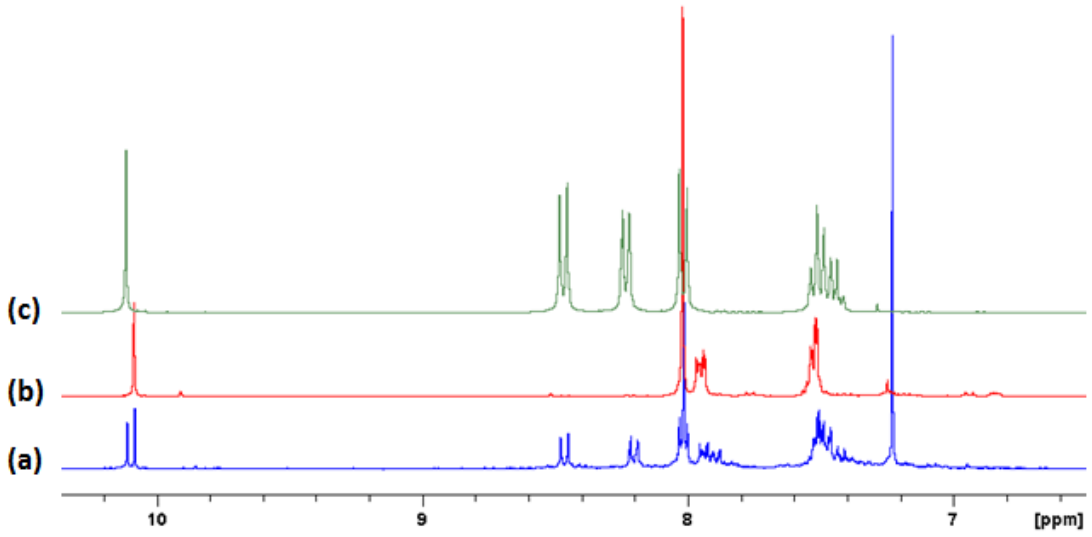

Figure 3.22. ^{1}H NMR spectra of crude product mixture containing both **67a** and **68** (blue), and purified **67a** (red) and **68** (green)

A search of the literature suggested it may have been possible to increase the yield of **67a** through deoxygenation of the isolated azoxy-aldehyde **68** using commercially available triethyl phosphite.[172] Thus, **68** was dissolved in a mixture of toluene and triethyl phosphite and heated under reflux for a period of 18 hr. ^{1}H NMR spectral analysis of the resulting crude product showed little conversion of the azoxy to the azo-aldehyde (~15%). The percentage conversion was improved incrementally up to a maximum of 50% upon heating of the reaction mixture under microwave irradiation for a period of up to 3 hr, at temperatures ranging from 75 ^{o}C to 170 ^{o}C. However, in all cases, the amount of the azo-aldehyde produced was offset by the significant degradation of the starting material and/or product under the extreme conditions.

The low isolated yield of **67a** and the failure to significantly enhance it by deoxygenation of **68**, coupled with the poor reproducibility of the reaction, led us to pursue a more efficient route to the desired azo-aldehyde **67a**.

3.2.4.ii Synthesis of the azo-aldehyde precursor 67a, starting from 4-(phenylazo)benzoic acid (71)

Having abandoned the route outlined in scheme 3.4, we adopted a procedure which described an alternative synthesis of **67a**,[173] the precursor to the oxime **52a** (scheme 3.6). Starting from commercially available 4-(phenylazo)benzoic acid (**71**) reduction with lithium aluminium hydride (LAH) yielded the primary alcohol **72a** as an orange solid in 66% yield. Following oxidation of **72a** with Dess-Martin periodinane (DMP), the desired aldehyde **67a** was obtained in 97% yield. In the case of both **72a** and **67a**, the ^{1}H NMR spectral data corresponded to that reported in the literature.[173] Finally, the oxime **52a** was obtained in 94% yield following condensation of **67a** with hydroxylamine hydrochloride in the presence of pyridine. The ^{1}H NMR spectra of **67a** and **52a** are shown below (figure 3.23). The azo-aldehyde **67a** is unusual in the sense that its spectrum displays a broad singlet at a chemical shift of 8.01 ppm which integrates for 4 protons. This is most likely due to poor resolution of the signals of two pairs of equivalent protons. Formation of the oxime from the aldehyde was confirmed by loss of the signal for the aldehyde proton at 10.11 ppm, and the appearance of a new signal characteristic of an oxime imino proton at 8.20 ppm.

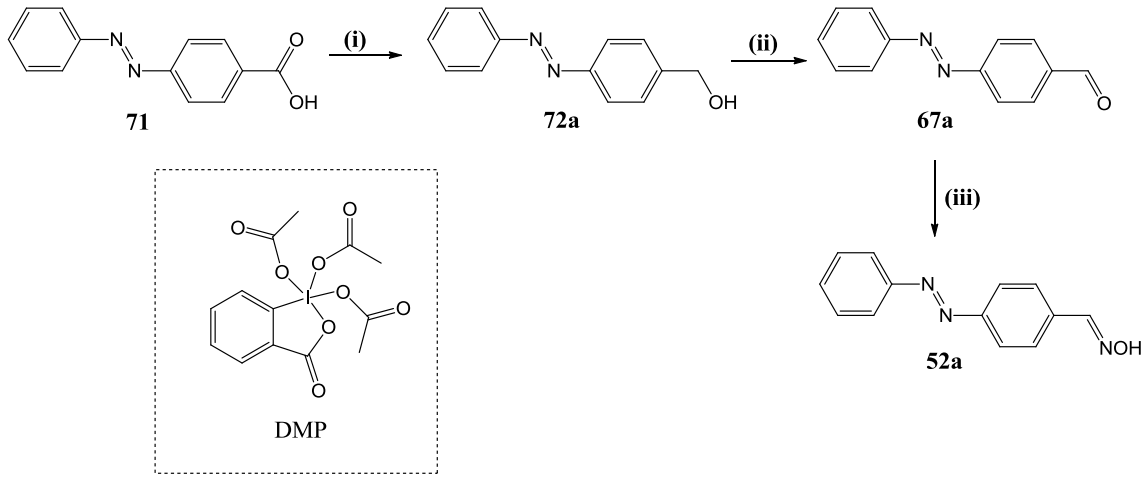

(i) LAH, THF, 30 min

(ii) DMP, DCM, 1 hr

(iii) $NH_2OH.HCl$, pyridine, EtOH, MW (P_{max} = 300 W, T = 120 °C), 1 hr

Scheme 3.6. Optimised synthesis of the azobenzene-oxime **52a**

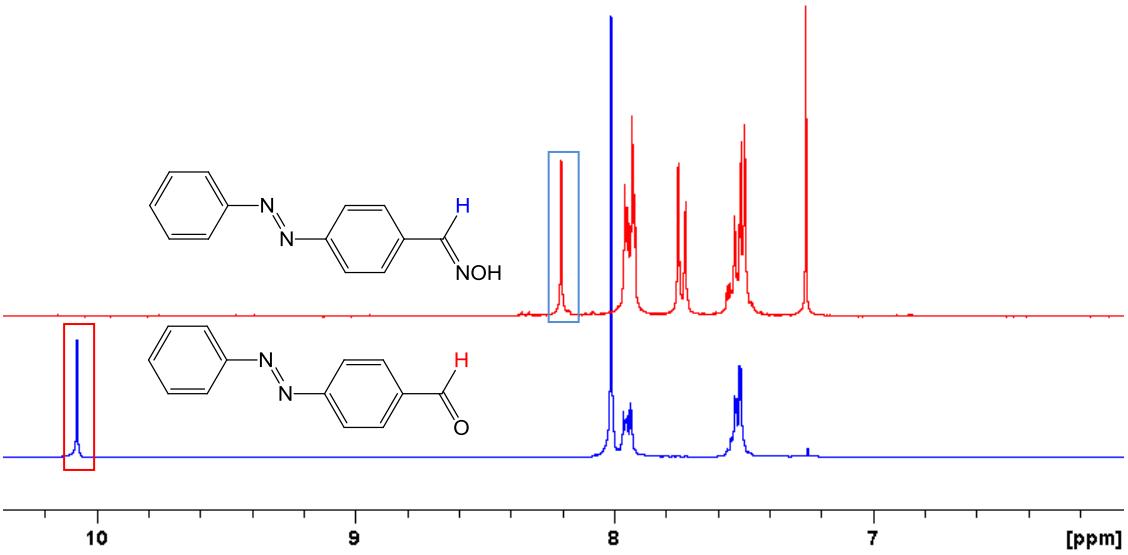

Figure 3.23. ^{1}H NMR spectra of the azo-aldehyde **67a** (blue) and the azo-oxime **52a** (red)

3.2.4.iii Synthesis of azo-aldehyde precursor 67b

Synthesis of the regioisomeric oxime **52b** required initial preparation of the *meta*-disubstituted azo-aldehyde **67b**. This aldehyde was arrived at by a slightly different route to that used to access **67a**. 3-(Phenylazo)benzoic acid is not commercially available, and the synthetic route adopted started with condensation between nitrosobenzene (**73**) and the substituted aniline **74b** in the presence of acetic acid (scheme 3.7). Chromatographic separation of the crude product mixture gave the desired product **72b** as an orange oil in 82% yield. The oxime **52b** was obtained following oxidation to the aldehyde **67b**, and subsequent condensation with $NH_2OH.HCl$ under microwave irradiation gave the final product **52b** as an orange solid, with a total yield of 85% over the two steps.

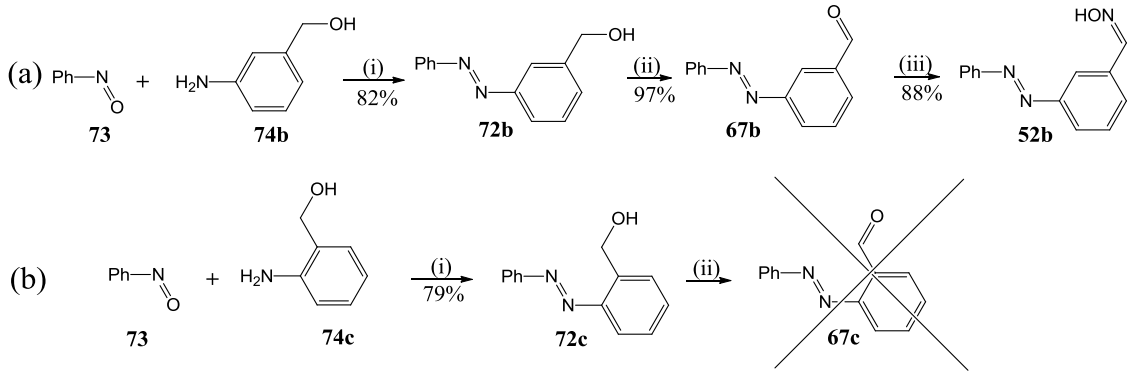

(i) CH_3COOH, 0 ^oC for 1 hr, then rt for 3hr for **72b**, 18 hr for **72c**

(ii) DMP, DCM, 1hr

(iii) $NH_2OH.HCl$, pyridine, EtOH, MW (P_{max} = 300 W, T = 120 ^oC), 1 hr

Scheme 3.7. (a) Synthesis of the oxime **52b**; (b) attempted synthesis of oxime **52c**

Efforts to synthesise the regioisomeric azo-oxime **52c** proved unsuccessful. While the primary alcohol **72c** could be obtained under the same conditions used for **72b** (albeit with a longer reaction time of 18 hr), attempted oxidation to the desired aldehyde **67c** with DMP resulted in degradation of the starting material. This was evidenced in the ^1H NMR spectrum of the crude product, which showed no characteristic aldehyde peaks. Additionally, over the course of an hour, the colour of the reaction mixture changed from orange, which is characteristic of azobenzene compounds, to black, indicating loss of the azo group.

3.2.6 Cyclisation reaction of 73c

Since the primary alcohol **72c** was unsuitable for oxidation to the corresponding aldehyde, we attempted instead to exploit it for the synthesis of the azo-alkyne **75**, which is analagous to **54** but has a longer linker between the phenyl ring and the alkyne (scheme 3.8). Thus, nucleophilic substitution of propargyl bromide with **72c** was attempted. This reaction was carried out in the presence of NaH to deprotonate the alcohol proton, with a view to subsequent nucleophilic attack of propargyl bromide by the alkoxide anion. However, the ^1H NMR spectrum of the resulting crude product showed no evidence of the desired alkyne **75**. Also, significantly, the colour of the

solution changed from orange to brown during the reaction, suggesting reactivity involving the N=N group.

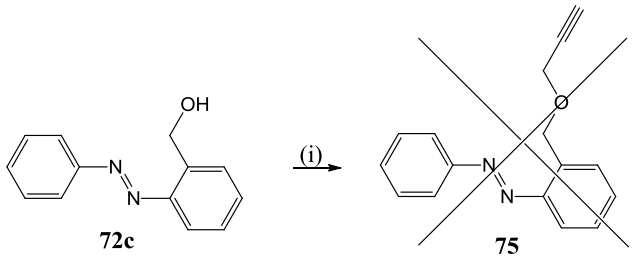

(i) $BrCH_2C(CH)$, NaH, DMF, 1 hr

Scheme 3.8. Attempted reaction to form the azo-alkyne **75**

A search of the literature uncovered an interesting reaction in which an electron deficient azo group undergoes nucleophilic attack by a primary alcohol (scheme 3.9).[174] This led us to conclude that an intramolecular attack of the alcohol (alcoholate anion) of **72c** on the adjacent azo group may be preferential to intermolecular reaction with propargyl bromide. This hypothesis was supported by the results of two trial reactions; one in which **72c** was heated under reflux in DMF in the absence of base for 1 hr, and another in which it was stirred with NaH in DMF under argon for 1 hr. In both cases, the ^{1}H NMR spectra of the sample following work-up corresponded to that observed for the crude product resulting from the attempted synthesis of the propargyl ether **75**. In light of this, we propose that when a strong base is present, an intramolecular cyclisation of **72c** occurs following deprotonation of the alcohol group. The resulting alkoxide ion attacks the adjacent azo group, ultimately yielding the heterocylic product **76** [scheme 3.10 (a)]. In the absence of base, thermal activation is sufficient to allow attack of the azo group by the alcohol, which loses its proton after the addition [scheme 3.10 (b)].

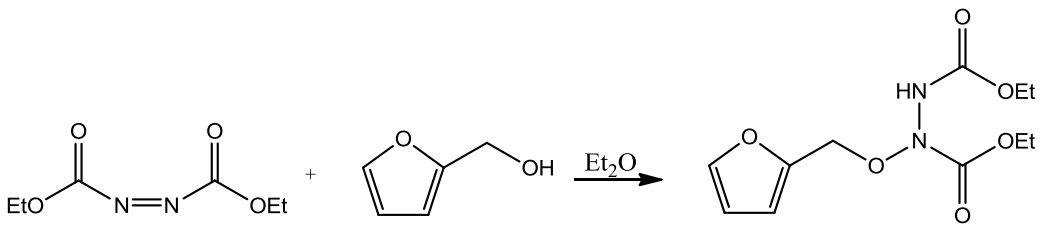

Scheme 3.9. Nucleophilic attack of an azo group by an alkoxide ion[174]

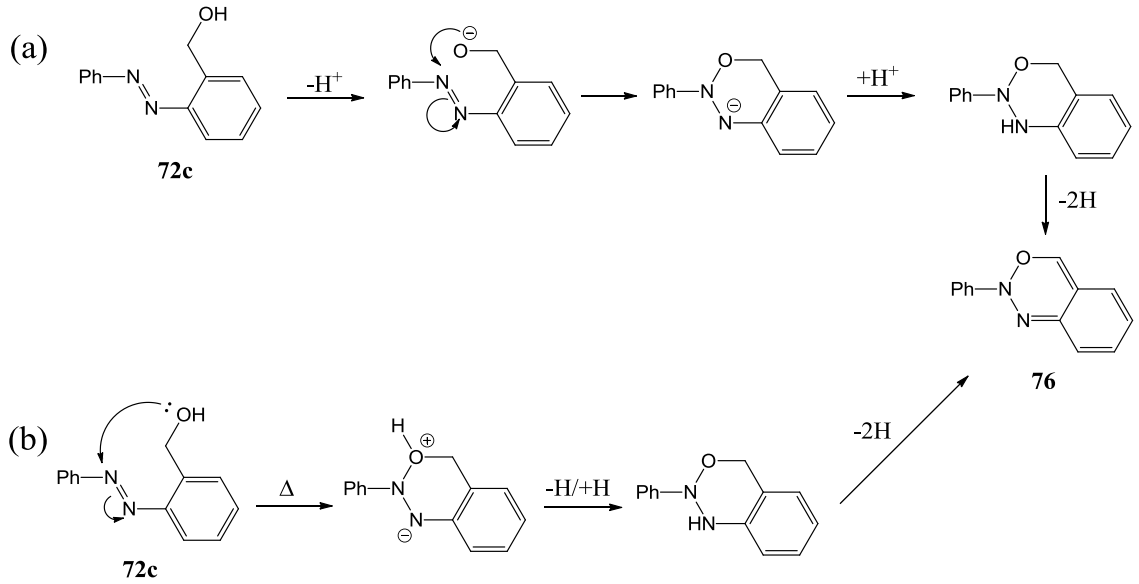

Scheme 3.10. Proposed mechanism of formation of the heterocyclic product **76** (a) with and (b) without base

In addition to mass analysis, formation of **76** is supported by ^{1}H, ^{13}C DEPTQ and $^{1}H^{1}H$ COSY NMR spectral data. The ^{1}H NMR spectrum of the product (figure 3.24) displays a narrow doublet at a chemical shift of 8.39 ppm, which corresonds to the proton of the heterocycle adjacent to the oxygen atom. The DEPTQ NMR spectrum supports formation of a product containing three quaternary carbon atoms (figure 3.25), while the $^{1}H^{1}H$ COSY spectrum in particular proved useful in the characterisation of the product; the coupling between relevant protons is highlighted in figure 3.26.

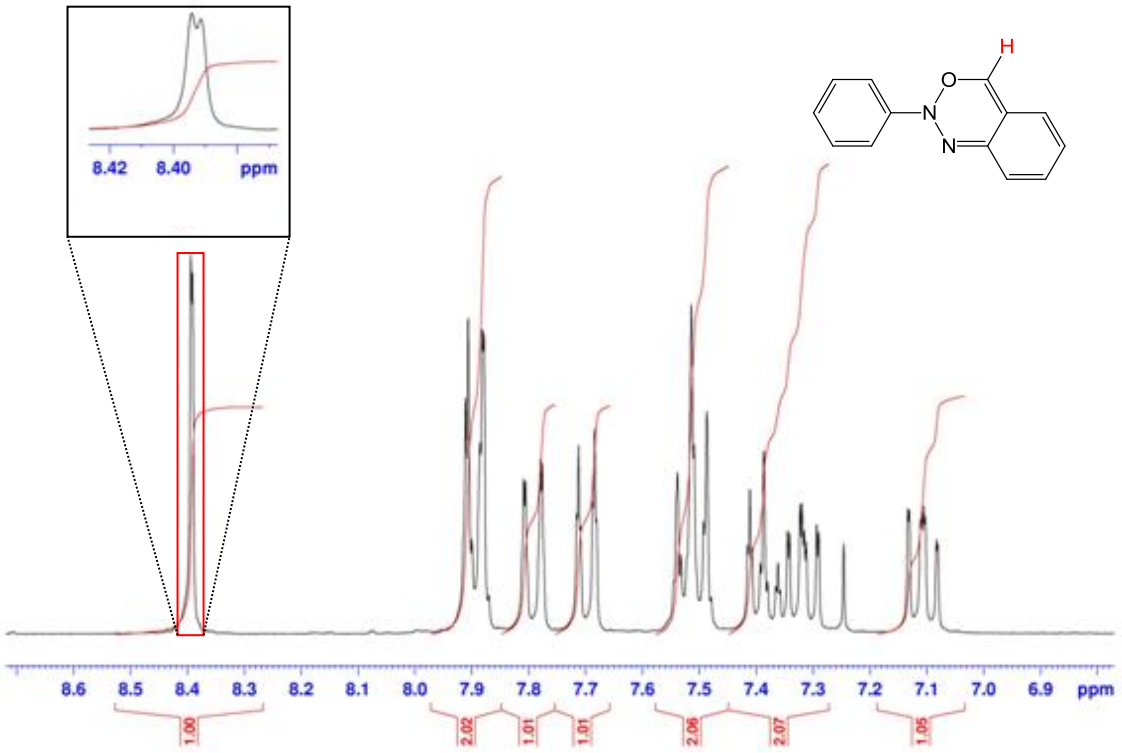

Figure 3.24. ^{1}H NMR spectrum of **76**

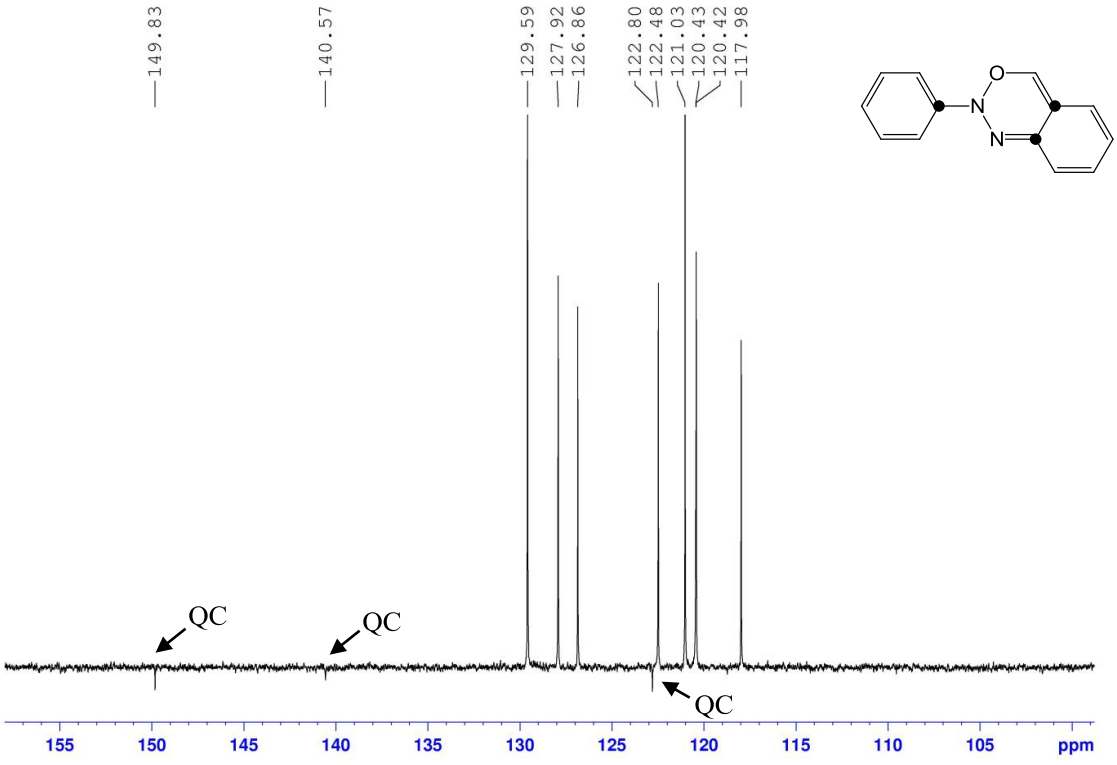

Figure 3.25. DEPTQ NMR spectrum of **76**

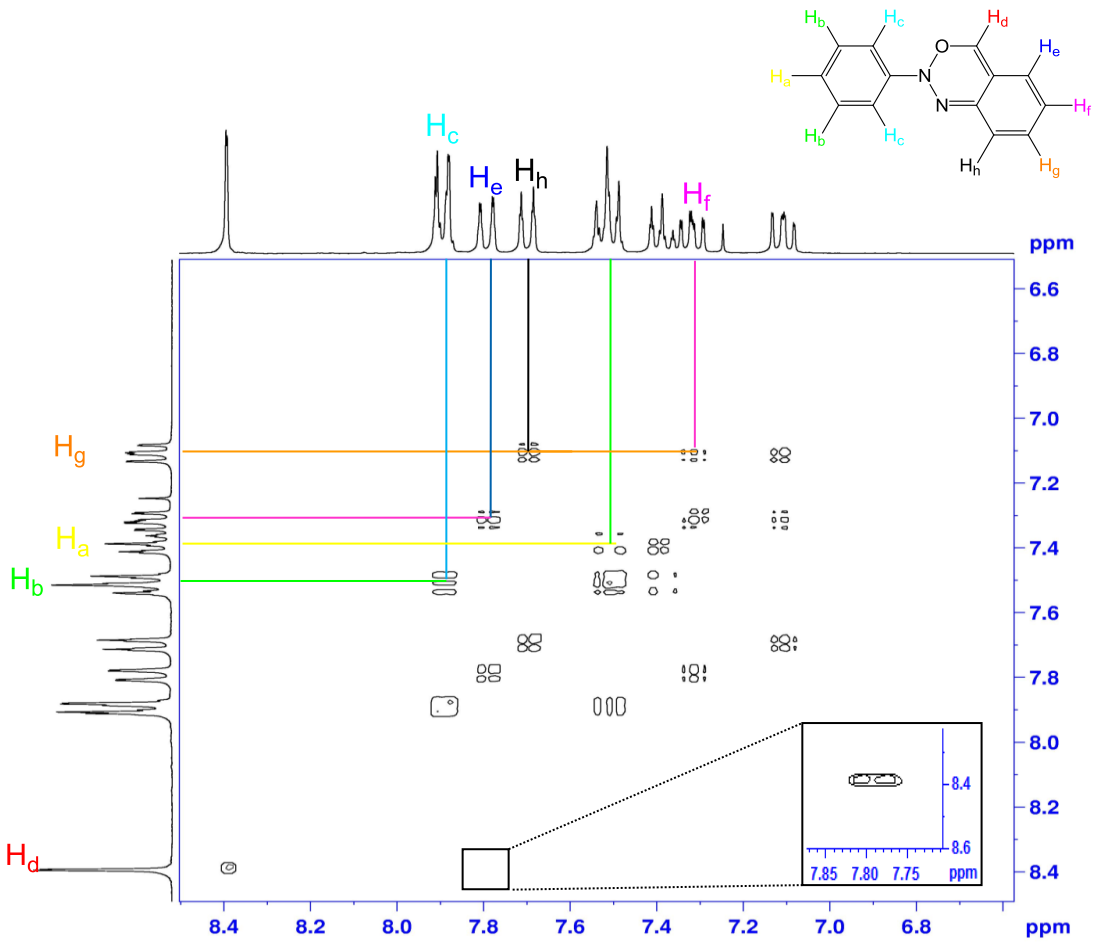

Figure 3.26. ^{1}H COSY NMR spectrum of **76**, with an expansion of a region inset highlighting coupling between protons H_d and H_e

3.2.7 Small molecule cycloadditions with oximes 52a & 52b

Before considering conjugation to DNA of the nitrile oxides **78a** and **78b**, to be derived *in situ* from the oximes **52a** & **52b** respectively, we were interested in a simple NOAC study of the azo-oximes **52**. In each case, the nitrile oxide was first generated *in situ* by treatment of the parent oxime with Ch-T in aq. EtOH and trapped with propargyl phenyl ether (**14**) in a one-pot reaction, forming the cycloadducts **77a** and **77b** as orange solids with isolated yields of 89% and 46% respectively (scheme 3.11).

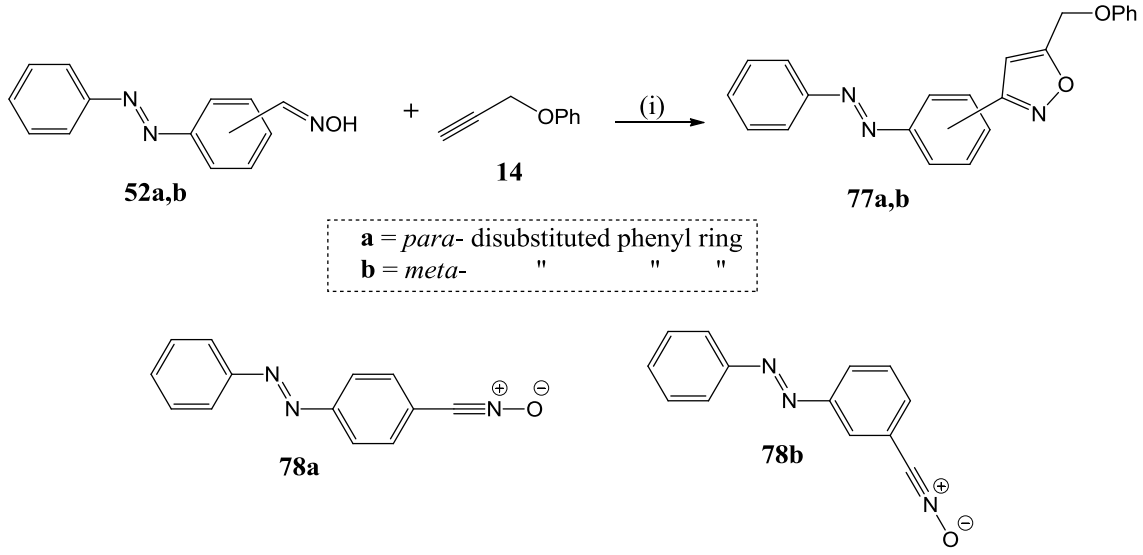

(i) Ch-T, EtOH/H_2O, 40 ^{o}C, 1 hr

Scheme 3.11. Synthesis of cycloadducts **77a** and **77b**

The high yield of the *para*-disubstiuted cycloadduct **77a** in relation to the *meta*-disubstituted product **77b** is most likely due to electronic effects. The nitrile oxide functionality of the *para*-disubstituted azobenzene **78a** is in conjugation with the entire azobenzene system; it may therefore lose electron density through the π system to the azo group, which has been shown previously to have some electrophilic character (section 3.2.6, page 75). As the NOAC involves the transfer of electrons from the HOMO of the dipolarophile to the LUMO of the dipole,[56] any loss of electron density from the latter will activate it towards cycladdition. Since the nitrile oxide group of the *meta*-disubstituted azobenzene **78b** is not in conjugation with the azo group, this activation does not occur; these electronic effects may be responsible for the yield of **77a** being significantly larger than that of **77b**.

The ^{1}H NMR spectra of the cycloadducts **77a** and **77b** are shown in figure 3.27. In each case, the signals for the isoxazole proton at ~6.7 ppm and the methylene protons at approximately ~5.2 ppm are characteristic of 3,5-disubstituted isoxazoles. The cycloadduct **77b** displays more signals in the aromatic region due to its lack of symmetry.

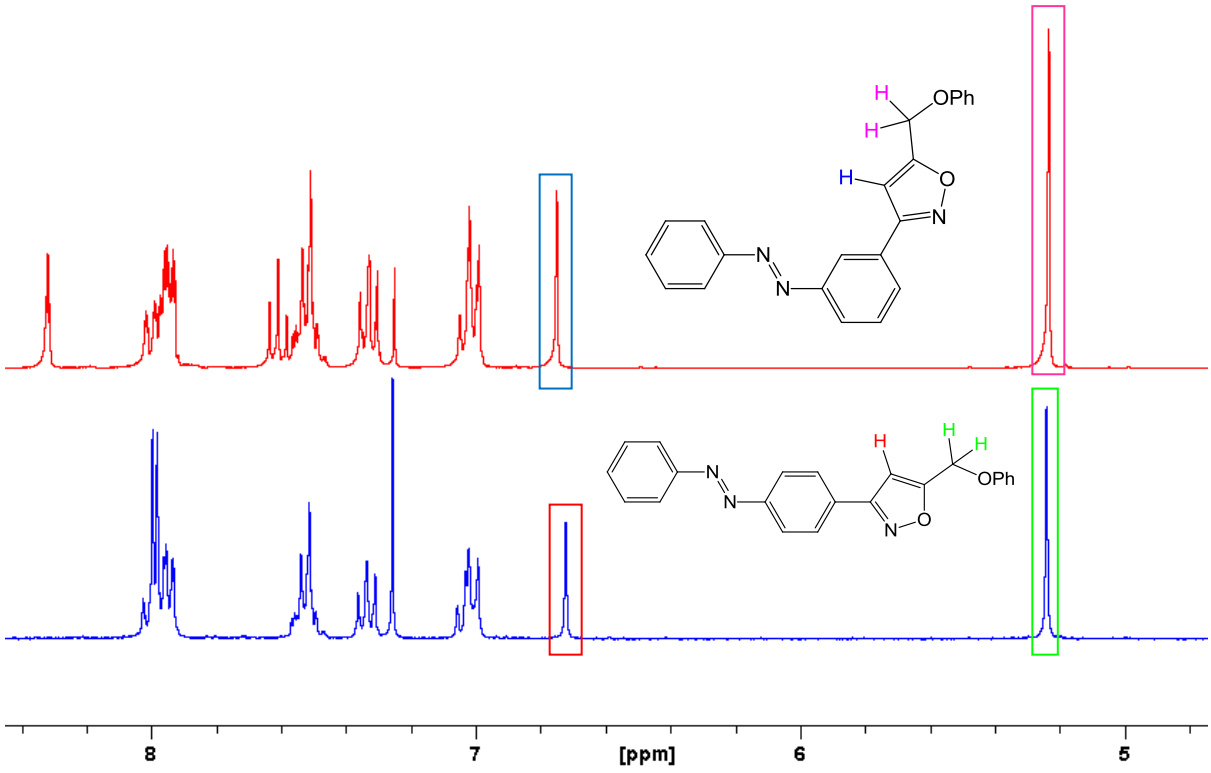

Figure 3.27. ^{1}H NMR spectra of cycloadducts **77a** (blue trace) and **77b** (red trace)

3.2.8 Site specific introduction of the azobenzene photoswitch to DNA

3.2.8.i Modification at the 3'-terminus

To begin to explore the application of click cycloaddition chemistry to the synthesis of nucleic acid derivatives bearing photoresponsive groups, we chose commercially available CPG supported 2'-*O*-propargyl uridine (**79**) as starting material. We believed the propargyl moiety borne on the ribose would function as a dipolarophile. Whilst it may be more sterically hindered than the propargyl phenyl ether used in the small molecule study, we expected it to be sufficiently available to function to trap the transient nitrile oxide. The resin loaded propargyl uridine also has the 5'-OH group available for oligonucleotide chain extension.

Agitation of a suspension of **79** in the presence of 30 equiv. of the oxime **52a** and 30 equivalents of Ch-T, in aqueous ethanol overnight at room temperature, furnished the isoxazole cycloadduct **81a** by way of NOAC to the transient dipole **78a**. Cleavage from the resin under standard conditions ($MeNH_2$, 65 ^{o}C, 30 min) yielded an aqueous

sample of the conjugate **82a** (scheme 3.12); analysis by RP-HPLC showed that the reaction proceeded in near quantitative yield (figure 3.28).

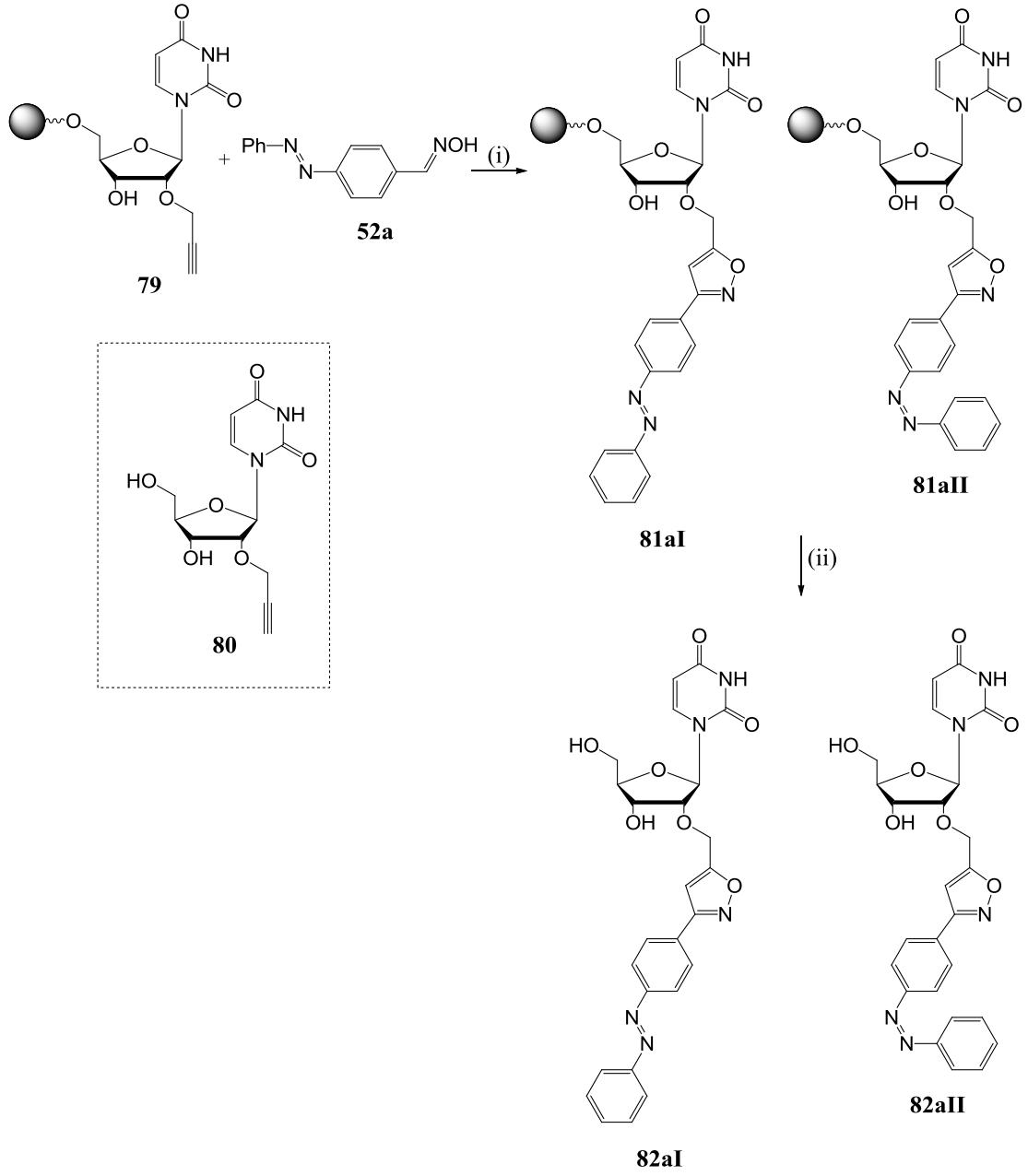

(i) Ch-T, EtOH/H_2O, rt, 18 hr

(ii) $MeNH_2$, 65 ^oC, 30 min

Scheme 3.12. Solid phase cycloaddition to form the conjugates **82a**

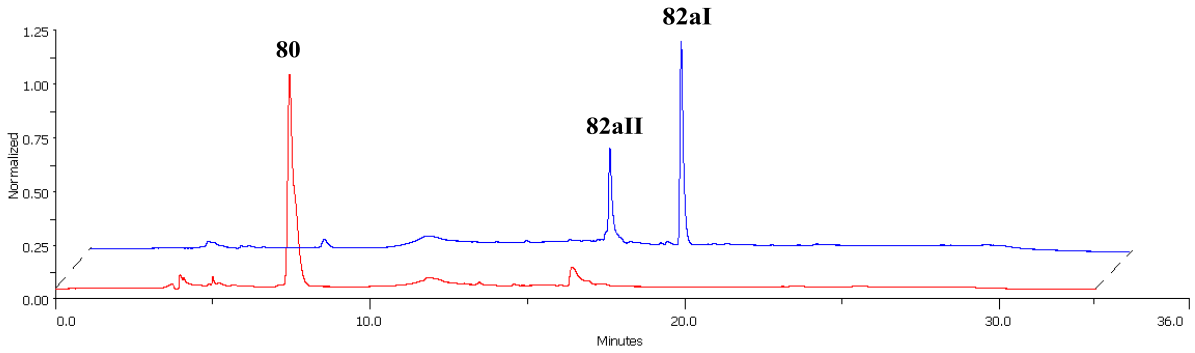

Figure 3.28. Overlaid chromatograms of the azobenzene-labelled nucleoside **82a** (blue trace) and the starting material reference, 2'-*O*-propargyl uridine (**80**) (red trace)

Significantly, the chromatogram of **82a** shows evidence of two products of differing retention time (**82aI** and **82aII**); one with the pendant azobenzene in the *cis* conformation and one where the substituents around the azo functionality have a *trans* relationship. Since the HPLC system was equipped with a diode-array detector (DAD), it was possible to use the software to analyse the UV profile of each individual peak within the chromatogram. Thus, it was apparent that the later eluting, major product (**82aI**) had a local maximum at 325 nm, whereas the early eluting, minor product (**82aII**) did not absorb at this wavelength (figure 3.29).

Under the classifications for azobenzenes described by Rau[137] (see section 3.1.2.iv, page 49), our product can be characterised as the 'azobenzene type'. The *trans* isomers of this class are known to have a λ_{max} in the region of ~325 nm, while the *cis* isomers do not absorb light in this region. From this it was possible to conclude that in the major product (**82aI**) the azobenzene moiety had *trans* configuration, and in the minor product (**82aII**) the azo group had *cis* configuration.[†]

[†] Any future compound numbers which are suffixed by '**I**', will denote the pendant azobenzene in the *trans* geometry, while those which are suffixed by '**II**' will refer to *cis* geometry

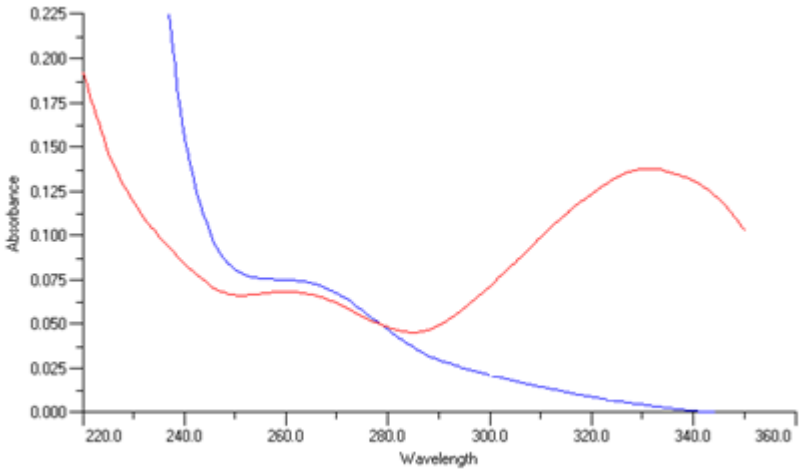

Figure 3.29. UV spectra of the *trans*- and *cis*-azobenzene appended nucleoside conjugates **82aI** (red) and **82aII** (blue) of **82a**

Having proved the concept that nucleic acid derivatives bearing an azobenzene photoswitch could be prepared by NOAC chemistry on the solid phase, we attempted to access a photoswitch-bearing oligonucleotide by standard phosphoramidite coupling chemistry on a DNA synthesiser starting from the solid-supported cycloadduct **81a** (scheme 3.13). Firstly, the short 3-mer **83a** was grown; thymidine monomers were selected as these are the most 'simple' and require no protecting group. Standard conditions for automated DNA synthesis were adopted, and following cleavage of the crude product from the resin, analysis of the resulting aqueous sample **84a** by RP-HPLC showed that all the starting material had been consumed. MALDI-TOF MS analysis confirmed formation of the desired product. Thus, the presence of the isoxazole-linked azobenzene did not interfere negatively with oligonucleotide chain extension.

With this information to hand, we endeavoured to grow an oligonucleotide containing a mixture of natural bases, with their standard protecting groups. Starting from the solid-supported **81a**, the mixed 4-*mer* **85a** was grown. Deprotection and cleavage from the resin gave an aqueous solution of **86a**; HPLC and MALDI-TOF MS analysis confirmed quantitative formation of the desired product. In the case of both the 3-mer **84a** and the mixed 4-mer **86a**, the chromatograms showed evidence of both the *cis* and *trans* isomers of the azobenzene-bearing oligonucleotides (figure 3.30). The successful syntheses of these oligonucleotides suggest that, within the innate

restrictions of solid phase synthesis, *e.g.* length of sequence, any desired sequence of DNA can be made bearing the isoxazole-azobenzene moiety at the 3'-terminus.

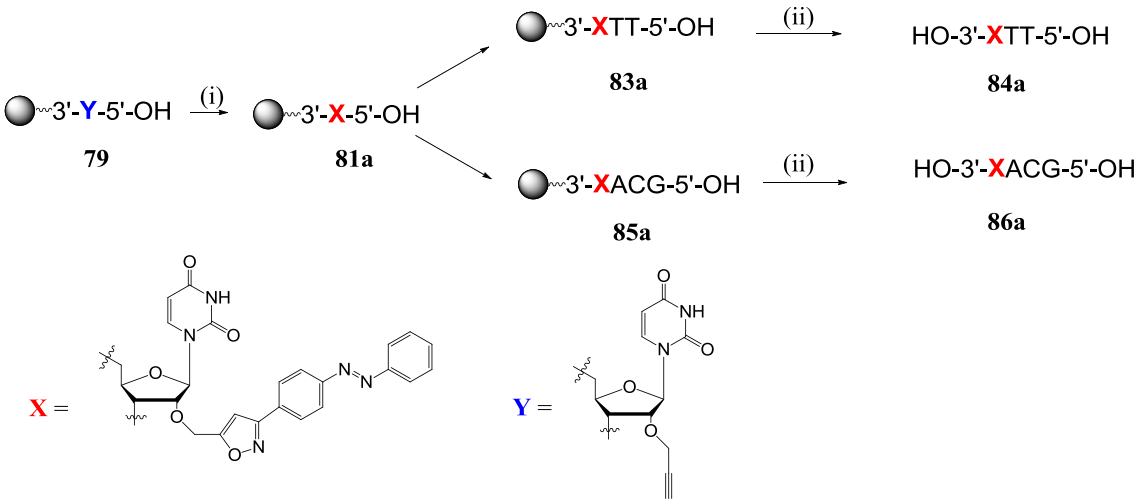

(i) Ch-T, **52a**, EtOH/H_2O, 18 hr, rt

(ii) $MeNH_2$, 65 °C, 30 min

Scheme 3.13. Synthesis of 3'-modified azobenzene-oligonucleotide conjugates **84a** and **86a**

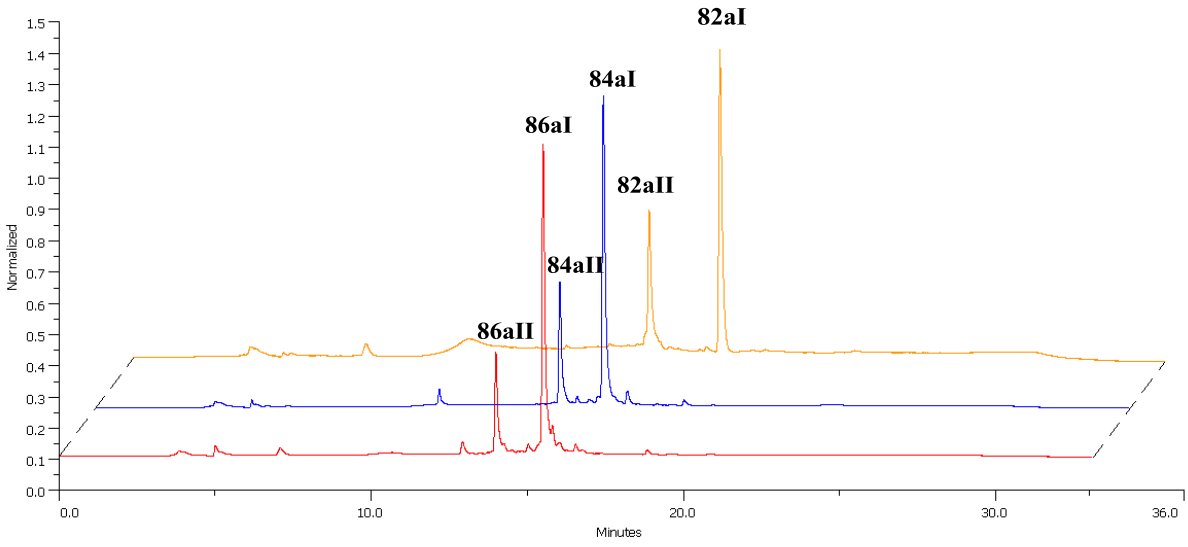

Figure 3.30. HPLC traces of azobenzene-labelled nucleosides/oligonucleotides; starting material reference, **82a** (orange trace), 3-*mer*, **84a** (blue trace), and mixed 4-*mer*, **86a** (red trace)

3.2.8.ii Modification at the 5'-terminus

To broaden the scope of this chemistry, incorporation of the azobenzene moiety at the 5' end and in the middle of an oligonucleotide chain was explored. The approach adopted to achieve these goals is summarised in scheme 3.14. Commercially available 2'-*O*-propargyl uridine phorphoramidite (**88**) was coupled to CPG-T_4 (**87**). Manual solid phase coupling[‡] was considered necessary as the commercial pack size of the phosphoramidite (100 µmol) was deemed too small to install on the DNA synthesiser under standard dilution conditions. The alkyne-functionalised oligonucleotide was then installed on the synthesiser and standard oxidation, capping and deblocking procedures were carried out. At this point the propargyl bearing 5-*mer* **89** was removed from the system and a small portion was cleaved from the resin to act as a reference before any further steps were attempted. HPLC and MALDI-TOF MS analysis of the cleaved oligonucleotide **90** confirmed quantitative formation of the desired product. Cycloaddition was carried out on the solid phase with the nitrile oxide **78a** (generated *in situ* from the oxime **52a** by the Ch-T protocol) using the previously optimised conditions, yielding the resin-bound cycloadduct **91a**. As with earlier examples, HPLC analysis of an aqueous sample of the cleaved cycloadduct **92a** demonstrated complete consumption of the starting material, and formation of both *cis* and *trans* isomers of the azobenzene-modified oligonucleotide. As before, MALDI-TOF MS analysis confirmed formation of the desired product. Thus, a strategy for the modification of oligonucleotides at the 5'-terminus was demonstrated.

[‡] For a description of manual phosphoramidite coupling on the solid phase, see section 2.2.3, page 34

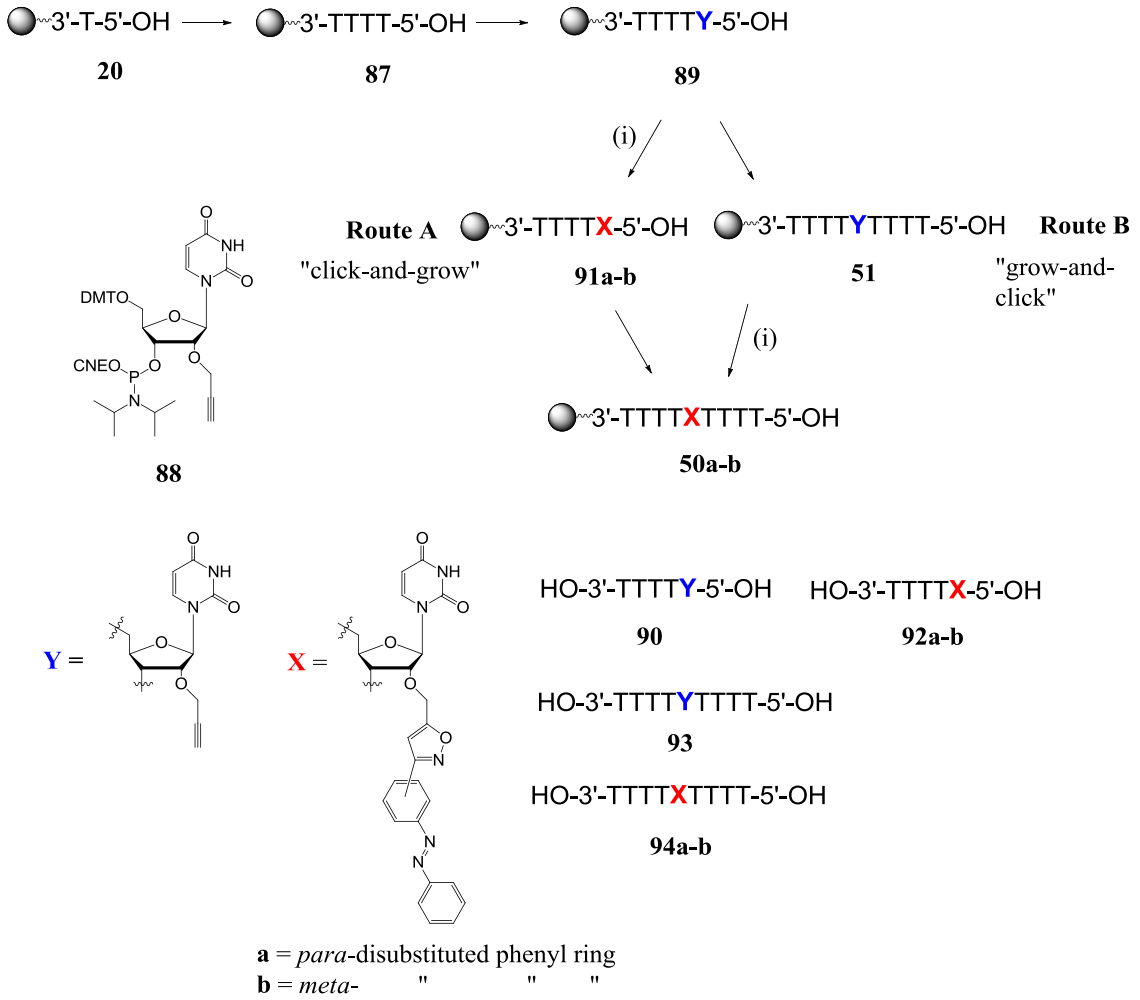

Scheme 3.14. Synthesis of the azobenzene modified oligonucleotides **50a-b** by routes A and B

3.2.8.iii Modification at an internal position

Two strategies were considered for the prepartion of oligonucleotide substrates bearing the azobenzene photoswitch at an internal position. These we dubbed the 'grow-and-click' or the 'click-and-grow' approach. Employing the latter methodology, the azobenzene-conjugated 5-mer **91a** was installed on the DNA sythesizer as a substrate from which the 9-mer **50a** was grown. Characterisation of the cleaved product **94a** by HPLC and MALDI-TOF MS analysis confirmed succesful synthesis of an oligonucleotide bearing a pendant azobenzene moiety in the middle of the chain.

The alternative, 'grow-and-click' approach has also been demonstrated. Following manual coupling of the phosphoramidite **88** to CPG-T_4 (**87**), the resin-supported product **89** was installed on the DNA synthesiser and the propargyl bearing oligonucleotide **51** was grown. Cycloaddition between **51** and the nitrile oxide **78a**, which was prepared *in situ* following reaction of the oxime **52a** and Ch-T, successfully yielded the cycloadduct **50a**. Significantly, even though in this case the dipolarophile was borne in the middle of the sequence, no decrease in yield was observed with regard to the corresponding end-modified oligonucleotides **81a**, **83a** and **85a**. As expected, the HPLC trace of the cleaved product **94a** prepared by the 'click-and-grow' approach was identical to that prepared by the 'grow-and-click' approach.

Cycloaddition of **51** with the *in situ* generated *meta*-disubstituted nitrile oxide **78b** was carried out using the same experimental conditions used for the *para*-disubstituted isomer **78a**. Cleavage of the product **50b** from the resin yielded an aqueous sample of **94b**, which was characterised by HPLC (figure 3.31) and MALDI-TOF MS analysis. Comparison of the chromatograms of the regioisomeric products (**94a** and **94b**) shows evidence of both *cis* and *trans* isomers; the retention time of each was almost identical for both (**94a** and **94b**). Significantly, the yield of **50b** (~80% conversion) was noticably less than that of the isomeric cycloadduct **50a** (~95% conversion), in which the azo group is *para*- to the dipole functionality. This observation is directly parallel to the attenuated yield observed for formation of the cycloadduct **77b** in comparison to **77a** (section 3.2.7, page 79).

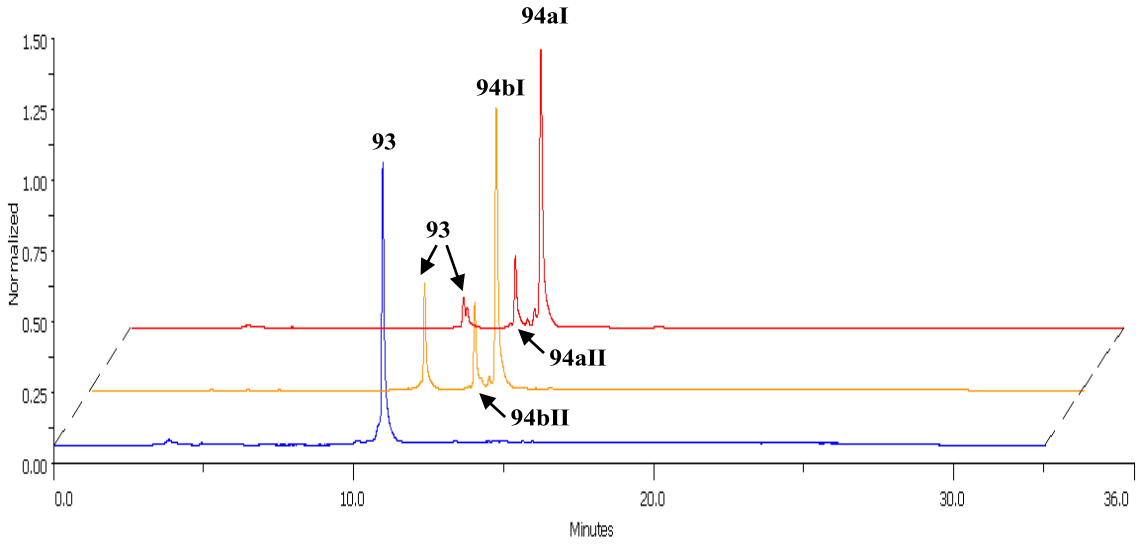

Figure 3.31. HPLC traces of crude oligonucleotide reaction products bearing an azobenzene photo-switch at an internal position; T_9–alkyne starting material reference **93** (blue), *meta*-disubstituted cycloadduct **94b** (orange), and *para*-disubstituted cycloadduct **94a** (red)

3.2.9 Photochemical characterisation of modified oligonucleotides 94a and 94b

A trawl of the literature reveals few examples in which the photochemistry and/or isomerisation kinetics of azobenzenes bearing a substituent in a position *meta*- to the azo group have been investigated. Fewer reports still directly compare these properties in isomeric 1,3- and 1,4-disubstituted azobenzenes. This is perhaps surprising, considering the distinctly different electronic characteristics one might expect of such regioisomers. We were therefore interested in exploring the photoresponsive properties of the novel azobenzene-modified oligonucleotides **94a** and **94b**. In particular, we were keen to explore the influence, or otherwise, of the conjugating isoxazole ring between the azobenzene units and the oligonucleotide chain, and thus wished to compare the characteristics of **94a** and **94b** to similar compounds reported in the literature.

Prior to examination of their photochemical properties, the crude samples of **94a** and **94b** (synthesised on a 1 µmol scale), were purified by preparative RP-HPLC to obtain an isolated sample of the *trans* isomer of each species. These isolated fractions were stored in brown eppendorf tubes to prevent light induced photo-isomerisation from the *trans* to the *cis* form.

The UV spectra of pure **94aI** and **94bI** were recorded, in turn, and a difference in the position of the π–π* absorption band of the pendant azobenzene moiety of each compound was noted. A smaller difference in the position of the n–π* band was also observed (table 3.2). The π–π* transition for the parent *cis* azobenzene is known to have a λ_{max} at 276 nm, and since these compounds' photochemistry closely resembles that of the parent azobenzene, the π–π* absorption bands for **94aII** and **94bII** are most likely overlapping with the local maximum absorbance of the nucleic acid portion of the molecule, which strongly aborbs light at a wavelength of 260 nm. The difference in the λ_{max} of the π–π* absorption band of **94aI** and **94bI** is evidence that the azobenzene portion of these two regioisomeric conjugates has different electronic character.[137]

Compound	***trans*-isomer**		***cis*-isomer**	
	π–π*	**n–π***	**π-π***	**n–π***
94a	336 nm	433 nm	-	433 nm
94b	323 nm	428 nm	-	428 nm

Table 3.2. Position of π–π* and n–π* absorbance bands for *trans* and *cis* isomers of azobenzene modified oligonucleotides **94a** and **94b**

In order to achieve the irradiated (Irr) photostationary states of the azobenzene-oligonucleotide conjugates **94a** and **94b**, the samples were exposed, in turn, to near-UV irradiation from a medium pressure Hg-Arc lamp at 366 nm. Irradiation at this wavelength induces excitation of the π–π* transition, culminating in *trans-cis* isomerisation of the azobenzene moiety. In each case, the degree of isomerisation was monitored by the decrease in absorption observed at 325 nm. This wavelength was chosen because, as is shown in table 3.2 and figure 3.32, both **94aI** and **94bI** have a λ_{max} at or near this wavelength, whereas **94aII** and **94bII** do not absorb light at all in this region. Therefore, the decrease in absorption at this wavelength is a useful qualitative tool to measure the degree of *trans–cis* isomerisation over time. After irradiation for a period of 10 min, no further decrease was observed in the intensity of this absorption (figure 3.33). Dark-adapted (DA) photostationary states were induced by excitation of the n-π* transition following irradiation at 436 nm for 2 min. Within

this time, restoration of the original absorbances of each sample at 325 nm was observed.

A sample of **94a** in both the Irr and DA photostationary states was analysed by RP-HPLC, with detection at 260 nm. In each case, the relative peak areas of **94aI** and **94aII** were used to determine the mole fraction of **94aII** (χ_{cis}) in the photostationary state. While a 'truer' value for χ_{cis} would result from HPLC detection at the isosbestic wavelength[§] of **94aI** and **94aII**, analysis of the UV-Vis spectral data of these compounds revealed negligible difference between the molar absorptivity (ε) of **94aI** and **94aII** at the detection wavelength of 260 nm. A parallel strategy was used to obtain the χ_{cis} values for **94b** in the photostationary state; these results are summarised in table 3.3. The HPLC traces of **94a** in the Irr and DA states are also shown (figure 3.34).

(a)

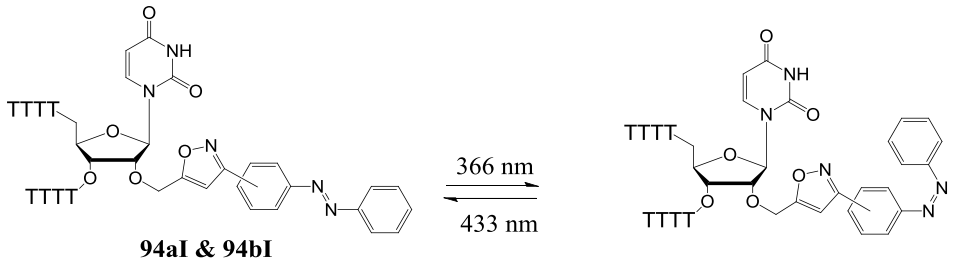

94aI & 94bI **94aII & 94bII**

(b)

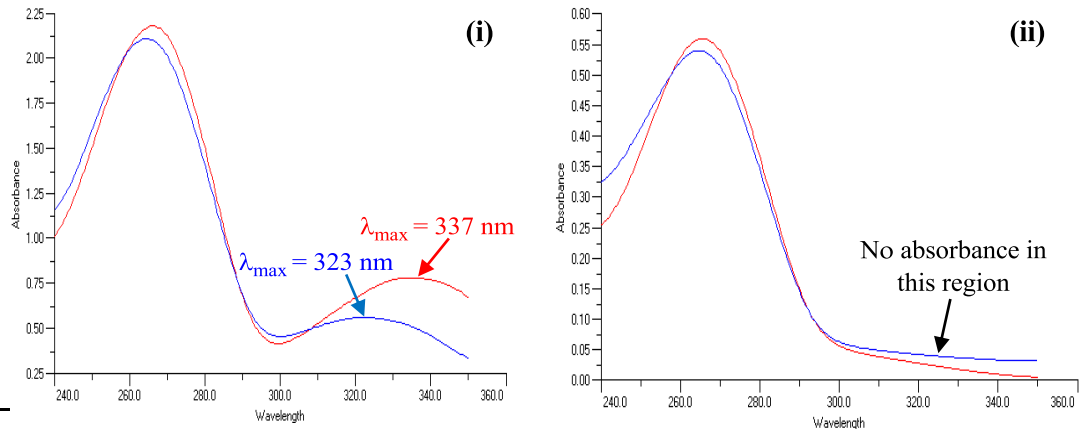

[§] An isobestic wavelength is a specific wavelength at which two chemical species have the same molar absorptivity (ε)

Figure 3.32. (a) Photo-isomerisation of azobenzene-modified oligonucleotides **94a** and **94b**; (b) UV spectra of (i) **94aI** (red) and **94bI** (blue), and (ii) **94aII** (red) and **94bII** (blue)

Compound	χ_{cis}	
	Irr	DA
94a	0.731	0.150
94b	0.825	0.188

Table 3.3. Mole fractions of *cis*-azobenzene appended oligonucleotides **94aII** and **94bII** (χ_{cis}) in the Irr and DA photostationary states at 26 °C.

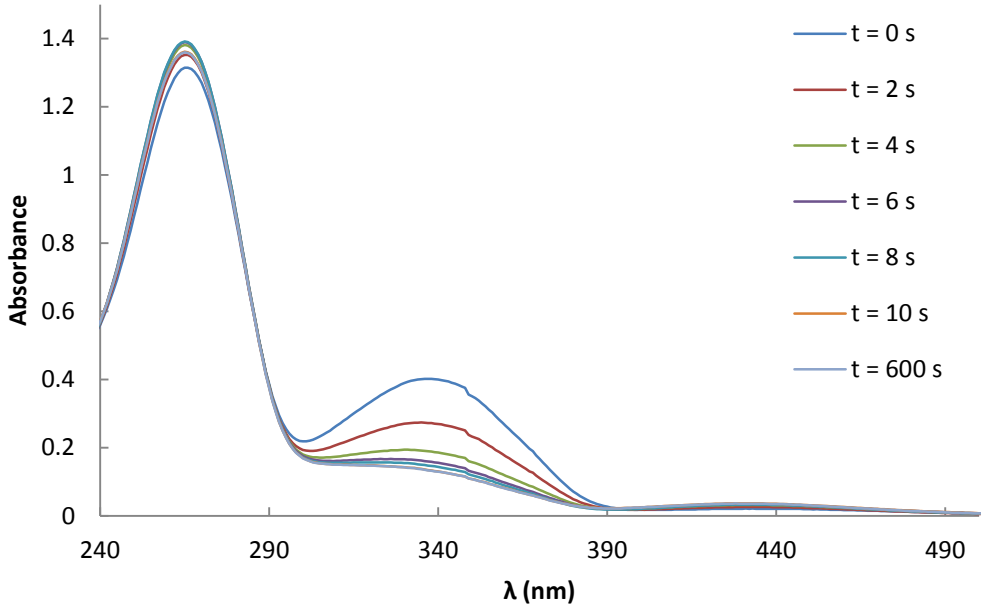

Figure 3.33. Overlaid UV/Vis spectra of **94a** upon irradiation at 366 nm for 0, 2, 4, 6, 8, 10 and 600 s; data for **94b** included in appendix (section 6.2, page 183).

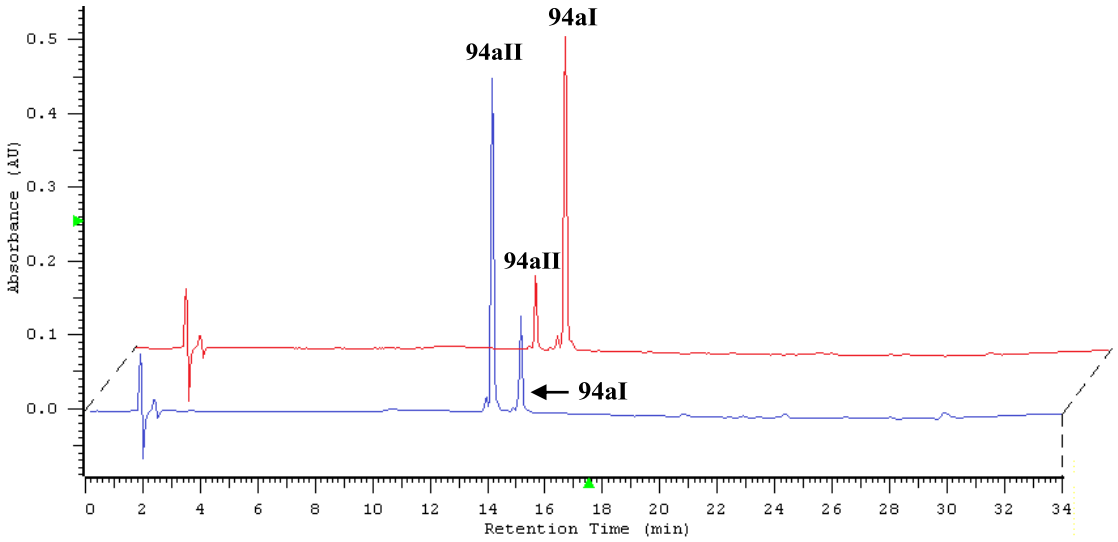

Figure 3.34. Overlaid HPLC traces of **94a** in the Irr (blue)and DA (red) photostationary states; data for **94b** included in appendix (section 6.2, page 183)

3.2.10 Thermal stability studies of 94aII and 94bII

The stability of the *cis* isomer of modified azobenzenes is an important criterion to consider in applications which require a bistable photoswitch. Many examples of photoresponsive biomolecules display efficient photoswitching between *trans* and *cis* forms, but the instability of the latter limits their effectiveness. The type and position of sustituent(s) on the azobenzene moiety has been shown to have a significant effect on both the photochemical and kinetic properties of these compounds (see section 3.1.2.iv, pages 49-52). Thus, the stabilities of the irradiated oligonucleotides **94a** and **94b** towards thermal *cis*-*trans* isomerisation were investigated.

Following irradiation at 366 nm for 10 minutes to achieve the Irr photostationary state, a series of UV spectra were recorded at temperatures ranging between 60 ^{o}C and 85 ^{o}C. The absorbances of **94a** and **94b** were measured at 325 nm over several hours; as thermal isomerisation from the *cis* to the *trans* form progressed the absorbance at 325 nm increased. A plot at each temperature of the normalised absorbance value [(A_t –

$A_0)/(A_\infty - A_0)]$** against time revealed that the thermal relaxation from *cis* to *trans* geometry observed first order kinetics (figure 3.35). Curve-fitting using the GraphPad Prism 5 software package gave the rate constant (k) for the *cis-trans* isomerisation at each temperature, and from these values an Arrhenius plot for the data was constructed (figure 3.36). The Arrhenius equation can be given in the form:

$$k = Ae^{E_A/RT} \quad (1)$$

or alternatively in its linear form,

$$\ln(k) = \ln(A) - E_A/R\ (1/T) \quad (2)$$

where A is the pre-exponential factor, E_A is the activation energy, R is the gas constant and T is the temperature. A plot of ln(k) versus 1/T for both **94a** and **94b** was linear, and application of linear regression analysis to the data gave an equation from which E_A and A could be derived. The Eyring equation similarly relates the rate constant (k) of a chemical process to temperature:

$$k = \frac{k_B T}{h} e^{\frac{-\Delta G^{\ddagger}}{RT}} \quad (3)$$

or written in its linear form:

$$\ln(k/T) = (-\Delta H^{\ddagger}/R)(1/T) + \ln(k_B/h) + \Delta S^{\ddagger}/R \quad (4)$$

where $\Delta H^{\ddagger}$ is the enthalpy of activation, k_B is Boltzmann's constant and $\Delta S^{\ddagger}$ is the entropy of activation. Hence, a plot of ln (k/T) versus 1/T gave a straight line for both **94a** and **94b** (figure 3.37), from which $\Delta H^{\ddagger}$ and $\Delta S^{\ddagger}$ could be obtained. The half-life ($t_{1/2}$) of a first order process at each temperature can be related to the rate constant (k):

$$t_{1/2} = \ln 2/k \quad (5)$$

** A_t = absorbance at time = t; A_0 = initial absorbance value; A_∞ = absorbance as t→∞

Since either the Arrhenius plot or the Eyring plot can be used to determine *k* at any temperature, the values of *k* at physiological temperature (37 °C) were obtained for **94a** and **94b** and, using equation 5, $t_{1/2}$ was calculated for each isomeric compound. The calculated values of the kinetic constants describing the thermal *cis–trans* isomerisation process for **94a** and **94b** are listed in table 3.4. Significantly, these point towards a slower relaxation from the *cis–trans* form for the *meta*-disubstituted isomer **94b** than for the *para*-disubstituted isomer **94a**.

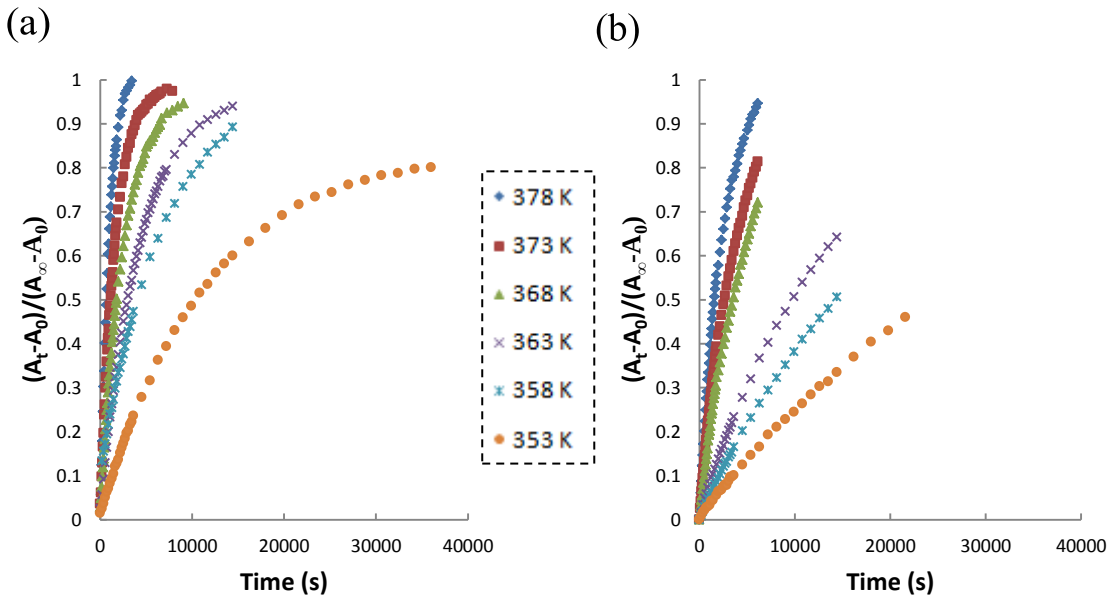

Figure 3.35. Plots of the normalised absorbance at 325 nm against time for the azobenzene-modified oligonucleotides **94a** (a) and **94b** (b)

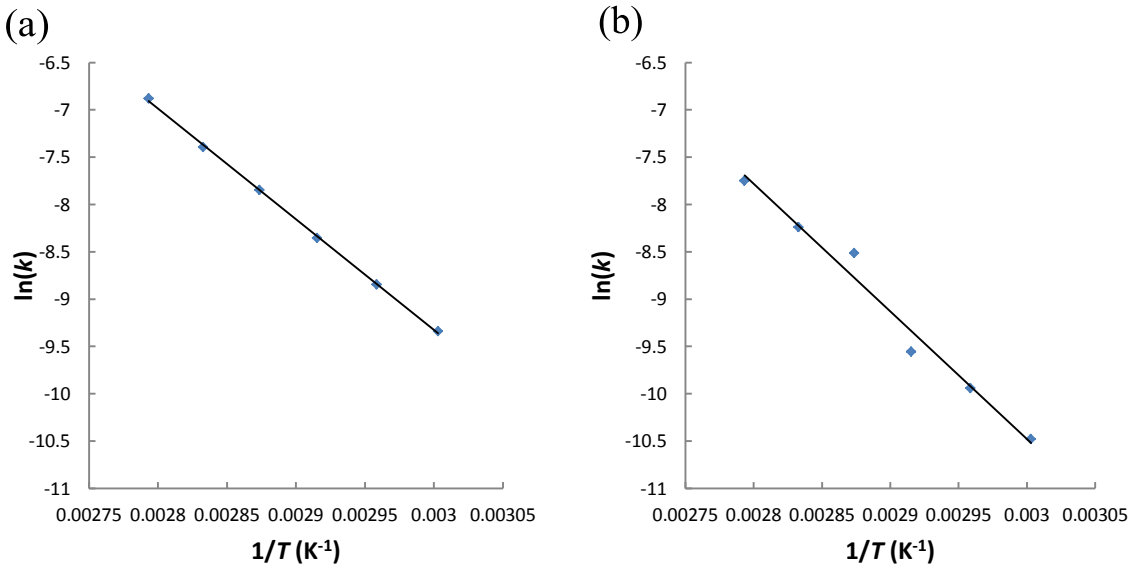

Figure 3.36. Arrhenius plots for the azobenzene-modified oligonucleotides **94a** (a) & **94b** (b)

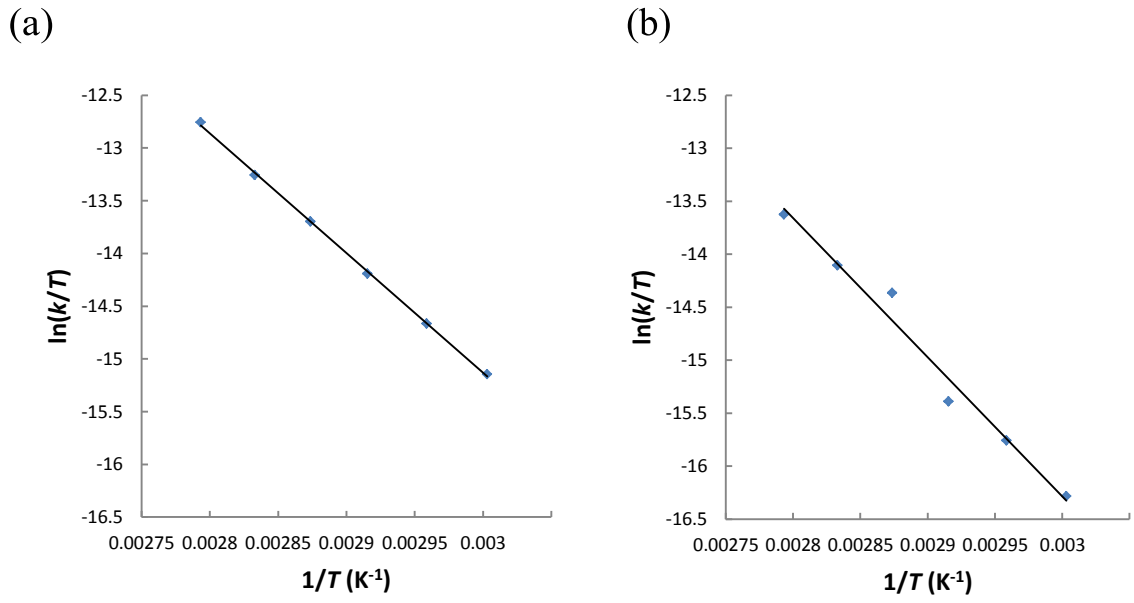

Figure 3.37. Eyring plots for the azobenzene-modified oligonucleotides **94a** (a) & **94b** (b)

Compound	E_{Act} (kJ·mol^{-1})	A (s^{-1})	$\Delta H^{\ddagger}$ (kJ·mol^{-1})	$\Delta S^{\ddagger}$ (J·mol^{-1}K^{-1})	$t_{1/2}$ at 37 °C (hr)
94a	97.25	1.549×10^{11}	94.37	-40.22	30.30
94b	112.18	1.065×10^{13}	109.22	-5.30	144

Table 3.4. Calculated kinetic constants describing the thermal *cis-trans* of isomerisation of **94a** and **94b**

The results from section 3.2.9, in addition to those highlighted in table 3.4, clearly show that the isomeric oligonucleotide conjugates **94a** and **94b** display different photochemical and kinetic behaviour. Amongst a limited number of literature studies comparing such properties in regioisomeric azobenzenes, Wang *et al.* have observed a sensitive relationship between the level of conjugation in substituted azobenzenes and the position of the π–π* absorption band.[175] Specifically, electron donating groups at the position *para* to the azo group were found to shift the π–π* band towards the visible end of the spectrum and to effect a significant decrease in the half-life of the *cis* isomers. The latter observation can be understood in terms of how the substituents affect the degree of single bond character in the azo moiety (figure 3.38). Groups at the 4-position are in conjugation with the azo group and so can increase its single bond character through resonance regardless of whether they are electron withdrawing or donating in nature. Since there is strong evidence to suggest that the transition state in going from *cis* to *trans* contains an N-N single bond (see section 3.1.2.iii, page 48), substituents contributing to a decrease in N/N bond order ought to result in a lowering of the activation energy for the isomerisation. Substituents present at the 3-position are not in conjugation with the azo group, therefore this effect does not occur and there is no lowering of the activation energy for *cis-trans* isomerisation by rotation of an N-N single bond. As a result, the half-life of the *cis* conformation of *meta*-disubstituted azobenzenes is longer than the corresponding *para*-disubstituted isomer.

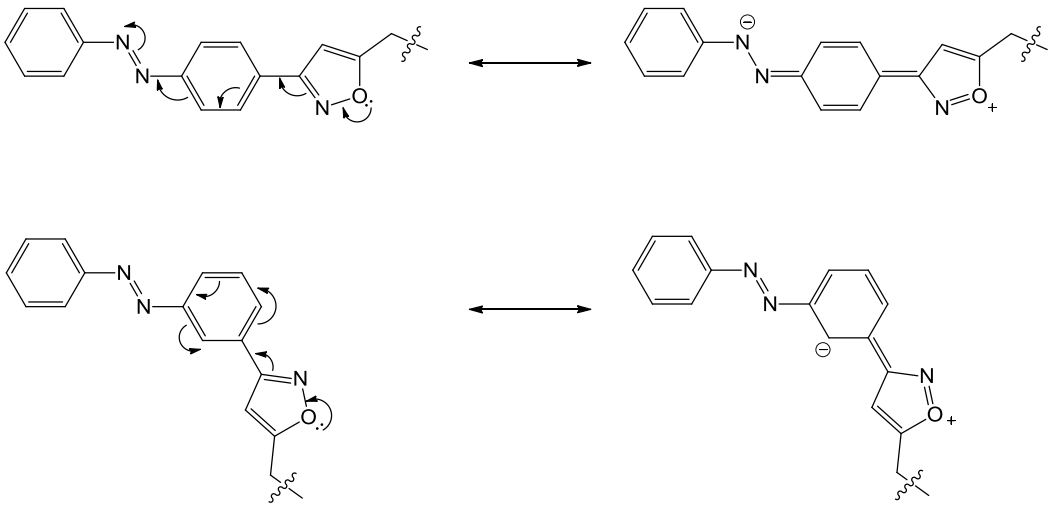

Figure 3.38. Mesomeric delocalisation opportunities for the isomeric isoxazole bearing azobenzenes **94a** and **94b**

Significantly, we have observed increased thermal stability of the *cis* form of a 1,3-disubstituted azobenzene. Whilst substitution at the 2-position has been reported to increase the half-life of *cis* azobenzenes in several cases,[142,176,177] this is generally attributed to the steric clash of the bulky substituents used with the rest of the molecule, thus destabilising the transition state in going from *cis* to *trans*. The exploitation of steric interference to reduce the rate of thermal relaxation may in addition have a negative impact on the efficiency of photo-isomerisation. It is unlikely that there is any significant difference in the sterics of the *cis*–*trans* transition state of our isomeric azobenzene-modified oligonucleotides, **94a** and **94b**, although it remains possible that this may play a minor role in the kinetics of the isomerisation. The most significant contribution to the increased thermal stability of **94bII** relative to **94aII**, however, is most likely the distinct electronic character of the two compounds (figure 3.38).

3.2.11 Conclusions

NOAC chemisty has been applied successfully in the generation of a series of substituted azobenzene cycloadducts. Small molecule examples demonstrate that this chemistry is successful for azobenzenes bearing either the alkyne, which may be linked *via* an amide or an ether group, or the dipole component of the click reaction.

Synthesis of azobenzene cycloadducts in which the isoxazole ring is in conjugation with the azobenzene moiety required initial preparation of the azo-oximes **52**, which were used to generate the nitrile oxides **77** *in situ* upon reaction with Ch-T. Condensation of nitrobenzaldehyde with the Grignard reagent **65** proved an inefficient route to the azo-aldehyde precursor **67a**, which was instead obtained in good yield in three steps from the azo-carboxylic acid **71a**. The *meta*-disubstituted isomer **67b** was also obtained in three steps, albeit *via* a slightly different route.

Solid phase NOAC proved to be a successful approach for the conjugation of an azobenzene moiety to nucleic acids. The *in situ* generated azo-nitrile oxides **77** underwent efficient cycloaddition with a range of oligonucleotides bearing a propargyl ether group at the 2'-position of the sugar. Oligonucleotides modified with azobenzene at the 3'- and 5'-ends were prepared, in addition to those bearing a pendant azobenzene moiety mid-sequence. In all cases, the reaction was remarkably clean and regiospecific.

The photochemical and kinetic properties of the azobenzene-modified oligonucleotides **94a** and **94b** were examined. A slight difference in the position of the π–π* absorbance band was observed between the *trans* isomers of the two compounds, highlighting a difference in the electronic properties of these two regioisomeric conjugates. The photoswitching efficiency of each compound was excellent, with both photostationary states established within minutes.

Thermal relaxation studies of the two compounds showed that the *cis* form of the *para*-disubstituted isomer **94a** had a significantly shorter half-life than the *cis* form of *meta*-disubstituted isomer **94b**. Conjugation between the isoxazole ring, when borne at the 4'-position of the azobenzene, and the azo group, is considered to increase the single bond character of the latter and thus to lower the activation energy of *cis*–*trans* isomerisation.

Azobenzene-functionalised oligonucleotides have been reported previously. However, the application of solid phase NOAC, which employs simple, easily prepared components of the click reaction, may help to broaden the scope of these photoresponsive modifications. In addition, use of 1,3-disubstituted azobenzenes

should be considered for applications which require a bistable photoswitch, since they may improve the thermal stability of the commonly unstable *cis*-azobenzene moiety without compromising the efficiency of photo-switching.

Chapter 4

Conjugation of small molecules to DNA/RNA by strain-promoted azide-alkyne cycloadditions (SPAAC)

4.1 Introduction

4.1.1 Copper-free click chemistry

Thus far, a detailed overview of several types of 1,3-dipolar cycloaddition has been given, and methodologies which exploit NOAC for the modification of nucleic acids have been demonstrated. One of the main advantages that NOAC can claim over the popular CuAAC is that no catalyst is required. As such, potential toxicity issues arising from the use of Cu(I) are avoided, which is of particular importance for biological applications. Indeed, other simple, efficient and selective copper-free approaches to biomolecule conjugation are in demand, and in this section the increasingly popular SPAAC will be discussed.

4.1.2 Bioorthogonal reactions

For a chemical reaction to be considered bioorthogonal, the functional groups in question must be mutually reactive under physiological conditions, yet remain inert to the biological environment;[178] such reactions represent a powerful tool for bioconjugation. However, it is only in the past decade, coinciding with the advent of the click chemistry ideology, that applications exploiting bioorthogonal reactions have been successfully employed. In many cases, the ultimate goal of these applications is the *in vivo* labelling of specific biomolecules.[179,180] This may be achieved *via* selective reaction between the biomolecule in question and a synthetic label, each of which have been suitably functionalised with complementary reactive groups. In biological systems, the cellular metabolic machinery can be exploited to incorporate modified monomers into proteins,[181] glycans,[182] lipids[183] and nucleic acids.[184] Exposure of these modified biomolecules to a labelling group, *e.g.* biotin, fluorescein, bearing a complementary reaction partner, *e.g.* azide, alkyne, may then yield the labelled biomolecule.

The majority of such applications utilise the azide group as one of the labelling components.[185] The azide moiety displays several characteristics which make it a prime candidate for bioorthogonal reactions. It is highly inert, yet displays unique reactivity under the right conditions. In addition, its small size facilitates incorporation into a variety of biomolecules without disrupting their overall structure. Also, unlike many other functional groups employed for coupling reactions in organic chemistry, azides are not present in biological compounds, and as such represent an ideal candidate for bioorthogonal transformations.

4.1.3 Strain-promoted azide-alkyne cycloadditions (SPAAC)

Bertozzi and co-workers have arguably been the main pioneers of bioorthogonal chemistry, and in particular have been responsible for the resurgence in interest in the SPAAC. The re-introduction of this chemical strategy arose from the need for an orthogonal, metal-free conjugation approach in biological systems; as such it was determined that the Huisgen azide-alkyne cycloaddition was an appropriate starting point.

Unlike the hugely popular copper-catalysed version, the convential Huisgen process exhibits sluggish kinetics with simple linear alkynes, and the conditions of high temperature and pressure required for efficient reaction are hardly ideal for biological applications.[52] In contrast, the reaction of cyclooctyne with neat phenyl azide was observed by Wittig and Krebs back in 1961 to proceed in an almost explosive manner.[186] The high reactivity is attributed to the significant ring strain in the system, which is released in the transition state and cycloaddition products resulting from the cyclic alkyne. It is important to note that reaction with a substituted cyclooctyne affords a mixture of regioisomeric cycloadducts, with little regioselectivity observed (scheme 4.1). For a discussion of the regiochemistry of azide-alkyne cycloadditions in terms of frontier orbital theory, see section 1.4.2.ii, page 20.

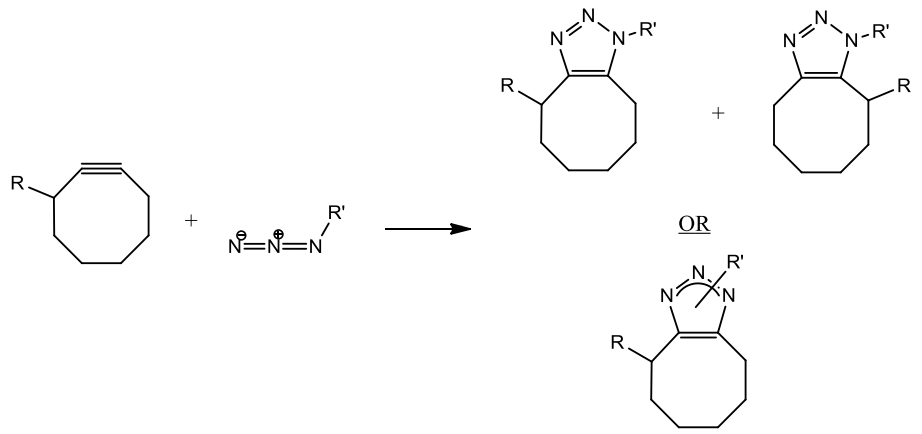

Scheme 4.1. Reaction of a substituted cyclooctyne with an azide to form a mixture of triazolyl cycloadducts

In 2004, Bertozzi *et al.* reported the first application of SPAAC to chemical biology. The biotin-labelled cyclooctyne **95b** was prepared from the parent compound **95a** and used to label azide-functionalised glycoproteins in cell lysates and on live cultured cells (scheme 4.2).[187]

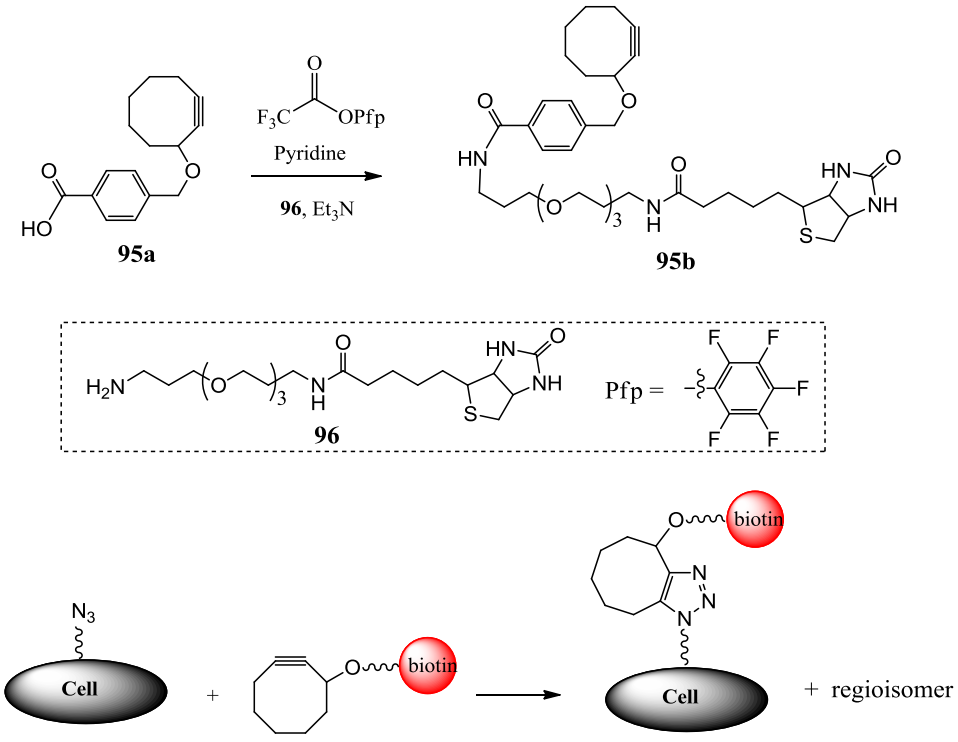

Scheme 4.2. Synthesis of the biotin-labelled strained alkyne **95b** and its application to cell surface labelling[187]

Whilst these results were most exciting, a study of the reaction kinetics of the cyclooctyne **95a** with some model azides indicated that there was room for improvement in terms of reactivity. Thus, in a separate study, Bertozzi and co-workers prepared the cyclooctyne derivatives **97a** and **98a** (figure 4.1).[188] Selection of compound **97a** was based on the hope that excision of the phenyl ring from **95a** would improve aqueous solubility and decrease the steric bulk near the reactive centre. In compound **98a**, an electron-withdrawing fluorine substituent was introduced at the propargylic position to lower the energy of the $LUMO_{dipolarophile}$ and promote reaction with the azide. In a series of model reactions, the rates of reaction of benzyl azide with the cyclooctynes **95a, 97a** and **98a** were compared. Whilst **95a** and **97a** displayed similar kinetics, significant rate enhancement was observed with the fluorinated cyclooctyne **98a**. Consequently, the biotinylated derivative, **98b**, was found to react more rapidly than the corresponding compounds **95b** and **97b** with azide-labelled glycoproteins in cell lysates and on cell surfaces.

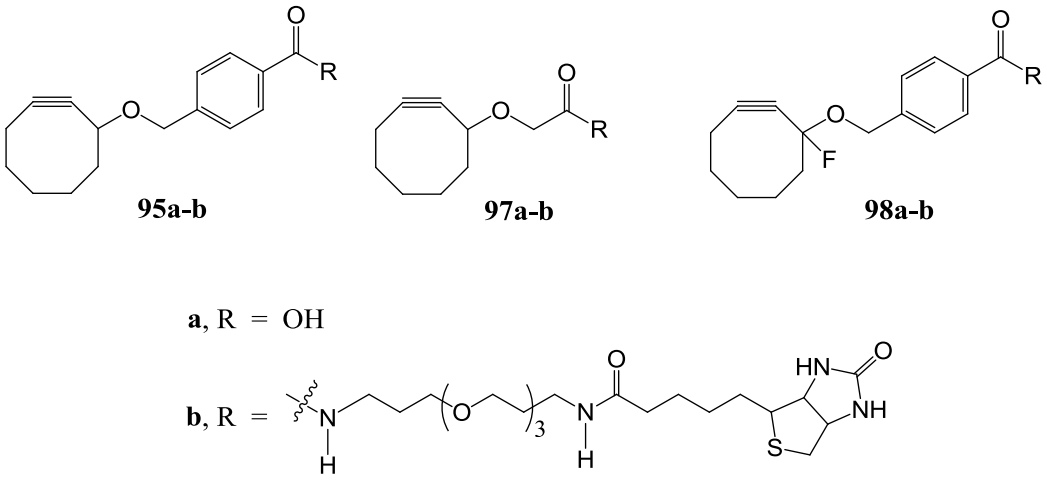

Figure 4.1. The cyclooctynes **95**, **97** and **98** prepared and investigated in SPAAC by Bertozzi *et al.*[188]

The Bertozzi group reported an additional increase in the rate of cycloaddition upon incorporation of a *gem*-difluoro group at the propargylic position of the cyclooctyne (**99**, figure 4.2).[189] Significantly, the extra electron-withdrawing group further activated the alkyne moiety without creating an electrophilic Michael acceptor capable of alkylating biological nucleophiles. Similar rate enhancement for the SPAAC was observed with the novel cyclooctyne **100**, which introduced further ring strain by

fusion of two aromatic rings to a cyclooctyne core.[190] Incorporation of an amide functionality within the cyclic scaffold, as in **101**, resulted in a further increase in reactivity.[191] The structurally related azacyclooctyne **102**, bearing an exocyclic amide bond, was also observed to undergo efficient cycloaddition with azides.[192,193] Other examples from the literature include the photocaged and tetramethoxy diarylcyclooctyne derivatives **103**[194] and **104.**[195]

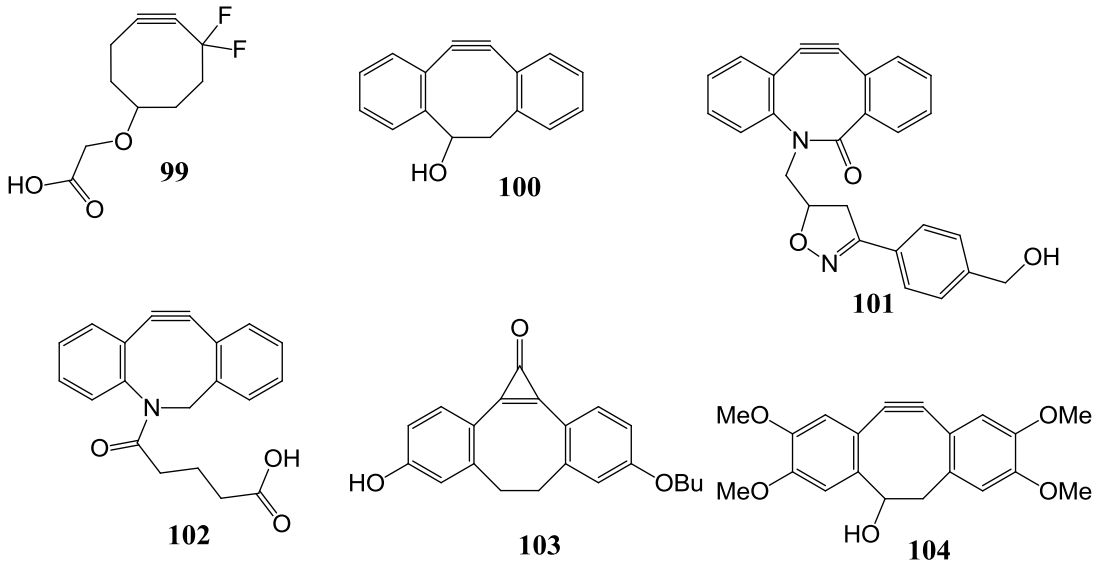

Figure 4.2. Cyclooctyne derivatives reported in copper-free click chemistry applications

Although aryl rings fused to the cyclooctyne scaffold may improve reactivity, the corresponding increase in lipophilic character may compromise the utility of these compounds in biological applications. In addition to the expected poorer water solubility, lipophilic compounds may engage in unwanted hydrophobic interactions with proteins. Indeed, even relatively hydrophilic cyclooctynes have been shown to experience issues of bioavailability and solubility. In one of the few *in vivo* applications of SPAAC, Bertozzi and co-workers found that the bioavailability of a biotinylated derivative of the cyclooctyne **99** was compromised by binding to serum albumin.[196]

The kinetic and lipophilicity data for the strained alkynes **95, 97-104** is summarised in table 4.1. Rate constants (*k*) are for the reaction with benzyl azide in acetonitrile. The calculated partition coeffecients (clogP) are a measure of molecular hydrophobicity, and were calculated using BioByte (embedded in ChemBioDraw 12.0) for the *N*-

methylamide derivative of carboxylic acids and the *N*-methyl carbamate derivative of alcohols (high clogP = high lipophilicity).[197]

Compound	clogP	k (x 10^{-3} M^{-1} s^{-1})	Ref.
95a	3.3	2.4	187
97a	1.7	1.3	188
98a	4.8	4.3	188
99	1.3	76	189
100	4.4	57	190
101	3.9	960	191
102	3.5	310	192,193
103	4.0	76	194
104	3.7	94	195

Table 4.1. clogP values and rate constants (*k*) for the reaction of the cyclooctynes **95, 97-104** with benzyl azide in acetonitrile[197]

Synthetic accessibility is another factor which determines the general value of a particular cyclooctyne. For example, the enhanced reactivity of the difluoroalkyne **99** has to some extent been overshadowed by a lengthy, poor yielding synthesis (10 steps, 1.2% yield),[179] while the syntheses of **100** (5 steps, 10% yield) and **102** (9 steps, 41% yield) are also ineffecient. The simple cyclooctynes **95a** (4 steps, 52% yield) and **97a** (4 steps, 10% yield) present less of a synthetic challenge, but are as discussed less valuable as a result of their inferior reactivity.

4.1.4 Strain-promoted modification of nucleic acids

In the wake of recent developments such as DNA sequencing and RNAi diagnostics and therapeutics, there is an ever increasing demand for efficient bioconjugation strategies for oligonucleotides. While conjugation using CuAAC has proven popular, issues exist relating to Cu(I) mediated oxidative cleavage of DNA and cytotoxicity resulting from

copper contamination in nucleic acid products.[191,198] Careful selection of Cu(I) stabilising ligands has been shown recently to avoid DNA degradation and even facilitate CuAAC in living organisms.[199] Nonetheless, chemistries which avoid the use of copper are still preferable for the preparation of oligonucleotide conjugates. Our group has previously reported oligonucleotide conjugation by strain-promoted nitrile oxide cycloaddition (SPNOC) on the solid phase,[200] while others have reported a similar approach employing azides as the dipole.[201,202] However, these studies also differ in that they have concentrated on solution over solid phase conjugation. The appeal of solid phase conjugation includes ease of purification and the possibility to automate; as such the next goal of our research was to design a methodology for the resin-supported post-synthetic modification of nucleic acids using the SPAAC approach. A further goal was demonstration of the SPAAC with simple, non-fluorinated monocyclic octynes as an alternative to the more commonly employed diarylcyclooctynes. The benefits of employing a simple cyclic alkyne in strain-promoted cycloadditions should include ease of synthetic access and superior kinetics with bulky azides. In addition, the decreased lipophilicity and steric bulk may be advantageous for drug delivery, biomedical and imaging applications, where aqueous solubility and a decreased tendency to interact with hydrophobic proteins are paramount. Advanced applications in which the 'click' reaction is carried out *in vivo* between genetically encoded azides and cyclooctyne lablels may also proceed more smoothly. Thus, the goal was to develop post synthetic oligonucleotide conjugation on the solid phase by strain promoted cycloaddition between azide dipoles and simple monocyclic octynes, as summarised in scheme 4.3.

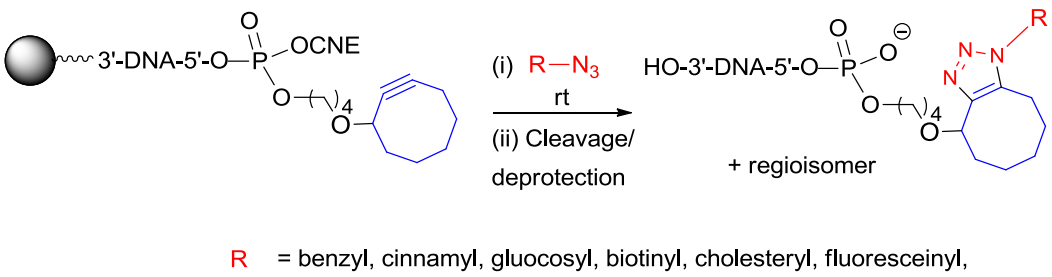

Scheme 4.3. Resin-supported, post-synthetic oligonucleotide conjugation by SPAAC

4.2 Results and Discussion

4.2.1 Synthesis of the resin-supported DNA-cyclooctynes 110 and 112

The strategy for the synthesis of cyclooctyne-linked oligonucleotides required initial preparation of **108** as the key intermediate (scheme 4.4). The synthesis of **108** has been reported previously by our research group.[200] Starting from commercially available cycloheptene (**105**), the already known bicycle **106** was obtained following condensation with bromoform in the presence of potassium *tert*-butoxide.[203] Following electrocyclic ring opening of **106**, the intermediate *trans*-allylic cation was captured with 1,4-butanediol to afford the bromo alcohol **107**, which was used without further purification. Finally, treatment of **107** with sodium hydride induced loss of HBr and furnished the cyclooctyne derivative **108**. For each synthetic step, reaction progress was monitored by TLC, with the exception of the formation of **108**, since the starting material and product displayed identical retention factors in a range of solvent systems. This reaction was thus monitored by ^{1}H NMR spectroscopy following work-up of a small sample of the reaction mixture (figure 4.3). Disappearance of the characteristic olefinic proton resonance was indicative of the consumption of compound **107**. In addition, a slight downfield shift in the signal for the proton on the chiral carbon atom was observed in the product **108**. Significantly, the cyclooctyne **108** is prepared in just three steps, with an overall yield of 33%. In terms of synthetic accessibility, this compares well with the simple cyclooctynes **95a** (4 steps, 52% yield)[187] and **97a** (4 steps, 10% yield),[188] and is significantly more efficient than the tedious and low-yielding syntheses of **100** and **102** (see section 4.1.3, page 106).

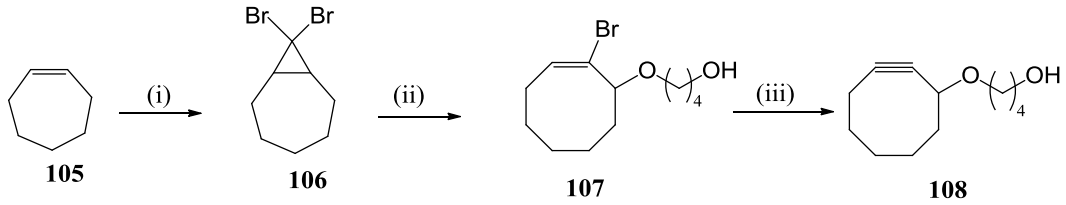

(i) $CHBr_3$, KO*t*Bu, pentane, rt, 24 hr

(ii) $AgClO_4$, 1,4-butanediol, toluene/pyridine, reflux, 4 hr

(iii) NaH, DMF, 1 hr

Scheme 4.4. Synthesis of the cyclooctyne derivative **108**[200]

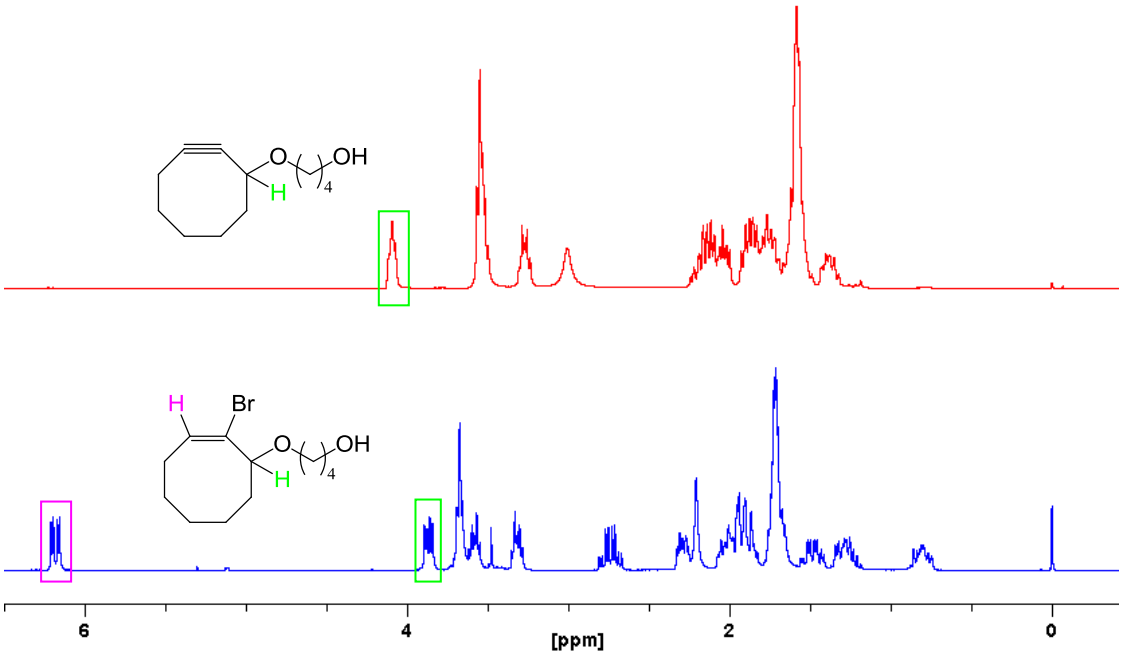

Figure 4.3. ^{1}H NMR spectra of the bromoalkene intermediate **3** and the cyclooctyne **4**

The presence of a pendant hydroxy group on the cyclooctyne **108** facilitated straightforward conversion to the corresponding phosphoramidite **109**, which was achieved following reaction with 2-cyanoethyl-*N,N,N',N'*-tetraisopropylphosphoramidite (**16**) in the presence of BMT as activator (scheme 4.5). In addition to a signal at 147.2 ppm characteristic of the desired phosphoramidite **109**, the ^{31}P NMR spectrum showed a number of signals in the region of ~10-30 ppm suggestive of some P(V) impurities (figure 4.4). It was determined that these by-products were not likely to be detrimental to coupling with oligonucleotides; thus compound **109** was used without further purification.

Coupling between the CPG-oligonucleotides **24** and **28** and the phosphoramidite **109** was carried out manually on the solid phase,[††] employing BMT as an activator (scheme 4.5). Following cleavage of the DNA-cyclooctyne conjugate from the resin, successful coupling was confirmed by HPLC and MALDI-TOF MS analysis.

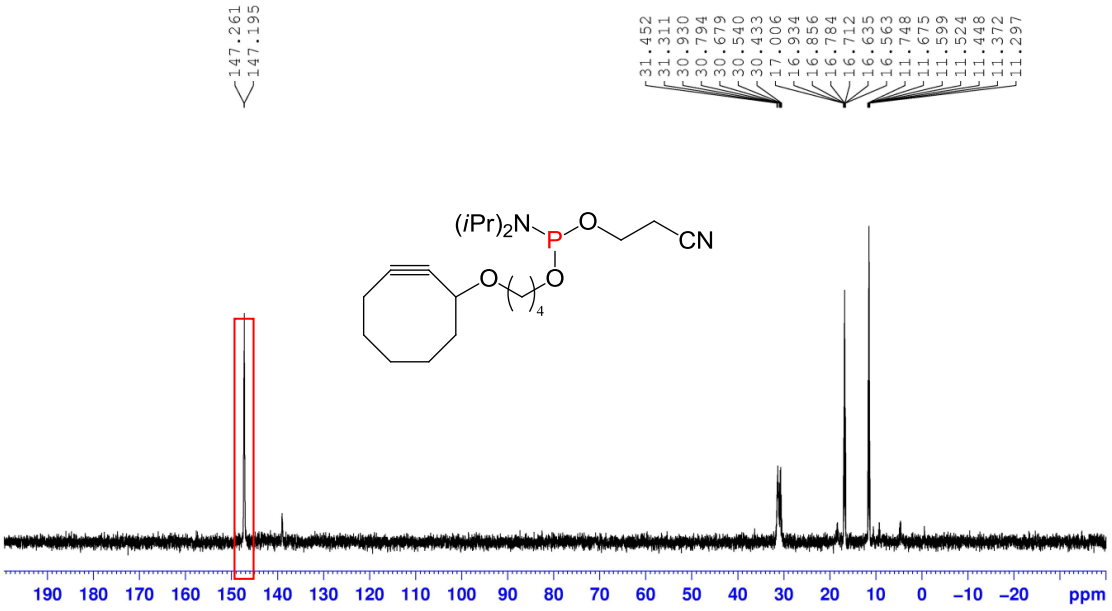

Figure 4.4. ^{31}P NMR spectrum of crude phosphoramidite **109**

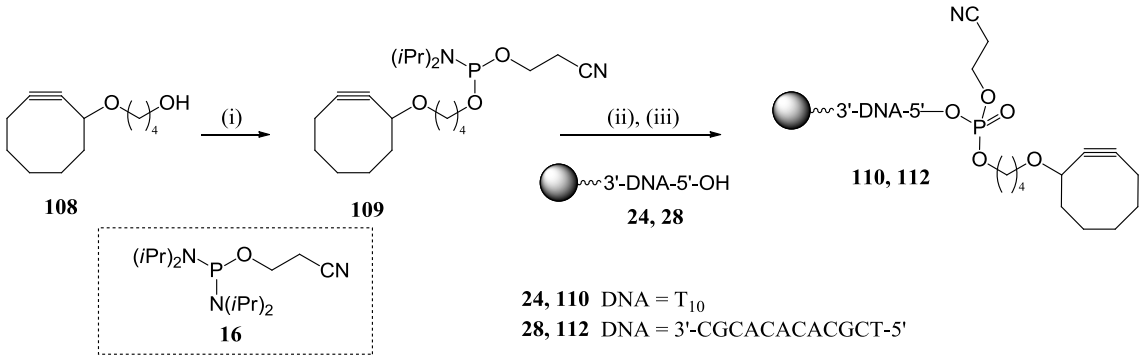

(i) BMT, **16**, CH_3CN, rt, 30 min

(ii) BMT, CH_3CN, rt, 30 min

(iii) I_2 (0.1 M) THF-pyridine-H_2O

Scheme 4.5. Synthesis of resin-bound DNA-cyclooctyne conjugates **110** and **112**

[††] For a description of manual phosphoramidite coupling on the solid phase, see section 2.2.3, page 34

4.2.2 Selection and synthesis of azide labels

To demonstrate the utility of solid phase SPAAC with the DNA-cyclooctynes **110** and **112**, a range of azides were required. For initial proof of concept studies we selected the small, simple dipoles benzyl azide (**114**) and cinnamyl azide (**115**). The former was commercially available, while the latter, a known compound,[204] was prepared by nucleophilic displacement of cinnamyl bromide with sodium azide.

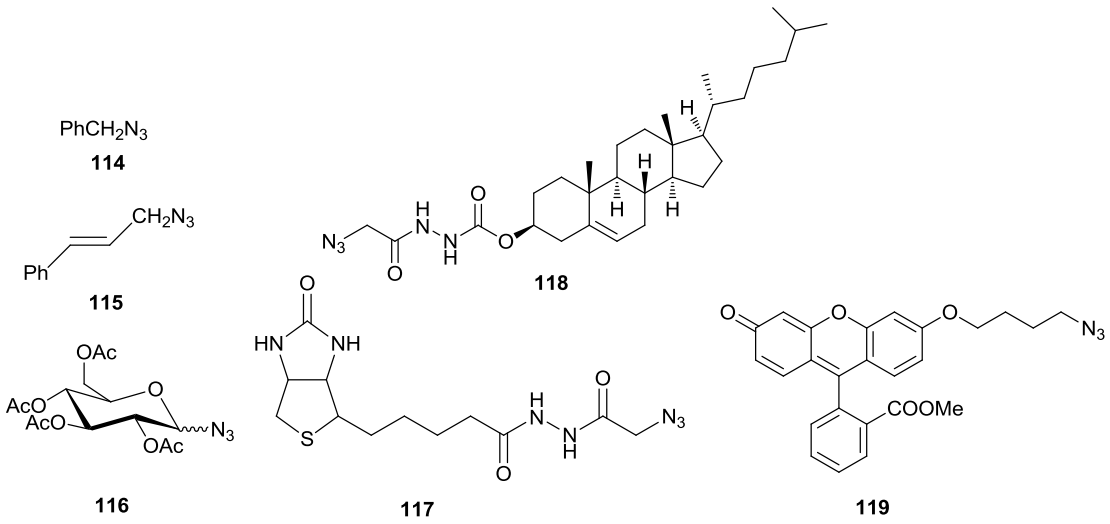

Figure 4.5. Azide reaction partners for SPAAC to DNA-cyclooctynes **110** and **112**

More complex azides were required to investigate the success of coupling with biologically relevant labels, *e.g.* those used in imaging or biomedical applications. Oligonucleotide-carbohydrate conjugates have the potential for improved cellular uptake;[205] with this in mind the commercially available glucose label **116** was selected as a relevant partner. For the same reason, the cholesterol azide **118** was selected. Conjugation of oligonucleotides to lipophilic moieties has been shown to assist crossing of the lipid bilayer, and so provides hope of a non-toxic alternative to cationic liphophilic or polymeric delivery systems.[202,206] The preparation of compound **118** required access to the azidohydrazide **122** as a key building block; this was obtained in two steps from ethyl bromoacetate (scheme 4.6). Nucleophilic displacement of **120** with sodium azide proceeded quantitatively to give the intermediate **121**,[204] which was used without further purification. Reaction of **121** with hydrazine monohydrate

afforded the azido compound **122**, which was coupled with commercially available cholesterol chloroformate (**124**) to yield the desired product **118**.

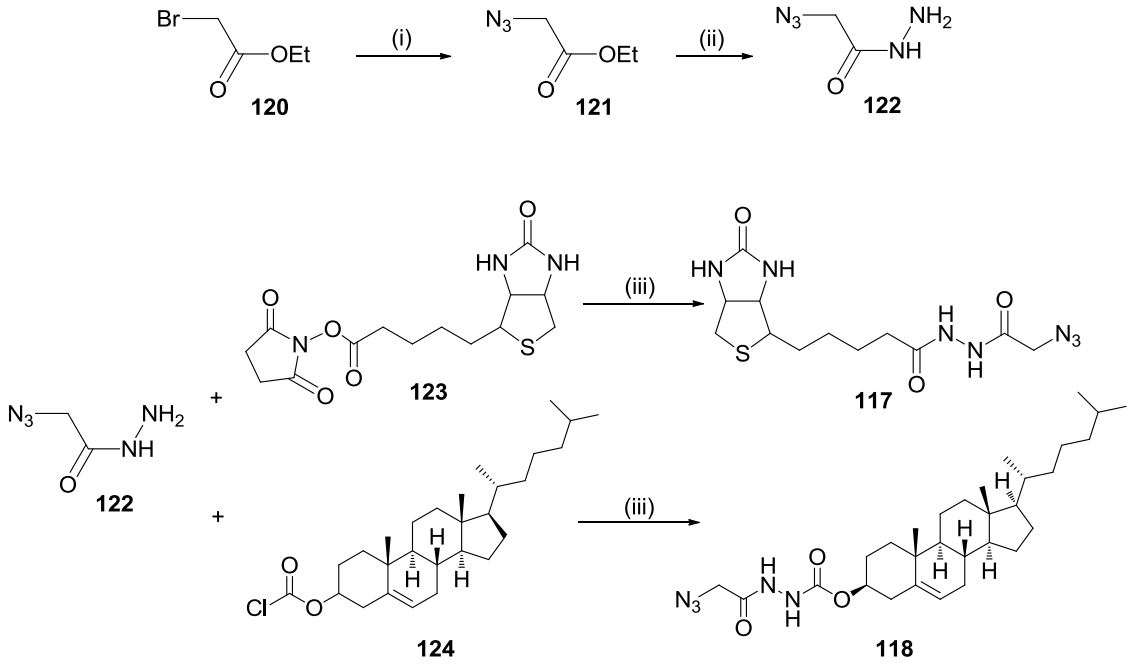

(i) NaN_3, H_2O/Me_2CO, rt, 30 min

(ii) $NH_2NH_2.H_2O$, EtOH, rt, 2 hr

(iii) Et_3N, DMF, rt, 18 hr

Scheme 4.6. Synthesis of the biotin and cholesterol azide labels, **117** and **118**

The ^1H NMR spectral data for **118** is shown (figure 4.6). While most of the signals are densely located in the region of ~0.7-2.0 ppm, some diagnostic signals are seen in the downfield region. The two NH proton signals present as broad singlets at 8.19 and 6.75 ppm, while the olefinic proton of the cholesterol moiety is represented by a narrow doublet at 5.38 ppm. Other characteristic signals include the multiplet resonance at ~4.6 ppm which represents the proton *geminal* to the oxygen atom of the carbamate group, and the singlet at 4.08 ppm corresponding to the methylene protons adjacent to the azide moiety.

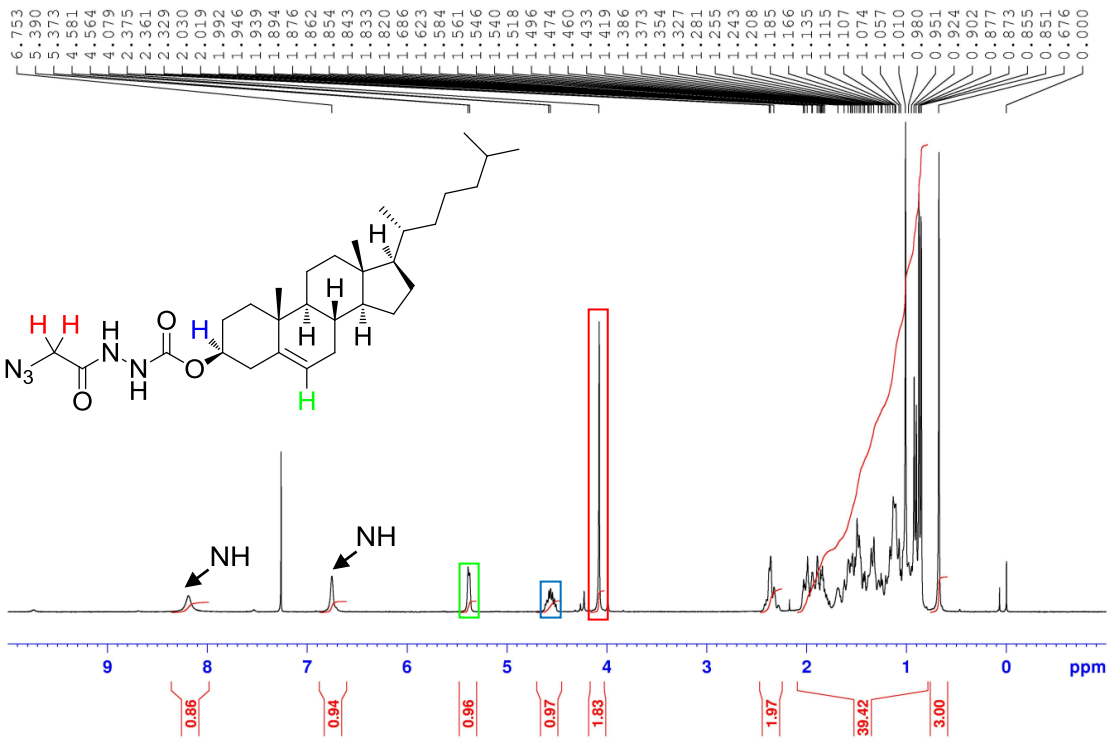

Figure 4.6. ^{1}H NMR spectrum of the cholesterol azide **118**

Synthesis of the biotin-labelled azide **117** followed a parallel route to that described for the preparation of the cholesterol compound **118**, with the final step involving coupling of **122** with the biotin NHS-ester **123** (scheme 4.6). Biotinylation is commonly employed to detect biomolecules by exploiting the strong binding interaction between biotin and the protein streptavidin. Conjugation of streptavidin to a reporter enzyme such as horseradish peroxidise (HRP) can facilitate both qualitative and quantitative detection of various biomolecules.[207]

The labelling of oligonucleotides with fluorescent probes can have obvious benefits in terms of bio-imaging; the fluorescein labelled azide **119** was therefore deemed to be an interesting candidate for our studies. The synthesis of **119** required initial preparation of the key intermediates **125** and **126** (scheme 4.7). Compound **126** was known in the literature,[208] and was obtained from reaction between 2 equiv. of 1,4-dibromobutane and 1 equiv. of sodium azide. Coupling of **126** with the fluorescein methyl ester **125** (itself prepared following reflux of the parent fluorescein in methanolic sulphuric acid for 12 hr) furnished the desired fluoroscein azide **119** in 69% yield.

The ^{1}H NMR spectrum of **119**, in which some of the characteristic signals are highlighted, is shown below (figure 4.7). The two pairs of methylene protons adjacent to the oxygen and nitrogen atoms in the alkyl chain appear as triplets in the range of ~3.4-4.1 ppm. The methyl protons of the ester group present as a singlet at 3.64 ppm, and the relative integration of this signal to the two CH_2 signals is ~3:2:2.

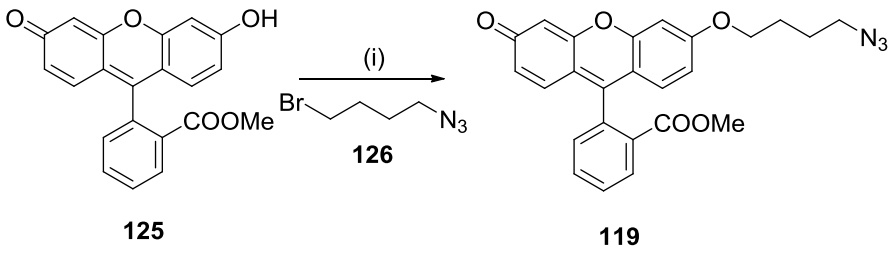

(i) K_2CO_3, DMF, 70 ^{o}C, 2 hr

Scheme 4.7. Synthesis of fluorescein azide **119**

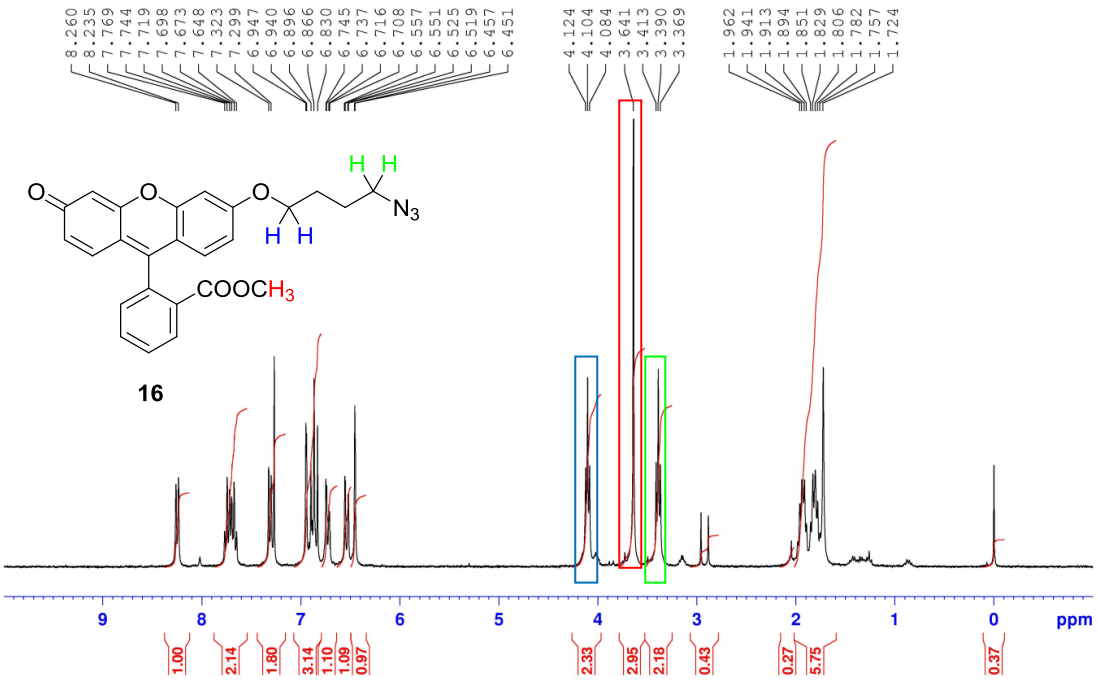

Figure 4.7. ^{1}H NMR spectrum of the fluorescein azide **119**

4.2.3 SPAAC on the solid phase

4.2.3.i Cycloadditions with the CPG-T_{10}-cyclooctyne 110

Exploratory cycloadditions were carried out between the simple azido compounds **114** and **115** and the resin-bound T_{10}-cyclooctyne **110** (scheme 4.8). These reactions were performed on a 0.2 µmol scale, and initially a large excess (90 equiv.) of azide was used to ensure complete reaction. To assist in solubility, aqueous DMSO was employed as solvent; the volume used was such that the working concentration of the azido compounds was ~140 mM. Encouragingly, complete conversion of the starting material to the desired triazolyl products **127a,b** was observed following agitation of the reaction mixture at rt for 30 min. This was evidenced by HPLC and MALDI-TOF MS analysis of the cleaved conjugates **128a,b**.

Significantly, two product peaks of similar magnitude were observed in each case. This was unsurprising, as azide-alkyne cycloadditions are known to exhibit little regioselectivity in the absence of a catalyst. This loss in regioselectivity is seen as an acceptable trade-off for the non-toxic metal-free conditions used. The regioisomeric products elute slightly later than the starting material, and the cycloaddition reaction displays a small preference for formation of the later eluting regioisomer (figure 4.8).

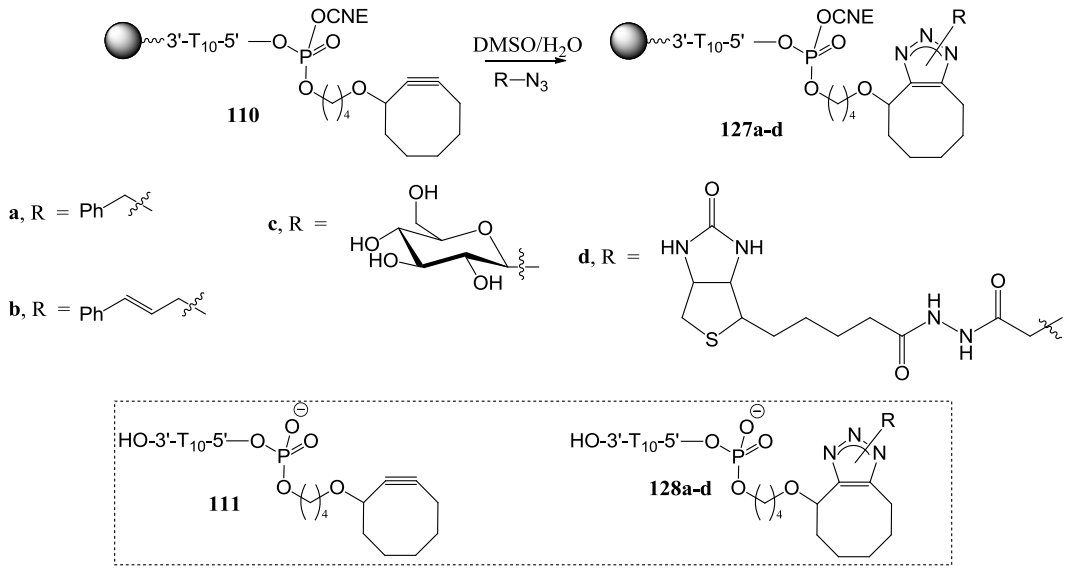

Scheme 4.8. Solid phase SPAAC to form the resin-bound cycloadducts **127a-d**

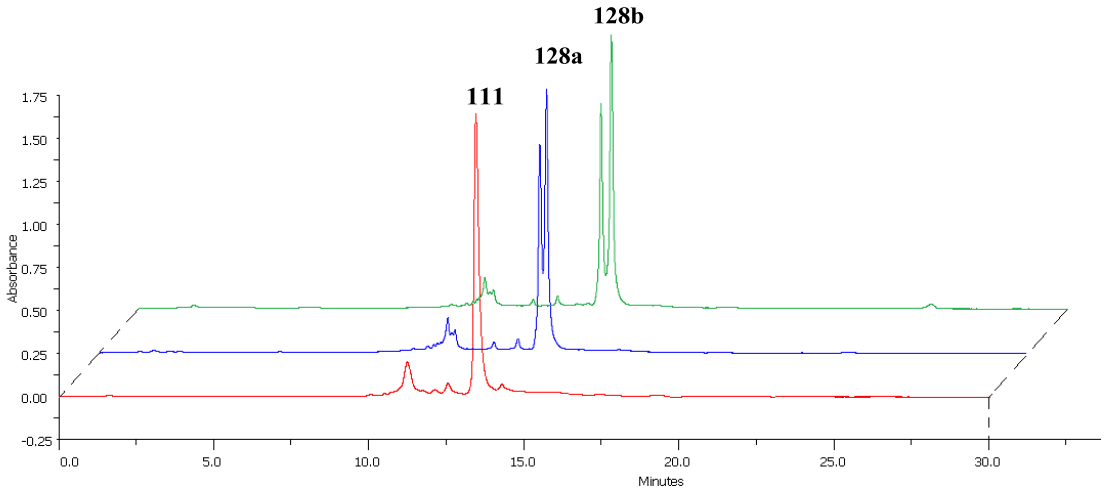

Figure 4.8. Overlaid chromatograms of the T_{10}-cyclooctyne **111** (red) and the crudeT_{10}-triazolyl cycloadducts **128a** (blue) and **128b** (green)

When considering the optimised conditions for cycloaddition, we turned to the findings of a previous study by our research group, in which the solid phase strain-promoted nitrile oxide cycloaddition (SPNOC) of the CPG-DNA-cyclooctyne **110** with a range of simple nitrile oxides was investigated (scheme 4.9).[200] In each case, agitation of **110** in the presence of *in situ* generated nitrile oxide (30 mM, 16 equiv.) in aqueous EtOH for 10 min was sufficient for completion of reaction. Guided by these results, cycloaddition of **110** was once more attempted with benzyl azide (**114**) in 50% aqueous DMSO, this time with a lower concentration and number of equivalents of the azide (50 mM, 20 equiv.). Unfortunately, these conditions were found to be insufficient for complete reaction. Subsequently, the concentration of **114** was increased from 50 to 140 mM and reaction with the resin-bound DNA-cyclooctyne **110** was re-attempted. Gratifyingly, quantitative conversion of **110** to the triazolyl cycloadduct **127a** was in this case observed following deprotection/cleavage of the product and analysis by RP-HPLC. Employment of these conditions in the cycloaddition of **110** with cinnamyl azide (**115**) gave similar results. These findings demonstrate that while reaction of the DNA-cyclooctyne **110** displays slower kinetics with azides than with nitrile oxides, similar reaction rates can be achieved by increasing the effective concentration of the azide dipole.

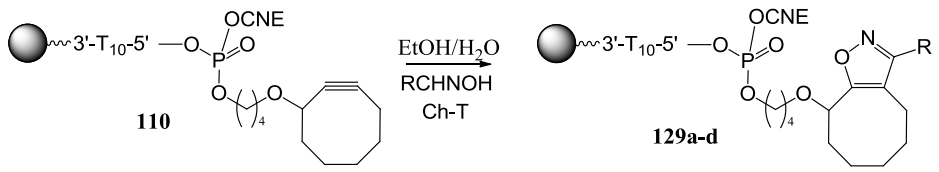

a, R = Ph

b, R = 1-Naphthyl

c, R = 2-Fluorophenyl

d, R = 1-Pyrenyl

e, R = 2-(2-Hydroxyethoxy)phenyl

Scheme 4.9. Modification of CPG-DNA-cyclooctynes by SPNOC

Having completed proof of concept studies with the small azides **114** and **115**, the potential for conjugation of some more complex labels was investigated. Thus, the glucose and biotin azides **116** and **117** were investigated. Pure DMSO was necessary to solubilise the azido sugar **116**, and a 140 mM solution was prepared. Agitation of the resin-bound T_{10}-cyclooctyne **110** in the presence of 20 equiv. of **116** for 4 hr was found to be sufficient for complete conversion of the starting material to the product **127c**. Following cleavage of the products from the solid support, HPLC analysis showed peak splitting, which was attributed to employment of the sugar **116** as a mixture of anomers (figure 4.9). MALDI-TOF MS analysis of the products **128c** indicated that deacetylation of the glucose moiety had occurred under the basic conditions of the cleavage/deprotection protocol.

Similar conditions were employed for cycloaddition with the biotin azide **117**. In this case, 90% aqueous DMSO was the solvent of choice. Again, 4 hr reaction time was required, after which cleavage of the product **127d** from the resin and analysis by HPLC confirmed complete consumption of the starting material **110**. Consistent with previous observations, two sharp regioisomeric product peaks were observed, and the formation of the products **128d** was supported by MALDI-TOF MS. Interestingly, the sugar and biotin conjugates **128c,d** had a shorter retention time than the parent T_{10}-cyclooctyne starting material, **111** (figure 4.9).

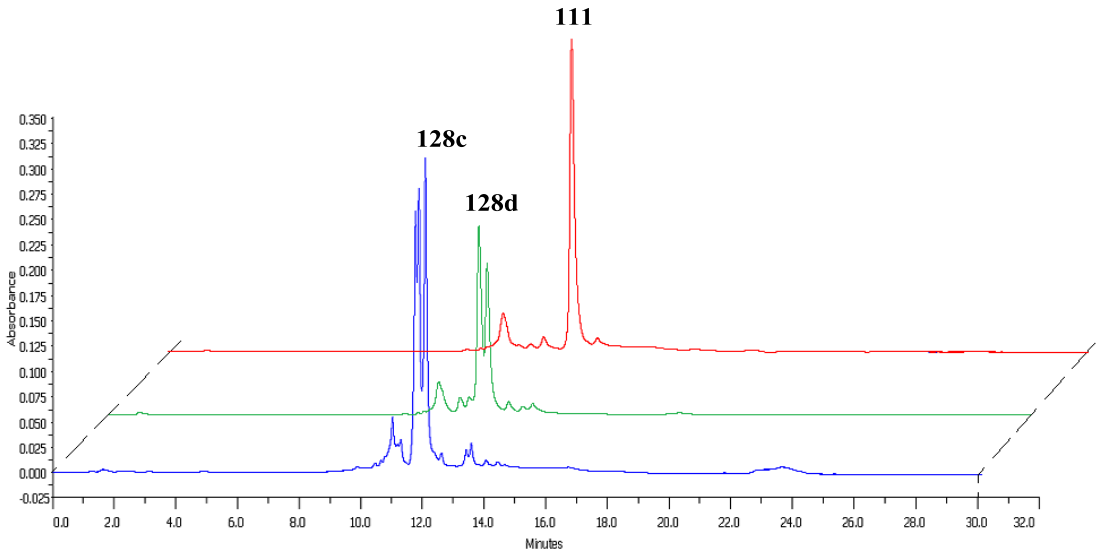

Figure 4.9. Overlaid chromatograms of the crude T_{10} triazolyl cycloadducts **128c** (blue) and **128d** (green), and the T_{10}-cyclooctyne starting material **111** (red)

Since the electronics of the azide has been shown to have little influence on the outcome of strain-promoted cycloadditions,[188] the slower reaction of the CPG-T_{10}-cyclooctyne **110** with **116** and **117** has been attributed to their increased steric demand in comparison to the azides **114** and **115**. It is also encouraging that the observed reaction rates compare favourably with those reported for SPAAC involving activated dibenzocyclooctynes conjugated to RNA.[202,209] The required reaction times and solvent composition for formation of the SPAAC cycloadducts **128a-d** is summarised in table 4.2.

Azide	Reaction solvent	Reaction time	Product
114	50% aq. DMSO	30 min	**128a**
115	50% aq. DMSO	30 min	**128b**
116	DMSO	4 hr	**128c**
117	DMSO	4 hr	**128d**

Table 4.2. Reaction conditions for formation of T_{10} conjugates **128a-d** from the azides **114**-**117** and the DNA-cyclooctyne **110**

4.2.3.ii Cycloadditions with CPG-mixed 12-mer-cyclooctyne 112

Having demonstrated the success of SPAAC with a decathymidine sequence and the azides **114-117**, the compatibility of a mixed DNA sequence, containing all 4 bases with their standard protecting groups, was next explored (scheme 4.10). The CPG-12-*mer* **28** (3'-CGCACACACGCT-5') was selected and the cyclooctyne introduced in a manner described in section 4.2.1.

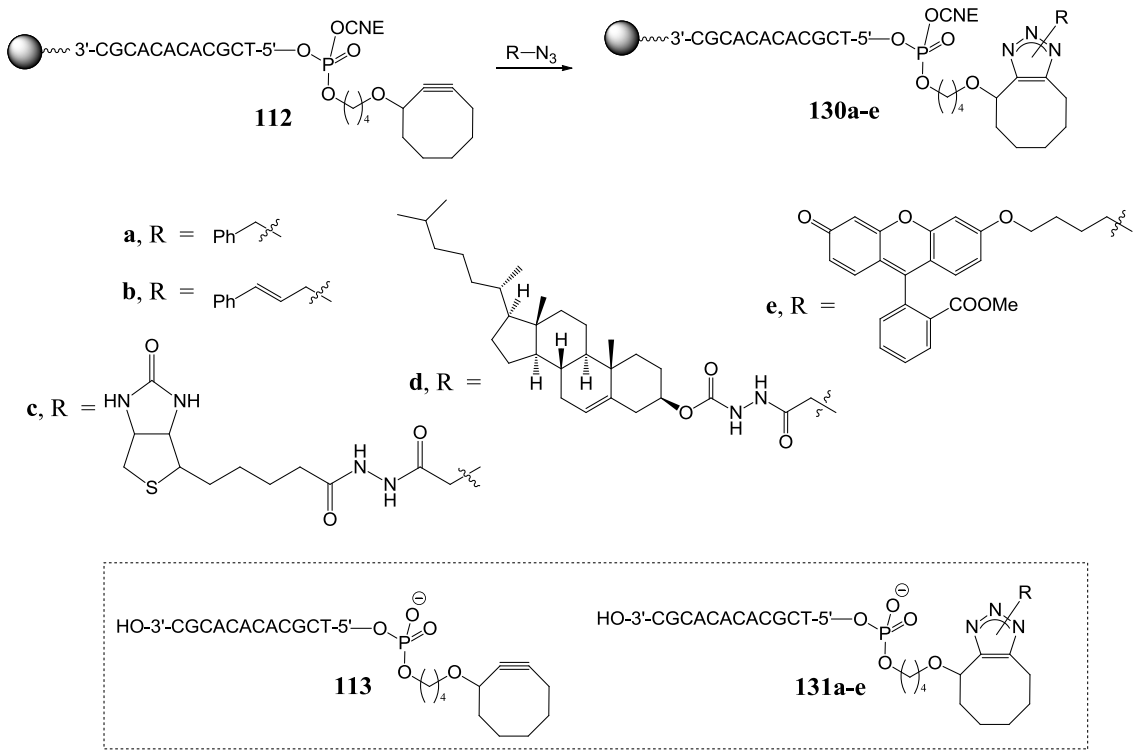

Scheme 4.10. Solid phase SPAAC to form the resin-bound cycloadducts **130a-e**

Preliminary cycloadditions with the DNA-cyclooctyne **112** focused on the simple benzyl and cinnamyl labelled azides **114** and **115**. In each case a solution of the azide (20 equiv., 140 mM) in 50% aqueous DMSO was added to the resin-bound 12-*mer*-cyclooctyne **112** in an eppendorf tube and the mixture was agitated for 30 min at room temperature. Following deprotection and cleavage of the reaction products **130a,b** (28 % NH_4OH, rt, 24 hr), the HPLC traces of the crude products showed complete consumption of the starting material (figure 4.10). The profile of each chromatogram was quite similar to that observed for the T_{10} products, with the similar polarity characteristics of the starting material and the products resulting in little difference in retention times. Co-injection of a sample of the DNA-cyclooctyne **113** with the

product sample in each case confirmed that the two major peaks did indeed represent the regioisomeric products. The regioselectivity was also very similar to that observed for the T_{10} cycloadducts.

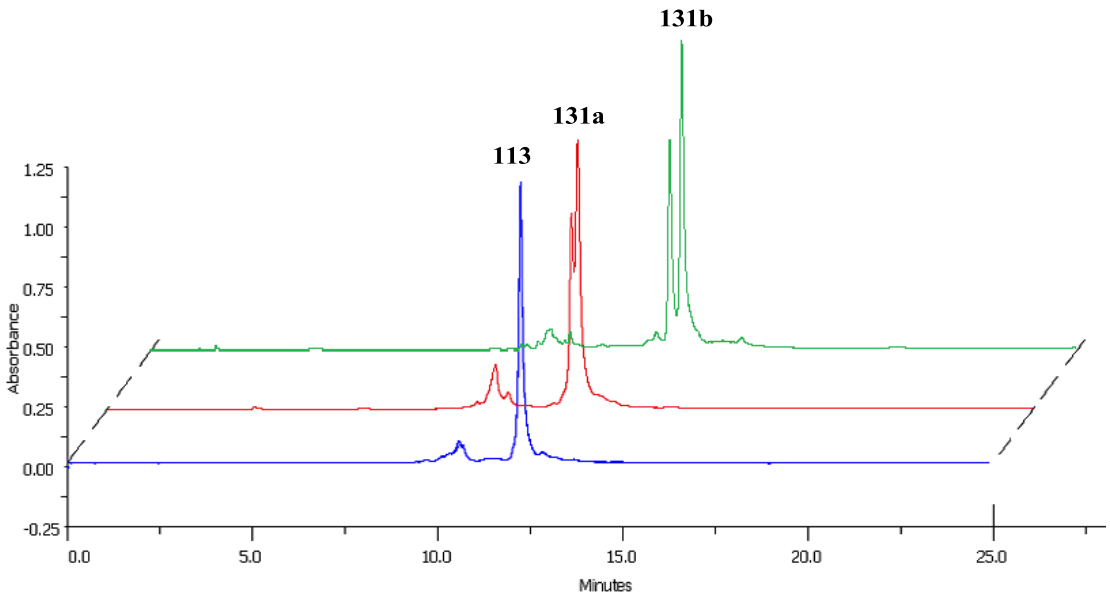

Figure 4.10. Overlaid chromatograms of the DNA-cyclooctyne starting material **113** (blue) and the crude DNA-triazolyl cycloadducts **131a** (red) and **131b** (green)

Reaction of **112** with the biotin azide **117** was found to proceed smoothly under identical reaction conditions to those used for the preparation of the analogous T_{10}-cycloadduct **127d**. Deprotection and cleavage from the resin yielded a crude sample of **131c**. In this case, purification of the product was deemed necessary; this was achieved by preparative RP-HPLC. Removal of impurities was confirmed by re-injection of the pure fractions (figure 4.11). These were then combined, concentrated and analysed by MALDI-TOF MS, which confirmed the structural integrity of the product **131c**.

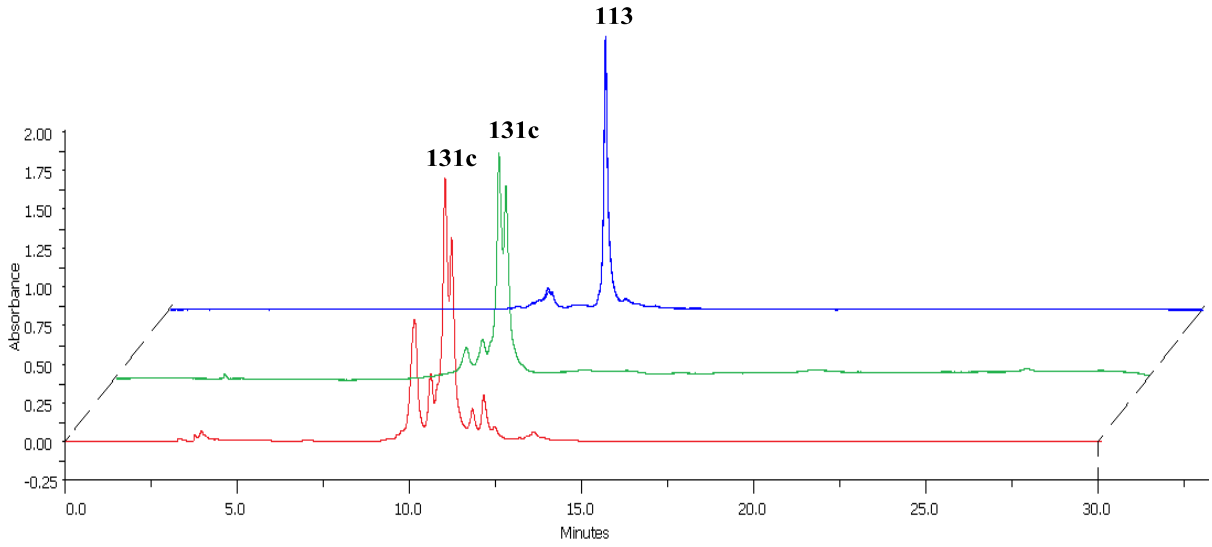

Figure 4.11. Overlaid chromatograms of crude (red) and purified (green) biotin cycloadduct **131c**, and DNA-cyclooctyne starting material **113** (blue)

As discussed in section 4.2.2, the conjugation of lipids to oligonucleotides is known to improve cellular uptake. However, despite advances in the post-synthetic modification of oligonucleotides, the conjugation of steroidal groups remains non-trivial. Two recent reports have employed CuAAC in the preparation of steroidal oligonucleotide conjugates. In one example, the key ligation step is carried out on the monomeric scale.[206] The modified monomer is then incorporated into an oligonucleotide sequence using standard phosphoramidite coupling methodology. In the second example, microwave-assisted click conjugation is performed with a resin-bound oligonucleotide-alkyne.[202] Since the minimum acceptable concentration of copper for pharmaceutical applications is 15 ppm,[210] a non-toxic, catalyst-free alternative for the conjugation of lipids to nucleic acids would have obvious advantages.

Solubility can be an issue for steroidal compounds, but the cholesterol azide **118** was found to be satisfactorily soluble in chloroform. Reaction beween the DNA-cyclooctyne **112** and **118** (20 equiv., 140 mM) was thus carried out on a 0.2 µmol scale, employing chloroform as the solvent. After 24 hr agitation at room temperature, the crude reaction products **130d** were deprotected and cleaved from the resin using the standard protocol and analysed by RP-HPLC. Problems arose initially in the analysis due to the strong retention of the lipophilic conjugate by the non-polar C18 column.

Consequently, the product HPLC trace showed no evidence of cycloaddition. However, employment of a less-polar C8 phase resulted in weaker retention of the product, and two peaks representing the regioisomeric cycloadducts were observed at 23.2 and 23.8 min (figure 4.12). As a consequence of the slow elution of the regioisomeric products, considerable peak broadening was observed, although significant separation from the earlier eluting impurities was nonetheless achieved. This facilitated relatively straighforward purification of the crude products by preparative HPLC, yielding a pure sample of **131d**. This was analysed by MALDI-TOF MS, which confirmed formation of the desired product.

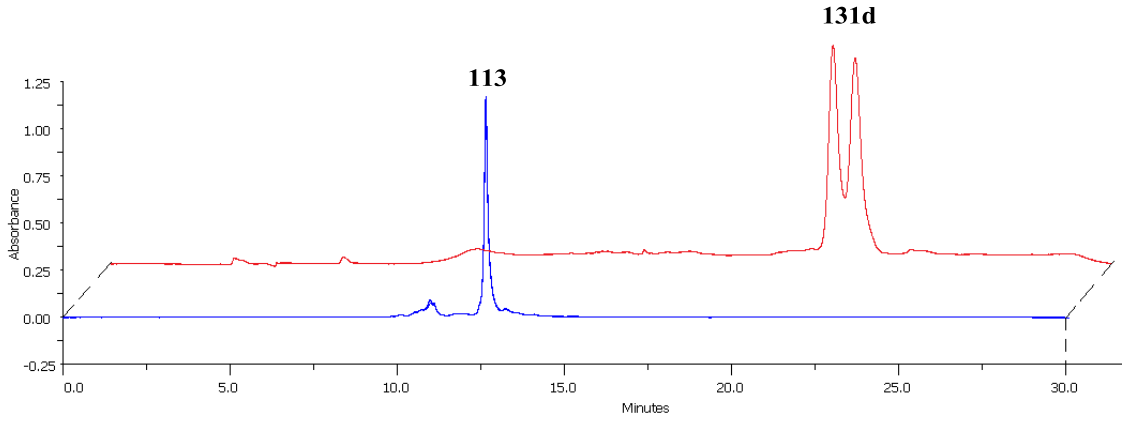

Figure 4.12. Overlaid chromatograms of the crude DNA-cyclooctyne starting material **113** (blue) and the pure cholesterol cycloadduct **131d** (red)

In recent years fluorescent tags have replaced radioactive labels as one of the most useful tools for probing cellular mechanisms. We wished to investigate the compatibility of the azido compound **119** with the SPAAC approach, with a view to preparation of fluorescently labelled oligonucleotides. Original cycloadditions employed either 90% aqueous DMF, DMSO or $CHCl_3$ as the reaction solvent. Following agitation of the CPG-DNA-cyclooctyne **112** in the presence of the fluorescein azide **119** (20 equiv., 140 mM) overnight at room temperature, reaction work-up involved washing away the excess azide with a suitable organic solvent, *e.g.* $CHCl_3$. After extensive washing the resin still displayed an intense yellow colour and was highly fluorescent, as would have been expected if the resin-bound oligonucleotide has been trapped by the fluorescein azide **119**. However, upon exposure of the solid-supported reaction products to the basic cleavage/deprotection conditions, the yellow colour was

seen to gradually fade, before disappearing altogether. At this point, we hypothesised that this loss of colour was due to hydrolysis of the ester moiety, which was convalently linked to the fluorescein chromophore, leading to a non-fluorescent lactone.[211] Nonetheless, we continued with the characterisation of these colourless samples. The HPLC traces of the crude products displayed double peaks typical of regioisomeric cycloaddition products (figure 4.13), and reactions were deemed to be 85-100% complete on the basis of the relative areas of the starting material and product peaks. Following purification of a representative sample by preparative HPLC, MALDI-TOF MS analysis supported formation of the proposed lactone form of the cycloadduct (compound **131f**). The structure of **131f** and its proposed mechanism of formation are shown in scheme 4.7. The loss of fluorescence can be attributed to the loss of conjugation resulting from formation of the lactone ring.

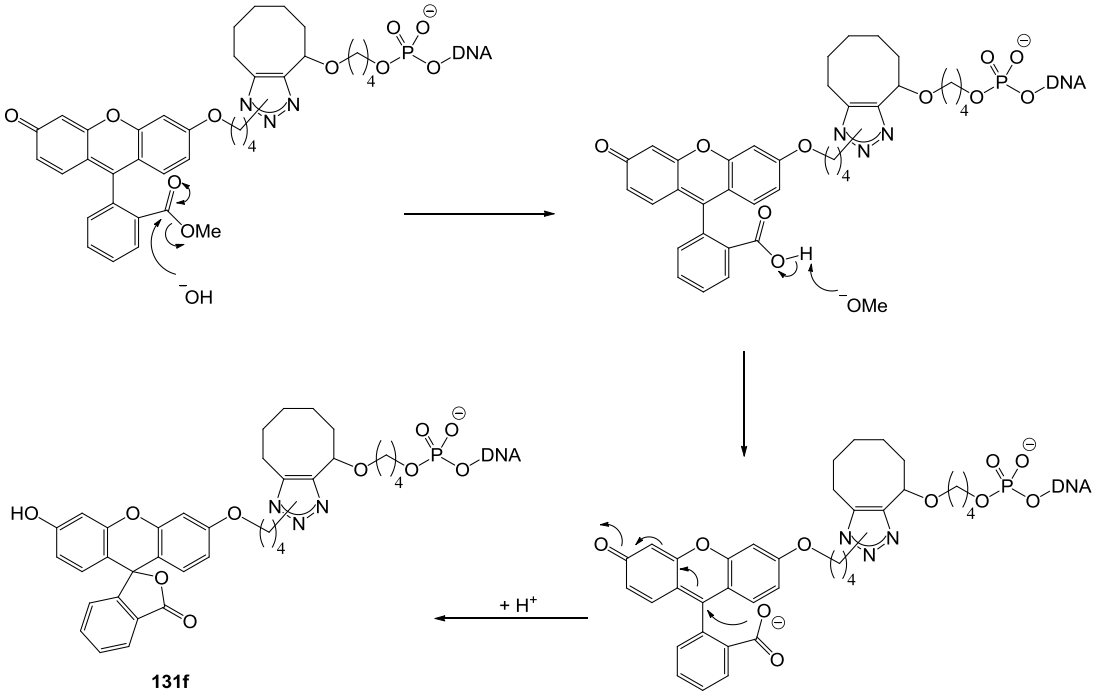

Scheme 4.11. Proposed mechanism for formation of the spiro-lactone product

The instability of the fluorescein methyl ester under the basic conditions required for deprotection/cleavage lead us to pursue a solution phase approach to this cycloaddition. By initial cleavage of **112** from the resin and reaction of the resulting DNA-cyclooctyne **113** with the fluroescein azide **119** in the solution phase, exposure of the fluorescein ester to base can be avoided, and thus the highly fluorescent

tetracyclic skeleton is preserved. Indeed, this approach, employing 20 equiv. of azide (110 mM in DMF) with a reaction time of 18 hr, yielded an intensely coloured solution after work-up. However, HPLC analysis of this sample demonstrated only ~35% conversion to the desired products. This could be increased to 80% conversion upon doubling the amount of the azide used to 40 equiv. Following purification of the triazolyl products **131e** by HPLC, MALDI-TOF MS analysis confirmed that the structural integrity of the fluorescein chromophore was indeed intact. The HPLC traces of the the oligonucleotides conjugates **131e** and **131f** are shown in figure 4.13.

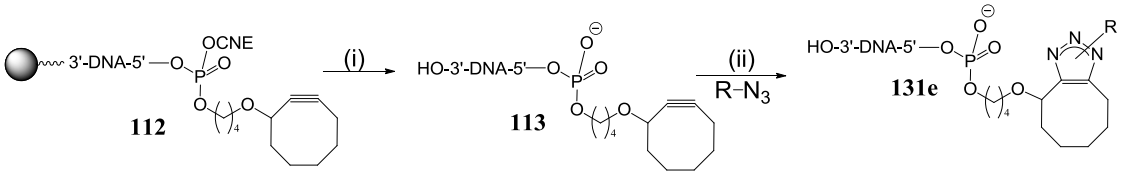

DNA = 3'-CGCACACACGCT-5'

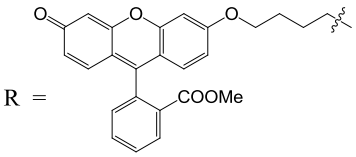

(i) 28% aq. NH_4OH, rt, 24 hr

(ii) DMF, rt, 18 hr

Scheme 4.12. SPAAC in the solution phase

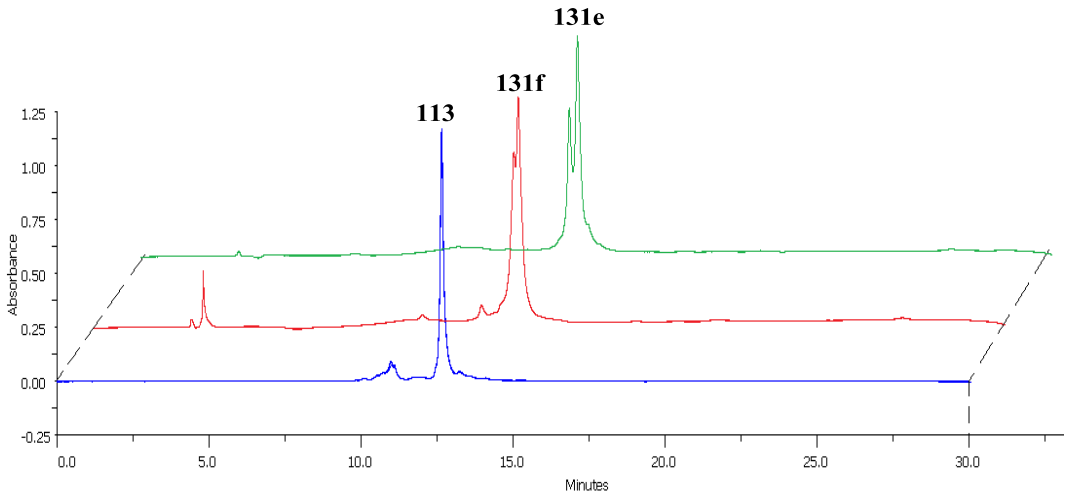

Figure 4.13. Overlaid chromatograms of the DNA-cyclooctyne starting material **113** (blue), and the purified triazolyl cycloadducts **131f** (red) and **131e** (green)

Azide	Reaction solvent	Reaction Time	Product
114	DMSO:H_2O 1:1	30 min	**131a**
115	DMSO:H_2O 1:1	30 min	**131b**
117	DMSO:H_2O 9:1	4 hr	**131c**
118	$CHCl_3$	24 hr	**131d**
119[a]	DMSO:H_2O 9:1	18 hr	**131e**
119	$CHCl_3$:H_2O 9:1	18 hr	**131f**

[a] This reaction was conducted in solution phase

Table 4.3. Conditions for the preparation of DNA-triazolyl conjugates **131a-f**

4.2.4.iii Cycloadditions with CPG-2'-OMe RNA-cyclooctynes

DNA is a relatively robust biomolecule with respect to RNA, which can be tricky to handle due to its sensitivity to various nucleases present on the skin or in the typical lab environment. Therefore, when attempting to apply a new methodology to the modification of RNA, it is often useful for initial proof of concept studies to focus on DNA. Owing to the vastly similar structure and chemical properties of these two biomolecules, results obtained with DNA more often than not translate well to RNA. The next goal of the project was to investigate the compatibility of the SPPAC approach outlined above with RNA for the provision of sequences labelled with groups likely to increase their stability, cellular delivery or visibility, *e.g.* fluorescent tagging; these conjugates may have significant benefits when employed in RNAi applications.

Initial studies focused on the CPG-$\underline{U}_4$-cyclooctyne[‡‡] **134**, which was prepared following coupling of the cyclooctyne-phosphoramidite **109** to the resin-bound $\underline{U}_4$ sequence **132** (scheme 4.13) using a procedure parallel to that outlined in section 4.2.1. The RNA

[‡‡] Underlined base denotes a 2'-OMe protected nucleoside

used was blocked at the 2'-position of each sugar with an OMe group. Use of the 2'-OMe 'blocking group' is popular when working with RNA, as it increases stability and nuclease resistance without interfering with the intracellular RNAi machinery.[10]

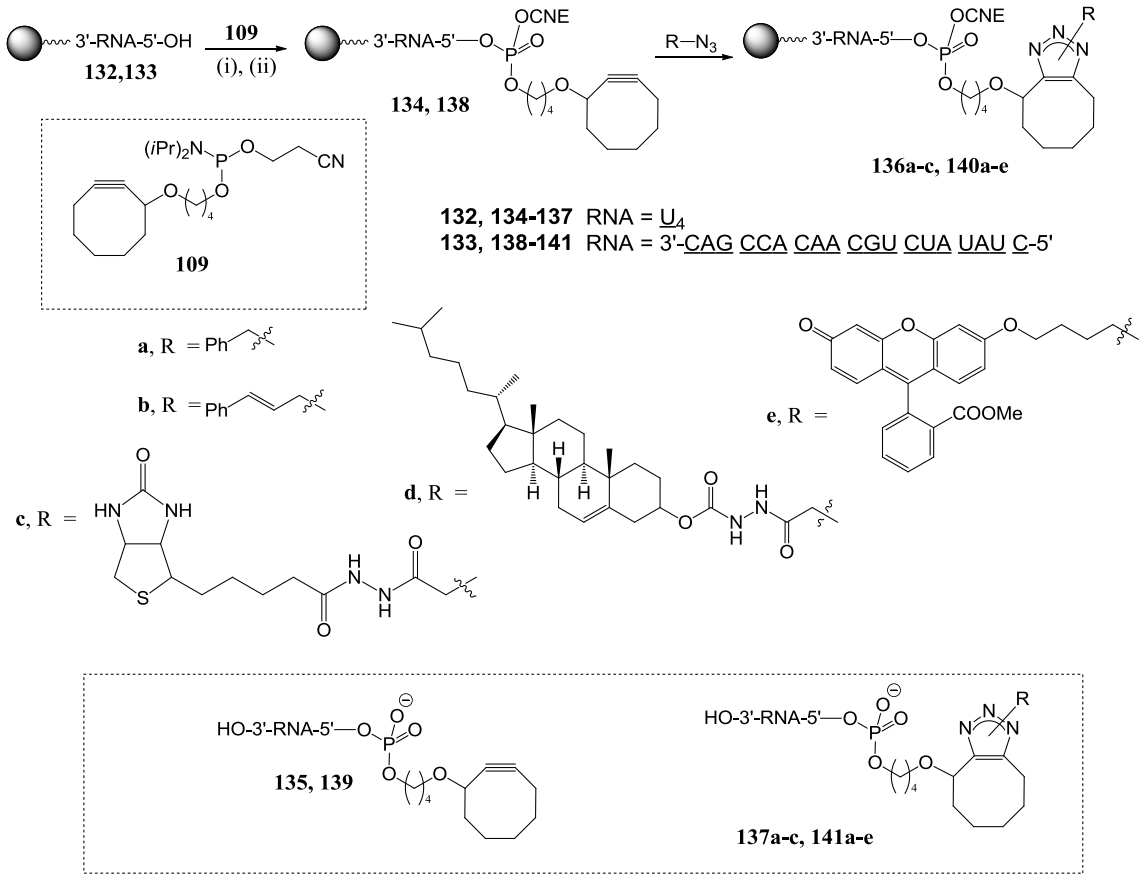

(i) BMT, CH_3CN, rt, 30 min

(ii) I_2 (0.1 M) THF-pyridine-H_2O

Scheme 4.13. Synthesis of 2'-OMe RNA-triazolyl conjugates by SPAAC

The benzyl, cinnamyl and biotin azides **114, 115** and **117** were chosen as test cases, and a large excess (~100 equiv.) was used to drive each reaction to completion. Agitation of the reaction mixtures for 2 hr in aqueous DMSO was followed by work-up and cleavage from the resin. The work-up procedure for 2'-OMe RNA was the same as that used for DNA. HPLC analysis of the products **137a-c** demonstrated complete consumption of the starting material in each case (figure 4.14).

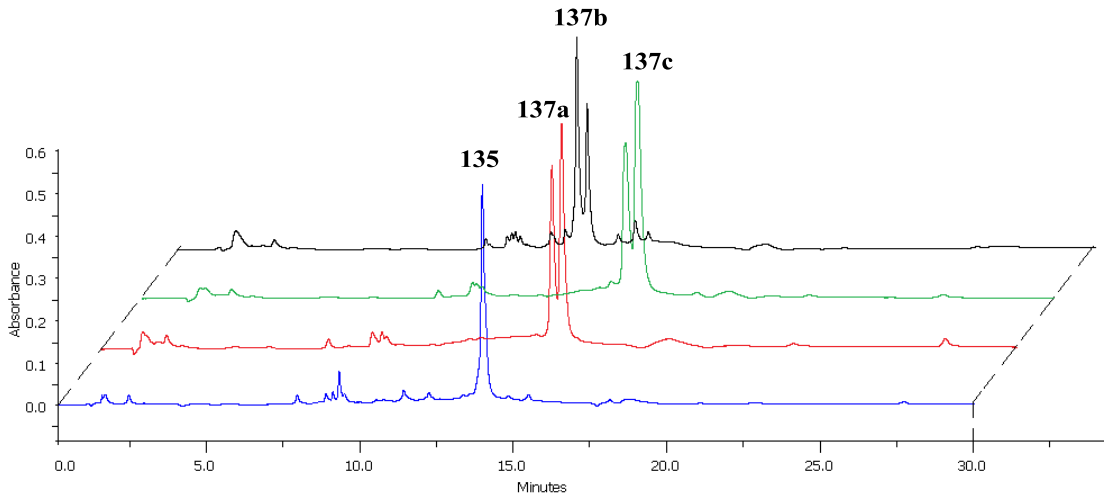

Figure 4.14. Overlaid chromatograms of the U_4-cyclooctyne **135** (blue), and the U_4-triazolyl cycloadducts **137a** (red), **137b** (green) and **137c** (black)

The results observed with the U_4-cyclooctyne confirmed that SPAAC was successful with a small RNA sequence. Conjugation to a more complex sequence was next investigated. Thus, the resin-bound 2'-OMe RNA-cyclooctyne conjugate **138**, a 19-*mer* containing all four bases with their standard protecting groups, was prepared. This sequence was also the approximate length of those employed for formation of synthetic siRNA duplexes; as such its compatibility with the SPAAC methodology could provide a novel route to modified siRNAs on the solid phase.

Cycloaddition of **138** with the benzyl and cinnamyl azides **114** and **115** was carried out under parallel conditions to those employed for the analogous reaction with the DNA-cyclooctyne **112**. Thus, following 30 minutes agitation of the reaction mixture at room temperature and cleavage from the resin, analysis of the crude products by HPLC showed that all of the starting material had been consumed. Notably, the chromatograms of the crude reaction products **141a,b** contained more early eluting impurities than the corresponding DNA cycloadducts (figure 4.15). These impurities can be traced back to the RNA-cyclooctyne starting material, and were attributed to failed sequences arising from the synthesis of the 19-*mer* RNA. Even if the coupling efficiency of each step is > 98%, these failed sequences can build up during the synthesis of a relatively long oligonucleotide. In this case, however, it was reasonably simple to remove these impurities by preparative HPLC. As a representative example, the HPLC traces of crude and purified **141a** are shown in figure 4.16.

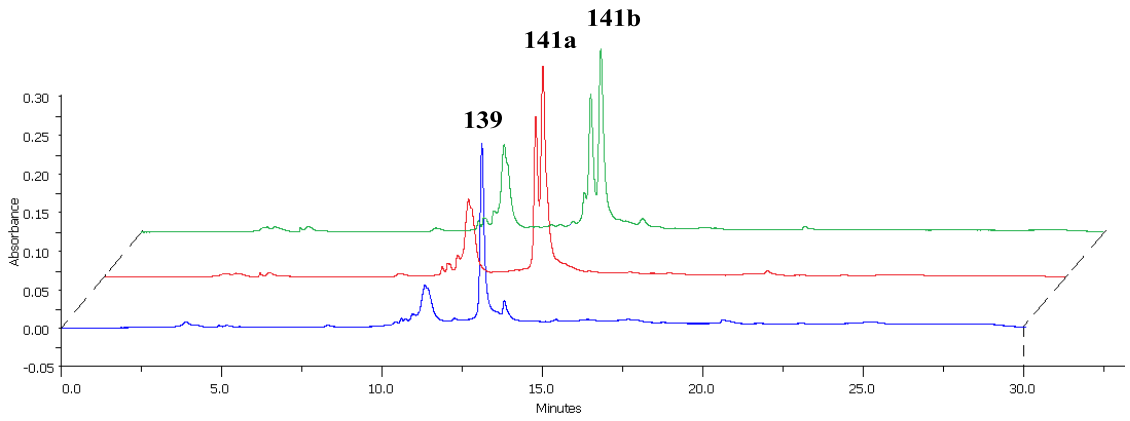

Figure 4.15. Overlaid chromatograms of the crude RNA-cyclooctyne starting material **139** (blue), and the crude RNA-triazolyl cycloadducts **141a** (red) and **141b** (green)

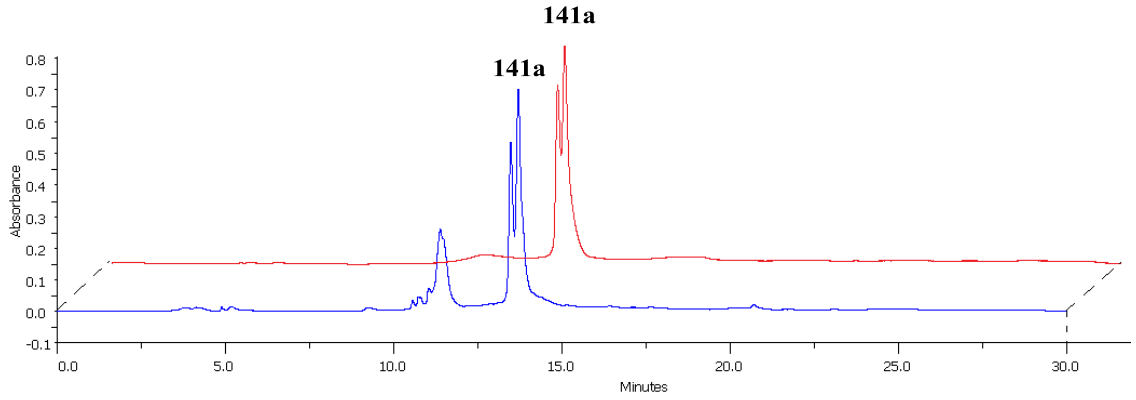

Figure 4.16. Overlaid chromatograms of crude (blue) and purified (red) benzyl cycloadduct **141a**

Investigation of cycloaddition with the more complex azides **117** and **118** employed the same optimised conditions used for reaction with DNA. Consequently, the cycloadduct **140c** was formed in near quantitative yield after 4 hr reaction beween **138** and the biotin azide **117** (20 equiv., 140 mM). Similarly, after 24 hr agitation of **138** in a suspension of the cholesterol azide **118** in $CHCl_3$, the resin-bound RNA-conjugate **140d** was formed. Cleavage/deprotection and purification by HPLC yielded the cycloadducts **141c,d** (figure 4.17), which were further characterised by MALDI-TOF MS.

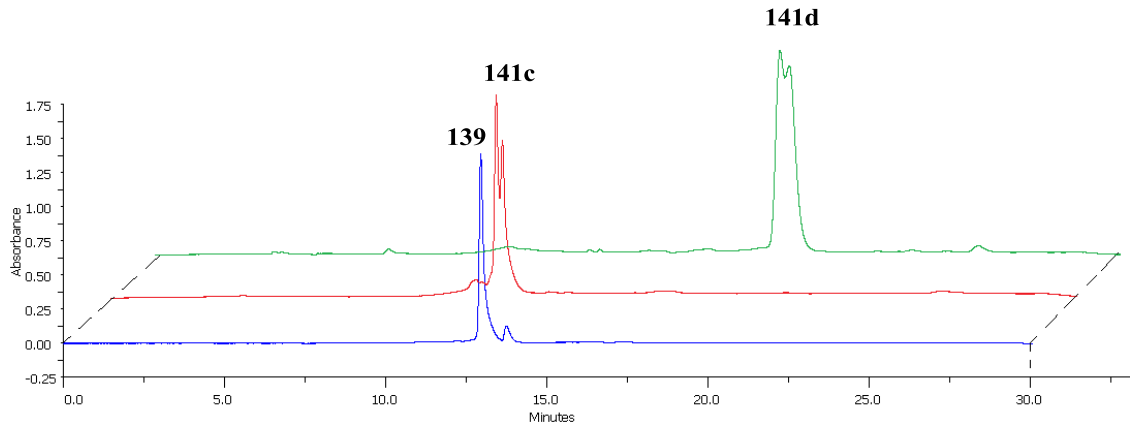

Figure 4.17. Overlaid chromatograms of purified RNA-cyclooctyne starting material **139** (blue), and purified triazolyl cycloadducts **141c** (red) and **141d** (green)

The instability of the the fluorescein methyl ester group under the basic conditions necessary for deprotection/cleavage guided the approach to the preparation of a fluorescently labelled RNA-conjugate. A sample of the RNA-cyclooctyne **139**, purified by preparative HPLC, was agitated in the presence of a solution of the fluorescein azide **119** in DMF for 18 hr at room temperature. HPLC analysis of the products following work-up demonstrated complete consumption of the starting material **139** (figure 4.18), and MALDI-TOF MS analysis confirmed formation of the triazolyl cycloadduct **141e**.

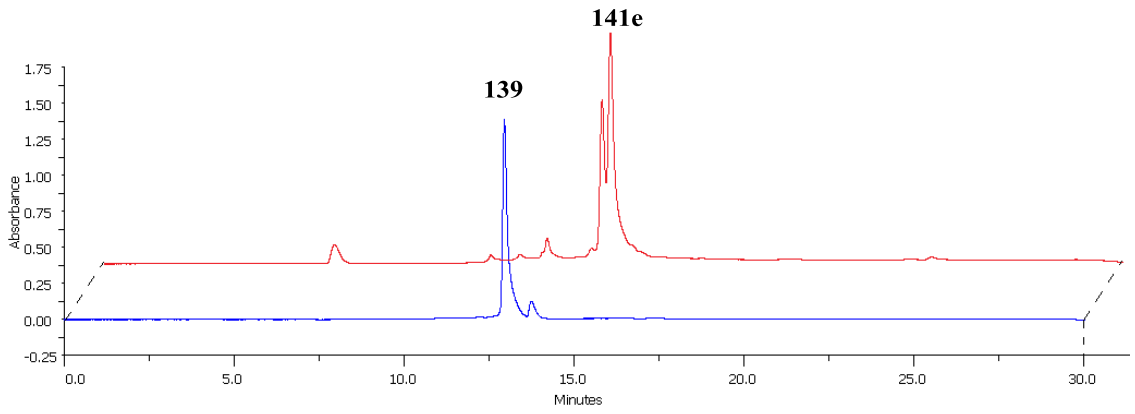

Figure 4.18. Overlaid chromatograms of purified RNA-cyclooctyne **139** (blue), and the crude fluorescein cycloadduct **141e** (red)

4.2.5 Conclusions

Solid phase SPAAC conjugation of several biologically interesting labels to both DNA and 2'-OMe RNA has been demonstrated. This methodology employs mild, copper-free conditions and is high yielding, efficient and broad in scope. Although the rate of reaction of these cyclooctyne-functionalised oligonucleotides is slower with azides than with nitrile oxide dipoles at similar concentrations,[200] this can be compensated by increasing the concentration of azide in the reaction mixture. While application of SPAAC to oliognucleotide conjugation has been reported previously,[201,212] these examples require lengthy (10 steps), non-trivial syntheses to produce a suitable cyclooctyne conjugate. In contrast, the DNA/RNA-cyclooctynes employed here can be obtained in five synthetic steps,[200] and still undergo efficient SPAAC with azide dipoles. Compatibility of this methodology has been demonstrated with azides of varying steric and electronic demands, including biotin, fluorescein, and cholesterol; the resulting conjugates may prove valuable in an array of bioanalytical and therapeutic applications. Indeed, the general approach described here could potentially be used to modify nucleic acids with a variety of structurally and functionally diverse labels, which need only be functionalised with a simple azide moiety to facilitate attachment.

4.2.6 Future Work

- Expand the scope of the pre-synthetic approach to chemically modified oligonucleotides by employing a wider range of alkyne click partners bearing labels of varying synthetic and biological interest.
- Determine the photochemical properties of a range small molecule and oligonucleotide-azobenzene conjugates to establish the existence, or not, of a relationship between the extent of conjugation between the azobenzene moiety and the linker (isoxazole) unit to nucleic acids, *e.g.* compare the the λ_{max} of the π- π* and n- π* transitions of the azobenzene unit in the cycloadducts **77a,b** with the oligonucleotide-conjugates **94a,b**.
- Develop a synthetic route to **67c**; perhaps attempt reduction of the primary alcohol **74c** to the aldehyde **142** prior to condensation with nitrosobenzene to form the azobenzene, which may avoid reactivity at the azo group. Preparation of the *ortho*-substituted oligonucleotide-azobenzene conjugate **94c** and comparison of its photochemical and kinetic properties with those of **94a** and **94b** may yield further insight into the nature of the *trans-cis* equilibrium of these isoxazole-linked azobenzene conjugates.

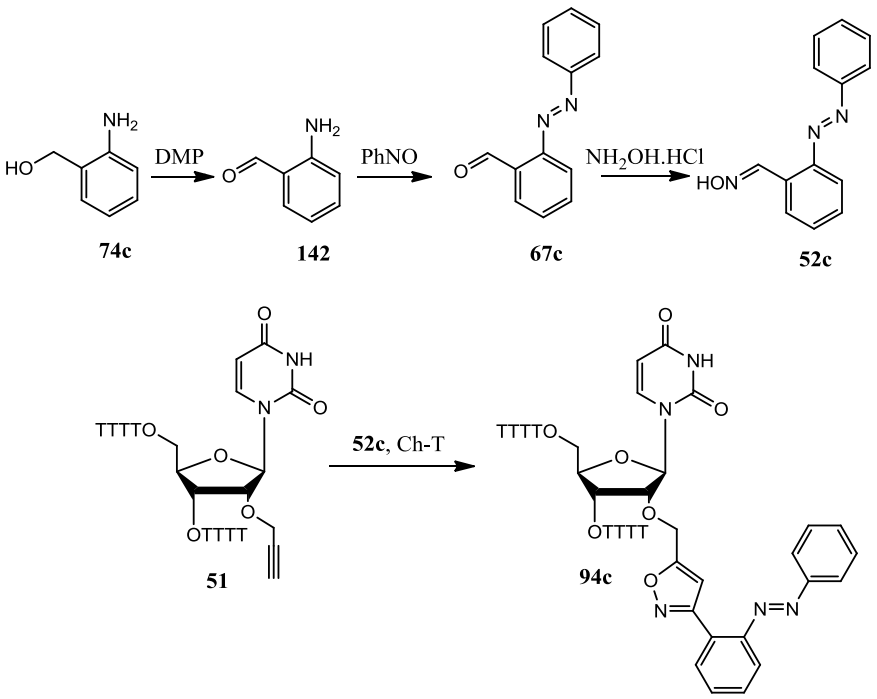

Scheme 4.14. Proposed synthesis of *ortho*-substituted oligonucleotide-conjugate **94c**

- Prepare an oligonucleotide-AB conjugate bearing the photoresponsive unit at an internal position, analogous to **94**, and investigate the melting properties of the duplex composed from such a sequence with a complementary strand of DNA. This experiment will inform on the influence of the isoxazole-modification on the thermal stability of the duplex under the Irr and DA adapted conditions.
- Investigate the potential of labelled siRNAs prepared using the methodology described in chapter 4 to effect RNAi in a biological environment. A key experiment should be designed to compare the ability of a cholesterol-labelled siRNA analogue of **141d** and a native unlabelled duplex to effect knockdown of a particular gene, *e.g.* green fluorescent protein gene. In such a case the lipophilic character of the cholesterol moiety may be expected to assist siRNA in crossing the cell's lipid bilayer.

Chapter 5

Experimental

5.1 Instrumentation

Standard reagents were supplied by either Apollo Scientific, TCI Europe, or Sigma-Aldrich and were used as received without further purification. Solvents were distilled before use and purified according to standard procedures. Analytical TLC was performed on precoated (250 μm) silica gel 60 F-254 plates from Merck. All plates were visualised by UV irradiation and/or staining with Hanessian's stain (5 g $(NH_4)_6Mo_7O_{24}.4H_2O$, 1 g $Ce(SO_4)_2$, 10 mL conc. H_2SO_4 in 90 mL H_2O) followed by heating. Flash chromatography was performed using silica gel 32–63 μm, 60 Å. Electrospray (ESI) mass spectra were collected on an Agilent Technologies 6410 Time of Flight LC/MS. NMR spectra were obtained with a Bruker instrument at 25 °C (^1H at 300 MHz; ^{13}C at 75 MHz, ^{31}P at 121 MHz). Chemical shifts are reported in ppm downfield from TMS as standard. NMR spectra are recorded in $CDCl_3$ unless otherwise stated. UV-Vis spectra were recorded with a Jasco V-630BIO spectrophotometer at 25 °C. Infrared spectra were recorded as KBr discs or liquid films between KBr plates using a Perkin Elmer System 2000 FT-IR spectrometer. Melting point analyses were carried out using a Stewart Scientific SMP 1 melting point apparatus.

All materials used in DNA/RNA synthesis were supplied by either Link Technologies or ChemGenes. Oligonucleotide synthesis was carried out on an Expedite DNA/RNA synthesiser on a 1 μmol scale using standard DNA and RNA phosphoramidites. Standard nucleobase protecting groups were used. BMT (0.2 M) was used as activating agent. Oxidation was performed using 8:1:1 THF:pyridine:H_2O containing 20 mM I_2. Deprotection/cleavage of both native and modified DNA/2'-OMe RNA was achieved following incubation in either:

(i) 40% aqueous CH_3NH_2 (500 μL) at 65 ^oC for 30 minutes (for oligonucleotides containing thymine bases only)

(ii) 28% aqueous NH_4OH (500 μL) at 25 ^oC for 24 hr (for mixed sequences of oligonucleotides containing all four bases)

CH_3NH_2/ NH_4OH was evaporated using a concentrator. The CPG was washed with H_2O (3 x 150 μL aliquots), and all solutions and washings were combined to afford an

aqueous solution of DNA, which was analysed and if necessary, purified, by RP-HPLC on a Nucleosil column (unless otherwise stated) under the following conditions:
Column: Nucleosil C18 (4.6 x 250 mm). Buffer A: 0.1 M TEAAc, pH 6.5, 5% (v/v) MeCN, buffer B: 0.1 M TEAAc, pH 6.5, 65% (v/v) MeCN. Gradient: 0-4.3 min, 5% B; 4.3-16.6 min, 5→100% B. Flow rate: 1.0 mL/min. Detection at 260 nm with a diode array detector.
DNA/2'-OMe RNA was desalted with illustra™ NAP™-10 Sephadex™ G-25 DNA grade columns purchased from GE Healthcare. Mass spectral data was obtained by MALDI-TOF MS recorded by Metabion, Germany, unless otherwise stated.

5.2 Generation of phorphoramidite monomers by NOAC

5.2.1 General procedure for the synthesis of oximes 13a-c

A solution of the required aryl aldehyde **12a-c** (1.00 g, 6.02 mmol) and hydroxylamine hydrochloride (1.26 g, 18.1 mmol) in EtOH (35 mL) was stirred at room temperature for 10 min, after which a solution of sodium acetate (1.69 g, 24.1 mmol) in H2O (15 mL) was added. The mixture was heated under reflux for 40 min. Following solvent removal under reduced pressure the crude product, obtained as a white solid, was taken up in EtOAc (30 mL), washed with H_2O (3 x 20 mL) and dried over anhydrous magnesium sulfate. Removal of the solvent under reduced pressure yielded the pure product as a white solid in excellent yield.

2-(2-Hydroxyethoxy)benzaldehyde oxime (13a)

Yield: 96%, m.p. = 98-100 ^{o}C

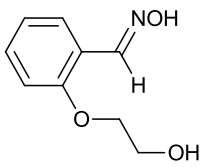

^{1}H NMR δ 8.41 (s, 1H, CHNOH), 7.58 (d, J = 7.8 Hz, 1H, ArH), 7.35 (t, J = 7.8 Hz, 1H, ArH), 7.03-6.95 (m, 2H, ArH), 4.17 (t, J = 4.0 Hz, 2H, ArOCH2), 3.98 (t, J = 4.0 Hz, 2H, C<u>H</u>$_2$OH); ^{13}C NMR δ 157.0, 147.8 (ArCO & CHNOH), 131.2, 128.9, 121.6, 121.2, 113.7, (1 x ArC, 4 x ArCH), 70.7, 61.2 (2 x CH_2); IR (KBr) 3388, 3219, 1601, 1251, 764 cm^{-1}; HRMS (ESI) calcd for 204.0631 [M + Na]$^{+}$, found 204.0640.

3-(2-Hydroxyethoxy)benzaldehyde oxime (13b)

Yield: 86%, m.p. = 94-96 ^{o}C

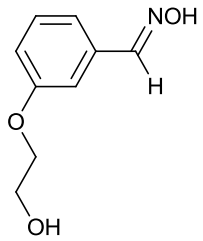

^{1}H NMR δ 8.11 (s, 1H, C<u>H</u>NOH), 7.88 (br s, 1H, CHNO<u>H</u>), 7.33-7.28 (m, 1H, ArH), 7.19-7.12 (m, 2H, ArH), 6.98-6.94 (m, 1H, ArH), 4.12 (t, J = 3.9 Hz, 2H, ArOCH$_2$), 3.98 (t, J = 3.9 Hz, 2H, CH$_2$OH); ^{13}C NMR δ 156.9, 147.7 (ArCO & CHNOH), 131.2, 128.8, 121.6, 121.2, 113.6 (1 x ArC, 4 x ArCH), 70.6, 61.2 (2 x CH_2); IR (KBr) 3350, 3154, 1595, 1262, 907, 795 cm^{-1}; HRMS (ESI) calcd for $C_9H_{12}NO_3$ 182.0812 [M + H] +, found 182.0809.

4-(2-Hydroxyethoxy)benzaldehyde oxime (13c)

Yield: 88%, m.p. = 109-111 ^{o}C

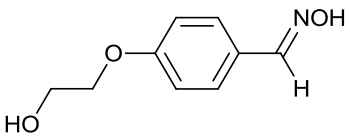

^{1}H NMR δ 8.09 (s, 1H, C<u>H</u>NOH), 7.52 (d, J = 8.4 Hz, 2H, ArH), 7.32 (br s, 1H, CHNO<u>H</u>), 6.93 (d, J = 8.7 Hz, 2H, ArH), 4.12 (t, *J* = 3.9 Hz, 2H, ArOCH$_2$), 4.00-3.97 (t, *J* = 3.9 Hz, C<u>H</u>$_2$OH), 2.05 (br s, 1H, CH$_2$O<u>H</u>); ^{13}C NMR δ 160.1, 149.9 (ArCO & CHNOH), 128.6 (2 x ArCH), 125.2 (ArC), 114.8 (2 x ArCH), 69.3, 61.4 (2 x CH_2); IR (KBr) 3262, 1605, 1259, 836 cm^{-1}; HRMS (ESI) calcd for 204.0631 [M + Na] +, found 204.0622.

5.2.2 General procedure for the synthesis of cycloadducts 15a-c

To a round-bottomed flask containing oxime (274 mg, 1.5 mmol) and Ch-T (427 mg, 1.9 mmol) in ethanol (5 mL) and water (5 mL) was added propargyl phenyl ether (100 mg, 0.75 mmol). The mixture was stirred for 18 hr at room temperature after which analysis by TLC (hexane:EtOAc, 6:4) indicated complete reaction. After removal of the solvent under reduced pressure, the residue was taken up in EtOAc (30 mL) and the solution was washed with 5% NaOH (3 x 10 mL). The organic layer was dried over anhydrous magnesium sulphate and the solvent was removed under reduced pressure. The crude products were purified by flash column chromatography (hexane:EtOAc, 6:4) to give the cycloadduct in good yield.

2-(2-[5-(Phenoxymethyl)isoxazol-3-yl]phenoxy)ethanol (15a)

Colourless oil; Yield: 81%, R_f = 0.304 (hexane:EtOAc, 7:3)

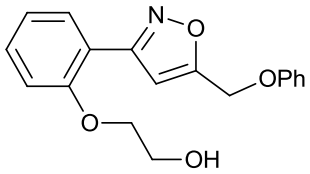

^{1}H NMR δ 7.77-7.70 (m, 1H, ArH), 7.50-7.25 (m, 3H, ArH), 7.08-6.97 (m, 5H, ArH), 6.76 (s, 1H, isox-H), 5.20 (s, 2H, CH_2OPh), 4.18 (t, *J* = 4.5 Hz, 2H, $ArOCH_2$), 3.93-3.90 (t, *J* = 4.5 Hz, 2H, CH_2OH), 3.24 (br s, 1H, $CH_2O\underline{H}$); ^{13}C NMR δ 167.4, 160.4, 157.8, 156.7 (4 x ArC), 131.4, 129.8, 129.7, 121.8, 121.6 (6 x ArCH), 118.4 (ArC), 114.8, 113.9 (3 x ArCH), 104.2 (isox-CH), 70.9, 61.3, 61.1 (3 x CH_2); IR (film) 3400, 1601, 1245, 755 cm^{-1}; HRMS (ESI) calcd for $C_{18}H_{18}NO_4$ 312.1230 $[M + H]^+$, found 312.1242

2-(3-[5-(Phenoxymethyl)isoxazol-3-yl]phenoxy)ethanol (15b)

White solid; Yield: 68%, m.p. = 70-72 ^{o}C

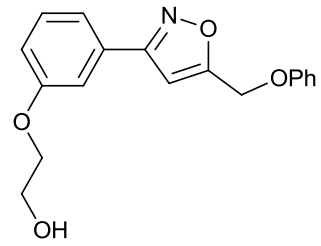

^{1}H NMR δ 7.38-7.28 (m, 5H, ArH), 7.04-6.96 (m, 4H, ArH), 6.61 (s, 1H, isox-H), 5.17 (s, 2H, C$\underline{H}_2$OPh), 4.12 (t, *J* = 4.2 Hz, 2H, ArOCH_2), 3.96 (t, *J* = 4.2 Hz, 2H, C$\underline{H}_2$OH), 2.42 (br s, 1H, $CH_2O\underline{H}$); ^{13}C NMR δ 168.7, 162.4, 159.1, 157.8 (4 x ArC), 130.1 (ArCH), 130.0 (ArC), 129.7, 121.9, 119.8, 116.8, 114.8, 112.5 (8 x ArCH), 101.5 (isox-CH), 69.4, 61.4, 61.3 (3 x CH_2); IR (KBr) 3208, 1600, 1260, 1231, 885, 755 cm^{-1}; HRMS (ESI) calcd for $C_{18}H_{18}NO_4$ 312.1230 [M + H] +, found 312.1233.

2-(4-[5-(Phenoxymethyl)isoxazol-3-yl]phenoxy)ethanol (15c)[§§]

White solid; Yield: 65%, m.p. = 95-97 ^{o}C

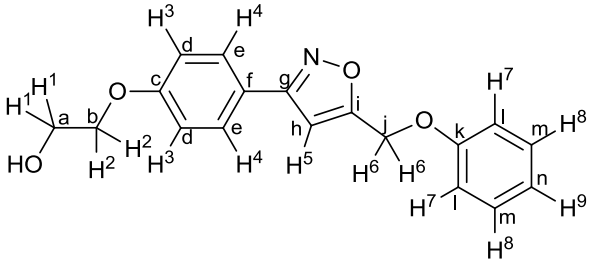

^{1}H NMR δ 7.75 (d, *J* = 8.4 Hz, 2H, H^4), 7.32 (t, *J* = 7.5 Hz, 2H, H^8), 7.04-6.98 (m, 5H, $H^{3,7,9}$), 6.59 (sl br s, 1H, H^5), 5.20 (sl br s, 2H, H^6), 4.14 (t, *J* = 4.4 Hz, 2H, H^2), 3.99 (t, *J* = 4.4 Hz, 2H, H^1), 2.03 (br s, 1H, OH); ^{13}C NMR δ 168.4, 162.1, 160.1, 157.8 ($C^{c,g,i,k}$), 129.7 (C^e), 128.3 (C^m), 121.9 ($C^{d/l/n}$), 121.7 (C^f), 114.9 ($C^{d/l/n}$), 114.8 ($C^{d/l/n}$), 101.1 (C^h), 69.3

[§§] A detailed discussion of the characterisation of **15c** is presented in the appendix (section 6.1)

(C^{b}), 61.5 ($C^{a/j}$), 61.4 ($C^{a/j}$); IR (KBr), 3438, 1613, 1258, 1238, 842 cm^{-1}; HRMS (ESI) calcd for $C_{18}H_{18}NO_4$ 312.1230 [M + H] +, found 312.1245.

5.2.3 General procedure for the synthesis of phosphoramidites 17a-c

The required cycloadduct **15** (100 mg, 0.32 mmol), and BMT (31 mg, 0.16 mmol) were placed in a dried round bottomed flask under an argon atmosphere. Anhydrous acetonitrile (5 mL) was added to the flask followed by diisopropylamine (23 µl, 0.16 mmol) and 2-cyanoethyl-*N,N,N',N'* tetraisopropylphosphorodiamidite (112 µl, 0.35 mmol). The reaction mixture was stirred for 30 minutes at room temperature after which TLC analysis (hexane:EtOAc, 1:1) showed complete consumption of the starting alcohol. The reaction mixture was diluted with ethyl acetate (25 mL) and washed with aqueous sodium bicarbonate (10 x 3 mL). The organic layer was dried over anhydrous sodium sulfate and the solvent was removed under reduced pressure to give the crude phosphoramidite, which was purified by flash column chromatography (hexane:EtOAc, 3:7) with elution under a positive pressure of nitrogen gas, yielding a colourless oil in each case.

2-Cyanoethyl 2-(2-[5-(phenoxymethyl)isoxazol-3-yl]phenoxy)ethyl *N,N*-diisopropylphosphoramidite (17a)

R_f = 0.83 (hexane:EtOAc, 3:7)

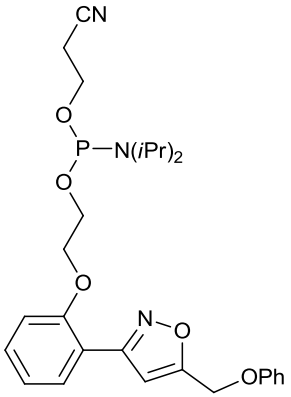

^{1}H NMR δ 7.94 (dd, *J* = 7.7, 1.7 Hz, 1H, ArH), 7.43-7.31 (m, 3H, ArH), 7.07-6.98 (m, 6H, ArH and isox-H), 5.19 (s, 2H, CH_2OPh), 4.25-4.22 (m, 2H), 4.16-3.54 (m, 6H), 2.55-2.51 (m, 2H), 1.19-1.14 (m, 12H); ^{31}P NMR δ 148.8.

2-Cyanoethyl 2-(3-[5-(phenoxymethyl)isoxazol-3-yl]phenoxy) ethyl *N,N*-diisopropylphosphoramidite (17b)

R_f = 0.83 (hexane:EtOAc, 3:7)

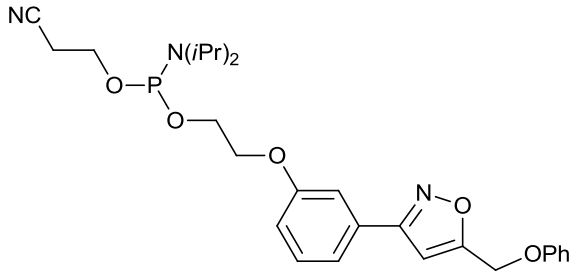

^{1}H NMR δ 7.39-7.32 (m, 5H, ArH), 7.05-6.98 (m, 4H, ArH), 6.64 (s, 1H, isox-H), 5.21 (s, 2H, CH_2OPh), 4.20 (t, *J* = 5.1 Hz, 2H), 4.10-3.49 (m, 6H), 2.63 (t, *J* = 6.4 Hz, 2H), 1.20 (dd, *J* = 6.8, 2.1 Hz, 12H); ^{31}P NMR δ 149.1.

2-Cyanoethyl 2-(4-[5-(phenoxymethyl)isoxazol-3-yl]phenoxy)ethyl *N,N*-diisopropylphosphoramidite (17c)

Rf = 0.83 (hexane:EtOAc, 3:7)

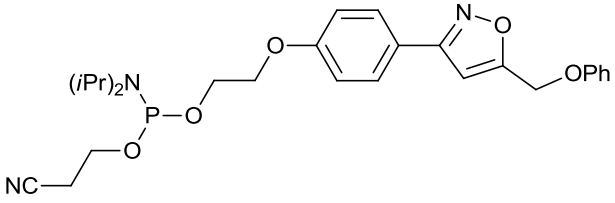

^{1}H NMR δ 7.73 (d, *J* = 8.7 Hz, 2H, ArH), 7.32 (t, *J* = 7.6 Hz, 2H, ArH), 7.04-6.95 (m, 5H, ArH), 6.59 (s, 1H, isox-H) 5.20 (s, 2H, CH_2OPh), 4.29 (t, *J* = 5.1 Hz, 2H, CH_2), 4.10-3.77 (m, 4H), 3.70-3.57 (m, 2H), 2.63 (t, *J* = 6.5 Hz, 2H), 1.20 (dd, *J* = 6.8, 2.9 Hz, 12H); ^{31}P NMR δ 149.0.

5.2.4 General procedure for manual conjugation of phosphoramidite monomers to CPG-DNA–OH; preparation of 22, 26 and 30

To manually couple the phosphoramidites **17a-c** to the resin supported nucleoside/oligonucleotide, **20**, **24** or **28**, separate solutions of the phosphoramidite (500 µL, 100 mM in anh. CH_3CN) and of BMT (500 µL, 0.3 mM in anh. CH_3CN), both in 1 mL syringes were attached to either end of a DNA synthesis column containing CPG-DNA (1 µmol). The mixture was reacted for 15 minutes at room temperature with mixing between the two syringes. This reaction was repeated with a second portion of each of a new solution of the phosphoramidite and BMT. The CPG was washed with CH_3CN (5 x 2 mL) prior to treatment with oxidizer (700 µL, 0.1 M Iodine solution in THF: pyridine: water; 8:1:1). Further washing with CH_3CN (2 x 5 mL) and drying yielded the resin-bound DNA-conjugates **22**, **26** or **30**. Deprotection/cleavage was followed by analysis by RP-HPLC.

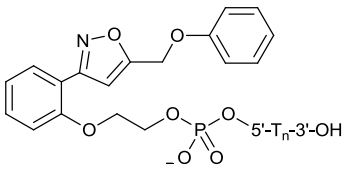

23a n = 1; **27a** n = 10

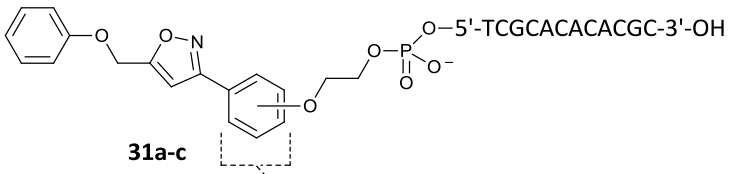

31a-c

a = *ortho*-substitution
b = *meta*- "
c = *para*- "

Compound	Mass calculated	Mass found
23a	638.1510 [M + Na^+]	638.1534 [M + Na^+][a]
27a	3353	3353
31a	3948	3949
31b	3948	3949
31c	3948	3949

[a] LC/MS-ESI-TOF mass data

Table 5.1. Mass data for the oligonucleotide conjugates **23a**, **27a** and **31a-c**

5.3 Site specific introduction of azobenzene to DNA by NOAC

5.3.1 General procedure for the synthesis of the aryl oximes 57b-c

To a solution of the aldehyde (50 mmol) in EtOH (10 mL) was added hydroxylamine hydrochloride (7.24 g, 75 mmol) and pyridine (6.07 mL, 75 mmol). The resulting solution was heated for 30 min under microwave irradiation (T = 125 ^{o}C, P_{max} = 300 W) and after completion of reaction, the solution was cooled to 0 ^{o}C and water (5 mL) was added. This precipitated the pure product, which was filtered off as a white solid in excellent yield.

2-Fluorobenzaldehyde oxime (57b)

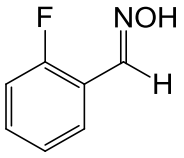

Yield: 95%, m.p. = 61-62 ^{o}C (lit. value = 61.8-62.3 ^{o}C)[73]

^{1}H NMR spectral data corresponded to that reported in the literature; (200 MHz, $CDCl_3$) δ 9.20 (br s, 1H, OH), 8.38 (s, 1H, CH=N), 7.77 (t of d, 1H, *J* = 7.4, 1.8 Hz), 7.37 (t of dd, 1H, *J* = 7.8, 5.3, 1.8 Hz), 7.16 (br t, 1H, *J* = 7.5 Hz), 7.09 (ddd, 1H, *J* = 10.4, 8.2, 1.2 Hz).[73]

1-Naphthaldehyde oxime (57c)

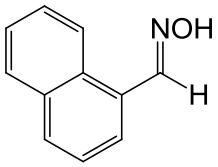

Yield: 92%, m.p. = 96-97 ^{o}C (lit. value 96 ^{o}C)

^{1}H NMR data corresponded that reported in the literature; (400 MHz, CDCl3) δ 8.82 (s, 1H), 8.48 (d, J = 8.3 Hz, 1H), 7.93-7.87 (m, 2H), 7.78 (d, J = 7.0 Hz, 1H), 7.62-7.46 (m, 3H).[71]

5.3.2 Synthesis of the ether linked isoxazole cycloadducts 55a-d

5.3.2.i General procedure for synthesis of the cycloadducts 55a-c

To a solution of the oxime (1.27 mmol) in EtOH (2.5 mL) was added a solution of Ch-T (289 mg, 1.27 mmol) in H_2O (2.5mL). The resulting solution was stirred for 10 min at room temperature, after which it was added to a solution of the alkyne **54**[213] (100 mg, 0.423 mmol) in EtOH (5 mL). This solution was then heated for 1 hr at 40^{o}C, after which the reaction mixture was cooled to -20 ^{o}C, yielding the product as an orange precipitate in good yield.

3-Phenyl-5-((4-(phenylazo)phenoxy)methyl)isoxazole (55a)

Yield: 91 %, m.p. = 125-127 ^{o}C

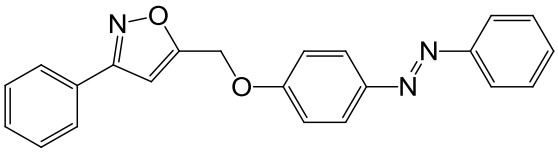

^{1}H NMR δ 7.97-7.81 (m, 6H, ArH), 7.53-7.45 (m, 6H, ArH), 7.11 (d, 2H, *J* = 8.8 Hz, ArH), 6.69 (s, 1H, isox-H), 5.28 (s, 2H, CH_2); ^{13}C NMR δ 167.9, 162.6, 160.0, 152.6, 147.7 (5 x ArC), 130.7, 130.3, 129.1, 129.0 (6 x ArCH), 128.6 (QC), 126.9, 124.9, 122.7, 115.0 (8 x ArCH), 101.7 (isox-CH), 61.5 (CH_2); HRMS (ESI) calcd for $C_{22}H_{18}N_3O_2$ 356.1402 $[M + H]^+$, found 356.1402.

3-(2-Fluorophenyl)-5-((4-(phenylazo)phenoxy)methyl)isoxazole (55b)

Yield: 86 %, m.p. = 108-109 ^{o}C

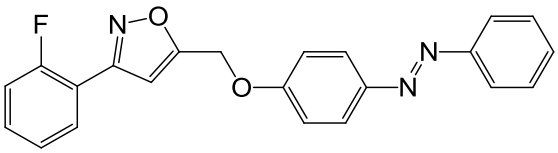

^{1}H NMR δ 8.02-7.87 (m, 5H, ArH), 7.53-7.40 (m, 4H, ArH), 7.27-7.10 (m, 4H, ArH), 6.84 (d, 1H, *J* = 3.5 Hz, isox-H), 5.29 (s, 2H, CH_2); ^{13}C NMR δ 167.6 (d, *J* = 1.8 Hz, ArC), 160.3 (d, *J* = 250.3 Hz, ArC-F), 160.0, 158.0, 152.6, 147.7 (4 x ArC), 131.9 (d, *J* = 8.5 Hz, ArCH), 130.7, 129.1, 129.1, 124.8 (6 x ArCH), 124.7 (d, *J* = 3.5 Hz, ArCH), 122.7 (2 x ArCH),

116.7 (d, *J* = 11.8 Hz, ArC), 116.4 (d, *J* = 21.7 Hz, ArCH), 115.0 (2 x ArCH), 104.3 (d, *J* = 9.0 Hz, isox-CH), 61.4 (CH_2) ; HRMS (ESI) calcd for $C_{22}H_{17}FN_3O_2$ 374.1299 $[M + H]^+$, found 374.1295.

3-(Naphthalen-1-yl)-5-((4-(phenylazo)phenoxy)methyl)isoxazole (55c)

Yield: 86 %, m.p. = 112-114 ^oC

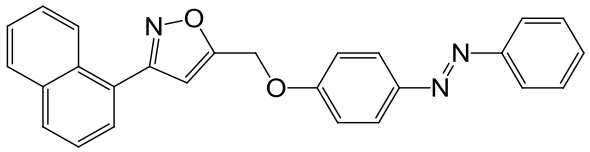

^1H NMR δ 8.39-8.35 (m, 1H ArH), 7.98-7.88 (m, 6H, ArH), 7.71 (d, *J* = 6.6 Hz, 1H, ArH), 7.57-7.45 (m, 6H, ArH), 7.15 (d, *J* = 8.2 Hz, 2H, ArH), 6.72 (s, 1H, isox-H), 5.37 (s, 2H, CH_2); ^{13}C NMR δ 167.2, 167.8, 160.0, 152.6, 147.7, 133.8, 130.9 (7 x ArC), 130.7, 130.5, 129.1, 128.6, 127.9, 127.2 (7 x ArCH), 126.4 (ArC), 125.4, 126.5, 125.2, 124.9, 122.7, 115.0 (9 x ArCH), 105.1 (isox-CH), 61.6 (CH_2); HRMS (ESI) calcd for $C_{26}H_{20}N_3O_2$ 406.1550 $[M + H]^+$, found 406.1558.

5.3.2.ii Synthesis of the cycloadduct 55d

To a solution of 2-nitrobenzaldehyde oxime **57d** (211 mg, 1.27 mmol) in EtOH (2.5 mL) was added a solution of Ch-T (434 mg, 1.91 mmol) in H_2O (2.5mL). The resulting solution was stirred for 20 min at rt, after which it was added to a solution of the alkyne[213] (100 mg, 0.423 mmol) in EtOH (5 mL). This solution was then heated for 1 hr at 40^oC. Once the reaction was complete, EtOAc (20 mL) was added, the organic layer was washed with 1 M NaOH (3 x 10 mL) and dried over anhydrous magnesium sulphate. Removal of the solvent under reduced pressure yielded the crude product, which was purified by flash column chromatography (Hex:EtOAc, 4:1) to yield the product as an orange solid.

3-(2-nitrophenyl)-5-((4-(phenylazo)phenoxy)methyl)isoxazole (55d)

Yield: 35 %, m.p. = 96-98 ^{o}C

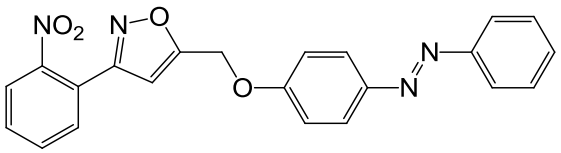

^{1}H NMR δ 8.02 (d, *J* = 7.7 Hz, 1H, ArH), 7.95 (d, *J* = 9.0 Hz, 2H, ArH), 7.90-7.88 (m, 2H, ArH), 7.72-7.64 (m, 3H, ArH), 7.53-7.45 (m, 3H, ArH), 7.11 (d, *J* = 9.0 Hz, 2H, ArH), 6.51 (s, 1H, isox-H), 5.31 (s, 2H, CH_2); ^{13}C NMR δ 167.8, 160.1, 159.9, 152.7, 148.6, 147.8 (6 x ArC), 133.1, 131.7, 130.8, 130.6, 129.1, 124.8, 124.6 (9 x ArCH), 124.0 (ArC), 122.7, 115.1 (4 x ArCH), 104.0 (isox-CH), 61.4 (CH_2); HRMS (ESI) calcd for $C_{22}H_{17}N_4O_4$ 401.1244 $[M + H]^+$, found 401.1243.

5.3.3 General procedure for the synthesis of amide linked cycloadducts (62-64)

To a solution of the oxime **57a** (138 mg, 1.14 mmol) in EtOH (2.5 mL) was added a solution of Ch-T (259 mg, 1.14 mmol) in H_2O (2.5 mL). The resulting solution was stirred for 10 min at room temperature, after which it was added to a solution of the alkyne[169] (100 mg, 0.380 mmol) in EtOH (5 mL). This solution was then heated for 1 hr at 40^{o}C, after which the reaction mixture was cooled to -20 ^{o}C, yielding the product as an orange precipitate in good yield.

2-(Phenylazo)-N-((3-phenylisoxazol-5-yl)methyl)benzamide (62)

Yield: 78%, m.p. = 136-138 ^{o}C

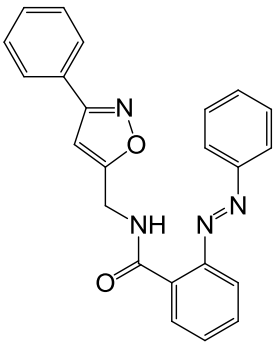

^{1}H NMR δ 9.29 (br t, *J* = 5.5 Hz, 1H, NH), 8.44-8.40 (m, 1H, ArH), 7.86-7.73 (m, 5H, ArH), 7.62-7.42 (m, 8H, ArH), 6.55 (s, 1H, isox-H), 4.89 (d, *J* = 5.5 Hz, 2H, CH_2); ^{13}C NMR δ 169.4, 165.9, 162.6, 152.3, 149.5 (5 x ArC), 132.4, 132.2, 131.7, 131.7 (4 x ArCH), 130.5 (ArC), 130.1, 129.6, 128.9 (5 x ArCH), 128.8 (ArC), 126.8, 123.2, 115.9 (5 x ArCH), 100.7 (isox-CH), 36.0 (CH_2); HRMS (ESI) calcd for $C_{23}H_{19}N_4O_2$ 383.1503 $[M + H]^+$, found 383.1513.

3-(Phenylazo)-N-((3-phenylisoxazol-5-yl)methyl)benzamide (63)

Yield: 81%, m.p. = 160-161 ^{o}C

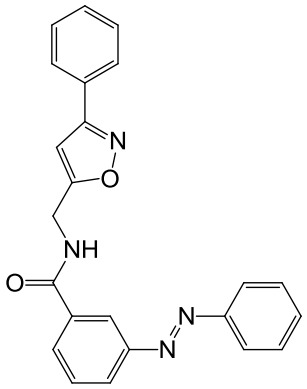

^{1}H NMR δ 8.31 (t, *J* = 1.8 Hz, 1H, ArH), 8.07 (d, *J* = 8.0 Hz, 1H, ArH), 7.98 (d, *J* = 7.8 Hz, 1H, ArH), 7.94-7.90 (m, 2H, ArH), 7.79-7.75 (m, 2H, ArH), 7.62-7.42 (m, 7H, ArH), 7.04 (br t, *J* = 5.8 Hz, 1H, NH), 6.60 (s, 1H, isox-H), 4.85 (d, *J* = 5.8 Hz, 2H, CH_2); ^{13}C NMR δ 169.1, 166.9, 162.8, 152.5, 152.4, 134.6 (6 x ArC), 131.6, 130.1, 129.7, 129.2, 128.9 (8 x ArCH), 128.7 (ArC), 126.8, 126.7, 123.0, 120.6 (6 x ArCH), 100.8 (isox-CH), 35.8 (CH_2); HRMS (ESI) calcd for $C_{23}H_{19}N_4O_2$ 383.1503 $[M + H]^+$, found 383.1501.

4-(Phenylazo)-N-((3-phenylisoxazol-5-yl)methyl)benzamide (64)

Yield: 70%, m.p. = 198-199 ^{o}C

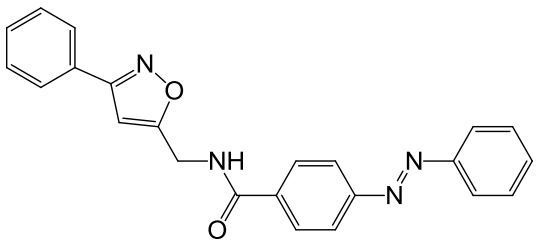

^{1}H NMR δ 7.98-7.94 (m, 6H, ArH), 7.81-7.78 (m, 2H, ArH), 7.54-7.44 (m, 6H, ArH), 6.78 (br t, *J* = 5.9 Hz, 1H, NH), 6.62 (s, 1H, isox-H), 4.86 (d, *J* = 5.9 Hz, 2H, CH_2) ; ^{13}C NMR δ 168.9, 166.7, 162.8, 154.6, 152.5, 135.2 (6 x ArC), 131.7, 130.2, 129.2, 129.0 (6 x ArCH), 128.7 (ArC), 128.1, 126.9, 123.1, 123.1 (8 x ArCH), 108.8 (isox-CH), 35.8 (CH_2); HRMS (ESI) calcd for $C_{23}H_{19}N_4O_2$ 383.1503 $[M + H]^+$, found 383.1500.

5.3.4 Synthesis of 4-(phenylazo)benzaldehyde (67a) by the Grignard method

To a 1 M solution of ethylmagnesium bromide (24 mL) in THF (34 mL) was added a solution of aniline (1.15 g, 12.3 mmol) in THF (10 mL) under an atmosphere of argon at 0 ^{o}C. The mixture was stirred gently at 55 ^{o}C for 45 min to complete the evolution of ethane. The resulting solution of the phenyliminodimagnesium intermediate **65** was added to a solution of 4-nitrobenzaldehyde (227 mg, 1.50 mmol) dissolved in THF (10 mL) at 0 ^{o}C under argon, where upon the colour of the mixture turned a deep reddish-brown colour. The coloured mixture was stirred at 55 ^{o}C for 3 hr, after which it was quenched with aqueous NH_4Cl (20 mL), extracted with diethyl ether (3 x 30 mL), and washed with 1 M HCl (3 x 30 mL) to remove any unreacted aniline. After washing with water (1 x 30 mL), the organic layer was dried over anhydrous $MgSO_4$ and concentrated under reduced pressure, yielding the crude product as a dark reddish-brown oil, which was purified by flash column chromatography (hexane:EtOAc, 9:1) giving the desired product **67a** as a red solid.

Yield: 38%, m.p. = 118-119 ^{o}C

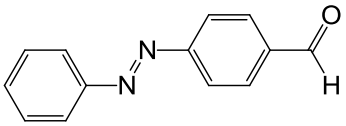

^{1}H NMR δ 10.08 (s, 1H, CHO), 8.01 (br s, 4H, ArH), 7.96-7.93 (m, 2H, ArH), 7.53-7.51 (m, 3H, ArH); ^{13}C NMR δ 191.6 (CHO), 155.9, 152.6, 137.5 (3 x ArC), 132.0 (ArCH), 130.7 (2 x ArCH), 129.2 (2 x ArCH), 123.3 (2 x ArCH), 123.3 (2 x ArCH); HRMS (ESI) calcd for $C_{13}H_{11}N_2O$ 210.0793 $[M + H]^+$, found 210.0880.

5.3.5 Synthesis of 4-(phenylazo)benzaldehyde (67a) starting from 4-(phenylazo)benzoic acid

5.3.5.i Synthesis of 4-(phenylazo)phenylmethanol (72a)

To a solution of 4-(phenylazo)benzoic acid (1.00 g, 4.42 mmol) in anhydrous THF (25 mL) was added LAH (210 mg, 5.53 mmol) at 0 ^{o}C, and the resulting mixture was stirred at rt for 30 min. The remaining LAH was then quenched with 3 % KOH. The resulting solution was diluted with EtOAc (30 mL) and washed with brine (1 x 10 mL). The combined organic layers were dried over anhydrous $MgSO_4$ and concentrated under reduced pressure to yield the product as an orange solid (619 mg, 66 %).

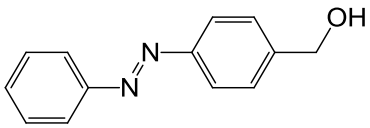

Yield: 66%, m.p. = 140-142 ^{o}C (lit. value = 142 ^{o}C)[214]

^{1}H NMR data corresponded that reported in the literature; (500 MHz, CDCl3) δ 7.90 (d, J = 8.0 Hz, 4H), 7.52.7.45 (m, 5H), 4.76 (s, 2H).[173]

5.3.5.ii Synthesis of 4-(Phenylazo)benzaldehyde (67a)

To a solution of 4-(phenylazo)phenylmethanol (**72a**) (300 mg, 1.41 mmol), in anhydrous DCM (10 mL) was added DMP (730 mg, 1.72 mmol). The resulting solution was stirred at rt for 1 hr. The solvent was then removed under reduced pressure and the resulting orange solid was dissolved in EtOAc (30 mL). This solution was washed with saturated $NaHCO_3$ (10 mL), brine (10 mL) and water (10 mL). The organic layer was then dried over anhydrous sodium sulphate and concentrated under reduced pressure, yielding the pure product as an orange solid (289 mg, 97 %).

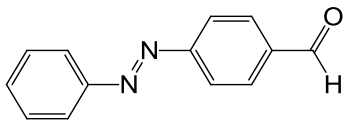

^{1}H NMR data corresponded to that observed for the product obtained using the Grignard method (see section 5.3.4, page 147).

5.3.6 Synthesis of of 3-(phenylazo)benzaldehyde (67b)

5.3.6.i Synthesis of 3-(phenylazo)phenylmethanol (72b)

The amine **74b** (500 mg, 4.06 mmol) was added to a solution of nitrosobenzene (652 mg, 6.09 mmol) in CH_3COOH (5 mL) at 0 ^oC. The resulting mixture was stirred at this temperature for 1 hr, after which it was warmed to rt and stirred for another 3 hr. EtOAc was added and the organic layer was washed with aqueous $NaHCO_3$ (3 x 20 mL) to remove the CH_3COOH. The organic layer was then dried over anhydrous $MgSO_4$ and concentrated under reduced pressure, yielding an orange solid as the crude product. This was then purified by flash column chromatography (hexane:EtOAc, 6:4), giving the product as an orange oil in good yield.

Yield: 82%, m.p. = 35-36 ^oC

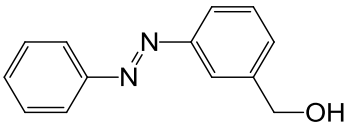

^{1}H NMR δ 7.93-7.90 (m, 3H, ArH), 7.85 (dt, *J* = 6.8, 1.9 Hz, 1H, ArH), 7.55-7.45 (m, 5H, ArH), 4.79 (s, 1H, CH_2); ^{13}C NMR δ 152.9, 152.6, 142.1 (3 x ArC), 131.1, 129.4, 129.3, 129.1, 122.9, 122.6, 120.6 (9 x ArCH), 64.9 (CH_2); HRMS (ESI) calcd for $C_{13}H_{13}N_2O$ 213.1022 $[M + H]^+$, found 213.1030.

5.3.6.ii Synthesis of 3-(phenylazo)benzaldehyde (67b)

To a solution of 3-(phenylazo)phenylmethanol (**72b**) (300 mg, 1.41 mmol), in anhydrous DCM (10 mL) was added DMP (1.20 g, 2.82 mmol). The resulting solution

was stirred at rt for 3 hr. The solvent was then removed under reduced pressure and the resulting orange solid was dissolved in EtOAc (30 mL). This solution was washed with saturated $NaHCO_3$ (10 mL), brine (10 mL) and water (10 mL). The organic layer was then dried over anhydrous sodium sulphate and concentrated under reduced pressure, yielding the pure product as an orange solid.

Yield: 71%, m.p. = 53-56 ^{o}C

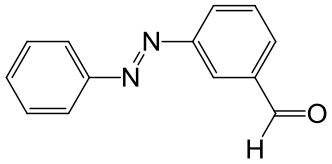

^{1}H NMR δ 10.04 (s, 1H, CHO), 8.32 (t, *J* = 1.8 Hz, 1H ArH), 8.10 (dt, *J* = 7.9, 1.3 Hz, 1H, ArH), 7.93-7.89 (m, 3H, ArH), 7.58 (t, *J* = 7.9 Hz, ArH); ^{13}C NMR δ 191.6 (CHO), 152.8, 152.3, 137.3 (3 x ArC), 131.7, 131.1, 129.8, 129.2, 128.7, 123.8, 123.2 (9 x ArCH); HRMS (ESI) calcd for $C_{13}H_{11}N_2O$ 211.0866 $[M + H]^+$, found 211.0868.

5.3.7 General procedure for the synthesis of 3- & 4-(phenylazo)benzaldehyde oximes (52a,b)

To a solution of the aldehyde (350 mg, 1.66 mmol) in EtOH (10 mL) was added hydroxylamine hydrochloride (173 mg, 2.49 mmol) and pyridine (2.49 mmol, 0.201 mL). The resulting solution was heated for 1 hr under microwave irradiation (T = 125 ^{o}C, P_{max} = 300 W). Water (5 mL) was then added and the resulting orange precipitate was filtered off to yield pure product in excellent yield.

3-(Phenylazo)benzaldehyde oxime (52b)

Yield: 88%. m.p. = 101-103 ^{o}C

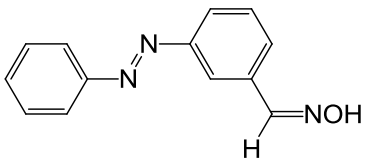

^{1}H NMR δ 8.37 (br s, 1H, NOH), 8.26 (s, 1H, CHNOH), 8.13 (t, *J* = 1.7 Hz, 1H, ArH), 7.96-7.91 (m, 3H, ArH), 7.71 (d, *J* = 7.7 Hz, 1H), 7.56-7.48 (m, 4H, ArH); ^{13}C NMR δ 152.9, 152.5 (ArC), 149.8 (CHNOH), 133.1 (ArC), 131.4, 129.6, 129.2, 129.0, 124.4, 123.0, 121.6 (9 x ArCH); HRMS (ESI) calcd for $C_{13}H_{12}N_3O$ 226.0975 $[M + H]^+$, found 226.0979.

4-(Phenylazo)benzaldehyde oxime (52a)

Yield : 94 %, m.p. = 151-152 ^{o}C

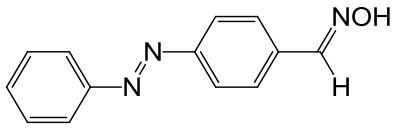

^{1}H NMR δ 8.20 (s, 1H, CHNOH), 7.96-7.92 (m, 4H, ArH), 7.74 (d, J = 8.5 Hz, 2H, ArH), 7.60 (br s, 1H, NOH), 7.56-7.49 (m, 3H, ArH); ^{13}C NMR δ 153.3, 152.6 (2 x ArC), 149.7 (CHNOH), 134.4 (ArC), 131.4, 129.2, 127.8, 123.3, 123.0 (9 x ArCH); HRMS (ESI) calcd for $C_{13}H_{12}N_3O$ 226.0975 $[M + H]^+$, found 226.0986.44

5.3.8 General procedure for the synthesis of the isoxazole cycloadducts 77a-b

The oxime **52** (150 mg, 0.667 mmol) was dissolved in EtOH (3 mL) and Ch-T (152 mg, 0.667 mmol) was added, followed by H_2O (1 mL). The resulting solution was stirred for 10 min at rt. The alkyne **14** (29 mg, 0.222 mmol) was then added followed by EtOH (1.5 mL) and H_2O (0.5 mL). The reaction was heated at 40 ^{o}C for 1 hr, after which H_2O (30 mL) was added and the aqueous layer was extracted with DCM (3 x 10 mL). Following drying of the combined organic extracts over anhydrous magnesium sulphate, the solvent was removed under reduced pressure. The resulting crude product was purified by flash column chromatography (hex:EtOAc, 4:1) to the pure product as an orange solid.

5-(phenoxymethyl)-3-(3-(phenylazo)phenyl)isoxazole (77b)

Yield: 46%, m.p. = 105-107 ^{o}C

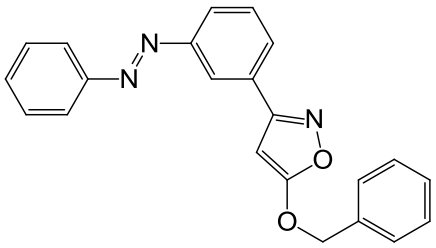

^{1}H NMR δ 8.32 (t, *J* = 2.1 Hz, 1H, ArH) 8.01-7.93 (m, 4H, ArH), 7.61 (t, *J* = 7.8 Hz, 1H, ArH), 7.57-7.49 (m, 3H), 7.36-7.30 (m, 2H, ArH), 7.05-6.99 (m, 3H, ArH), 6.75 (s, 1H, isox-H), 5.24 (s, 2H, CH_2); ^{13}C NMR δ 168.9, 162.1, 157.8, 153.0, 152.5 (5 x ArC), 131.4 (ArCH), 129.8 (ArC), 129.8, 129.7, 129.2, 129.0, 124.7, 123.0, 122.0, 121.1, 114.8 (13 x ArCH), 101.5 (isox-CH), 61.5 (CH_2); HRMS (ESI) calcd for $C_{22}H_{18}N_3O_2$ 356.1394 $[M + H]^+$, found 356.1391.

5-(phenoxymethyl)-3-(4-(phenylazo)phenyl)isoxazole (77a)

Yield: 89%, m.p. = 121-122 ^{o}C

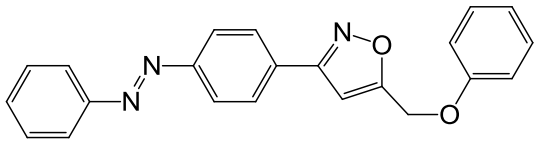

^{1}H NMR δ 8.04-7.93 (m, 6H, ArH), 7.60-7.50 (m, 3H, ArH), 7.34 (t, *J* = 8.1 Hz, 2H, ArH), 7.06-7.00 (m, 3H, ArH), 6.72 (s, 1H, isox-H), 5.24 (s, 2H, CH_2); ^{13}C NMR δ 169.0, 161.9, 157.8, 153.5, 152.6 (5 x ArC), 131.4 (ArCH), 131.0 (ArC), 129.7, 129.2, 127.7, 123.4, 123.0, 122.0, 114.8 (13 x ArCH), 101.4 (isox-CH), 61.5 (CH_2); HRMS (ESI) calcd for $C_{22}H_{18}N_3O_2$ 356.1394 $[M + H]^+$, found 356.1393.

5.3.9 Synthesis of 2-(phenylazo)phenyl)methanol (72c)

Procedure was the same as that used to prepare **72b**, except reaction time was 18 hr.

Yield = 79%, m.p. = 76-79 ^{o}C

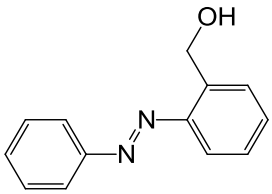

^{1}H NMR δ 7.90 (d, *J* = 8.2 Hz, 2H, ArH), 7.82 (d, *J* = 6.6 Hz, 1H, ArH), 7.57-7.42 (m, 6H, ArH), 5.04 (d, *J* = 4.8 Hz, 2H, CH_2), 3.17 (br t, *J* = 4.8 Hz, 1H, OH); ^{13}C NMR δ 152.5, 150.2, 138.7 (3 x ArC), 131.4, 131.4, 129.3, 129.1, 128.4, 123.0, 128.1 (9 x ArCH), 63.0 (CH_2OH); HRMS (ESI) calcd for $C_{13}H_{11}N_2$ 195.0917 [$(M + H)^+ - H_2O$], found 195.0919.

5.3.10 Synthesis of 2-phenyl-2*H*-benzo[*d*][1,2,3]oxadiazine (76)

5.3.10.i With base

The primary alcohol **72c** (68 mg, 0.319 mmol) was dissolved in DMF (5 mL) and sodium hydride (11 mg, 0.478 mmol) was added under an atmosphere of argon. After one hour stirring at rt, the reaction was quenched at 0 ^{o}C with MeOH (10 mL), and EtOAc (30 mL) was added. The organic layer was washed several times with H_2O (3 x 10 mL), dried over anhydrous $MgSO_4$, and concentrated under vacuum, yielding the crude product as a brown solid. This was purified by flash column chromatography (hexane:EtOAc, 6:4), giving the pure product as an off-white solid in 73% yield.

5.3.10.ii Without base

The primary alcohol **72c** (118 mg, 1.80 mmol) was dissolved in DMF (5 mL) and the resulting solution heated under reflux for 1 hr. After this time, the solvent was removed under reduced pressure, yielding a pure sample of product **76** in quantitative yield.

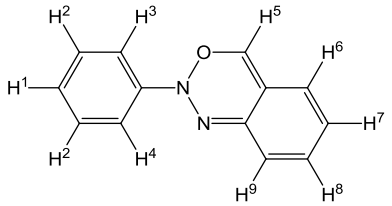

^{1}H NMR δ 8.39 (d, *J* = 0.9 Hz, 1H, H^{5}), 7.91 (d, *J* = 7.6, Hz, 2H, H^{3}), 7.84 (dd, *J* = 8.9, 0.9 Hz, 1H, H^{6}), 7.72 (d, *J* = 8.5 Hz, 1H, H^{9}), 7.52 (t, *J* = 7.6 Hz, 2H, H^{2}), 7.42-7.33 (m, 2H, H^{1}, H^{7}), 7.14 (t, *J* = 8.5 Hz, 1H, H^{8}); ^{13}C NMR δ 149.8, 140.6 (2 x ArC), 129.6, 127.9 , 126.9 (4 x ArCH), 122.8 (ArC), 122.5, 121.0, 120.4, 120.4, 118.0 (6 x ArCH); HRMS (ESI) calcd for $C_{13}H_{11}N_2O$ 211.0871 [$(M + H)^{+}$], found 211.0875.

5.3.11 Synthesis of the 2'-*O*-propargylated oligonucleotides 89 and 51

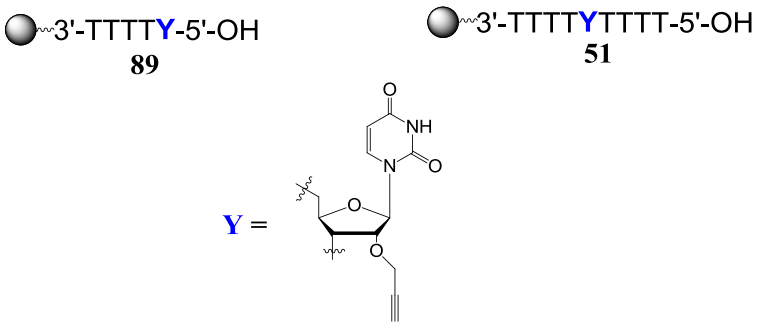

Separate solutions of the phosphoramidite **88** (500 µL, 100 mM in anhydrous CH_3CN), and BMT (500 µL, 0.3 mM in anhydrous CH_3CN), both in 1 mL syringes were attached to either end of a DNA synthesis column containing the CPG-T_4 **87** (1 µmol). The mixture was reacted for 15 min at rt with mixing between the two syringes. This reaction was repeated with a second portion each of a new solution of the phosphoramidite and BMT. The column was then re-installed on the oligonucleotide synthesiser where standard washing, capping, oxidation and deblocking programmes were carried out. Where the oligonucleotide **89** was required, the column was removed from the synthesiser at this point. Where the oligonucleotide **51** was required, the column was left installed on the synthesiser and the remaining DNA phosphoramidites were coupled using the standard procedure. Deprotection/cleavage of the resin-bound oligonucleotides was followed by RP-HPLC analysis.

5.3.12 Synthesis of the azobenzene-oligonucleotide conjugates 82, 84, 86, 92 and 94

HO-3'-**X**-5'-OH **82a**

HO-3'-**X**TT-5'-OH **84a**

HO-3'-**X**ACG-5'-OH **86a**

HO-3'-TTTT**X**-5'-OH **92a-b**

HO-3'-TTTT**X**TTTT-5'-OH **94a-b**

X =

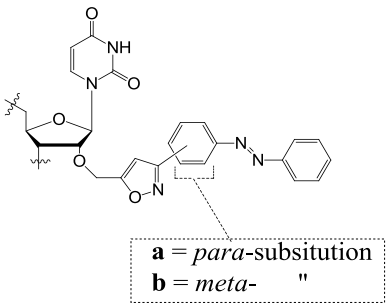

To a solution of the azo-oxime, **52** (30 µL, 250 mM in EtOH) was added a solution of Ch-T (10 µL, 750 mM in 1:1 EtoH:H_2O). This was then agitated at rt for 10 minutes to facilitate formation of the nitrile oxide, after which 20 µL (3.6 µmol) of this nitrile oxide solution was added to the CPG-2'-*O*-propargylated nucleic acid material (0.12 µmol). The mixture was agitated at rt for 24 hr, after which the excess starting material was washed away with DMSO (10 x 200 µL) and CH_3CN (2 x 200 µL). Deprotection/cleavage of the resin-bound oligonucleotides was followed by analysis and if necessary, purification by RP-HPLC.

Compound	Mass calculated	Mass found
82a	528.1490 [M + Na^+]	528.1463 [M + Na^+][a]
84a	1113	1115
86a	1436	1437
90	1498	1501
92	1721	1723
93	2716	2714
94a	2938	2937
94b	2938	2936

[a] LC/MS-ESI-TOF mass data

Table 5.2. Mass data for azobenzene- and alkyne-modified oligonucleotide conjugates

5.3.13 Photochemical characterisation of the azobenzene-oligonucleotide conjugates 94a and 94b

5.3.13.i Photo-switching of azobenzene-oligonucleotide conjugates 94a and 94b

A medium pressure Hg-Arc lamp (100 W, Engelhard Hanovia of Canada Ltd.) was used to effect photo-isomerisation of the azobenzene moieties. A band-pass filter was used for irradiation at 366 nm (4.13 W) and a cut-off filter was used for irradiation >400 nm (435 nm, 3.36 W) in combination with a water filter (1 cm) to prevent warming of the samples.

5.3.13.ii UV analysis of E → Z photoswitching following irradiation at 366 nm

UV spectra of solutions of the azobenzene-oligonucleotide conjugates **94a** and **94b** (15 µM in Milli-Q H_2O) were measured following irradiation at 366nm for 2, 4, 6, 8, 10 and 600 seconds. The appearance/disappearance of the λ_{max} at ~325 nm was used to monitor the degree of isomerisation.

5.3.13.iii Determination of the mole fraction of the cis-azobenzene appended 9-mers 98aII and 98bII (χ_{cis}) in the photostationary state using RP-HPLC

Solutions of the azobenzenze-oligonucleotides conjugates **94a** and **94b** (15 µM in Milli-Q H_2O) were analysed by RP-HPLC on a Hichrom C18 column following irradiation at 366 nm for 10 min and at >400 nm for 2 min. The χ_{cis} values for **94a** and **94b** in both photostationary states were quantified from the relative peak areas of **94aI** and **94aII**, and **94bI** and **94bII**.

5.3.14 Thermal stability studies of the cis-azobenzene appended 9-mers 98aII and 98bII

Following irradiation to the *cis* form at 366 nm for 10 min, UV spectra of the azobenzene-oligonucleotides conjugates **94a** and **94b** (10 µM in buffer: 10 mM pH 7.0 $Na_xH_xPO_4$, 100 mM NaCl, 0.5 mM EDTA) were measured at regular intervals up to a

period of 10 hr. This procedure was carried out at the following temperatures; 60, 65, 70, 75, 80, 85 °C. The normalised absorbance values $[(A_t-A_0)/A_\infty-A_0)]$ at 325 nm were plotted against time, and by curve-fitting using the GraphPad Prism 5 software package, the rate constants (*k*) at each temperature were obtained. Arrhenius and Eyring plots were generated from these data, and from these plots a range of kinetic constants were obtained for the *cis-trans* isomerisation process of both **94a** and **94b** (see table 3.4, page 96)

5.4 Conjugation to DNA/RNA by SPAAC

5.4.1 Synthesis of the biotin and cholesterol azides 117 and 118

5.4.1.i Synthesis of 2-azidoacetohydrazide (122)

To a solution of ethyl 2-azidoacetate[204] (2.0 g, 15.5 mmol) in EtOH (10 mL) was added hydrazine hydrate (1.3 mL, 25.3 mmol). The mixture was allowed to stir at rt for 2 hr after which TLC analysis (DCM:MeOH, 9:1) indicated complete consumption of starting material. Following removal of the solvent under reduced pressure, the crude product was purified by flash column chromatography (DCM:MeOH, 9:1) to yield a colourless oil (1.6 g, 90 %).

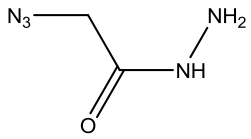

^{1}H NMR δ 8.14 (br s, 1H, N<u>H</u>NH$_2$), 4.06 (br s, 2H, NHN<u>H</u>$_2$), 4.01 (s, 2H, CH_2); ^{13}C NMR δ 167.5 (C=O), 51.6 (CH_2N_3); HRMS (ESI) calcd for $C_2H_5N_5ONa$ 138.0386 $[M + Na]^+$, found 138.0390.

5.4.1.ii Synthesis of N'-2-azidoacetyl biotin hydrazide (117)

To a solution of the biotin-NHS ester **123**[215] (870 mg, 2.55 mmol) and 2-azidoacetohydrazide **122** (352 mg, 3.06 mmol) in anhydrous DMF (20 mL) was added TEA (1.5 mL, 20.4 mmol). The resulting mixture was stirred overnight at rt under an atmosphere of argon. Following removal of particulate matter by filtration, the filtrate was evaporated to yield the crude product as a white solid, which was washed with DCM (5 x 10 mL) to yield pure product (745 mg, 86%).

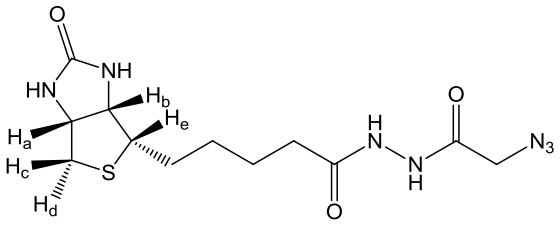

^{1}H NMR (DMSO-d_6) δ 10.05 (br s, 1H, NH), 9.86 (s, 1H, NH), 6.43 (s, 1H, NH), 6.36 (s, 1H, NH), 4.33-4.29 (m, 1H, $H_{a/b}$), 4.16-4.12 (m, 1H, $H_{a/b}$), 3.89 (s, 2H, CH_2N_3), 3.14-3.07 (m, 1H, $H_{c/d/e}$), 2.86-2.80 (m, 1H, $H_{c/d/e}$), 2.60-2.56 (m, 1H, $H_{c/d/e}$), 2.14 (t, 2H, J = 7.2 Hz, CH_2C=O), 1.64- 1.30 (m, 6H, 3 x CH_2); ^{13}C NMR (DMSO-d_6) δ 170.9 (C=O), 166.3 (C=O), 162.7 (C=O), 61.0, 59.2, 55.4, 49.3, 39.7, 32.9, 28.0, 27.9, 25.0 (9 x alkyl C); HRMS (ESI) calcd for $C_{12}H_{20}N_7O_3S$ 342.1343 $[M + H]^+$, found 342.1352.

5.4.1.iii Synthesis of cholesteryl 2-(2-azidoacetyl)hydrazine carboxylate (118)

To a solution of 2-azidoacetohydrazide (**122**) (0.62 g, 5.39 mmol), and TEA (620 µL) in DCM (50 mL) was added a solution of cholesterol chloroformate (**124**) (2.00 g, 4.45 mmol) in DCM (100 mL). The resulting mixture was stirred at rt overnight. The solvent was removed under reduced pressure and the crude product was purified by flash column chromatography (hexane:EtOAc, 7:3) to yield a white solid (800 mg, 34%).

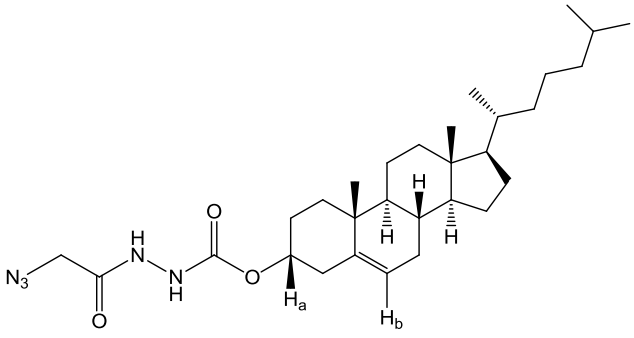

^{1}H NMR δ 8.19 (s, 1H, NH), 6.75 (s, 1H, NH), 5.38 (d, 1H, *J* = 5.1 Hz, H_b), 4.62-4.51 (m, 1H, H_a), 4.08 (s, 2H, CH_2N_3), 2.40-2.33 (m, 2H, alkyl H), 2.03-0.85 (m, 38H, alkyl H), 0.68 (s, 3H, CH_3); ^{13}C NMR δ 166.2 (C=O), 155.5 (C=O), 139.3 (C=CH_b), 123.0 (C=CH_b), 56.7, 56.1, 51.5, 50.0, 42.3, 39.7, 39.5, 38.2, 36.9, 36.5, 36.2, 35.8, 31.9, 31.8, 28.2, 28.0, 27.9, 24.3, 23.8, 22.8, 22.6, 21.0, 19.3, 18.7, 11.9 (25 x alkyl C); Anal. calcd for $C_{30}H_{49}N_5O_3$: C 68.27; H 9.36; N 13.27, Found: C 68.02; H 9.39; N 13.33.

5.4.2 Synthesis of the fluorescein azide 119

To a solution of 1-azido-4-bromobutane [216] (270 mg, 1.26 mmol) in anhydrous DMF (5 mL) was added fluorescein methyl ester **125** [217] (314 mg, 0.90 mmol) and potassium carbonate (170 mg, 1.23 mmol). The mixture was heated to 70 ^{o}C under an argon atmosphere for 2 hr after which TLC analysis (DCM:MeOH, 9:1) indicated complete reaction. The mixture was diluted with EtOAc (20 mL) and washed with water (3 x 10 mL). The organic layer was dried over anhydrous $MgSO_4$ and the solvent was removed under vacuum to yield an orange-brown solid. This was washed with hexane (6 x 10 mL) to remove the excess azide, thus yielding the product as an orange-brown solid which was used without further purification (276 mg, 69%).

Methyl 2-(6-(4-azidobutoxy)-3-oxo-3*H*-xanthen-9-yl)benzoate (119)

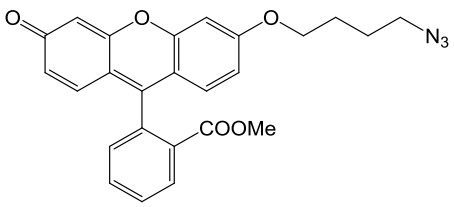

^{1}H NMR δ 8.25 (d, 1H, *J* = 7.5 Hz), 7.77-7.65 (m, 2H, ArH), 7.31 (d, 1H, *J* = 7.2 Hz, ArH), 6.95-6.83 (m, 3H, ArH), 6.73 (d, 1H, *J* = 8.7 Hz, ArH), 6.54 (d, 1H, *J* = 9.6 Hz, ArH), 6.45 (s, 1H, ArH), 4.10 (t, 2H, *J* = 6.0 Hz, OCH_2), 3.64 (s, 3H, $COOCH_3$), 3.39 (t, 2H, *J* = 6.6 Hz, CH_2N_3) 1.98-1.73 (m, 4H, -CH_2CH_2-); ^{13}C NMR δ 185.5, 165.6, 163.3, 158.9, 154.2, 150.3, 134.5, 132.7, 131.1, 130.5, 130.2, 130.2, 129.7, 129.7, 128.9, 117.4, 114.8, 113.6, 105.6, 100.8 (4 x ArC, 3 x ArCO, 1 x ArC=O, 1 x $COOCH_3$, 11 x ArCH), 68.1, 52.3, 51.03,

26.2, 25.6 (4 x CH_2, 1 x $COO\underline{C}H_3$); HRMS (ESI) calcd for $C_{25}H_{22}N_3O_5$ 444.1554 $[M + H]^+$, found 444.1574.

5.4.3 General procedure for the synthesis of the T_{10}-triazolyl conjugates 128a-d

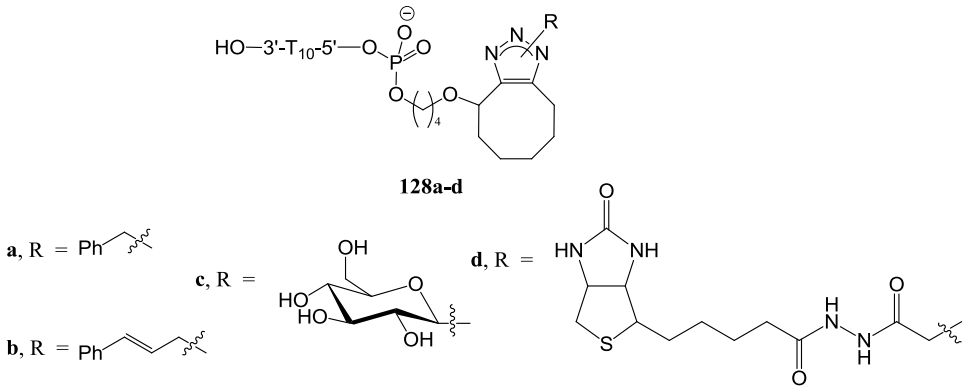

To solid supported T_{10}-cyclooctyne **24** (0.2 µmol) in an eppendorf tube was added a solution of the azide in DMSO (20 µL of a 200 mM stock solution, 4.0 µmol, 20 equivalents). The final volume was adjusted to 30 µL with DMSO and water according to the solubility of the azide (table 5.3), and the mixture was agitated at rt. After completion of reaction, the supernatant liquid was removed by syringe and the CPG was washed firstly with a suitable organic solvent (5 x 300 µL, see table 5.3) and then H_2O (1 x 300 µL). Deprotection/cleavage of the resin-bound oligonucleotides was followed by RP-HPLC analysis.

R group	Reaction solvent	Work-up solvent	Reaction Time	Product
Benzyl	DMSO:H_2O, 1:1	CH_3CN	30 min	**128a**
Cinnamyl	DMSO:H_2O, 1:1	CH_3CN	30 min	**128b**
Glucose	DMSO	CH_3CN	240 min	**128c**
Biotin	DMSO:H_2O, 9:1	DMSO	240 min	**128d**

Table 5.3. Reaction conditions and work-up procedures for the synthesis of the DNA-conjugates **128a-d**

R group	Mass calculated	Mass found	Product
Benzyl	3371	3371	**128a**
Cinnamyl	3397	3395	**128b**
Glucose	3443	3443	**128c**
Biotin	3579	3579	**128d**

Table 5.4. Mass data for the cleaved DNA-conjugates **128a-d**

5.4.4 Synthesis of the mixed 12-*mer* DNA-triazolyl conjugates 131a-f

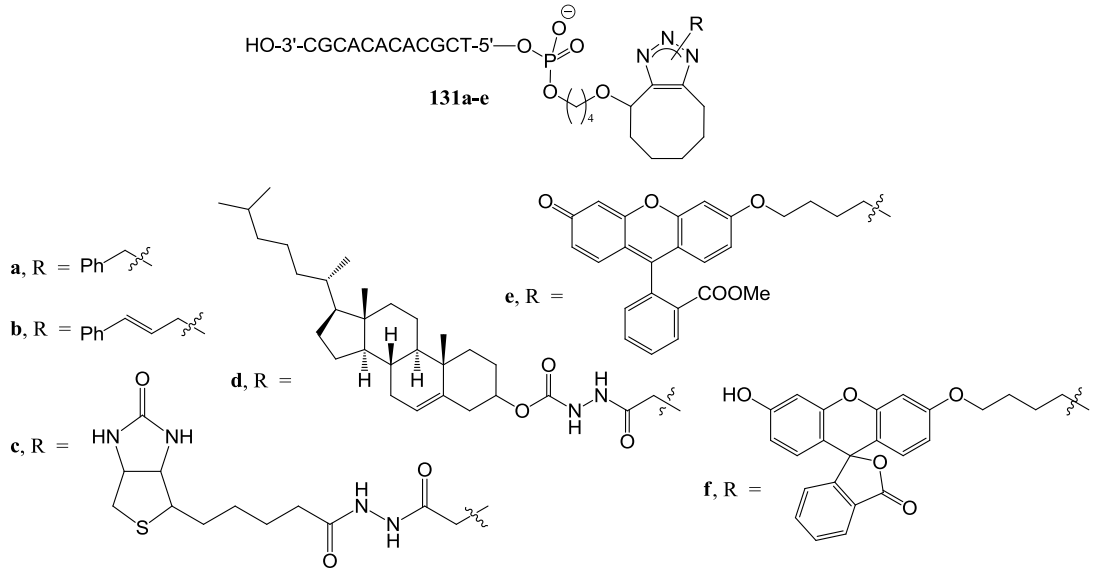

5.4.4.i General procedure for the synthesis of the mixed 12-mer DNA-triazolyl conjugates 131a-c

To the solid supported DNA-cyclooctyne **112** (0.14 µmol) in an eppendorf tube was added a solution of the azide (10 µL of a 280 mM stock solution in DMSO, 2.8 µmol, 20 equivalents). The volume was adjusted to 20 µL with DMSO and water according to the solubility of the azide (table 5.5) and the reaction mixture was agitated at rt. After completion of the reaction, the CPG was washed firstly with a suitable organic solvent (5 x 300 µL, see table 5.5) and then H_2O (1 x 300 µL). Deprotection/cleavage of the resin-bound oligonucleotides was followed analysis and if necessary, purification, by RP-HPLC.

5.4.4.ii Synthesis of the cholesterol-labelled DNA conjugate 131d

To the solid supported DNA-cyclooctyne **112** (0.14 μmol) in an eppendorf tube was added a solution of the cholesterol azide **118** (20 μL of a 140 mM stock solution in $CHCl_3$, 2.8 μmol, 20 equivalents). The reaction mixture was agitated at rt overnight. The CPG was then washed firstly with $CHCl_3$ (5 x 300 μL) and then H_2O (1 x 300 μL). Deprotection/cleavage of the resin-bound oligonucleotide was followed by RP-HPLC analysis and purification on a Phenomenex C8 column.

5.4.4.iii Synthesis of the non-fluorescent DNA conjugate 131f

To the solid supported DNA-cyclooctyne **112** (0.14 μmol) in an eppendorf tube was added a solution of the fluorescein azide **119** (10 μL of a 280 mM stock solution in $CHCl_3$, 2.8 μmol, 20 equivalents). The volume was adjusted to 20 μL with $CHCl_3$ (table 5.5) and the reaction mixture was agitated at rt overnight. The CPG was then washed firstly with $CHCl_3$ (5 x 300 μL) and then H_2O (1 x 300 μL). Deprotection/cleavage of the resin-bound oligonucleotide was followed by analysis and purification by RP-HPLC

5.4.4.iv Synthesis of the fluorescent DNA conjugate 131e

Following deprotection/cleavage of the CPG-DNA-cyclooctyne **112**, a solution of the resulting DNA-cyclooctyne **113** (125 μL, 200 μM, 0.025 μmol) was evaporated to dryness. To this was added a solution of the fluorescein azide **119** (4.5 μL of a 112 mM stock solution in DMSO, 1.0 μmol, 40 equivalents) and H_2O (0.5 μL). Following agitation overnight at rt, H_2O (300 μL) and EtOAc (300 μL) were added and the aqueous layer was washed with EtOAc (10 x 300 μL) to remove the excess azide. Any remaining EtOAc was removed under vacuum and the resulting aqueous solution was analysed and purified by RP-HPLC.

R group	Reaction solvent	Work-up solvent	Reaction Time	Product
Benzyl	DMSO:H_2O 1:1	CH_3CN	30 min	**131a**
Cinnamyl	DMSO:H_2O 1:1	CH_3CN	30 min	**131b**
Biotin	DMSO:H_2O 9:1	DMSO	4 hr	**131c**
Cholesterol	$CHCl_3$	$CHCl_3$	24 hr	**131d**
Fluorescein (ester)	DMSO:H_2O 9:1	EtOAc	18 hr	**131e**[a]
Fluorescein (lactone)	$CHCl_3$:H_2O 9:1	$CHCl_3$	18 hr	**131f**

[a] This reaction was conducted in the solution phase

Table 5.5. Reaction conditions and work-up procedures for synthesis of the DNA conjugates **131a-f**

R group	Mass calculated	Mass found	Product
Benzyl	3967	3969	**131a**
Cinnamyl	3993	3996	**131b**
Biotin	4175	4176	**131c**
Cholesterol	4361	436	**131d**
Fluorescein (ester)	4277	4277	**131e**
Fluorescein (lactone)	4262	4262	**131f**

Table 5.6. Mass data for the DNA-conjugates **131a-f**

5.4.5 General procedure for the synthesis of the $\underline{U}_4$-triazolyl conjugates 136a-c

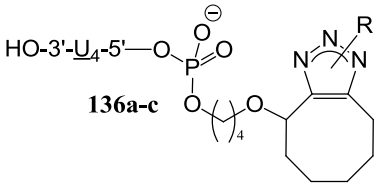

a, R = 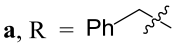

b, R = 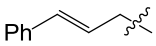

c, R = 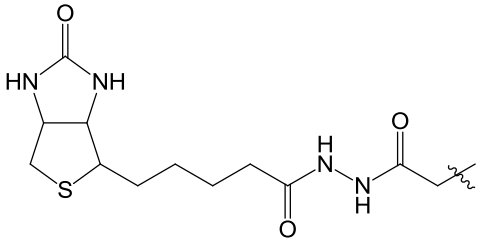

To the solid supported $\underline{U}_4$-cyclooctyne **134** (0.1 µmol) in an eppendorf tube was added a solution of the azide (40 µL of a 250 mM stock solution in DMSO, 10 µmol, 100 equivalents) and H_2O (10 µL). The reaction mixture was agitated at rt for 2 hr. The CPG was then washed firstly with DMSO (5 x 300 µL, see table 4.3) and then H_2O (1 x 300 µL). Deprotection/cleavage of the resin-bound oligonucleotides was followed by RP-HPLC analysis.

5.4.6 Synthesis of the 2'-OMe RNA-triazolyl conjugates 141a-e

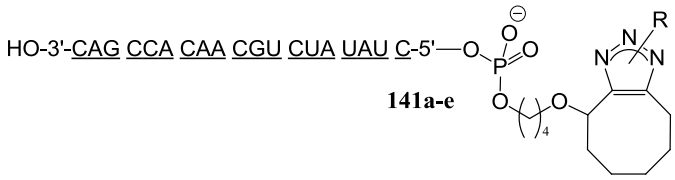

a, R = 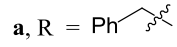

b, R = 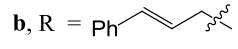

c, R = 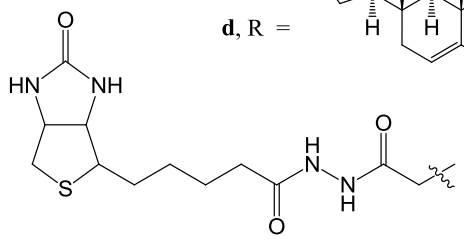

d, R = 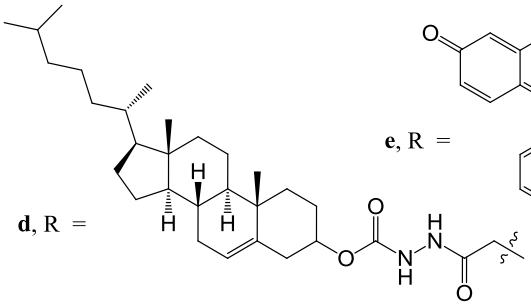

e, R = 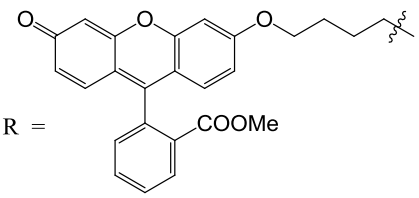

5.4.6.i General procedure for the synthesis of the 2'-OMe RNA-triazolyl conjugates 141a-c

To the solid supported 2'-OMe RNA-cyclooctyne **138** (0.14 μmol) in an eppendorf tube was added a solution of the azide (10 μL of a 280 mM stock solution in DMSO, 2.8 μmol, 20 equivalents). The volume was adjusted to 20 μL with DMSO and water according to the solubility of the azide (table 5.7) and the reaction mixture was agitated at rt. After completion of the reaction, the CPG was washed firstly with a suitable organic solvent (5 x 300 μL, see table 5.7) and then H_2O (1 x 300 μL). Deprotection/cleavage of the resin-bound oligonucleotides was followed by RP-HPLC analysis and purification.

5.4.6.ii Synthesis of the cholesterol-labelled 2'-OMe RNA conjugate 141d

To the solid supported 2'OMe RNA-cyclooctyne **138** (0.14 μmol) in an eppendorf tube was added a solution of the cholesterol azide **118** (20 μL of a 140 mM stock solution in $CHCl_3$, 2.8 μmol, 20 equivalents). The reaction mixture was agitated at rt overnight. The CPG was then washed firstly with $CHCl_3$ (5 x 300 μL) and then H_2O (1 x 300 μL). Cleavage/deprotection, analysis and purification by RP-HPLC on a Phenomenex C8 column followed according to the procedures described above.

5.4.4.iii Synthesis of the fluorescein-labelled 2'-OMe RNA conjugate 141e

Following deprotection and cleavage of the CPG-RNA-cyclooctyne **138** from the resin**,** the resulting crude sample of the RNA-cyclooctyne **139** was purified by RP-HPLC. The purified sample (125 μL, 200 μM, 0.025 μmol) was then evaporated to dryness. To this was added a solution of the fluorescein azide **119** (4.5 μL of a 112 mM stock solution in DMSO, 1.0 μmol, 40 equivalents) and H_2O (0.5 μL). Following agitation overnight at rt, H_2O (300 μL) and EtOAc (300 μL) were added and the aqueous layer was washed with EtOAc (10 x 300 μL) to remove the excess azide. Any remaining EtOAc was removed under vacuum and the resulting aqueous solution was analysed by RP-HPLC.

R group	Reaction solvent	Work-up solvent	Reaction Time	Product
Benzyl	DMSO:H_2O 1:1	CH_3CN	30 min	**141a**
Cinnamyl	DMSO:H_2O 1:1	CH_3CN	30 min	**141b**
Biotin	DMSO:H_2O 9:1	DMSO	4 hr	**141c**
Cholesterol	$CHCl_3$	$CHCl_3$	18 hr	**141d**
Fluorescein (ester)	DMSO:H_2O 9:1	EtOAc	18 hr	**141e**[a]

[a] This reaction was conducted in solution phase

Table 5.7. Reaction conditions and work-up procedures for preparation of the 2'-OMe RNA conjugates **141a-e**

R group	Mass calculated	Mass found	Product
Benzyl	6624	6623	**141a**
Cinnamyl	6650	6650	**141b**
Biotin	6831	6833	**141c**
Cholesterol	7018	7020	**141d**
Fluorescein (ester)	6931	6934	**141e**

Table 5.8. MS data for the 2'-OMe RNA conjugates **141a-e**

Bibliography

(1) Watson, J. D.; Crick, F. H. *Nature* **1953**, *171*, 737.
(2) http://web.jjay.cuny.edu/~acarpi/NSC/12-dna.htm, accessed 10/06/2012.
(3) Fire, A.; Xu, S. Q.; Montgomery, M. K.; Kostas, S. A.; Driver, S. E.; Mello, C. C. *Nature* **1998**, *391*, 806.
(4) Meister, G.; Tuschl, T. *Nature* **2004**, *431*, 343.
(5) Tomari, Y.; Zamore, P. D. *Genes & Development* **2005**, *19*, 517.
(6) Samuelson, A. V.; Klimczak, R. R.; Thompson, D. B.; Carr, C. E.; Ruvkun, G. *Cold Spring Harbor Symp. Quant. Biol.* **2007**, *72*, 489.
(7) Bettencourt-Dias, M.; Goshima, G. *Methods Mol. Biol. (Totowa, NJ, U. S.)* **2009**, *545*, 39.
(8) DasGupta, R.; Gonsalves, F. C. *Methods Mol. Biol. (Totowa, NJ, U. S.)* **2008**, *469*, 163.
(9) Jeong, J. H.; Mok, H.; Oh, Y. K.; Park, T. G. *Bioconj. Chem.* **2009**, *20*, 5.
(10) Chiu, Y. L.; Rana, T. M. *RNA* **2003**, *9*, 1034.
(11) Czauderna, F.; Fechtner, M.; Dames, S.; Aygun, H.; Klippel, A.; Pronk, G. J.; Giese, K.; Kaufmann, J. *Nucleic Acids Res.* **2003**, *31*, 2705.
(12) Soutschek, J.; Akinc, A.; Bramlage, B.; Charisse, K.; Constien, R.; Donoghue, M.; Elbashir, S.; Geick, A.; Hadwiger, P.; Harborth, J.; John, M.; Kesavan, V.; Lavine, G.; Pandey, R. K.; Racie, T.; Rajeev, K. G.; Rohl, I.; Toudjarska, I.; Wang, G.; Wuschko, S.; Bumcrot, D.; Koteliansky, V.; Limmer, S.; Manoharan, M.; Vornlocher, H. P. *Nature* **2004**, *432*, 173.
(13) Feldkamp, U.; Niemeyer, C. M. *Angew. Chem., Int. Ed.* **2006**, *45*, 1856.
(14) Gu, Q.; Cheng, C.; Gonela, R.; Suryanarayanan, S.; Anabathula, S.; Dai, K.; Haynie, D. T. *Nanotechnology* **2006**, *17*, R14.
(15) Keren, K.; Krueger, M.; Gilad, R.; Ben-Yoseph, G.; Sivan, U.; Braun, E. *Science* **2002**, *297*, 72.
(16) Kinsella, J. M.; Ivanisevic, A. *Langmuir* **2007**, *23*, 3886.
(17) Heilemann, M.; Kasper, R.; Tinnefeld, P.; Sauer, M. *J. Am. Chem. Soc.* **2006**, *128*, 16864.
(18) Roelfes, G.; Feringa, B. L. *Angew. Chem., Int. Ed.* **2005**, *44*, 3230.
(19) do Nascimento, C.; Barbosa, R. E. S.; Issa, J. P. M.; Watanabe, E.; Ito, I. Y.; Monesi, N.; Albuquerque, R. F. *Microbiol. Res.* **2008**, *163*, 403.
(20) Xu, H. M.; Zhang, S.; Liu, D. P.; Liang, C. C. *Mol. Biotechnol.* **2001**, *17*, 183.
(21) Ugarte-Uribe, B.; Perez-Rentero, S.; Lucas, R.; Avino, A.; Reina, J. J.; Alkorta, I.; Eritja, R.; Morales, J. C. *Bioconj. Chem.* **2010**, *21*, 1280.
(22) Walther, C.; Meyer, K.; Rennert, R.; Neundorf, I. *Bioconj. Chem.* **2008**, *19*, 2346.
(23) http://www.linktech.co.uk/support/knowledge_base/27_choosing-a-synbase-solid-support, accessed 01/03/2012.
(24) Andersen, N. K.; Spacilova, L.; Jensen, M. D.; Kocalka, P.; Jensen, F.; Nielsen, P. *Nucleic Acids Symp. Ser.* **2008**, *52*, 149.
(25) Godeau, G. S., Cathy; Barthelemy, Philippe. *J. Med. Chem.* **2008**, *51*, 4374.
(26) Werder, S. M., Vladimir L.; Haener, Robert. *Org. Lett.* **2008**, *10*, 2011.
(27) Gutsmiedl, K.; Fazio, D.; Carell, T. *Chem.--Eur. J.* **2010**, *16*, 6877.
(28) Kuijpers, W. H. A.; Huskens, J.; Koole, L. H.; van Boeckel, C. A. A. *Nucleic Acids Res.* **1990**, *18*, 5197.
(29) Jäger, S.; Rasched, G.; Kornreich-Leshem, H.; Engeser, M.; Thum, O.; Famulok, M. *J. Am. Chem. Soc.* **2005**, *127*, 15071.
(30) Livak, K. J.; Hobbs, F. W.; Zagursky, R. J. *Nucleic Acids Res.* **1992**, *20*, 4831.
(31) Augustin, M. A.; Ankenbauer, W.; Angerer, B. *J. Biotechnol.* **2001**, *86*, 289.
(32) Giller, G.; Tasara, T.; Angerer, B.; Muhlegger, K.; Amacker, M.; Winter, H. *Nucleic Acids Res.* **2003**, *31*, 2630.
(33) Tasara, T.; Angerer, B.; Damond, M.; Winter, H.; Dorhofer, S.; Hubscher, U.; Amacker, M. *Nucleic Acids Res.* **2003**, *31*, 2636.

(34) Baccaro, A.; Weisbrod, S. H.; Marx, A. *Synthesis-Stuttgart* **2007**, 1949.
(35) Gramlich, P. M. E.; Wirges, C. T.; Gierlich, J.; Carell, T. *Org. Lett.* **2008**, *10*, 249.
(36) Hill, K. W.; Taunton-Rigby, J.; Carter, J. D.; Kropp, E.; Vagle, K.; Pieken, W.; McGee, D. P. C.; Husar, G. M.; Leuck, M.; Anziano, D. J.; Sebesta, D. P. *J. Org. Chem.* **2001**, *66*, 5352.
(37) Comstock, L. R.; Rajski, S. R. *Nucleic Acids Res.* **2005**, *33*, 1644.
(38) Singh, I.; Vyle, J. S.; Heaney, F. *Chem. Commun.* **2009**, 3276.
(39) Kolb, H. C.; Finn, M. G.; Sharpless, K. B. *Angew. Chem., Int. Ed.* **2001**, *40*, 2004.
(40) Craig, T. W.; Harvey, G. R.; Berchtold, G. A. *J. Org. Chem.* **1967**, *32*, 3743.
(41) Ferraris, D.; Drury, W. J.; Cox, C.; Lectka, T. *J. Org. Chem.* **1998**, *63*, 4568.
(42) Dirksen, A.; Dawson, P. E. *Bioconj. Chem.* **2008**, *19*, 2543.
(43) Montalbetti, C.; Falque, V. *Tetrahedron* **2005**, *61*, 10827.
(44) Burgess, K.; Ibarzo, J.; Linthicum, D. S.; Russell, D. H.; Shin, H.; Shitangkoon, A.; Totani, R.; Zhang, A. J. *J. Am. Chem. Soc.* **1997**, *119*, 1556.
(45) Maddani, M. R.; Prabhu, K. R. *J. Org. Chem.* **2010**, *75*, 2327.
(46) Gothelf, K. V.; Jørgensen, K. A. *Chem. Rev.* **1998**, *98*, 863.
(47) Curtius, T. *Ber. Dtsch. Chem. Ges.* **1883**, *16*, 2230.
(48) Buchner, E. *Ber. Dtsch. Chem. Ges.* **1888**, *21*, 2637.
(49) Beckmann, E. *Ber. Dtsch. Chem. Ges.* **1890**, *23*, 3331.
(50) Werner, A.; Buss, H. *Chem. Ber.* **1894**, *27*, 2193.
(51) Diels, O.; Alder, K. *Justus Liebigs Ann. Chem.* **1928**, *460*, 98.
(52) Huisgen, R. *Angew. Chem., Int. Ed.* **1963**, *2*, 565.
(53) Sustmann, R. *Pure Appl. Chem.* **1974**, *40*, 569.
(54) Sustmann, R. *Tetrahedron Lett.* **1971**, *12*, 2717.
(55) Sustmann, R.; Trill, H. *Angew. Chem., Int. Ed.* **1972**, *11*, 838.
(56) Fleming, I. *Frontier Orbitals and Organic Chemical Reactions*; Wiley, 1977.
(57) Michael, A. *J. Prakt. Chem.* **1893**, *48*, 94.
(58) Huisgen, R.; Szeimies, G.; Möbius, L. *Chem. Ber.* **1967**, *100*, 2494.
(59) Tornoe, C. W.; Christensen, C.; Meldal, M. *J. Org. Chem.* **2002**, *67*, 3057.
(60) Rostovtsev, V. V.; Green, L. G.; Fokin, V. V.; Sharpless, K. B. *Angew. Chem., Int. Ed.* **2002**, *41*, 2596.
(61) Hein, J. E.; Fokin, V. V. *Chem. Soc. Rev.* **2010**, *39*, 1302.
(62) Kolb, H. C.; Sharpless, K. B. *Drug Discovery Today* **2003**, *8*, 1128.
(63) Binder, W. H.; Sachsenhofer, R. *Macromol. Rapid Commun.* **2007**, *28*, 15.
(64) Lutz, J.-F. *Angew. Chem., Int. Ed.* **2007**, *46*, 1018.
(65) Chen, L.; Li, C.-J. *Adv. Synth. Catal.* **2006**, *348*, 1459.
(66) Aragao-Leoneti, V.; Campo, V. L.; Gomes, A. S.; Field, R. A.; Carvalho, I. *Tetrahedron* **2010**, *66*, 9475.
(67) Durek, T.; Becker, C. F. W. *Biomol. Eng.* **2005**, *22*, 153.
(68) El-Sagheer, A. H.; Brown, T. *Chem. Soc. Rev.* **2010**, *39*, 1388.
(69) Padwa, A. *1,3-Dipolar Cycloaddition Chemistry*; Wiley, 1984.
(70) Feuer, H.; Torssell, K. *Nitrile Oxides, Nitrones, and Nitronates in Organic Synthesis: Novel Strategies in Synthesis*; Wiley-Interscience, 2008.
(71) Ramón, R. n. S.; Bosson, J.; Díez-González, S.; Marion, N.; Nolan, S. P. *J. Org. Chem.* **2010**, *75*, 1197.
(72) Jain, N.; Kumar, A.; Chauhan, S. M. S. *Tetrahedron Lett.* **2005**, *46*, 2599.
(73) Mallory, F. B.; Mallory, C. W. *J. Am. Chem. Soc.* **1985**, *107*, 4816.
(74) Chiarino, D.; Napoletano, M.; Sala, A. *Synth. Commun.* **1988**, *18*, 1171.
(75) Halling, K.; Torssell, K. B. G.; Hazell, R. G. *Acta Chem. Scand.* **1991**, *45*, 736.
(76) Tsuge, O.; Kanemasa, S.; Suga, H. *Chem. Lett.* **1986**, 183.
(77) Gi, H.-J.; Xiang, Y.; Schinazi, R. F.; Zhao, K. *J. Org. Chem.* **1997**, *62*, 88.

(78) De la Cruz, P.; Espildora, E.; Garcia, J. J.; De la Hoz, A.; Langa, F.; Martin, N.; Sanchez, L. *Tetrahedron Lett.* **1999**, *40*, 4889.
(79) Torsell, K. B. G.; Hazell, A. C.; Hazell, R. G. *Tetrahedron* **1985**, *41*, 5569.
(80) Mukaiyama, T.; Hoshino, T. *J. Am. Chem. Soc.* **1960**, *82*, 5339.
(81) Iffland, D. C.; Yen, T.-F. *J. Am. Chem. Soc.* **1954**, *76*, 4083.
(82) Kornblum, N. In *Organic Reactions*; John Wiley & Sons, Inc.: 2004.
(83) Sheremetev, A. B.; Makhova, N. N.; Friedrichsen, W. *Adv. Heterocycl. Chem.* **2001**, *78*, 65.
(84) Hassner, A.; Lokanatha Rai, K. M. *Synthesis* **1989**, *1989*, 57.
(85) Padmavathi, V.; Reddy, K. V.; Padmaja, A.; Venugopalan, P. *J. Org. Chem.* **2003**, *68*, 1567.
(86) Cossio, F. P.; Morao, I.; Jiao, H.; Schleyer, P. v. R. *J. Am. Chem. Soc.* **1999**, *121*, 6737.
(87) Rastelli, A.; Gandolfi, R.; Sarzi AmadÃ¨, M. *J. Org. Chem.* **1998**, *63*, 7425.
(88) Meyer, A. G.; Easton, C. J.; Lincoln, S. F.; Simpson, G. W. *J. Org. Chem.* **1998**, *63*, 9069.
(89) Kozikowski, A. P. *Acc. Chem. Res.* **1984**, *17*, 410.
(90) Sharma, S.; Pathak, V. N.; Madan, H.; Sharma, A. *Indian J. Heterocycl. Chem.* **2010**, *19*, 337.
(91) Karthikeyan, K.; Seelan, T. V.; Lalitha, K. G.; Perumal, P. T. *Bioorg. Med. Chem. Lett.* **2009**, *19*, 3370.
(92) Maurya, R.; Ahmad, A.; Gupta, P.; Chand, K.; Kumar, M.; Jayendra; Rawat, P.; Rasheed, N.; Palit, G. *Med. Chem. Res.* **2011**, *20*, 139.
(93) Mazzei, M.; Sottofattori, E.; Dondero, R.; Ibrahim, M.; Melloni, E.; Michetti, M. *Farmaco* **1999**, *54*, 452.
(94) Karabasanagouda, T.; Adhikari, A. V.; Girisha, M. *Indian J. Chem., Sect B: Org. Chem. Incl. Med. Chem.* **2009**, *48*, 430.
(95) Loh, B.; Vozzolo, L.; Mok, B. J.; Lee, C. C.; Fitzmaurice, R. J.; Caddick, S.; Fassati, A. *Chem. Biol. Drug Des.* **2010**, *75*, 461.
(96) Stork, G.; Danishefsky, S.; Ohashi, M. *J. Am. Chem. Soc.* **1967**, *89*, 5459.
(97) Easton, C. J.; Hughes, C. M.; Kirby, K. D.; Savage, G. P.; Simpson, G. W.; Tiekink, E. R. T. *J. Chem. Soc., Chem. Commun.* **1994**, 2035.
(98) Fuentes, J. A.; Maestro, A.; Testera, A. M.; Banez, J. M. *Tetrahedron: Asymmetry* **2000**, *11*, 2565.
(99) Gutsmiedl, K.; Wirges, C. T.; Ehmke, V.; Carell, T. *Org. Lett.* **2009**, *11*, 2405.
(100) Algay, V.; Singh, I.; Heaney, F. *Org. Biomol. Chem.* **2010**, *8*, 391.
(101) Romeo, R.; Giofre, S. V.; Iaria, D.; Sciortino, M. T.; Ronsisvalle, S.; Chiacchio, M. A.; Scala, A. *Eur. J. Org. Chem.* **2011**, 5690.
(102) Karskela, M. H., Mia; Virta, Pasi; Loennberg, Harri. *Bioconj. Chem.* **2010**, *21*, 748.
(103) Kocalka, P. A., Nicolai K.; Jensen, Frank; Nielsen, Poul. *ChemBioChem* **2007**, *8*, 2106.
(104) Andersen, N. K.; Chandak, N.; Brulikova, L.; Kumar, P.; Jensen, M. D.; Jensen, F.; Sharma, P. K.; Nielsen, P. *Bioorg. Med. Chem. Lett.* **2010**, *18*, 4702.
(105) Ostergaard, M. E.; Guenther, D. C.; Kumar, P.; Baral, B.; Deobald, L.; Paszczynski, A. J.; Sharma, P. K.; Hrdlicka, P. J. *Chem. Commun.* **2010**, *46*, 4929.
(106) James, D. E., Jean-Marc; Amigues, Eric; Schulz, Juergen; Vitry, Christiane; Bordenave, Thomas; Szlosek-Pinaud, Magali; Fouquet, Eric. *Tetrahedron Lett.* **2010**, *51*, 1230.
(107) Chittepu, P.; Sirivolu, V. R.; Seela, F. *Bioorg. Med. Chem. Lett.* **2008**, *16*, 8427.
(108) Seela, F.; Sirivolu, V. R. *Nucleosides, Nucleotides & Nucleic Acids* **2007**, *26*, 597.
(109) Smietana, M.; Johnson, R. B.; Wang, Q. M.; Kool, E. T. *Chem.--Eur. J.* **2004**, *10*, 173.
(110) Grecian, S.; Fokin, V. V. *Angew. Chem., Int. Ed.* **2008**, *47*, 8285.
(111) Lee, Y.-S.; Hyean Kim, B. *Bioorg. Med. Chem. Lett.* **2002**, *12*, 1395.
(112) Himo, F.; Lovell, T.; Hilgraf, R.; Rostovtsev, V. V.; Noodleman, L.; Sharpless, K. B.; Fokin, V. V. *J. Am. Chem. Soc.* **2005**, *127*, 210.

(113) Pelliccioli, A. P.; Wirz, J. *Photochem. Photobiol. Sci.* **2002**, *1*, 441.
(114) Corrie, J. E. T.; Barth, A.; Munasinghe, V. R. N.; Trentham, D. R.; Hutter, M. C. *J. Am. Chem. Soc.* **2003**, *125*, 8546.
(115) Yu, H. T.; Li, J. B.; Wu, D. D.; Qiu, Z. J.; Zhang, Y. *Chem. Soc. Rev.* **2010**, *39*, 464.
(116) Mayer, G.; Heckel, A. *Angew. Chem., Int. Ed.* **2006**, *45*, 4900.
(117) Lee, H. M.; Larson, D. R.; Lawrence, D. S. *ACS Chem. Biol.* **2009**, *4*, 409.
(118) Kawai, T.; Nakashima, Y.; Irie, M. *Adv. Mater.* **2005**, *17*, 309.
(119) Luo, S. J.; Chen, K. X.; Cao, L. C.; Liu, G. D.; He, Q. S.; Jin, G. F.; Zeng, D. X.; Chen, Y. *Opt. Express* **2005**, *13*, 3123.
(120) Lafuma, A.; Chodorowski-Kimmes, S.; Quinn, Francis X.; Sanchez, C. *Eur. J. Inorg. Chem.* **2003**, *2003*, 331.
(121) Andersson, J.; Li, S. M.; Lincoln, P.; Andreasson, J. *J. Am. Chem. Soc.* **2008**, *130*, 11836.
(122) Asanuma, H.; Shirasuka, K.; Yoshida, T.; Takarada, T.; Liang, X. G.; Komiyama, M. *Chem. Lett.* **2001**, 108.
(123) Zhu, M.-Q.; Zhang, G.-F.; Li, C.; Aldred, M. P.; Chang, E.; Drezek, R. A.; Li, A. D. Q. *J. Am. Chem. Soc.* **2011**, *133*, 365.
(124) Schulze, F. W.; Petrick, H. J.; Cammenga, H. K.; Klinge, H. *Z. Phys. Chem.* **1977**, *107*, 1.
(125) Monti, S.; Orlandi, G.; Palmieri, P. *Chem. Phys.* **1982**, *71*, 87.
(126) Kobayashi, T.; Degenkolb, E. O.; Rentzepis, P. M. *J. Phys. Chem.* **1979**, *83*, 2431.
(127) Lednev, I. K.; Ye, T.-Q.; Hester, R. E.; Moore, J. N. *J. Phys. Chem.* **1996**, *100*, 13338.
(128) Fliegl, H.; Koehn, A.; Haettig, C.; Ahlrichs, R. *J. Am. Chem. Soc.* **2003**, *125*, 9821.
(129) Beharry, A. A.; Woolley, G. A. *Chem. Soc. Rev.* **2011**, *40*, 4422.
(130) Norman, L. L.; Barrett, C. J. *J. Phys. Chem. B* **2002**, *106*, 8499.
(131) Kumar, G. S.; Neckers, D. C. *Chem. Rev.* **1989**, *89*, 1915.
(132) Naujok, R. R.; Paul, H. J.; Corn, R. M. *J. Phys. Chem.* **1996**, *100*, 10497.
(133) Rau, H.; Lueddecke, E. *J. Am. Chem. Soc.* **1982**, *104*, 1616.
(134) Curtin, D. Y.; Grubbs, E. J.; McCarty, C. G. *J. Am. Chem. Soc.* **1966**, *88*, 2775.
(135) Bandara, H. M. D.; Burdette, S. C. *Chem. Soc. Rev.* **2012**, *41*, 1809.
(136) Magee, J. L.; Shand, W.; Eyring, H. *J. Am. Chem. Soc.* **1941**, *63*, 677.
(137) Rau, H. *Photochemistry and Photophysics*; CRC Press, Boca Raton, FL, 1990; Vol. 2.
(138) Dong, Q.; Svoboda, K.; Tiersch, T. R.; Todd Monroe, W. *J. Photochem. Photobiol. B* **2007**, *88*, 137.
(139) Brode, W. R.; Gould, J. H.; Wyman, G. M. *J. Am. Chem. Soc.* **1952**, *74*, 4641.
(140) Gabor, G.; Fischer, E. *J. Phys. Chem.* **1971**, *75*, 581.
(141) Pozhidaeva, N.; Cormier, M.-E.; Chaudhari, A.; Woolley, G. A. *Bioconj. Chem.* **2004**, *15*, 1297.
(142) Nishioka, H.; Liang, X.; Asanuma, H. *Chem.--Eur. J.* **2010**, *16*, 2054.
(143) Asanuma, H.; Liang, X.; Komiyama, M. *Tetrahedron Lett.* **2000**, *41*, 1055.
(144) Woolley, G. A. *Acc. Chem. Res.* **2005**, *38*, 486.
(145) El Halabieh, R. H.; Mermut, O.; Barrett, C. J. *Pure Appl. Chem.* **2004**, *76*, 1445.
(146) Yager, K. G.; Barrett, C. J. *J. Photochem. Photobiol. A* **2006**, *182*, 250.
(147) Koumura, N.; Kudo, M.; Tamaoki, N. *Langmuir* **2004**, *20*, 9897.
(148) Wen, Y.; Yi, W.; Meng, L.; Feng, M.; Jiang, G.; Yuan, W.; Zhang, Y.; Gao, H.; Jiang, L.; Song, Y. *J. Phys. Chem. B* **2005**, *109*, 14465.
(149) Clavier, G.; Ilhan, F.; Rotello, V. M. *Macromolecules* **2000**, *33*, 9173.
(150) Renner, C.; Moroder, L. *ChemBioChem* **2006**, *7*, 868.
(151) Zhang, Y.; Erdmann, F.; Fischer, G. *Nat. Chem. Biol.* **2009**, *5*, 724.
(152) Schierling, B.; Noël, A. J.; Wende, W.; Hien, l. T.; Volkov, E.; Kubareva, E.; Oretskaya, T.; Kokkinidis, M.; Römpp, A.; Spengler, B.; Pingoud, A. *Proc. Natl. Acad. Sci. U. S. A.* **2010**, *107*, 1361.

(153) Bartels, E.; Wassermann, N. H.; Erlanger, B. F. *Proc. Natl. Acad. Sci. U. S. A.* **1971**, *68*, 1820.
(154) Fujita, D.; Murai, M.; Nishioka, T.; Miyoshi, H. *Biochem.* **2006**, *45*, 6581.
(155) Volgraf, M.; Gorostiza, P.; Szobota, S.; Helix, M. R.; Isacoff, E. Y.; Trauner, D. *J. Am. Chem. Soc.* **2006**, *129*, 260.
(156) Yamana, K.; Yoshikawa, A.; Nakano, H. *Tetrahedron Lett.* **1996**, *37*, 637.
(157) Asanuma, H.; Ito, T.; Komiyama, M. *Tetrahedron Lett.* **1998**, *39*, 9015.
(158) Asanuma, H.; Ito, T.; Yoshida, T.; Liang, X. G.; Komiyama, M. *Angew. Chem., Int. Ed.* **1999**, *38*, 2393.
(159) Asanuma, H.; Liang, X. G.; Yoshida, T.; Komiyama, M. *ChemBioChem* **2001**, *2*, 39.
(160) Robertson, J. M. *J. Chem. Soc.* **1939**, 232.
(161) Yamazawa, A.; Liang, X.; Asanuma, H.; Komiyama, M. *Angew. Chem., Int. Ed.* **2000**, *39*, 2356.
(162) Asanuma, H.; Tamaru, D.; Yamazawa, A.; Liu, M.; Komiyama, M. *ChemBioChem* **2002**, *3*, 786.
(163) Liu, M.; Asanuma, H.; Komiyama, M. *J. Am. Chem. Soc.* **2006**, *128*, 1009.
(164) Matsunaga, D.; Asanuma, H.; Komiyama, M. *J. Am. Chem. Soc.* **2004**, *126*, 11452.
(165) Ito, H.; Liang, X.; Nishioka, H.; Asanuma, H. *Org. Biomol. Chem.* **2010**, *8*, 5519.
(166) Nakamura, M.; Fukunaga, Y.; Sasa, K.; Ohtoshi, Y.; Kanaori, K.; Hayashi, H.; Nakano, H.; Yamana, K. *Nucleic Acids Res.* **2005**, *33*, 5887.
(167) Nakamura, M.; Fukunaga, Y.; Sasa, K.; Ohtoshi, Y.; Kanaori, K.; Hayashi, H.; Nakano, H.; Yamana, K. *Nucleic Acids Res.*, *33*, 5887.
(168) Casas-Solvas, J. M.; Martos-Maldonado, M. C.; Vargas-Berenguel, A. *Tetrahedron* **2008**, *64*, 10919.
(169) Ravalico, F.; James, S. L.; Vyle, J. S. *Green Chem.* **2011**, *13*, 1778.
(170) Okubo, M.; Takahashi, T.; Koga, K. *Bull. Chem. Soc. Jpn.* **1983**, *56*, 199.
(171) Reid, E. B.; Pritchett, E. G. *J. Org. Chem.* **1953**, *18*, 715.
(172) Guerrini, G.; Costanzo, A.; Bruni, F.; Selleri, S.; Casilli, L.; Giusti, L.; Martini, C.; Lucacchini, A.; Malmberg Aiello, P.; Ipponi, A. *Eur. J. Med. Chem.* **1996**, *31*, 259.
(173) Kim, Y.; Koh, M.; Kim, D. K.; Choi, H. S.; Park, S. B. *J. Comb. Chem.* **2009**, *11*, 928.
(174) Yur'ev, Y. K.; Zefirov, N. S. *Zh. Obshch. Khim.* **1959**, *29*, 2954.
(175) Wang, Q.; Gao, S.; Zhou, K.; Chen, W.; Niu, C.; Xi, Z. *Chin. J. Chem.* **2009**, *27*, 1582.
(176) Ghosh, S.; Usharani, D.; De, S.; Jemmis, E. D.; Bhattacharya, S. *Chem.--Asian J.* **2008**, *3*, 1949.
(177) Bunce, N. J.; Ferguson, G.; Forber, C. L.; Stachnyk, G. J. *J. Org. Chem.* **1987**, *52*, 394.
(178) Prescher, J. A.; Dube, D. H.; Bertozzi, C. R. *Nature* **2004**, *430*, 873.
(179) Baskin, J. M.; Prescher, J. A.; Laughlin, S. T.; Agard, N. J.; Chang, P. V.; Miller, I. A.; Lo, A.; Codelli, J. A.; Bertozzi, C. R. *Proc. Natl. Acad. Sci. U. S. A.* **2007**, *104*, 16793.
(180) Bernardin, A.; Cazet, A.; Guyon, L.; Delannoy, P.; Vinet, F.; Bonnaffe, D.; Texier, I. *Bioconjugate Chem.* **2010**, *21*, 583.
(181) Link, A. J.; Mock, M. L.; Tirrell, D. A. *Curr. Opin. Biotechnol.* **2003**, *14*, 603.
(182) Keppler, O. T.; Horstkorte, R.; Pawlita, M.; Schmidts, C.; Reutter, W. *Glycobiology* **2001**, *11*, 11R.
(183) Jao, C. Y.; Roth, M.; Welti, R.; Salic, A. *Proc. Natl. Acad. Sci. U. S. A.* **2009**, *106*, 15332.
(184) Salic, A.; Mitchison, T. J. *Proc. Natl. Acad. Sci. U. S. A.* **2008**, *105*, 2415.
(185) Debets, M. F.; van, d. D. C. W. J.; Rutjes, F. P. J. T.; van, D. F. L. *ChemBioChem* **2010**, *11*, 1168.
(186) Wittig, G.; Pohlke, R. *Chem. Ber.* **1961**, *94*, 3276.
(187) Agard, N. J.; Prescher, J. A.; Bertozzi, C. R. *J. Am. Chem. Soc.* **2004**, *126*, 15046.
(188) Agard, N. J.; Baskin, J. M.; Prescher, J. A.; Lo, A.; Bertozzi, C. R. *ACS Chem. Biol.* **2006**, *1*, 644.

(189) Baskin, J. M.; Prescher, J. A.; Laughlin, S. T.; Agard, N. J.; Chang, P. V.; Miller, I. A.; Lo, A.; Codelli, J. A.; Bertozzit, C. R. *Proc. Natl. Acad. Sci. U. S. A.* **2007**, *104*, 16793.
(190) Ning, X. H.; Guo, J.; Wolfert, M. A.; Boons, G. J. *Angew. Chem., Int. Ed.* **2008**, *47*, 2253.
(191) Jewett, J. C.; Sletten, E. M.; Bertozzi, C. R. *J. Am. Chem. Soc.* **2010**, *132*, 3688.
(192) Debets, M. F.; van Berkel, S. S.; Schoffelen, S.; Rutjes, F.; van Hest, J. C. M.; van Delft, F. L. *Chem. Commun.* **2010**, *46*, 97.
(193) Kuzmin, A.; Poloukhtine, A.; Wolfert, M. A.; Popik, V. V. *Bioconj. Chem.* **2010**, *21*, 2076.
(194) Poloukhtine, A. A.; Mbua, N. E.; Wolfert, M. A.; Boons, G. J.; Popik, V. V. *J. Am. Chem. Soc.* **2009**, *131*, 15769.
(195) Stockmann, H.; Neves, A. A.; Stairs, S.; Ireland-Zecchini, H.; Brindle, K. M.; Leeper, F. J. *Chem. Sci.* **2011**, *2*, 932.
(196) Chang, P. V.; Prescher, J. A.; Sletten, E. M.; Baskin, J. M.; Miller, I. A.; Agard, N. J.; Lo, A.; Bertozzi, C. R. *Proc. Natl. Acad. Sci. U. S. A.* **2010**, *107*, 1821.
(197) Debets, M. F.; Van Berkel, S. S.; Dommerholt, J.; Dirks, A. J.; Rutjes, F.; Van Delft, F. L. *Acc. Chem. Res.* **2011**, *44*, 805.
(198) Ustinov, A. V.; Korshun, V. A. *Russ. Chem. Bull.* **2006**, *55*, 1268.
(199) Soriano, d. A. D.; Wang, W.; Jiang, H.; Besanceney, C.; Yan, A. C.; Levy, M.; Liu, Y.; Marlow, F. L.; Wu, P. *J. Am. Chem. Soc.* **2010**, *132*, 16893.
(200) Singh, I.; Heaney, F. *Chem. Commun.* **2011**, *47*, 2706
(201) Delft, P. v.; Meeuwenoord, N. J.; Hoogendoorn, S.; Dinkelaar, J.; Overkleeft, H. S.; Marel, G. A. v. d.; Filippov, D. V. *Org. Lett.* **2010**, *12*, 5486.
(202) Yamada, T.; Peng, C. G.; Matsuda, S.; Addepalli, H.; Jayaprakash, K. N.; Alam, M. R.; Mills, K.; Maier, M. A.; Charisse, K.; Sekine, M.; Manoharan, M.; Rajeev, K. G. *J. Org. Chem.* **2011**, *76*, 1198.
(203) Skattebol, L.; Solomon, S. In *Organic Synthesis*; Wiley & Sons: New York, 1973; Vol. Coll. Vol. 5, p 306.
(204) Shi, F.; Waldo, J. P.; Chen, Y.; Larock, R. C. *Org. Lett.* **2008**, *10*, 2409.
(205) Zatsepin, T. S.; Oretskaya, T. S. *Chem. Biodiversity* **2004**, *1*, 1401.
(206) Godeau, G.; Staedel, C.; Barthelemy, P. *J. Med. Chem.* **2008**, *51*, 4374.
(207) Wilchek, M.; Bayer, E. A. *Anal. Biochem.* **1988**, *171*, 1.
(208) Yao, L.; Smith, B. T.; Aubé, J. *J. Org. Chem.* **2004**, *69*, 1720.
(209) Debets, M. F.; van, d. D. C. W. J.; Rutjes, F. P. J. T.; van, D. F. L. *ChemBioChem* **2010**, *11*, 1168.
(210) MacDonald, J. E.; Kelly, J. A.; Veinot, J. G. C. *Langmuir* **2007**, *23*, 9543.
(211) Li, C.; Henry, E.; Mani, N. K.; Tang, J.; Brochon, J.-C.; Deprez, E.; Xie, J. *Eur. J. Org. Chem.* **2010**, 2395.
(212) Jayaprakash, K. N.; Peng, C.-G.; Butler, D.; Varghese, J. P.; Maier, M. A.; Rajeev, K. G.; Manoharan, M. *Org. Lett.* **2010**, *12*, 5410.
(213) Casas-Solvas, J. M.; Martos-Maldonado, M. C.; Vargas-Berenguel, A. *Tetrahedron* **2008**, *64*, 10919.
(214) Fatas, P.; Longo, E.; Rastrelli, F.; Crisma, M.; Toniolo, C.; Jimenez, A. I.; Cativiela, C.; Moretto, A. *Chem.--Eur. J.* **2011**, *17*, 12606.
(215) Jiang, X. Z.; Ahmed, M.; Deng, Z. C.; Narain, R. *Bioconj. Chem.* **2009**, *20*, 994.
(216) Agnew, H. D.; Rohde, R. D.; Millward, S. W.; Nag, A.; Yeo, W. S.; Hein, J. E.; Pitram, S. M.; Tariq, A. A.; Burns, V. M.; Krom, R. J.; Fokin, V. V.; Sharpless, K. B.; Heath, J. R. *Angew. Chem., Int. Ed.* **2009**, *48*, 4944.
(217) Guarin, S. A. P.; Tsang, D.; Skene, W. G. *New J. Chem.* **2007**, *31*, 210.

Appendix

6.1 Detailed analysis of spectral data of a representative isoxazole cycloadduct

In order to characterise the novel compounds prepared in this thesis, a range of NMR spectra were gathered; these included ^{1}H (300 MHz), ^{13}C (75 MHz), DEPT (45, 90, 135), homonuclear and heteronuclear COSY, and ^{31}P (121 MHz). For all compounds initially the ^{1}H NMR spectra were examined, and resonance positions, multiplicity and relative integrations were recorded. Peaks were assigned based on resonance position and multiplicity. Homonuclear COSY data highlighted coupling between the protons and the ^{13}C peaks were assigned with the help of DEPT (45, 90, 135) spectra and as necessary heteronuclear COSY spectra.

NMR spectral data of 2-(4-(5-(phenoxymethyl)isoxazol-3-yl)phenoxy)ethanol (15c)

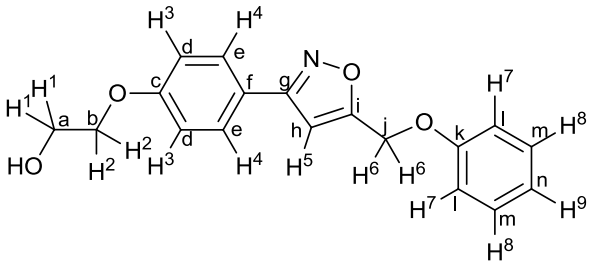

Included below is the NMR data which was used to assign peaks and characterise the structure of the isoxazole cycloadduct **15c**. All spectra are recorded in $CDCl_3$.

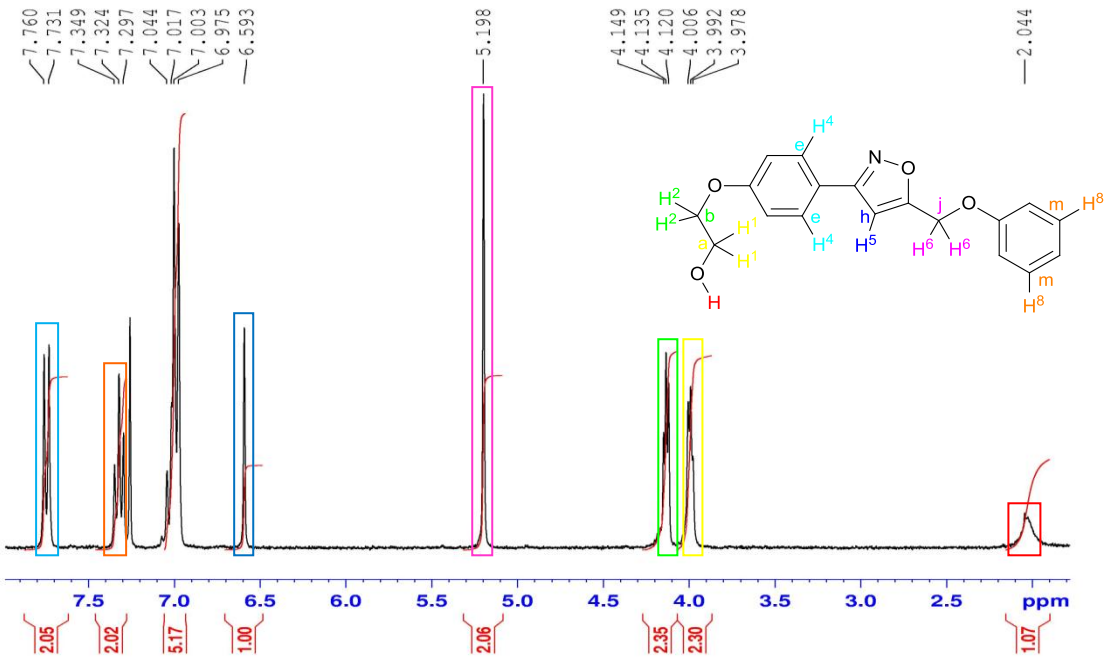

Figure 6.1. ^{1}H NMR spectrum of **15a**

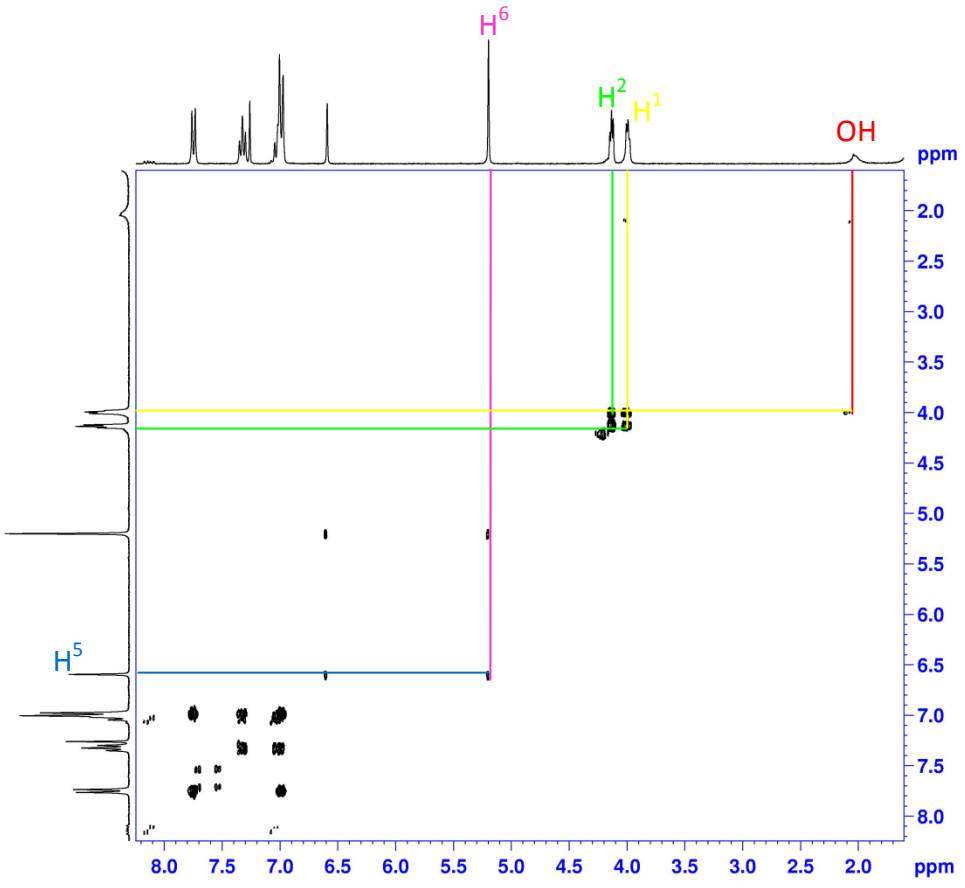

Figure 6.2. ^{1}H^{1}H COSY NMR spectrum of **15a**

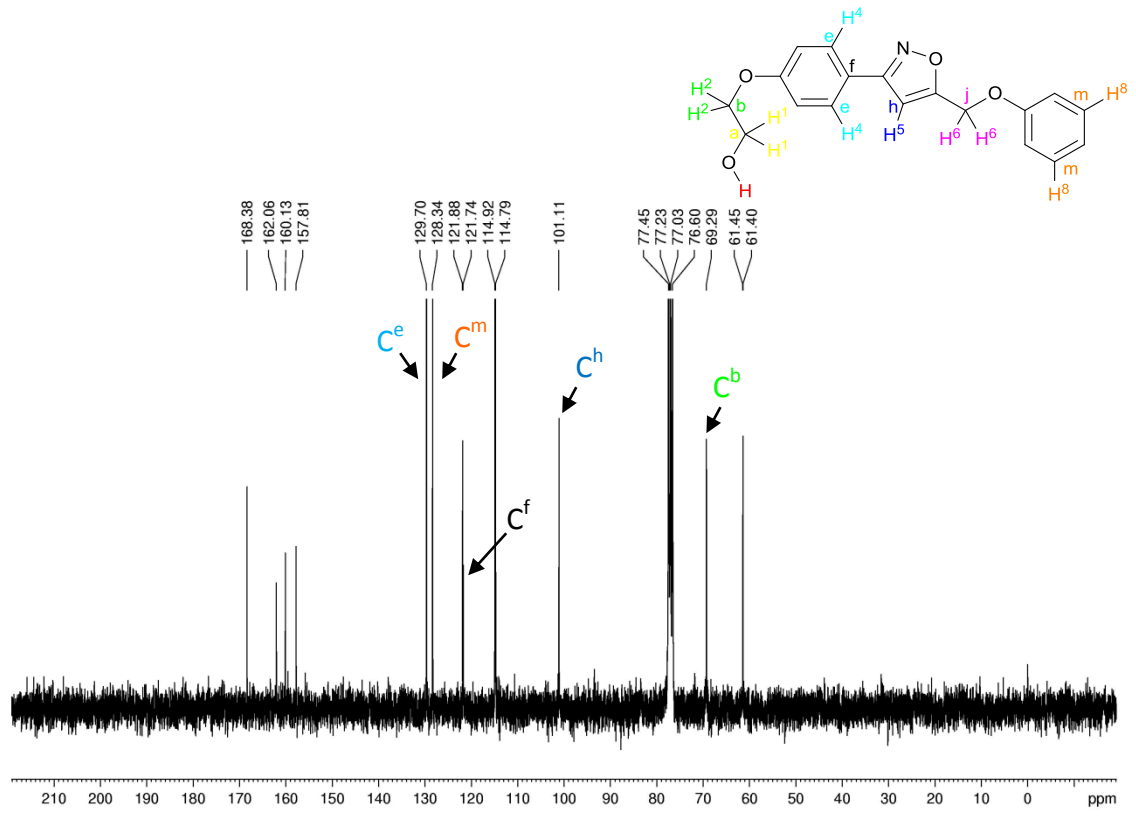

Figure 6.3. ^{13}C NMR spectrum of **15a**

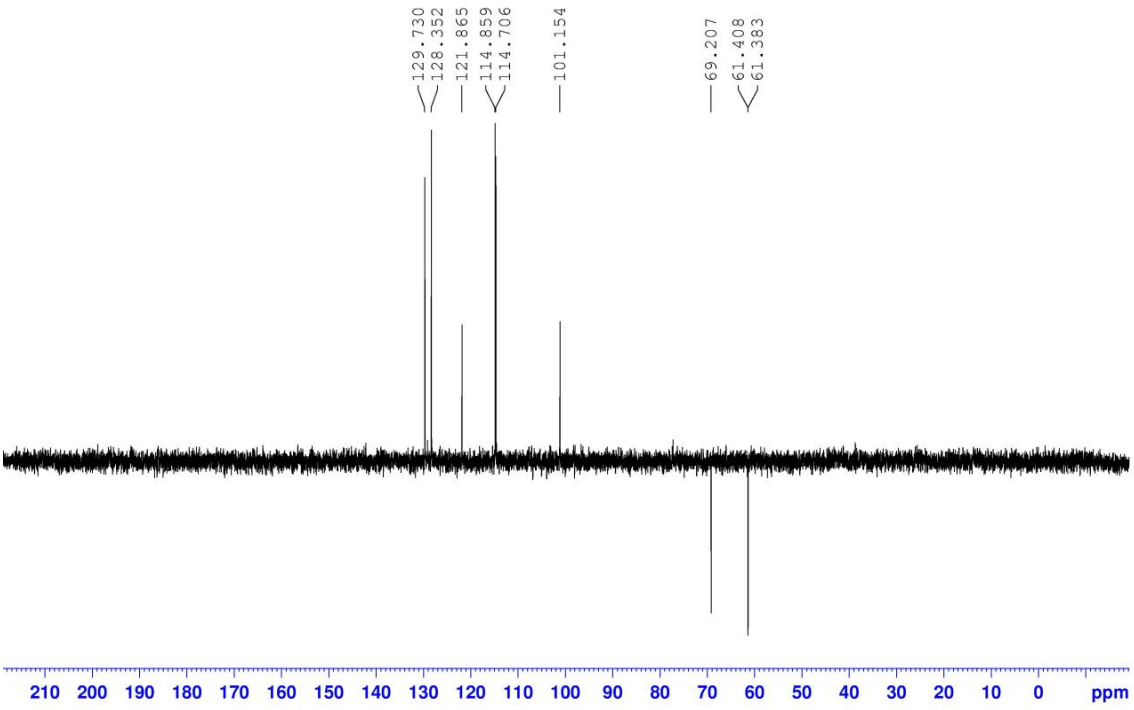

Figure 6.4. DEPT135 NMR spectrum of **15a**

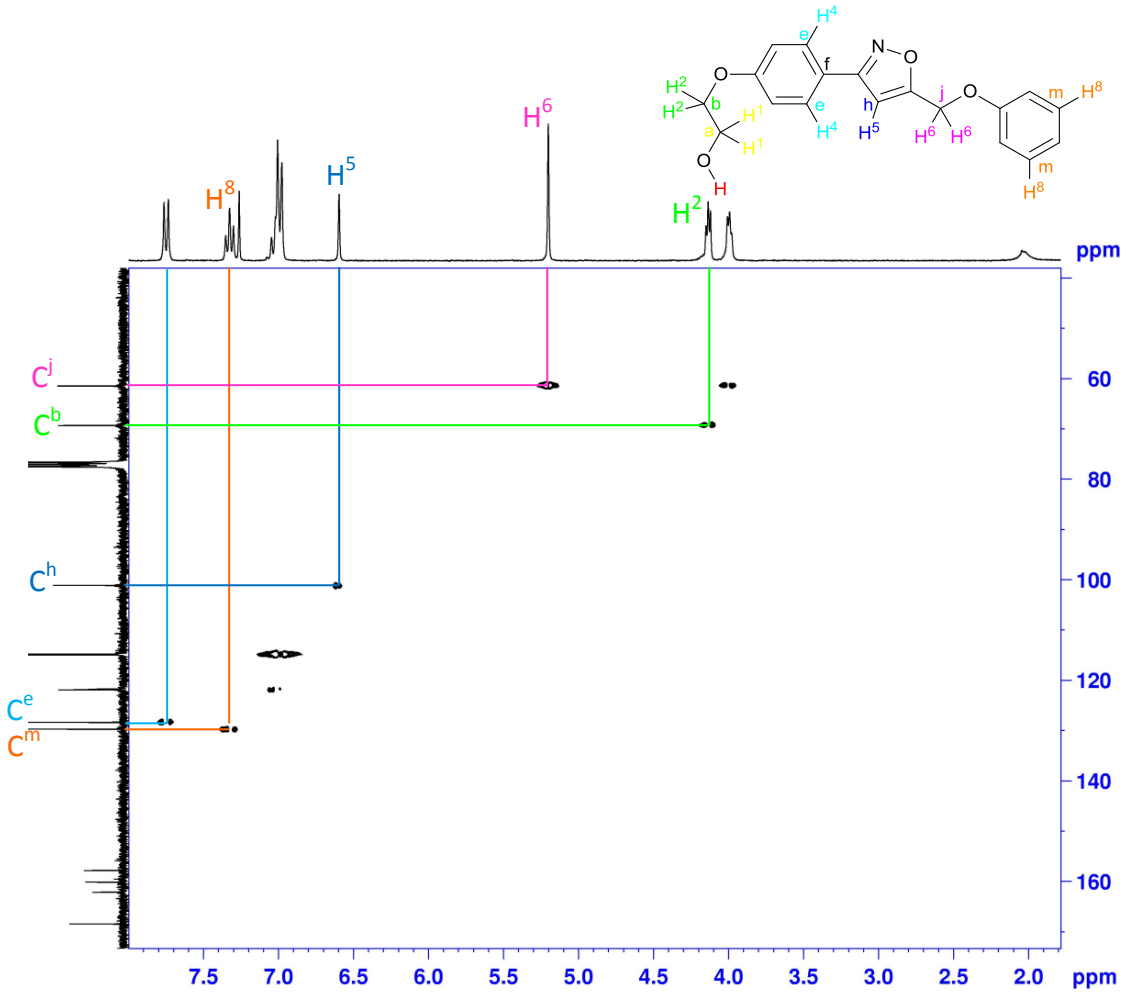

Figure 6.5. $^{1}H^{13}C$ COSY NMR spectrum of **15a**

The use of relative integrations and coupling constants in the ^{1}H NMR spectrum (figure 6.1) and a range of additional NMR spectra were used to assign the peaks. In the ^{1}H NMR spectrum, the aromatic peaks are located between 6.98 and 7.76 ppm. The isoxazole proton (H^{5}) presents as a singlet at 6.60 ppm. This chemical shift is typical of that observed for all 3,5-disubstituted isoxazoles prepared in this thesis. The next signal, integrating for two protons, represents the methylene protons H^{6}. Assignment of the protons H^{5} and H^{6} is confirmed by analysis of the $^{1}H^{1}H$ COSY spectrum (figure 6.2), which shows coupling between these protons. This ^{4}J coupling is perhaps surprising, although closer inspection of the ^{1}H NMR spectrum confirms slight broadening of the two signals in question.

The two signals at 4.14 and 3.99 ppm, each integrating for two protons, clearly represent the two sets of methylene protons H^1 and H^2. The final peak, a broad singlet at 2.04 ppm, is that of the OH proton. Assignment of the protons H^1 and H^2 is aided by analysis of the $^1H^1H$ COSY spectrum, which shows coupling between the signal at 3.99 ppm and the OH signal at 2.04 ppm. Therefore, the signal at 3.99 ppm must be that of the H^1 protons. The only coupling observed for the protons at 4.14 ppm is between those at 3.99 ppm; the peak at 4.14 ppm must therefore represent the H^2 protons.

The aromatic region of the ^1H NMR spectrum contains three discrete signals: a doublet at 7.75 ppm integrating for 2 protons, a triplet at 7.32 ppm integrating for 2 protons and a multiplet at 7.04-6.98 ppm integrating for 5 protons. Assignment of the aromatic protons requires consideration of the possible resonance structures of this molecule (figure 6.6). Each aromatic ring bears an electron donating alkoxy substitutuent. The lone pair of the oxygen can delocalise into the aromatic ring, which results in resonance structures for each ring with a negative charge at the positions *ortho* and *para* to the electron donating group. As the true structure is a weighted average of all the contributing resonance forms, the protons at the *ortho* and *para* positions will be shielded relative to those which are *meta* to the alkoxy group, and as such will appear further upfield. This will affect the H^3, H^7 and H^9 protons, which are all represented by the relatively upfield multiplet at 7.04-6.68 ppm. The more downfield signals at 7.75 ppm and 7.32 ppm therefore represent the H^4 and H^8 protons.

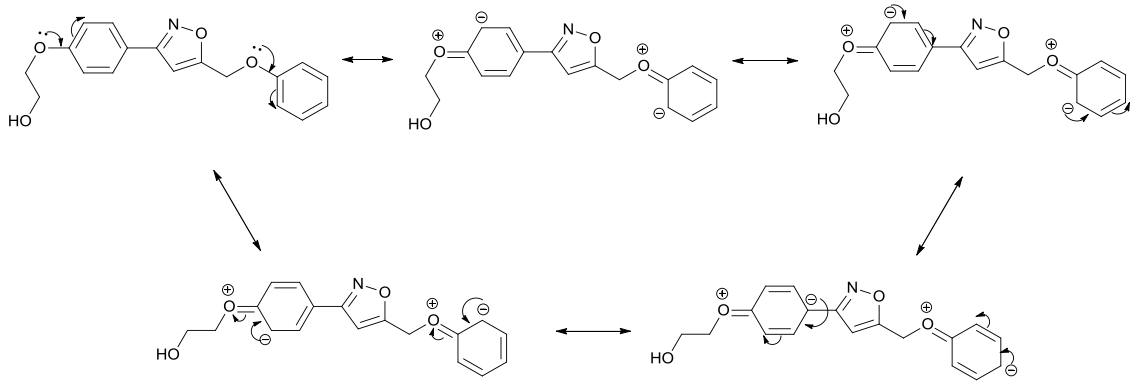

Figure 6.6. Selected resonance contributors for the cycloadduct **15c**

The doublet at 7.75 ppm integrates for 2 protons and has a coupling constant of 8.7 Hz, which suggests ^{3}J coupling to one other aryl proton. This doublet must therefore represent the H^4 protons, which are coupled to the adjacent H^3 protons. By elimination, this means the triplet at 7.32 ppm must correspond to the H^8 protons. As these are coupled to both the H^7 and H^9 protons, this singal would be expected to present as a doublet of doublets. However, due to overlappling of the two middle peaks of the signal, a triplet is observed. Table 6.1 below lists the assignments of all signals in the ^{1}H NMR spectrum of **15c**.

Entry	Peak (ppm)	Multiplicity	Coupling Constant (Hz)	Proton(s)
1	7.75	d	8.4	H^4
2	7.32	t	7.5	H^8
3	7.04-6.98	m	-	$H^{3,7,9}$
4	6.59	sl br s	-	H^5
5	5.20	sl br s	-	H^6
6	4.14	t	4.4	H^2
7	3.99	t	4.4	H^1
8	2.03	br s	-	OH

Table 6.1. Assignment of signals in the ^{1}H NMR spectrum of 15c

The ^{13}C NMR spectrum (figure 6.3) can be assigned with the help of DEPT135 (figure 6.4) and CH correlation (figure 6.5) spectra. A glance at the DEPT135 spectrum immediately reveals the idenitity of the CH_2 signals at 69.3, 61.5 and 61.4. Analysis of the CH correlation spectrum shows coupling between the carbon peak at 69.3 ppm and the H^2 protons (entry 6, table 6.1), confirming that this peak represents C^b. Due to the almost negligible difference in the chemical shift of the carbon atoms C^a and C^j (61.5 and 61.4 ppm), it is impossible to unambiguously assign these signals based on analysis of the CH correlation spectrum.

The aromatic and isoxazole carbon atoms resonate in the range of 168.4-101.1 ppm. Those carbons bearing a proton can be assigned following analysis of the CH

correlation spectrum. Coupling is observed between the peak at 101.1 ppm and the H^5 signal (entry 4, table 6.1); therefore this peak must represent C^h. Coupling is also observed between the carbon peaks at 129.7 and 128.3 and the protons H^4 (entry 1, table 6.1) and H^8 (entry 2, table 6.1), respectively. These peaks can therefore unambiguously be assigned as representing the carbons C^e (129.7 ppm) and C^m (128.3 ppm). The carbon signals at 121.9, 114.9 and 114.8 ppm are all coupled to protons within the multiplet at 7.04-6.98 ppm. These signals therefore represent carbon atoms C^d, C^l, and C^n, although individual assignment is impossible, as the signals representing protons H^3, H^7 and H^9 cannot themselves be distinguished.

Finally, analysis of the DEPT135 spectrum reveals signals representing quaternary carbon atoms at 168.4, 162.1, 160.1, 157.8 and 121.7. Of these signals, the peak at 121.7 ppm can be definitively assigned as the carbon C^f. This is logical, as it is the only quaternary carbon not directly bound to an electronegative atom, and is therefore less deshielded than the others. The remaining quaternary signals can be assigned as C^c, C^g, C^i and C^k.

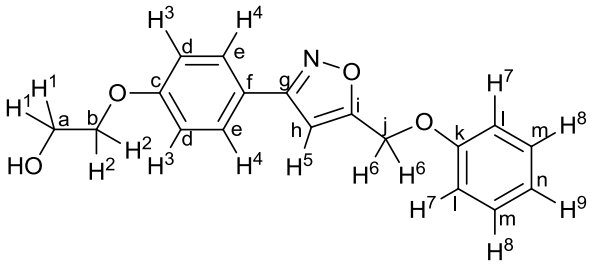

^{1}H NMR δ 7.75 (d, *J* = 8.4 Hz, 2H, H^4), 7.32 (t, *J* = 7.5 Hz, 2H, H^8), 7.04-6.98 (m, 5H, $H^{3,7,9}$), 6.59 (sl br s, 1H, H^5), 5.20 (sl br s, 2H, H^6), 4.14 (t, *J* = 4.4 Hz, 2H, H^2), 3.99 (t, *J* = 4.4 Hz, 2H, H^1), 2.03 (br s, 1H, OH); ^{13}C NMR δ 168.4, 162.1, 160.1, 157.8 ($C^{c,g,i,k}$), 129.7 (C^e), 128.3 (C^m), 121.9 ($C^{d/l/n}$), 121.7 (C^f), 114.9 ($C^{d/l/n}$), 114.8 ($C^{d/l/n}$), 101.1 (C^h), 69.3 (C^b), 61.5 ($C^{a/j}$), 61.4 ($C^{a/j}$).

6.2 Photochemical characterisation data for 94b

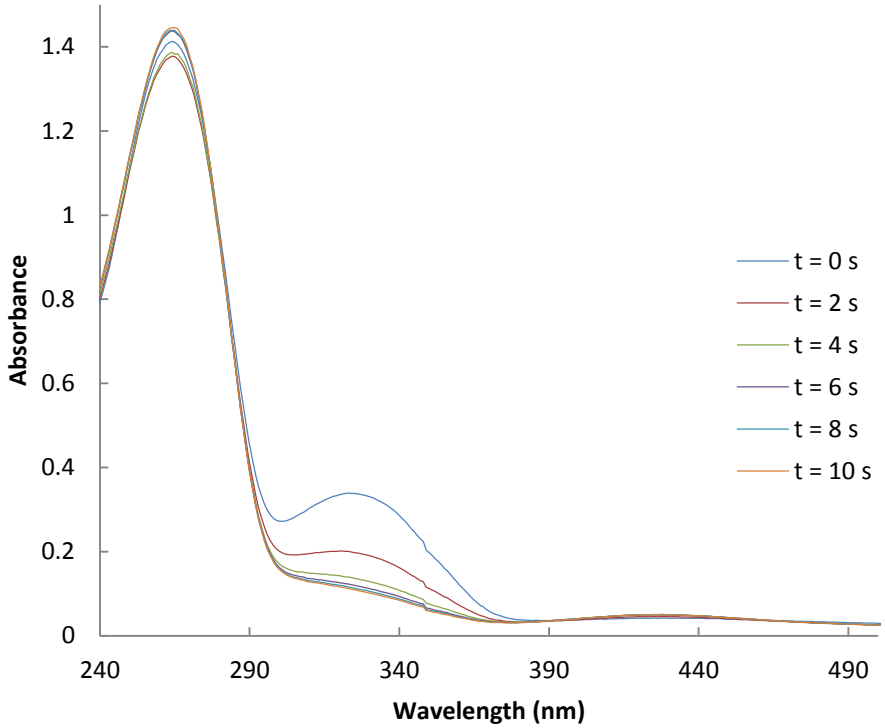

Figure 6.7. Overlaid UV/Vis spectra of **94b** upon irradiation at 366 nm for 0, 2, 4, 6, 8 and 10 s

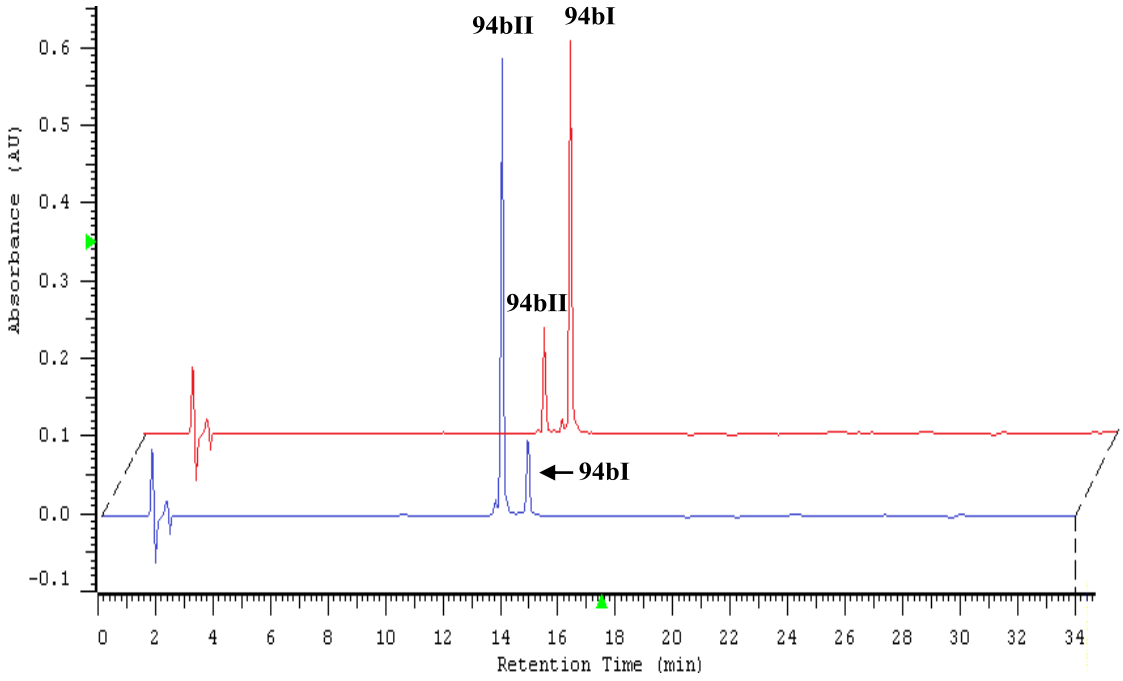

Figure 6.8. Overlaid HPLC traces of **94b** in the Irr (blue) and DA (red) photostationary states

6.3 Author publications